

eman ta zabal zazu



Universidad
del País Vasco

Euskal Herriko
Unibertsitatea

Pathological *ATAD3* variants and perturbed cholesterol metabolism in human and fly

Mikel Muñoz Oreja

Supervisors:

Ian J. Holt

Itxaso Martí

May 2023

Laburpena

Mitokondriak zelula eukarioto-nukleatu guztietan dauden bakterio tamainako organuluak dira. Beren funtzio behinenekoa da zelula behar duen energiari hornitzea, baina horrez gainera, mitokondriek zelularen hainbat funtzio garrantzitsutan hartzen dute parte, hala nola: nukleotido, aminoazido eta gantz azidoen metabolismoan, burdinaren homeostasian edo zenbait lipido, kinona, esteroide edo urearen biosintesian.

Mitokondrien beste ezaugarri garrantzitsu bat da bi mintzez inguratutako organulua dela, kanpo-mintza (OMM) eta barne-mintza (IMM) eta, horrek, gune ezberdinak bereizten ditu mitokondriarentzat baliagarriak direnak. Esate baterako, barne-mintza oso selektiboa da eta ioi txikiak ere ezin dute hura zeharkatu mintzeko garraiatzaileen laguntzarik gabe. Hartaz, gradiente elektrokimiko bat sortzen da barne-mintzaren bi aldeak bereizten dituen, eta gradiente horri esker da gai mitokondria energia sintetizatzeko. Labur, fosforilazio oxidatibo (OXPHOS) prozesuko lau proteina-konplexuak elektroioak garraiatzen dituzten bitartean, protoiak ponpatzen dira, eta, hala, gradiente elektrokimikoa sortzen da bostgarren konplexuak (ATP sintasak) ADPa eta fosfato inorganikoa elkartzeko erabiltzen duena. Horrela ATPa sortzen da, zelularen energia-molekula. Barne-mintzean, baita ere, gandorak sortzen dira; hau da, mitokondriaren barne aldera (matrizera) sartzen diren inbaginazioak, barne-mintzaren azalera handitzen dutenak, energiaren produkzioa areagotu dadin, besteak beste.

Beste organuluekiko nabarmen bereizgarria den ezaugarria dute mitokondriek, izan ere, animalietan beren DNA propioa duten (mitokondrietako DNA edo mtDNA) organulu bakarrak dira. Hala ere, giza mtDNA zirkularrek 37 gene baino ez dituzte kodetzen, eta mitokondrien beharrezko funtzioetarako eta izanerako behar dituzten gainerako proteinak nukleoan daude kodetuta eta zitoplasman sintetizatu behar dira, eta, azkenik, mitokondrietara garraiatu. Mitokondrietako DNAREN 37 gene horietatik, 13 dira proteina-kodetzaile, eta, gainontzekoek itzulpenerako beharrezko RNA elementuak kodetzen dituzte, RNA erribosomiko (rRNA) eta transferenteak (tRNA).

Mitokondrietako DNAREN herentzia ere berezia da; izan ere, nukleoan ez bezala, ernalkuntzaren ondorengo uneetan aitarengandik datozen mitokondriak eta

euren mtDNA deuseztatzen dira, eta, hartara, zigotoak amaren mtDNA baino ez du jasoko. Horri herentzia amatiarra esaten zaio.

Mitokondriak etengabe ari dira beren morfologia aldatzen, fusio eta fisio prozesu txandakatuen bidez, eta, hala, mitokondrien sare tubulatu bat osatzen dute, dinamina GTPasa, erretikulu endoplasmatico eta mikrotubuluaren elkarrekintzaz. Horrek, halaber, zelulako mitokondrien kopurua aldakorra izatea dakar, metabolismoa eta zelulen beharrianak bezalako bestelako faktore batzuek baldintzatuta, ere bai. Beraz, mitokondria bakoitzak mtDNA kopia kopuru aldakorra du.

Mitokondrietako DNA hori, baina, ez dago aske. Jakina da konplexu multimolekularrak osatzen dituela hainbat proteinekin, eta, egitura horiei, nukleotideak deritze. Nukleotideetako proteina batzuekin elkarrekintzak behinbetikoak dira eta beste batzuekin, berriz, aldi baterakoak. Nabarmentzekoa da mitokondrietako A transkripzio faktorea (TFAM) zeinak mtDNA paketatzen eta babesten laguntzen du.

Informazio horrekin guztiarekin, ez da harritzekoa gaixotasun mitokondrialak oso ohikoak izatea, baina ulertzen zailak ere bai; izan ere, gaixotasun horien kausak askotarikoak izan daitezke: mitokondrietako nahiz nukleoko geneek sor ditzakete, herentzian jasoak edo *de novo* gertatuak izan daitezke, eta, zelula edo ehun bereziak ala multisistemikoak izan daitezke. Hala ere, ohikoa izaten da beren eragin batzuk komunak izatea; hala nola, ATParen gabezia edo OXPHOS konplexuren baten edo batzuen aldaketak.

ATAD3, mitokondrietako mintzetako proteina, AAA+ familiako proteina da, eta, horregatik, domeinu eta funtzio bereizgarri batzuk ditu; hala nola, ATPasa domeinua, beste proteinetan eragiten duen domeinu funtzionala (nahiz eta funtzio hori askotarikoa izan daitekeen). ATAD3-ren kasuan, funtzio hori ezezaguna da zehazki, baina jakina da mitokondrietako DNA-rekin, edota nukleotideak osatzen dituzten hainbat proteinekin, elkarrekintzak dituela, mitokondrietako kolesterolaren gehiengoarekin ko-prezipitatzen duela, eta erretikulu endoplasmaticoarekin loturak sortzen dituela.

Gizakiak eboluzioan zehar gertatutako duplikazioetatik eratorritako hiru *ATAD3* gene dituzte, nukleoko lehenengo kromosoman bata bestearen segidan

kokatzen direnak (*ATAD3 A, B eta C*). Gene hauetan deskribaturiko mutazioak delezioak eta mutazio puntualak dira, batez ere, eta, tesi honen emaitzetan azaldu bezala, 2020. urtean, *ATAD3* geneetan duplikazioak ere deskribatu genituen gaixotasun-kausa. Gaixoen sintomatologia eta klinika aldakorra den arren, bereziki nabarmenak dira egoera multisistemikoak eta kasuen gehiengoak letalak dira jaio eta egun gutxitara. Aurreko ikerketa batek erakutsi zuen *ATAD3* genean delezio bialelikoak zituzten gaixoei kolesterolaren metabolismoan inplikaturiko geneak diferentzialki adierazita zizutela eta euren zelulek kolesterol libre gehiago zutela zitoplasman.

Tesi honen lehen kapituluak, *ATAD3* gaixoen zelulak erabili ziren ikerketa-iturri. Lehen aldiz, *ATAD3* gene-familian duplikazioak gaixotasunaren iturri ezarri genituen, eta, delezioen antzera, gaixotasun sindromiko larri bat eragiten zuen, entzefalopatia nabarmenekin, jaio eta berehala heriotzara zeramana. Gaixo haietako batean, 68 kb-ko duplikazio monoaleliko bat detektatu genuen *ATAD3B*-ren kopia bat eta *ATAD3A/C* fusio bat sortzen zituena. *ATAD3A/C* proteina fusioak 29 aminoazido zituen mutaturik eta horietako batzuk funtzionalki garrantzitsuak ziren proteinaren ATPasa domeinuan. Horietariko bat Arg466Cys mutazioa da, ATParen hidrolisian parte hartzen duen arginina behatz izeneko aminoazidoa aldatzen duena. Gerora, beste gaixo-familia batean Arg466Cys mutazio monoaleliko berbera, baina bera bakarrik, deskribatu genuen gaixotasun-kausa. Gaixo horiek helduak ziren eta batez ere atrofia optikoa eta bestelako sintoma neurologiko batzuk zituzten, baina duplikazio eta delezioen kasuan baino arinagoak.

Western blot eta antigorputzen detekzioaren bidez, ikusi genuen *ATAD3* proteina horiek adierazten zirela eta baita ere, gai ginela espezie mutante ezberdinak bereizteko nola proteinen abundantziagatik (*ATAD3* delezioak) ala banden migrazio-abiadurarengatik (*ATAD3 A/C* eta R466C gaixoak). Gaixoen beste fenotipo nabarmen bat zen zelula-barneko kolesterol-askea ia bikoitza zela, mutazio mota guztietan. Beraz, uste dugu bi fenotipo molekular horiek (proteina mutanteen identifikazioa eta kolesterol librearen emendioa) *ATAD3* gaixo potentzialen diagnosian lagungarri suerta daitezkeela, bestelako teknika genetiko eta klinikoekin konbinatuz.

Kolesterolaren biosintesian eta garraioan inplikaturiko zenbait proteinen adierazpen diferentziala detektatu genuen, batez ere, kolesterol-librea zelulatik kanpo ateratzeaz arduratzen diren mintz plasmatikoko ABCA1, ABCG1 eta SR-BI garraiatzaileena, zeina nabarmen txikiagoa zen. Horrek azalduko luke, hein batean behintzat, kolesterolaren akumulazioa. Lipido neutralak ere nabarmen ikus zitezkeen ATAD3 gaixoen zitoplasman, bestela ezin izaten dira detektatu zelula osasuntsuetan edo tratatu gabeetan; baina kontroletan kolesterolaren metabolismoa modulatu, badirudi kolesterolaren areagotzea lehenengotariko ezaugarri molekularra dela eta, lipido neutralena, berriz, sekundarioa edo. Hala ere, esperimentu horiek aditzera eman zuten kolesterolaren metabolismoaz gainera, beste lipido-bidezidor batzuk ere inplikatuta daudela ATAD3 gaixoetan.

ATAD3 gaixoen zitoplasman lisosomak akumulatzen zirela ikusi genuen, baita ere, baina zelulako materiala degradatzeko autofagia prozesuak ez zirudien bereziki aldatua. Gainera, lisosoma horietariko askok barnean mintz kontzentrikoak zituztela ikusi genuen, tipula itxura zutenak, eta gaixotasun lisosomalaren ezaugarri bereizgarri direnak. Hartara, gure modeloa da *ATAD3* mutatuak sortzen duen kolesterol librearen areagotze horrek, modu ez kontrolatuan kolesterolaren parte bat mintzetara joan dadila eragingo duela, eta horrek dituen efektu kaltegarriak saihesteko, zelulak lisosomen produkzioa handitzen duela. Kolesterol askoko mintz zati horiek liseritzen zailak direnez, tipula itxurako egiturak agertzen dira, liseritze prozesuan dauden bitartekari, autofagia fluxuan aldaketa nabarmenik gabe.

Hortaz, zelulako kolesterola eta lipidoen metabolismoko proteina gakoak modulatzeko desberdintasunak sor litzake *ATAD3* mutanteen zelulen eta kontrolen artean, eta, beharbada, estrategia terapeutiko baliagarriren bat aurki genezake. Nire esperimentuek erakutsi dute, kolesterolaren biosintesian, lipogenesian, garraioan edo kolesterolaren suplementazioan eragitean, orohar, kolesterola areagotzen dela, bai kontrol eta *ATAD3* gaixoetan. Horrek, beraz zaildu egiten du bi zelula moten arteko desberdintasunen identifikazioa, baina tratamendu batzuek etorkizunerako esperimentu berrien aukera zabaltzen zuten. Esate baterako, esfingosina fosfatoaren (S1P) suplementazioarekin kolesterolaren agregatu batzuk ikus zitezkeen kontroletan bakarrik, eta ez *ATAD3* zeluletan. Edo kolesterolaren biosintesia inhibitzen duen farmako batekin

(Ro 48-8071) kolesterolean ez, baina DNA mitokondrialaren erreplikazioan murrizpen nabarmena detektatu genuen.

Bigarren kapituluan, tesiko estantzian eta ondorengo urtean garatutako esperimentuak deskribatzen dira. Hemen gaixoen zeluletatik *Drosophila melanogaster* eulian esperimentatzera pasa nintzen. Euliaren R466C mutazio homologoa (R472C) zuten euliak sortu genituen, beren genomak dAtad3^{R472C} beste kopia bat txertatuz. Mutazioa eta bere ondorioak karakterizatzen hastean, hasieran, arazoak izan genituen fenotipoen kontsistentzia ez zelako berbera genotipo berbereko linea ezberdinetan. Arazo horiei esker, euliak hobeto karakterizatu ahal izan nituen eta nik neuk generatu dAtad3^{R472C} mutazioaren linea berri bat. Gainera, euli horietan kolesterol librea eta lipido neutralak detektatzeko arazoak izan nituen, mintzetako kolesterola detektatzeko sistema bat garatu genuen. Horretarako, perflingolisina O toxinarekin D4 domeinua erabili genuen, mintzeko kolesterolari batzen zaiona, mKate molekula fluoreszente bati lotuta zegoena. Estrategia hori jada erabili dute beste talde batzuek zeluletan, baina, guk, lehen aldiz, mKate-D4 hori eulian adieraztea lortu genuen, eta, hartara, *in vivo*, eulien ehunetan mintzetako kolesterola markatzea.

Horrela, ikusi genuen dAtad3^{R472C} larbetako neuroblastoek mKate-D4 markatzailearen agregatuak zituztela, mintzetan kolesterol-agregatuak zituztenaren seinale. Gainera, puntu horietariko asko lisosomekin gainjartzen zirela ikusi genuen, eta lisosoma gehiago zeudela dAtad3^{R472C} neuroblastoetan. Hortaz, datu horiek bat datoz zeluletan ikusitako kolesterolaren eta lisosomen emaitzekin, eta guk planteatutako modelo sendotzen dute. Izan ere, zelulen eta eulien datuak uztartuz, argi geratzen da ATAD3n mutazioek kolesterolaren emendio bat sortzen dutela, eta horri aurre egiten dietela lisosomen bidez liserituz, arestian aipatu bezala. Beraz, honek ATAD3 proteinak kolesterolaren metabolismoan duen inplikazioa argiago uzten du, eta iradokitzen du ATAD3ren ATPasa domeinua garrantzitsua izan daitekeela mitokondriako kolesterolaren erregulazioan.

Laburbilduz, tesi honek ATAD3 geneetan gertatzen diren mutazio berriak identifikatu ditu, eta, bereziki, horietako bat, ATParen hidrolisirako beharrezkoa den arginina behatz bat. Gaixoen zelulek kolesterolaren metabolismoa aldatu dutela ikusi dugu (bai librea eta bai mintzetakoa), eta hori ATAD3 patologiarekin

funtsean dagoela. Horrek gaixoen zeluletan sortzen dituen ondorio batzuk ere deskribatu ditugu, gaixotasunaren mekanismo molekularra ulertzen lagundu diezaguketenak, esaterako, lisosomen eragina eta inplikazioa ulertzen.

Table of contents

Abbreviations	4
General introduction	9
Mitochondria.....	10
Mitochondrial energy production	11
The mitochondrial genome.....	12
Replication, transcription and translation.....	14
The mitochondrial nucleoids.....	16
Mitochondrial diseases.....	17
Pathogenic mtDNA mutations	18
ATAD3	20
Hypothesis & Objectives	25
Chapter I: characterization of human primary fibroblast from <i>ATAD3</i> mutant patients	27
Introduction	28
The landscape of pathogenic <i>ATAD3</i> mutations	29
Cholesterol metabolism in the cell.....	33
Autophagy and the endolysosomal pathway	36
Materials & Methods	39
Cell culture	40
Immunocytochemistry.	40
Image capture and analysis.	41
Immunodetection of proteins.	41
Transmission electron microscopy	42
Quantification of mtDNA copy numbers.....	42
ATP levels analyzed by CellTiter-Glo (Promega).	42
Analysis of metabolic flux by SeaHorse (Agilent)	43
Table M1. Compounds, manufacturers	43
Table M2. Identity, source and dilutions of the primary and secondary antibodies used in the study.	44
Results	48
R1.1- <i>ATAD3</i> disease: genetics and clinical features.	49
R1.2- <i>ATAD3</i> protein-variant expression, identification and organization	54
R1.3- <i>ATAD3</i> antibodies.....	58

R1.4- Mitochondria and mitochondrial DNA phenotypes in ATAD3 mutant human primary fibroblast.....	67
R1.5- Extra-mitochondria effects of ATAD3 mutants	74
<i>R1.5.1-Free cholesterol accumulation and the expression of proteins implicated in cholesterol metabolism.....</i>	<i>74</i>
<i>R1.5.2-Neutral lipid accumulation.....</i>	<i>79</i>
<i>R1.5.3-Autophagy: autophagic flux, lysosomal abundance and activity & autophagy intermediates by TEM.....</i>	<i>83</i>
R1.6- Cholesterol and lipid metabolism modulation as a potential way of identifying, alleviating or treating ATAD3 mutants.	88
R1.7- Other potential ATAD3 patients	96
Chapter II: Generation of a new <i>in vivo</i> membrane-bound cholesterol reporter and its utilization in the <i>Atad3</i> R472C <i>Drosophila</i> model	103
Introduction.....	104
<i>Drosophila melanogaster</i> in the lab	105
UAS-Gal4 system for targeted gene expression	107
Materials & Methods.....	109
Cloning and transgenesis.....	110
Fly strains and maintenance	110
DNA extraction, PCR, electrophoresis and sequencing	111
<i>Drosophila</i> protein extraction and immunoblotting.....	111
<i>Drosophila</i> larval brain dissection and immunohistochemistry.....	112
Results	113
R2.1- Construction of a new membrane-cholesterol reporter for <i>Drosophila</i> : mKate-D4.....	114
R2.2- Generation and characterization of <i>dAtad3</i> ^{R472C} flies	115
<i>R2.2.1-Generation of UAS-dAtad3(R472C)-V5 flies.....</i>	<i>115</i>
<i>R2.2.2-Mutation severity assessment</i>	<i>118</i>
<i>R2.2.3- Membrane-bound cholesterol and lysosomes</i>	<i>121</i>
Discussion	125
ATAD3 pathological spectrum: genotype-phenotype correlates and diagnosis	127
OXPHOS <i>in vivo</i> and in cell models of ATAD3 disease.....	133
ATAD3 mitochondrial DNA and nucleoids	136
ATAD3 and cholesterol	137

Autophagy and lysosomes in relationship to cholesterol in the ATAD3 mutants	141
Modulation of cholesterol and lipid metabolism: mechanistic insights and future therapies for ATAD3 disease	145
<i>Sphingolipids</i>	149
ATAD3 antibodies	150
Approach to other diseases.....	152
Conclusions	153
Bibliography	156
Appendix	173
Publications during the PhD	174

Abbreviations

2DG	2-deoxyglucose
ABC	ATP-binding cassette
ABCA1	ATP Binding Cassette Subfamily A Member 1
ABCG1	ATP Binding Cassette Subfamily G Member 1
ACAT	Acyl CoA cholesterol acyltransferase
ADP	Adenosine diphosphate
AMP	Adenosine monophosphate
AMPK	AMP activated protein kinase
ATAD3	ATPase family AAA domain-containing protein 3
ATG	Autophagy-related proteins
ATG12	Autophagy related protein 12
ATG16	Autophagy related protein 16
ATG4	Autophagy related protein 4
ATGL	Adipose triglyceride lipase
Atglis	Atglistatin
ATP	Adenosine triphosphate
BiP	Binding immunoglobulin protein
BNE	Blue native electrophoresis
BrdU	Bromodeoxyuridine
CES1	Carboxylestersase 1
CLQ	Chloroquine
CNV	Copy number variant
COX II	Cyclooxygenase II
COX IV	Cyclooxygenase IV
CPT2	Carnitine Palmitoyltransferase 2
CYP11A1	Cytochrome P450 Family 11 Subfamily A Member 1
dbSNP	Single Nucleotide Polimosphism database
DDD	Deciphering Developmental Disorders
DFCP1	Double FYVE-containing protein 1
DNA	Deoxyribonucleic acid
DTT	Dithiothreitol
EEA1	Early Endosome Antigen 1
ER	Endoplasmic reticulum
ETC	Electron transport chain
FADH2	Flavin adenine dinucleotide

FBS	Fetal bovine serum
GABARAPs	Gamma aminobutyric acid receptor associated proteins
GFP	Green fluorescent protein
GRP78	Glucose regulated protein-78
GRSF1	G-Rich RNA sequence binding factor 1
GSEA	Gene set enrichment analysis
GTP	Guanosine triphosphate
H&E	Hematoxylin and eosin
HC	Homocysteine
HDL	High-density lipoproteins
HMG-CoA	3-hydroxy-3-methylglutaryl-CoA reductase
HSP60	Heat shock protein 60
ICC	Immunocytochemistry
IMM	Inner mitochondrial membrane
IMS	Intermembrane space
ISG	Interferon-stimulated gene
ISO	Isoproterenol
kb	kilobase
kDa	kilodalton
LAL	Lysosomal acid lipase
LAMP1	Lysosomal membrane protein
LC3	Microtubule-associated protein 1A/1B-light chain 3
LDL	Low-density lipoprotein
LHON	Leber's hereditary optic neuropathy
MAM	Mitochondria-associated membrane
MCP1	Monocyte chemoattractant protein 1
MEF	Mouse embryonic fibroblast
MELAS	Mitochondrial encephalomyopathy, lactic acidosis and stroke-like episodes
MPV17	Mitochondrial inner membrane protein 17
MRI	Magnetic Resonance Imaging
mtDNA	Mitochondrial DNA
mTOR	Mammalian target of rapamycin
NADH	Nicotinamide adenine dinucleotide
NAFLD	Non-alcoholic fatty liver disease

NAHR	Nonallelic homologous recombination
NCR	Non-coding region
nDNA	Nuclear DNA
NDUFB9	NADH:Ubiquinone oxidoreductase subunit B9
NDUSF4	Hereditary spastic paraplegia
NDUSF4	NADH:ubiquinone oxidoreductase subunit S4
NGS	Next generation sequencing
NIDDM	Non-insulin dependent diabetes
NPC	Niemann-Pick type C
NPC1	NPC Intracellular Cholesterol Transporter 1
OCR	Oxygen consumption rate
OMM	Outer mitochondrial membrane
OSC	3-oxidosqualene: lanosterol cyclase
OXPHOS	Oxidative phosphorylation
PBS	Phosphate-buffered saline
PCR	Polymerase chain reaction
PDHA1	Pyruvate dehydrogenase E1 subunit alpha 1
PE	Phosphatidylethanolamine
PFO	Perfringolysin O
PHRINL	Pontocerebellar hypoplasia, hypotonia, respiratory insufficiency syndrome, neonatal lethal
PKC	Protein kinase C
POLG	Polymerase gamma
POLRMT	Mitochondrial RNA polymerase
PPA1	Potential patient ATAD 1
PPA2	Potential patient ATAD 2
Rapa	Rapamycin
RIPA	Radioimmunoprecipitation assay buffer
RNA	Ribonucleic acid
RNAi	RNA interference
Ro	Ro 48-8071
Rot	Rotenone
RRF	Ragged-red fibers
rRNA	Ribosomal RNA
RT	Room temperature

RT-qPCR	Reverse transcription quantitative polymerase chain reaction
S1P	Sphingosine-1-phosphate
SDHA	succinate dehydrogenase subunit A
SDS-PAGE	Sodium dodecyl sulfate polyacrylamide gel electrophoresis
Sdz	Sandoz-58035
SERAC1	Serine active site containing 1
SOAT1	Sterol O-Acyltransferase 1
SPG15	Spastic paraplegia type 15
SPG7	Spastic paraplegia type 7
SPTLC	Serine palmitoyltransferase, long chain
SQSTM	Sequestosome 1
SR-BI	Scavenger receptor class B, type I
SREBP	Sterol regulatory element-binding protein
SREBP2	Sterol regulatory element-binding protein 2
StAR /STARD1	Steroidogenic acute regulatory protein
SURF1	cytochrome c oxidase assembly factor
TBS	Tris buffered saline
TCA	Tricarboxylic acid
TEFM	Mitochondrial transcription elongation factor
TEM	Transmission Electron Microscopy
TFAM	Mitochondrial transcription factor A
TFEB	Transcription Factor EB
TMS	Transmembrane segment
TOMM20	Translocase of outer mitochondrial membrane 20
tRNA	Transfer RNA
TSPO	Translocator protein
U18	U18666A
UAS	Upstream activation
VDAC	Voltage-dependent anion channel
WIPI	WD-repeat protein Interacting with phosphoinositides

General introduction

Mitochondria

Mitochondria are bacterium-sized organelles found in all nucleated eukaryotic cells. They are best known for energy production as they generate more than 90% of the cellular energy. As such they are known as the “powerhouses” of the cell. Notwithstanding this, mitochondria participate in many other cellular processes, such as amino acid, nucleotide and fatty acid metabolism, iron-sulfur cluster biogenesis, ion homeostasis, and the exclusive biosynthesis of some lipids, quinones, steroids and urea (Calvo & Mootha, 2010; Roger et al., 2017).

Across the vast heterogeneity in the eukarya domain, many organisms have achieved ecological specialization, that mainly differ on the way and amount of producing ATP and the end-products they generate (Martin & Mentel, 2010). Although, five major groups have been identified: aerobic mitochondria, anaerobic mitochondria, hydrogen-producing mitochondria, hydrogenosomes, and mitosomes, recent discoveries suggest that these organelles represent a functional continuum rather than a discrete set of classes (Roger et al., 2017). Few examples of eukaryotes that have lost mitochondria show us that, once again, every rule in biology has its exceptions and amitochondrial eukaryotes also do exist (Karnkowska et al., 2016).

Despite the diversity of mitochondria in current species, they all derive from a common ancestral organelle that originated from the integration of an endosymbiotic alphaproteobacterium into a host cell related to Asgard Archaea about 1.45 billion years ago (Roger et al., 2017; Wei et al., 2022). How and when this occurred is to date a matter of discussion, although two principal hypotheses can be distinguished: "mitochondria-early" hypotheses suggest that the mitochondrial symbiosis was among the first events in eukaryogenesis while "mitochondria-late" hypotheses hold that the mitochondrial symbiosis occurred after many other features of modern eukaryotes had already evolved (Roger et al., 2017). Regardless of how these initial stages played out, the transition from endosymbiotic bacterium to permanent organelle involved a massive number of evolutionary changes that occurred incrementally, until the integration of both cells was achieved. A key feature in achieving that was the origin of the mitochondrial protein import apparatus, which allowed host and symbiont compartments to mix genes and proteomes (Roger et al., 2017). In fact, it has been demonstrated that higher-order organisms have

progressively smaller mitochondrial genomes, which matches the observations that the translocation of mitochondrial genes to the nucleus is an ongoing process, alike the endosymbiosis that began billions of years back (Wei et al., 2022). The implications of these incursions need to be studied as they can potentially disrupt nuclear genes and cause disease (Turner et al., 2003; Wei et al., 2022).

Mitochondria are highly dynamic structures that are constantly changing their morphology according to the cellular needs and nutrient availability (Wai & Langer, 2016). Thus, despite the classical image of a rounded-shape mitochondria, the reality is that the continuous fission (or division) and fusion events with the involvement of many dynamin-related GTPases, the endoplasmic reticulum and microtubules, among others, rather form a tubular mitochondrial network that expands throughout the cytoplasm and interacts with different organelles (Lackner, 2014).

Internal cellular membranes are a feature of eukaryotic cells that enable compartmentalization, which allows unfettered specialization. Membranes themselves also serve as organizing centers, aided by numerous macromolecules that create microdomains where specific proteins attach, producing distinct functional spaces that augment cell capacity (Alberts et al., 2002). An exemplar is the mitochondria, which comprises an outer (OMM) and inner (IMM) mitochondrial membrane, whose interior is called the matrix, while the zone between the membranes is known as the intermembrane space (IMS). A characteristic of mitochondria is that the IMM is highly selective, not even small ions can pass without the aid of specific membrane-embedded transport proteins (Kühlbrandt, 2015). Consequently, an electrochemical gradient can be generated, across the IMM, but not the OMM (Fig. 11). The IMM is also distinguished by its deep invaginations into the matrix, called cristae; these enable a large surface area to be compressed in a small space (Kühlbrandt, 2015). These structural features and properties speak to the reason of existence of mitochondria: energy production.

Mitochondrial energy production

The primary role of mitochondria is considered to be the generation of cellular energy through the oxidative phosphorylation (OXPHOS) process. The OXPHOS system includes four of the five multi-subunit complexes that sequentially transfer electrons obtained from the tri-carboxylic acid (TCA) cycle and fatty acid oxidation. The

electron transport chain (ETC), located in the IMM, comprises four multisubunit complexes that receive electrons from reduced nicotinamide adenine dinucleotide (NADH) and flavin adenine dinucleotide (FADH₂). The transfer of electrons to compounds with higher oxidative potential is exergonic, releasing energy at each step. As the electrons reach the last step of the ETC, they react with oxygen (O₂) to produce water (H₂O). The energy produced is used to pump protons (H⁺) from the matrix to the IMS, resulting in a membrane potential of around 120-180 mV. The proton gradient is used by the ATP synthase or complex V to convert adenosine diphosphate (ADP) and inorganic phosphate into adenosine triphosphate (ATP), the cell's energy currency (Fig I1).

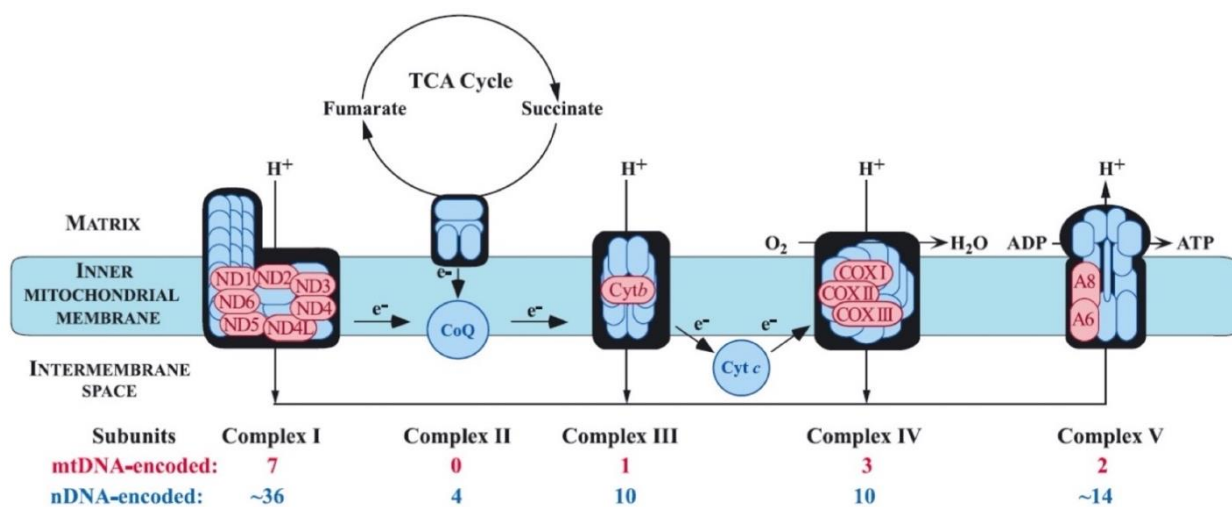


Figure I1. Schematic of the OXPHOS complexes and their component subunits. Multimeric protein complexes I–IV shuttle electrons along the respiratory chain, facilitated by the reduction of the cofactors coenzyme Q10 (Q) and cytochrome c (cyt c). Electron transfer is coupled to the transfer of protons (H⁺) across the inner mitochondrial membrane to generate a proton motive force, which is used by complex V (ATP synthase) to synthesize ATP. Seven subunits are part of complex I (ND1, ND2, ND3, ND4, ND4L, ND5, ND6), one belongs to complex III (cytochrome b), three to complex IV (COX1, COX2, COX3) and two are part of complex V (ATP6, ATP8). (From: Di Mauro, 2004).

The mitochondrial genome

Mitochondria are the only extra nuclear organelle in animals that have their own genome, mitochondrial DNA (mtDNA). The human mtDNA is a circular double stranded molecule of 16.5 kb and it encodes for 37 genes. 13 are protein encoding genes, while the remainder encode all the RNA elements required for the translation

of the protein-encoding transcripts, two ribosomal (rRNA) and 22 transfer (tRNA) RNAs (see translation below). The genetic information is unevenly distributed between the two DNA strands, with the heavy (H) -strand containing the majority of the genetic information, while the light (L) -strand encodes a single protein and eight transfer RNAs (Clayton, 1982). The genetic organization of mtDNA is remarkably efficient as, unlike nuclear DNA (nDNA), it has no introns and only one substantial non-coding region (NCR). The NCR contains essential *cis*-elements for replication and expression, including three promoters and two origins of replication (O_H and O_L), and many mtDNA contain a third strand of nucleic acid in the NCR (Fig. I2).

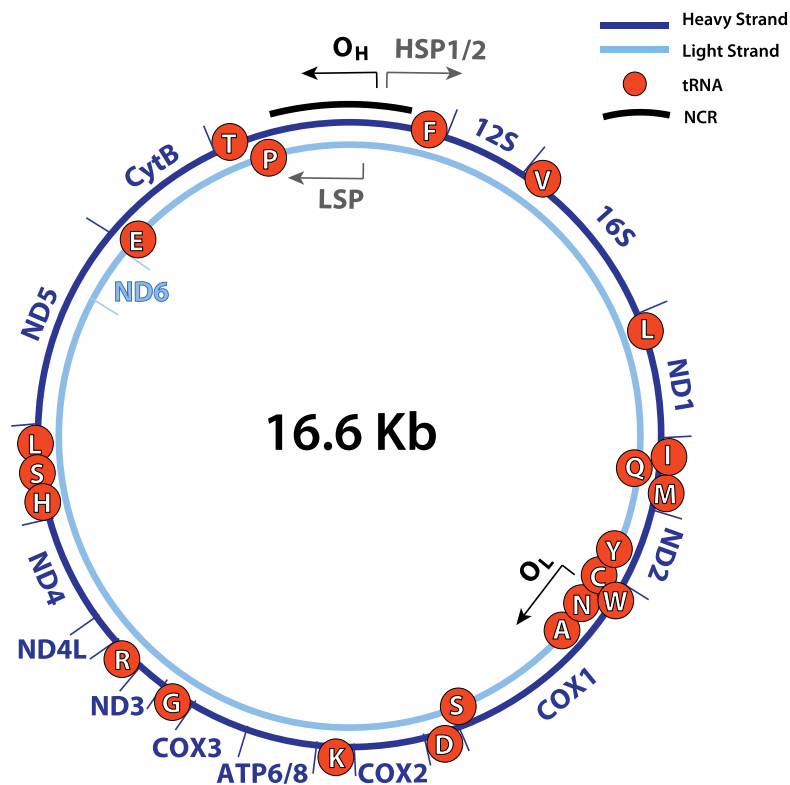


Figure I2. The human mitochondrial DNA genome. The 16.6Kb mtDNA encodes for 37 genes, including 22 tRNA (one letter code), 2 rRNA and 13 proteins part of the respiratory chain complexes. The NCR region contains regulatory elements. The origins of replication of the heavy (O_H) and light (O_L) strands and transcription promoters (HSP1-2, LSP) are also shown.

The same way cells have numerous mitochondria, each mitochondria have several copies of mtDNA molecules. Anywhere between 10% and 65% of mammalian mtDNA molecules contain a region of triple-stranded DNA, termed the mitochondrial displacement or D-loop (Kasamatsu et al., 1971). The D-loop maps to the NCR, and the third strand is commonly referred to as 7S DNA, based on its sedimentation properties. Of equal, or greater, abundance is the more recently discovered mitochondrial R-loop that also maps to the NCR and is formed of a 400-800

nucleotides of RNA, and is the complement of 7S DNA (Akman et al., 2016). Neither species is well understood, as they potentially have many roles in regulating mtDNA metabolism, including regulating the type of mechanism of replication and maintaining the balance between replication and transcription (Holt et al. 2019). The mitochondrial R-loop is also implicated in mtDNA segregation (Akman et al., 2016) and may be important for membrane attachment (Holt et al., 2019).

Like most DNA molecules, in its native state human mtDNA is tightly supercoiled. Supercoiling is regulated by topoisomerases (Kolesar et al., 2013); to date only TOP1mt and TOP3 alpha have been unequivocally linked to mtDNA metabolism. TOP3 alpha is the replicative mitochondrial topoisomerase, and mutations in the gene cause archetypal mtDNA disease (Nicholls et al., 2018). The role of TOP1mt is less clear, although it appears to affect mitochondrial protein synthesis and produces a clear footprint in the D-loop/R-loop region of the mitochondrial genome (Dalla Rosa et al., 2016).

One of the starkest differences between nuclear and mitochondrial DNA is the mode of transmission, with the latter being strictly maternally inherited. Shortly after fertilization, paternal mitochondria are selectively destroyed together with their mtDNA, thereby preventing transmission to the zygote, consequently the offspring inherit only the maternal mtDNA (Al Rawi et al., 2011). Maternal transmission of disease, as opposed to Mendelian, can therefore highlight the relevant genome (see pathogenic mtDNA mutations).

Replication, transcription and translation

Although conventional replication intermediates (RIs) similar to those found in the nucleus are detected in mitochondria (Holt et al. 2000), another distinguishing feature of mammalian mtDNA is that the majority of the time it has a highly unorthodox mechanism of replication. There are two competing hypotheses, which both agree that there is frequently a long delay between the initiation of leading and lagging strand DNA synthesis. In the strand displacement model (SDM), the displaced lagging strand template is coated with single-stranded binding protein (mtSSB), whereas in the transcript-dependent replication mechanism (TDM) the displaced strand is hybridized to mitochondrial transcripts (Reyes et al., 2013; Clayton, 1982). A major weakness of SDM is that short single-stranded regions are recognized to be

fragile sites in nuclear DNA replication despite their fleeting existence. SDM accentuates this hazard a thousand-fold, whereas TDM reduces the risk of breaks. Another theoretical advantage of TDM is that single-strand breaks in the displaced lagging-strand will be much easier to repair, and to repair faithfully (Holt & Jacobs, 2014).

Less controversy surrounds the core protein machinery of mtDNA replication, although it is in many ways quite remarkable. Three major enzymes are of bacteriophage origin, POLG (the mitochondrial DNA polymerase), POLRMT (the mitochondrial DNA polymerase) and Twinkle (the mitochondrial DNA helicase). Each is essential for mtDNA replication and each causes early embryonic lethality if ablated, and mutations in all three have been linked to human mtDNA disorders (Copeland, 2008). POLRMT is the core enzyme that synthesizes the two polycistronic transcripts from mtDNA from promoters within or at the periphery of the NCR. Although POLRMT can synthesize RNA on a single-stranded template without aid, the initiation of transcription on duplex DNA requires the melting action of mitochondrial transcription factor B2 (TFB2M) that is a site-specific binding protein, which determines the promoter sites. POLG depends on an accessory subunit POLG2 to synthesize long tracts of DNA (Carrodeguas et al., 2001), while mitochondrial transcription elongation factor (TEFM) serves the equivalent function for POLRMT (Minczuk et al., 2011). The clear implication is that TFB2M and TEFM play pivotal roles in determining whether POLRMT mediates RNA synthesis for replication or polycistronic transcription for protein production.

The 12S and 16S rRNA of the mitochondrial ribosome, together with tRNA-Val, are assembled with imported mitochondrial ribosomal proteins of the 39S mitochondrial large subunit and of the 28S small subunit, thus initiating the first steps of ribosome assembly (Richter-Dennerlein et al., 2016). Like the cytosolic ribosomes, mitochondrial ribosomes (mitoribosomes) are composed of a large and small subunit, but are characteristically more protein rich (and thus have an unusually low RNA content) compared to other ribosomal structures (Rorbach et al., 2016). Translation of the mitochondrial transcripts initiates with the mRNA binding to the 28S complex. Translation elongation then proceeds by cycles of aminoacyl-tRNAs binding, peptide bond formation, and displacement of deacylated tRNAs. The small ribosomal subunit is assembled at the mitochondrial nucleoid (He et al. 2012).

The 13 proteins products of the mtDNA are core components of the OXPHOS system. While the seven of complex I are numerically a minority they form the central core of the membrane embedded portion of the enzyme that translocates protons across the IMM, and without which the enzyme cannot be assembled let alone function (Tang et al., 2020). The three subunits of complex IV include the two catalytic subunits, and the single subunit of complex III is essential for its function. ATP subunit 6 (ATP6) controls proton re-entry for ATP synthesis, it is less clear, but still likely that the absence of the thirteenth protein, ATP subunit 8 (ATP8), is also needed for ATP production. The rest of the OXPHOS apparatus (80 or so proteins), and the hundreds of proteins required for the maintenance and expression of the mtDNA, along with over a thousand other mitochondrial components, are encoded in the nuclear genome and must be imported into the mitochondria after synthesis on cytosolic ribosomes (Tang et al., 2020).

The mitochondrial nucleoids

Despite once was believed mtDNA floats freely in the mitochondrial matrix, unprotected and prone to be damaged, because unlike nDNA it lacks histones to compact and protect it, we now know mtDNA is organized into multi-molecular clusters called nucleoids that are considered the unit of mtDNA inheritance (Bonekamp and Larsson, 2018) and are tightly bound to the mitochondrial inner membrane (IMM). On average, a primary fibroblast contains around 1800 nucleoids, although this can vary depending on cell cycle and metabolic activity (Bonekamp and Larsson, 2018). The number of mtDNA molecules per nucleoid is also tissue-specific and variable according to the bioenergetic needs of the cell, ranging over three orders of magnitude and is dependent on the physical separation of daughter mtDNAs called segregation (Clay Montier et al., 2009). Cancer cells can have 2-10 molecules per nucleoid (Iborra et al., 2004) while most primary fibroblast have a single copy of mtDNA (Kukat et al., 2011). Among the proteins that interact with mtDNA is the mitochondrial DNA polymerase γ (POLG), which associates with mtDNA transiently during mtDNA synthesis, while others like the mitochondrial DNA helicase Twinkle have a more prolonged interaction with the mitochondrial genome (Holt *et al.*, 2007; Bogenhagen et al., 2008; Gerhold et al., 2015). The mitochondrial transcription factor A (TFAM) is of particular importance, as it packages and protects the mtDNA from damage, while also regulating mtDNA expression and replication (Garstka *et al.*, 2003; Kang, Kim and Hamasaki, 2007). Additionally, studies have

suggested an intimate association between nucleoids and the mitochondrial translation machinery (He *et al.*, 2012). The number and organization of nucleoids are critical factors for the maintenance, expression, inheritance, and segregation of mtDNA within the cell.

Mitochondrial diseases

Mitochondrial diseases are among the most complex, but most common, of genetic diseases because they involve both nuclear and mitochondrial genomes and can be inherited or *de novo*; producing an immense heterogenic group, that ranges from a single affected tissue to several dysfunctional organs to multisystemic presentations. Patients with clinical onset in childhood often show severe and progressive presentations with nuclear gene disorders, while adult onset mitochondrial diseases usually include both nuclear and mitochondrial gene defects with predominantly mtDNA mutations (Lightowlers *et al.*, 2015). Despite the huge clinical variation, there are some consistent biochemical and morphological characteristics. One such feature is respiratory chain deficiency, which results in reduced enzymatic function of one or more OXPHOS complexes, leading to a simultaneous decrease in cellular oxygen consumption and ATP synthesis. Thus, the so-called primary mitochondrial disorders encompass a clinically heterogeneous group of diseases that arise as a result of dysfunction of the respiratory chain (Chinnery, 2021). Additionally, patients often show elevated levels of resting lactic acid in both their blood and cerebrospinal fluid. Histological examination of skeletal muscle sections can provide evidence of mitochondrial pathology. Basic muscle morphology can be assessed using hematoxylin and eosin (H&E), while the modified Gomori trichrome stain highlights connective tissue (light blue), muscle fibers (blue), and mitochondria (red), allowing the detection of ragged-red fibers (RRFs), which are characterized by a 'fiber cracking' appearance and abnormal subsarcolemmal proliferation of mitochondria (Fig. I3) (DiMauro, 2004). Although, RRFs have been a characteristic histopathological feature of mitochondrial disorders, hugely used for diagnostic purposes, as they have also been seen with normal aging and other muscle conditions (Greaves *et al.*, 2014 & Vincent *et al.*, 2016). Therefore, sequential COX/SDH histochemistry has been used to assess mitochondrial respiratory chain function in muscle cryosections, which measures the activities of complex IV (COX) and complex II (SDH)(Fig. I3) (Alston *et al.*, 2017). However, other OXPHOS complexes are not considered with this technique, such as complex I, which is the

largest and most commonly affected OXPHOS complex in mitochondrial disorders (von Kleist-Retzow et al., 1998). As a result, a high-throughput immunofluorescence assay has been developed to quantify the two most commonly affected OXPHOS components, namely complexes I and IV, along with a mitochondrial mass marker (porin) in individual muscle fibers on a single 10- μ m tissue section. Labelling laminin to define fiber boundaries facilitates the semi-automatic quantification of a large number of muscle fibers, and can be combined with the analysis of intensity, to increase accuracy (Fig. I3) (Alston et al., 2017). Overall, these features serve as important diagnostic markers for mitochondrial disorders.

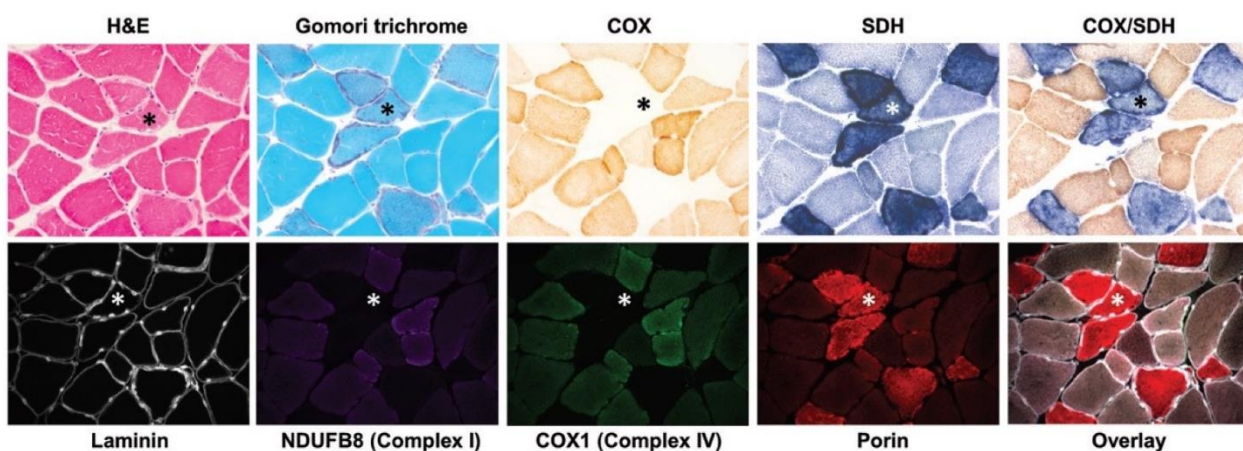


Figure I3. Histological and immunohistochemical examinations of mitochondrial pathology in primary mtDNA-related disease. Serial skeletal muscle (vastus lateralis) sections from a patient with a single, large-scale mtDNA deletion were stained with H&E and modified Gomori trichrome to assess basic muscle morphology and the presence of RRFs, respectively. The individual COX, SDH and sequential COX/SDH histochemical reactions show fibres manifesting mitochondrial accumulation and focal COX deficiency. Immunofluorescence assay that can quantify the levels of complex I (NDUFB8 subunit), complex IV (COX1 subunit), laminin, and a mitochondrial mass marker (porin), all within a single 10- μ m section. A highlighted COX-deficient fibre (*) shows focal accumulation of sarcolemmal mitochondria around the periphery of the fibre, and downregulated expression of both complex I and IV proteins (From Alston et al., 2017).

Pathogenic mtDNA mutations

The existence of transmissible traits in the cytoplasm was recognized in the early decades of the last century, and mutant mtDNAs in yeasts that result in respiratory deficiency were reported in the 1960s, the same decade that mtDNA was first visualized in human cells. In the 1980s, complex recombination events in plant mtDNA that yield toxic fusion proteins were identified as the cause of a tissue-specific mitochondrial disorder known as cytoplasmic male sterility. Many researchers

doubted that the findings from yeast and plant mtDNA were relevant to human conditions. On the other hand, as far back as 1971 maternal transmission of a rare cause of blindness, Leber's hereditary optic neuropathy (LHON) was recognized and in 1985, a large pedigree with a well-defined clinical syndrome, called MERRF, was reported to display strict maternal transmission (Rosing et al., 1985). However, it was not until early 1988, that pathogenic changes in mtDNA were first linked to human disease, when mtDNA deletions were found in many patients with mitochondrial myopathies; and at the end of the same year the first pathological point mutation in mtDNA was recorded, in patients with LHON (Holt et al., 1988; Wallace et al., 1988). Since, over 270 mutations have been identified, affecting every mitochondrial gene (Alston et al., 2017). The majority of these mutations involve either point mutations or large-scale rearrangements of the DNA (deletions and duplications) that directly impact OXPHOS function. Unique features of mtDNA-related disorders arise from key differences between mitochondrial and nuclear genetics. Firstly, mtDNA is maternally inherited and does not follow the classic Mendelian pattern, as paternal mtDNA is degraded after fertilization (Al Rawi et al., 2011). Secondly, while most nuclear genes have two alleles, the many mtDNA copies in the cells mean there are hundreds or thousands of copies of a certain mtDNA encoded gene.

The majority of mtDNA mutations are found in tRNA genes, even though they only represent about 10% of the mitochondrial genome's coding capacity. In contrast, mutations in protein-coding genes, which account for almost 70% of the genome, are less common (less than half of the cases). Mutations in the two rRNA genes are the rarest, accounting for only about 2% (Schon et al., 2012). This uneven distribution of mutation sites can be explained by the fact that tRNAs are more mobile than proteins and rRNAs and from an evolutionary perspective, there may be greater pressure to conserve proteins and rRNA sequences resulting in a higher tolerance for mutations affecting tRNA molecules. The most common pathological mtDNA mutation is m.3243A>G substitution in the *tRNA^{Leu}(UUR)* gene that can cause Mitochondrial Encephalomyopathy, Lactic Acidosis and Stroke-like episodes (MELAS) (Goto et al., 1990) or a combination of type II diabetes and deafness (NIDDM) (van den Ouweland et al., 1992).

Although the prevalence of mtDNA-related diseases is about 1 in 10,000, the frequency of the ten most common pathogenic mtDNA mutations is much higher, about 1 in 200, which indicates that many non-affected individuals carry sub-clinical

levels of potentially pathogenic mutant molecules (Chinnery et al., 2012). The explanation of this is that deleterious mutations are often heteroplasmic, meaning they affect some but not all copies of mtDNA. The clinical phenotype usually depends on the proportion of normal and mutant mtDNAs. Thus, heteroplasmic mtDNA mutations are considered recessive, only manifesting as a clinical phenotype when the mutant load exceeds approximately 70%, though this varies depending on the mutation, cell type, and tissue (Rossignol *et al.*, 2003). Other factors that influence the variable penetrance observed in mtDNA diseases are environmental toxins or epigenetic factors, for instance (Chinnery et al., 2012). Few exceptions to this general phenomena have been reported, such as a mutation in a tRNA that produced a multisystemic disorder and respiratory chain impairment despite the level of mutant mtDNA being lower than 25% (Sacconi *et al.*, 2008).

The first epidemiological nationwide study made in Spain estimated that from 2014 to 2020 the average incidence of mitochondrial diseases, both nDNA and mtDNA encoded, was of 1 in 500,000, while it was higher in children, about 1 in 100,000 (Bellusci et al., 2021). It is interesting to note that in the pediatric group nDNA mutations that affected mitochondria were much more prevalent than mtDNA mutations, but overall, mutations in mtDNA that accounted for mitochondrial disease were more abundant than those in nDNA (probably because the latter are harder to identify) (Bellusci et al., 2021). The most abundant type of mtDNA mutation were large-scale deletions (more than a third), while the most frequently mutated genes were *MT-RNR1* m.1555A>G in mtDNA and *TK2* in nDNA. For the relevance of this thesis, it is worth-mentioning that, according to this study, only 4 ATAD3A cases, all of them pediatric, were reported in the time between 1990 and 2020 in Spain (of 2761 total patients or 1105 in the nDNA group) (Bellusci et al., 2021).

ATAD3

ATAD3 is a member of the AAA+ protein family (ATPases associated with various cellular activities), a large group of proteins that are able to induce conformational changes in other various proteins and are characterized by the common structurally conserved ATPase domain. It is typical of these proteins to form oligomers at the C-terminal, usually hexamers, where the ATPase domain is located, and this is thought to be their biologically active form (Hanson & Whiteheart, 2005).

ATAD3 genes are conserved in multicellular organisms, but absent in unicellular organisms, including yeast (Gilquin et al., 2010). *ATAD3* is unique to higher eukaryotic organisms such as plants, nematodes, insects, and primates. No ortholog of this gene has been found in prokaryotic organisms, and although a far ortholog is present in protists and yeast, its characteristic domain is absent in *ATAD3* (Li & Rousseau, 2012). While haploid genomes typically contain only one copy of *ATAD3*, whole-gene duplication events have led to the presence of 3 copies in primates (*ATAD3A*, *B* and *C*) and up to 4 homologs have been reported, each located in a different chromosome, in some seed plants such as *Arabidopsis thaliana* with 35% identity and 52% similarity between the human *ATAD3A* and *A. thaliana*'s *ATAD3A1* (Kim et al., 2021).

In human, *ATAD3* gene-family is located in tandem on chromosome 1 at the 1p36.33 locus. Evidence of the homology of the 3 *ATAD3* genes is the high similarities between them. Both *ATAD3A* and *ATAD3B* contain 16 exons with slight variation in intron length and their protein sequences share a 93% identity, the most significant difference being the last exon of *ATAD3B*, which lacks the original stop codon and thus results in the extension of 62 aa, producing a protein of 648 aa and about 72 kDa (Gilquin et al., 2010). The addition of this aa sequence houses several potential phosphorylation sites and a putative transmembrane sequence. Another important difference is that the promoter of *ATAD3B* contains all the regulatory elements found in the promoter of *ATAD3A* plus two Myc-binding domains, five Pit1 binding domains, and a myogenin binding domain. The transcription factors that bind to these last two regulatory elements have been reported to express during embryogenesis, which could explain the limited expression of *ATAD3B* to tissues with high proliferative potential (embryonic and germinal areas), in comparison to the ubiquitously expressed *ATAD3A* (Schaffrik et al., 2006; Hubstenberger et al., 2008; Merle et al., 2012). Additionally, under certain conditions, *ATAD3B* has been observed to incorporate into *ATAD3A* homo-oligomers, forming *ATAD3A* and *ATAD3B* hetero-oligomers and modifying the C-terminal environment that has been shown to interact with nucleoid proteins like HSP60, and thus affect normal nucleoid function in mitochondria (Merle et al., 2012).

On the other hand, *ATAD3C* only contains the last 12 exons of *ATAD3A* and *ATAD3B* as the first 70 aa of *ATAD3A* are not translated in *ATAD3C* due to a mutation in the translational initiation site, resulting in initiation downstream. *ATAD3C* also differs in

the last exon, which produces a truncated C-terminal (Merle et al., 2012). Despite this difference, ATAD3C shares 87% identity with ATAD3A in the rest of its structure, but this difference might be indeed the reason why there is currently no experimental data on the expression of ATAD3C (Li & Rousseau, 2012).

ATAD3A boasts mainly two transcript variants, Q9NVI7 (634 aa, 71 kDa), Q9NVI7-2 (586 aa, 66.5 kDa) with the second isoform being the most predominant. Q9NVI7-2 lost the third exon, maintained in Q9NVI7, which is still conserved in the *Atad3b* of the most distant relative in the Hominidae family, the orangutan, but is absent in the rest of *Atad3b* from the hominids (Merle et al., 2012). Other transcript variants that seem to have a tissue specific expression (572 aa, 64 kDa only detected in adult heart) have been described, as well as some others that could potentially form, though their existence has not been proven yet (201 aa, 23 kDa) (Li et al., 2014). It is important to mention that some authors have reported that the 72 kDa band which would correspond to ATAD3B, could also be a hyper-phosphorylated form of ATAD3A and according to their results the 66.5 kDa canonical isoform would also be phosphorylated and both would be regulated mainly by protein kinase C (PKC) (Fang et al., 2010), though these experiments were conducted on immortalized cancer cell lines (Fang et al., 2010; Li et al., 2014).

The N-terminal domain, corresponding to aa 1-245, locates somewhere near the mitochondrial surface, with critical structural and functional sub-domains. The initial 50 aa, which include a proline-rich region, are an unstructured region, which represent a region in the peptide sequence that lacks a stable tertiary structure but potentially maintains interaction and functionality with many biomolecules (Na et al., 2018), as it has been observed by the removal of this region in other proteins (Ventorim et al., 2018). Similarly, loss of the 50 aa sequence in the ATAD3 N-terminal has been reported to promote ATAD3 pathological oligomerization (at its N-terminal end) and the recruitment and binding with Dynamin-related protein 1 (Drp1) that promotes mitochondrial fission (Zhao et al., 2019). Another important residue has been reported to be the Lys135 which is thought to be acetylated under normal basal conditions, whereas unknown stressed conditions can promote its deacetylation and subsequent oligomerization through the CC domain, leading to aberrant activation of the protein (Zhao et al., 2019). Two coiled-coil regions (CC1, aa 85-115 and CC2, aa 180-220) essential for interaction and oligomerization with other proteins follow the N-terminal (Gilquin et al., 2010). After the CC regions two transmembrane

segments come, transmembrane domain 1 and 2 (TM1, aa 225-242 and TM2, aa 247-264) for the integration of the protein into the OMM and the IMM, respectively, which correspond to the central part of the protein. The information necessary for ATAD3 targeting to mitochondria has been shown to be in these domains plus in the contiguous auxiliary import region (AIR, aa 280-290). On the other end, the C-terminal harbors the conserved and characteristic ATPase domain with the canonical Walker A (WA) and Walker B (WB) motifs, responsible for the binding and hydrolysis of the ATP, respectively. Several studies have demonstrated that ATP-binding is more relevant for some biological activities than ATP-hydrolysis, as evidenced by the dominant-negative behavior of the binding-deficient mutants but not hydrolysis-deficient ones (Gilquin et al., 2010). Besides, a common proteolytic domain conserved in other AAA+ ATPases (AFG3L2 or SPG7) has not been found in ATAD3A (Gerdes et al., 2012; Cooper et al., 2017; Baudier et al., 2017).

The exact sub-mitochondrial localization and positioning of ATAD3A has been an area of study itself for many research groups. The current version of the topic is that ATAD3A is a transmembrane protein whose C-terminal faces the matrix and crossing the IMM spans to the outer part of mitochondria, where the N-terminal is located. The C-terminal is in contact with the nucleoid (Ishihara et al., 2022) (referring to the nucleoid as mtDNA and the many proteins that interact with it permanently and transiently), nonetheless, it has not been fully elucidated whether there is a direct binding to mtDNA, as it could be through nucleoid-protein interaction (Bogenhagen et al., 2007; Gilquin et al., 2010). In the N-terminal, as well, it is not fully clear whether the N-terminal crosses the OMM and it is exposed to the cytosol or it stays under the protection of the OMM, in the IMS, but the presence of the two transmembrane domains (TM1 and TM2) suggest that ATAD3A crosses both membranes (Hubstenberger et al., 2010; Gilquin et al., 2010; Arguello et al., 2021).

ATAD3A has been observed to bound to specialized cholesterol-rich membrane domains with specific properties that facilitate nucleoid binding (Gerhold et al., 2015) distributed in distinct clusters of about 0.5-1 μ M separation through the mitochondrial network (Arguello et al., 2021), evidencing its structural role in membrane architecture. This membrane domains abundant in ATAD3A and cholesterol, also happen to be the regions where the IMM and OMM are most tightly connected, far from the cristae, and in tight connection with the ER, where ER-mitochondria junctions have been observed to be enriched, as well (Issop et al., 2015; Gerhold et

al., 2015; Hung et al., 2017). This enables ATAD3A to interact with ER components and co-participate in the various shared functions assigned to mitochondria and ER, complementing each other, such as the transport of several molecules and nutrients. However, rather than considering it an established structural ER-mitochondrial contact protein, as some have previously suggested (Baudier, 2018 & Scorrano et al., 2019), it is considered to be a transient ER-mitochondrial contact protein, that only binds for specific events or certain conditions (Arguello et al., 2021). For example, the interaction of a group of cytosolic, ER-associated and mitochondria exclusive proteins has been documented, where ATAD3A has been established a key central interactor, that associate under hormone-stimulation to facilitate the import and transfer of cholesterol from the ER, where it is synthesized, to the IMM, where it is metabolized by CYP11A1 as part of the steroidogenic pathways (Rone et al., 2012).

Apart from these structural functions, the oligomerization capacity attributed to members of the AAA+ family has been observed both in the N and C-terminals, with preferential formation of ATAD3A homo-oligomers in the distinct ATAD3A clusters dispersed throughout the mitochondrial network, suggesting the formation of a central channel that could induce conformational changes to other proteins using its ATPase domain (Arguello et al., 2021), as many proteins of the same family do (Hanson & Whiteheart, 2005). When analyzed by blue native electrophoresis (BNE), these oligomers have been seen to range from a predominant 900 kDa complex, that could correspond to a hexameric configuration, to smaller complexes that vary from 900-250 kDa, which would match with smaller oligomers (Goller et al., 2013; Peralta et al., 2019; Frazier et al., 2021).

Different mutations affect different parts of the ATAD3 sequence and, if the variant involves a residue or a region with important functional relevance, like some of the conserved domains, they can influence the protein in many different ways. To mention some: configurational and conformational changes, altered expression, altered oligomerization or affected binding or hydrolysis of ATPs (subsequently reducing its ATPase activity) can lead to disease-related states (Lang et al., 2020).

Hypothesis & Objectives

ATAD3 is a mitochondrial transmembrane protein mutations in which cause a range of multisystemic disorders characterized by neurological impairment. Although its precise function remains unknown, it has multiple interactors both outside and inside mitochondria. Specifically, ATAD3 co-purifies with cholesterol-rich platforms, is involved in the process of importing cholesterol into mitochondria, and cells with *ATAD3* deletions were found to have altered expression of a swathe of cholesterol-related factors and greatly elevated levels of free cholesterol. Thus, cholesterol metabolism is expected to be a fundamental part for ATAD3 protein, and so in ATAD3 disease. Therefore, this dissertation aims to study the molecular disease mechanism of ATAD3 disease with a particular focus on the relationship between ATAD3 and cholesterol metabolism, using both human and fly models.

Hence, the following objectives were proposed to be assessed:

1. To identify and characterize new pathological ATAD3 variants, paying especial attention to the molecular and cellular phenotypes to elucidate the molecular pathophysiology of the disease.
2. To establish laboratory diagnostic tools and markers of ATAD3 disease in based on shared characteristic molecular phenotypes of the different mutant fibroblast lines of the patients.
3. To understand the relation and implication of ATAD3 in the cholesterol metabolism and mitochondrial DNA axis.
4. To create new animal models and strategies in *Drosophila melanogaster* that aid the study of the impact of ATAD3 variants on cholesterol metabolism.
5. To develop pharmacological interventions with especial focus on lipid metabolism that facilitate to comprehend the mechanistic insights in ATAD3 disease, as well as the identification of therapeutic targets and potential drug treatments.

Chapter I: characterization of human primary fibroblast from *ATAD3* mutant patients

Introduction

The landscape of pathogenic *ATAD3* mutations

When studying and referring to different mutations and genetic rearrangements in the *ATAD3* locus, their functional and clinical implications are of special interest, and considering *ATAD3* gene-products will assemble in oligomers to form functional proteins, the proportion of the wild-type allele input to the oligomer is what determines the dysfunction of the protein. As such, for clarity and simplicity, when describing the zygosity of the mutations, we will use the terms monoallelic/biallelic to refer to each of the two alleles for a gene as a whole, rather than the terms homozygous/heterozygous, that refer to a particular mutation in each of the two alleles, and thus, avoid dubious terms such as compound heterozygotes that for the particular case of *ATAD3* are like homozygotes.

In 2016 *ATAD3A* was for the first time associated to mitochondrial dysfunction and disease, and several cases with pathological point mutations and deletions were described with their respective clinical phenotypes (Harel et al., 2016). From a genetic point of view, the cases that have been reported since still fall in those two major groups (point mutants and deletions), which we will talk about in the following lines, and in 2020 duplications within the *ATAD3* locus, low-copy repeats arising by intrachromosomal nonallelic homologous recombination (NAHR) (Carvalho & Lupski, 2016), expanded the genetic variability, that we will unravel in the results section of this thesis (Gunning et al., 2020; Frazier et al., 2021). The clinical symptoms vary depending on the exact mutation and its severity, which complicates the task of grouping and classifying, as will be further disclosed in the succeeding paragraphs. However, and since this thesis is not mainly clinic, I have not been very strict with detailing every clinical symptom and making subtle distinctions, but I rather have followed the criteria in OMIM which distinguishes two main groups of clinical syndromes HAYOS and PHRINL.

In the group of *ATAD3A* point mutants, the first reported mutations in 2016 included a *de novo* monoallelic missense variant in *ATAD3A* (c.1582C>T; p.Arg528Trp) detected in 5 unrelated children that displayed a syndromic neurodevelopmental disorder, which has been denominated Harel-Yoon syndrome (HAYOS, OMIM: 617183) (Harel et al., 2016). One of them also had another monoallelic variant, c.9645G>A, in *ATAD3A* and also presented Klinefelter syndrome. Functional studies conducted on *Drosophila* revealed that expressing the mutation ubiquitously resulted

in lethality. However, when the mutation was expressed specifically in muscles, 90% lethality was observed, accompanied by decreased mitochondrial content, aberrant mitochondrial morphology, and increased autophagic vacuoles. These findings indicate that the mutation functions as a toxic gain-of-function allele, causing a decrease in mitochondria in both neurons and muscle (Harel et al., 2016). Years later, more patients with the same c.1582C>T; p.Arg528Trp variant in *ATAD3A* have been reported with similar clinical symptoms (AlAyed et al., 2020; Lepelley et al., 2021). In the original publication, Harel and colleagues also reported the case of 2 adults from the same family with an inherited biallelic missense variant in *ATAD3A* (c.158C>T; p.Thr53Ile), with distantly related monoallelic unaffected parents, that presented in a milder form and was catalogued as a recessive HAYOS (Harel et al., 2016). The next year another group reported in a family of 2 affected siblings a missense and a nonsense variant that produced a biallelically mutated *ATAD3A* (c.230T>G; p.Leu77Arg and c.634C>T; p.Gln212X) that led to PHRINL and died within the first week of life (Peeters-Scholte et al., 2017). Four more individuals were reported to have the same p.Leu77Arg mutation in one allele and exon three and four deletion in the other, which translated in a milder disease course with yet very similar symptoms (Skopkova et al., 2023). In 2019 another family was identified with unaffected consanguineous parents, 4 affected siblings with PHRINL and 1 unaffected. The affected individuals had a biallelic missense mutation in *ATAD3A* (c.1217T>G; p.Leu406Arg), while the rest only had the variant in one allele (Peralta et al., 2019). The same year, a patient coming from consanguineous unaffected parents was identified with a biallelic missense variant in *ATAD3A* (c.251C>T; p.Thr84Met) that led to a milder form of HAYOS (Al Madhoun et al., 2019). This variant had been previously reported in the Single Nucleotide Polymorphism database (dbSNP) with uncertain clinical significance but it had very low frequency in the population (0.0002), and a significant alleviation of the symptoms was reported by the authors with the implementation of a ketogenic diet treatment (Al Madhoun et al., 2019). Another biallelic variant (c.528+3A>G) in *ATAD3A* was reported with a putative implication in splicing that predicted to produce a premature stop codon which resulted in a 69 amino acids shorter transcript. The patient had unaffected consanguineous parents and she presented some sort of milder HAYOS that started manifesting at 5-8 months after birth, with several ocular phenotypes and progressive cerebral and cerebellar atrophy. Ketogenic diet was tried with this patient with no measurable clinical improvements (Hanes et al., 2020). A patient was reported with

a biallelic missense mutation (c.980G>C; Arg327Pro) that died within months after birth with unknown clinical symptoms. Functional studies of the equivalent mutation in *Drosophila* showed this is a severe loss of function allele that causes neurogenesis defects and developmental lethality (Yap et al., 2021).

Besides the point mutants, Harel and colleagues also identified in a newborn with unrelated parents a maternally inherited 38 kb deletion, that affected ATAD3A in one allele, and a paternally inherited 68 kb deletion, that affected ATAD3A and ATAD3B in the other. This translated into a multisystemic disorder with a characteristic pontocerebellar hypoplasia that was lethal in the first week of life (Harel et al., 2016). In the following years, different research groups reported similar cases. In 2017 biallelic deletions that spanned about 38 kb and produced an ATAD3 A/B fusion gene were identified in 5 newborns from 4 families (2 of them were consanguineous) (Desai et al., 2017). The fusion protein was predicted to be similar to ATAD3A (isoform II) except from 2 missense variants (Ile7Val and Asp73Glu) and its expression which was expected to be reduced as it was under the promotor of *ATAD3B* (Desai et al., 2017). Similar to the patient described by Harel and colleagues, multisystemic failures were diagnosed and pontocerebellar hypoplasia was a common feature. 4 of these newborns deceased in the first week of life and the last one after seven months. Thus, from a clinical point of view, these kinds of cases have been classified under a common umbrella as recessive deletion syndromes or Pontocerebellar hypoplasia, Hypotonia, Respiratory Insufficiency syndrome, Neonatal Lethal (PHRINL) (OMIM: 618810). This study also showed that fibroblasts from two of these patients had altered lipid and cholesterol metabolism with increased and enlarged mtDNA foci as well as aberrant clumped mitochondria (Desai et al., 2017), phenotypes that were confirmed in an *Atad3* muscle conditional knockout mouse (Peralta et al., 2018). Similarly, at the end of the same year, another group reported 4 cases from 3 families, of which 2 had consanguineous parents, with recessive biallelic deletions affecting *ATAD3A* and *ATAD3B*, that presented PHRINL and died within the first week of life (Peeters-Scholte et al., 2017). Later in 2021 two more biallelic deletions were reported, a patient with a 67 kb deletion in one allele including *ATAD3A* and *ATAD3C* and a 38 kb deletion in the other including *ATAD3A* and *ATAD3B*, and the other patient with a biallelic 38 kb deletion in *ATAD3A* and *ATAD3B* (Yap et al., 2021).

There are some cases and mutants that for various reasons do not fit in the aforementioned classification or need specific mention. One would be a combination of two variants in *ATAD3A* that was reported in two siblings from unrelated parents that showed a milder form of HAYOS. One was a missense variant (c.1609T>A; p.Trp537Arg) inherited from the mother while the second was a 15 bp deletion (c.1614+2+16del; p.Gln503Pro fs*11) inherited from the father, meaning it produced an amino acid substitution and a frame shift of 11 nucleotides after the stop codon in the 3'-UTR region (Dorison et al., 2020). Yap and colleagues also reported a patient with a 38 kb deletion in one allele and a missense substitution in the other (c.229C>G; p.Leu77Val). The patient died with two years-old and presented a global developmental delay. Equivalent mutation in *Drosophila* showed this is a partial loss of function allele that produces some locomotion defects as well as accumulation of autophagic intermediates in adult muscles. This missense variant had already been described by Peeters-Scholte and colleagues in combination with a nonsense mutation, as abovementioned. They also reported two siblings presenting PHRINL with a biallelic deletion of exons three and four and a point mutation in one allele (c.150C>G; p.Phe50Leu), which resulted to be a severe loss of function allele in *Drosophila*, and another unrelated patient that showed the same missense variant in one allele but a three nucleotide deletion that results in a non-frameshift amino acid deletion (c.1703-05del; p.Lys568del) that translates in mild hypotonia in the patient, who is not deceased. Three more siblings were reported with a duplication in one allele that produced a frame shift (c.1141dup; p.Val381Glyfs*17) and a missense mutation in the other (c.508C>T; p.Arg170Trp) that presented moderate cognition problems and ataxia but where alive. *Drosophila* corroborated that this missense variant is also a partial loss of function allele (Yap et al., 2021).

There also need to be mentioned *ATAD3* mutants that have been associated to other established diseases, like the first monoallelic missense mutation in *ATAD3A* (c.1064G>A; Gly355Asp) associated to an existing disease, Hereditary Spastic Paraplegia (HSP) found in a mother and her son (Cooper et al., 2017). Neither of the two patients did seem to have any other affected genes related with HSP, and this mutation affected the Walker A motif and thus diminished the ATPase activity, though it was not possible to elucidate whether this mutation was inherited or *de novo* for the mother. Besides the characteristic altered mitochondrial morphology, patient-derived fibroblast and differentiated neurons showed an increased lysosomal mass

and autophagy upregulation (Cooper et al., 2017). A few years later, Lepelley and colleagues added to the variety of neurology-associated ATAD3 phenotypes the observation of up-regulated immune-related type I Interferon (IFN) signaling in four of five previously reported cases. They also reported 2 new patients (a toddler and an adult) where an already described point mutation in *ATAD3A* was found in each (c.1582C>T; p.Arg528Trp and c.1064G>A; p.Gly355Asp) (Lepelley et al., 2021). Besides the ATAD3-associated phenotypes these patients presented persistently elevated type I Interferon-stimulated gene (ISG) expression in blood, as well as systemic sclerosis (Lepelley et al., 2021), both of which are linked and have been associated to errors in the immune system that cause type I interferonopathies (Crow & Manel, 2015; Skaug & Assassi, 2020). This type of studies reinforce the need of studying these diseases with a wider perspective and they evidence the risk of over-classifying genotypes and phenotypes as shown by the c.1064G>A; p.Gly355Asp *ATAD3A* variant reported in two patients with spastic paraparesis, where only one of them had elevated type I IFN expression (Lepelley et al., 2021).

Cholesterol metabolism in the cell

Cholesterol is a lipid that belongs to the sterol subgroup which basically are modified steroids with a hydroxyl group, and thus it is a highly hydrophobic molecule (Luo et al., 2020). However, it is one of a kind molecule because besides the rigid steroid-like four rings, it has the hydroxyl polar group in one end (that intercalates between the polar heads of the phospholipids in membranes) and a flexible isooctyl chain on the other end (that locates in the center of the phospholipid bilayer) (Fig. I4A) (Subczynski et al., 2017). The four-ring structure confers special biophysical properties which increase cohesion and packing of neighboring lipids. Biological membranes acquire distinct regions and domains because of the lipid-lipid, lipid-protein and protein-protein interactions that form in them, and cholesterol is indeed placed close to saturated lipids rather than unsaturated lipids, creating a specialized more rigid region which reduces the fluidity and permeability of the membranes (Subczynski et al., 2017). This is the case of classic lipid rafts that are formed when cholesterol molecules bind to sphingolipids and this attracts certain proteins that create specialized functional membrane regions.

Its distribution also varies among the different parts of the cell. Cholesterol is enriched in the plasma membrane making up about a quarter of its lipids, while the

rest are phospholipids, sphingomyelin and glycolipids. Cholesterol is also abundant in the endosome pathways and part of the Golgi apparatus. On the other hand, the endoplasmic reticulum has low cholesterol amounts (about 1% of total cholesterol).

Cholesterol in mammals can be acquired by *de novo* synthesis (about 70%) or by dietary uptake (about 30%), though it can vary considerably. Dietary cholesterol is basically absorbed by the intestine, processed by the liver and then distributed throughout the body in lipoproteins, usually in the form of low-density lipoproteins (LDLs). At the cell surface, LDL receptor (LDLR) is the main responsible for the uptake of cholesterol via the endocytic pathways of the cell (Fig.14B) (Luo et al., 2020). *De novo* biosynthesis of cholesterol and important processing steps occur in the endoplasmic reticulum from acetyl CoA through the mevalonate pathway until the first sterol is formed: lanosterol. Then several modifications occur until cholesterol is generated, who can be further processed into oxysterols (which makes them more hydrophilic and thus bioactive), cholesteryl esters (which usually are seen as storage cholesterol forms that can account for the principal form of cholesterol in some specialized cells like macrophages, for instance). An important form of cholesterol is the unesterified cholesterol (also called free cholesterol), which is obtained from conversion of lipid-droplet stored cholesteryl esters or from the lipoproteins that enter the cell, and it is the form that is distributed to the different cellular membranes (Fig. 14B). After synthesis cholesterol rapidly exits endoplasmic reticulum (evidenced by the low levels in the ER), where it usually goes to the nearby Golgi tubules, mitochondria or endosomes (Ikonen et al., 2008).

Cholesterol can be transported inside the cells mainly by vesicular and non-vesicular ways. Vesicular ways include endocytic/exocytic pathways aided by the cytoskeleton which transfer cholesterol through different cellular membranes, while non-vesicular ways encompass lipid transfer proteins and direct membrane contacts.

The principal regulators of overall cholesterol metabolism in the cells are the sterol regulatory element binding proteins (SREBPs) and liver X receptors (LXRs), who activate a series of cascades that increase and decrease cholesterol levels, respectively. In the biosynthetic process, a key enzyme is also the ER glycoprotein HMGCR whose catalytic domain in the cytosol converts HMG-CoA to mevalonate, and it is considered to be the rate-limiting step in cholesterol biosynthesis (Luo et al., 2020). Another important regulatory mechanism is the conversion of unesterified to

esterified cholesterol, catalyzed by acyl CoA cholesterol acyltransferase (ACAT, also named sterol O acyltransferase or SOAT). Inversely, when unesterified cholesterol is needed, de-esterification occurs at acid endocytic compartments catalyzed by acid lipases, such as lysosomal acid lipase (LAL) (Fig. I4B). Niemann-Pick type C proteins (NPC) need to be mentioned, as they locate to endosomes, where they are required for the cholesterol recruitment and exit from the endosomal system, being crucial in cholesterol transport and implicated in disease states (Karten et al., 2009).

Most cells cannot catabolize cholesterol, except hepatocytes, adrenal cells and gonadal cells (Luo et al., 2020); thus, they rely on cholesterol efflux for its release outside the cell. To do that, most cells have four ways to transfer free cholesterol to apolipoprotein A-I who will generate high-density lipoproteins (HDLs) that will transport the cholesterol back to the liver where it can go to the bile (and transform into bile acids) or finally be excreted from the body. Those four ways consist of two passive mechanism: aqueous diffusion and scavenger receptor class B, type I (SR-BI) facilitated; and two active mechanisms involving the ATP-binding cassette (ABC) transporters ABCA1 and ABCG1, all of them located in the plasma membrane (Fig. I4B) (Phillips et al., 2014). Mutations in ABCA1, for instance, produce Tangier disease where patients have minimum HDL and apoA-I levels and huge amounts of accumulated cholesteryl esters (Luo et al., 2020).

Mitochondria in relationship to cholesterol has been especially studied in the context of steroidogenesis, where a key step that converts cholesterol to pregnenolone occurs at the inner mitochondrial membrane by CYP11A1. In that process steroidogenic acute regulatory proteins StAR/STARD1 (which belong to the family of StAR-related lipid transfer proteins, START), in the outer mitochondrial membrane, facilitate the transfer of cholesterol to the inner part of mitochondria with the interaction of many mitochondrial and some cytosolic proteins. Some of them are the translocator protein (TSPO), voltage-dependent anion channel (VDAC) or even ATAD3A. The current model is that STARD1 moves cholesterol to the outer mitochondrial membrane, where a distinct cholesterol pool is formed that is more accessible to be transported through TSPO to CYP11A1 at the inner membrane where it can be metabolized. ATAD3A helps bringing the outer and the inner mitochondrial membranes close to each other to facilitate this proposed mechanism (Elustondo et al., 2016).

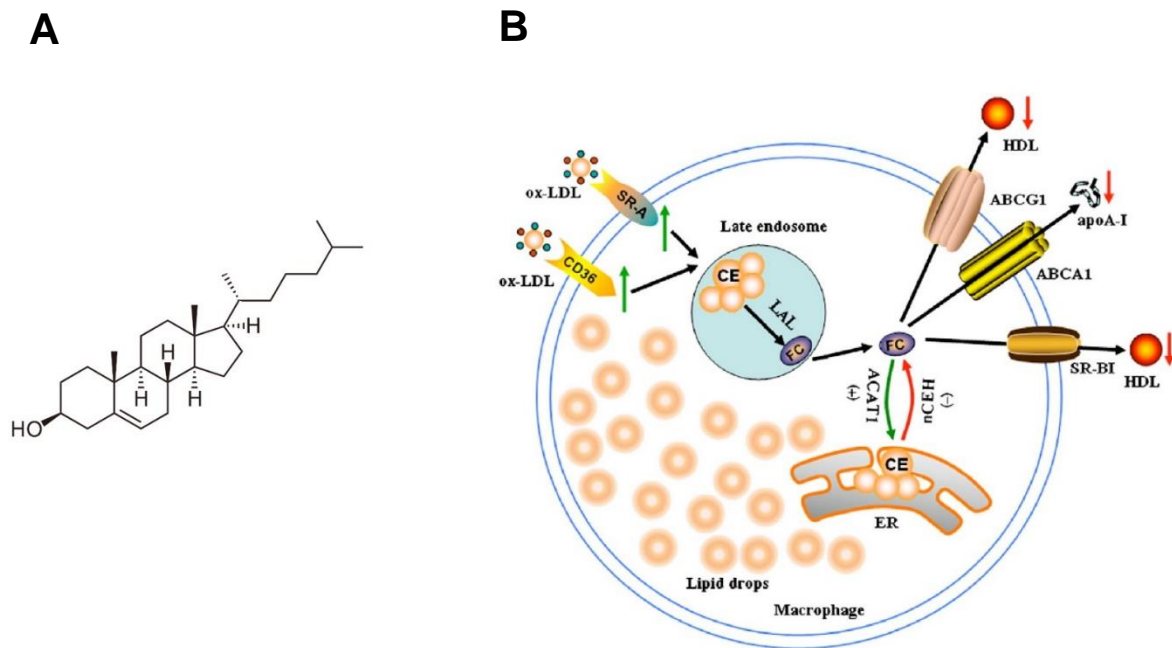


Figure 14. Simplified intracellular cholesterol trafficking pathways. (A) Structure of a cholesterol molecule with its four rings, the hydroxyl group and the isooctyl tail in the other. **(B)** Oxidized-LDL (ox-LDL) enter the cell and contribute to the cholesteryl ester pool in the cell. Cholesterol is found in the cell as cholesteryl esters (CE) or free-cholesterol (FC) and it can be interconverted in either way by different enzymes: ACAT1/SOAT1 converts FC to CE, while CE is converted to FC by nCEH/CES1 or by LAL found in the lysosomes. Free cholesterol is exported from the cell via the plasma membrane transporters ABCG1, ABCA1 and SR-BI which efflux cholesterol into HDLs to the circulation. (From: Luo et al., 2012)

Autophagy and the endolysosomal pathway

Cells rely on a continuous balance between synthesis/biogenesis and degradation/turnover for a correct homeostasis and health. The principal catabolic mechanisms in the cell are ubiquitin-proteasomal degradation of proteins and autophagy. Sometimes, as part of programmed cell death, entire cells can be degraded, but most of the time, specific cellular demands require certain cell parts, organelles or intracellular components to be degraded by autophagy to prevent damage or reuse them for other purposes. Usually carbon source shifts, overall nutrient unavailability and energy scarcity are the main activators of autophagy, but numerous processes have been reported to trigger it (Klionsky & Emr, 2000).

Three types of autophagy have been described in the literature depending on the way cellular material is degraded: microautophagy, which occurs when usually small molecules in the cytoplasm are directly sequestered and hydrolyzed in the lysosomes; chaperone-mediated autophagy which refers to the sequestration of

certain proteins to the lysosomes by chaperone action, and macroautophagy that consists on the degradation of cellular material by the direct implication of vesicles called autophagosomes and their subsequent fusion with the lysosomes (Hansen et al., 2018).

Macroautophagy, or autophagy hereafter, can be divided into several sequential steps where many autophagy-related proteins (ATGs) and cellular components take place (Fig. 15). To simplify, the process is initiated by the formation of double membrane vesicles called autophagosomes or phagophores, followed by their elongation and sequestration of different cellular material (called cargo), continued by the fusion of the mature autophagosomes with lysosomes to form autophagolysosomes or autolysosomes that degrade that cargo with the lysosomal enzymes (Hansen et al., 2018).

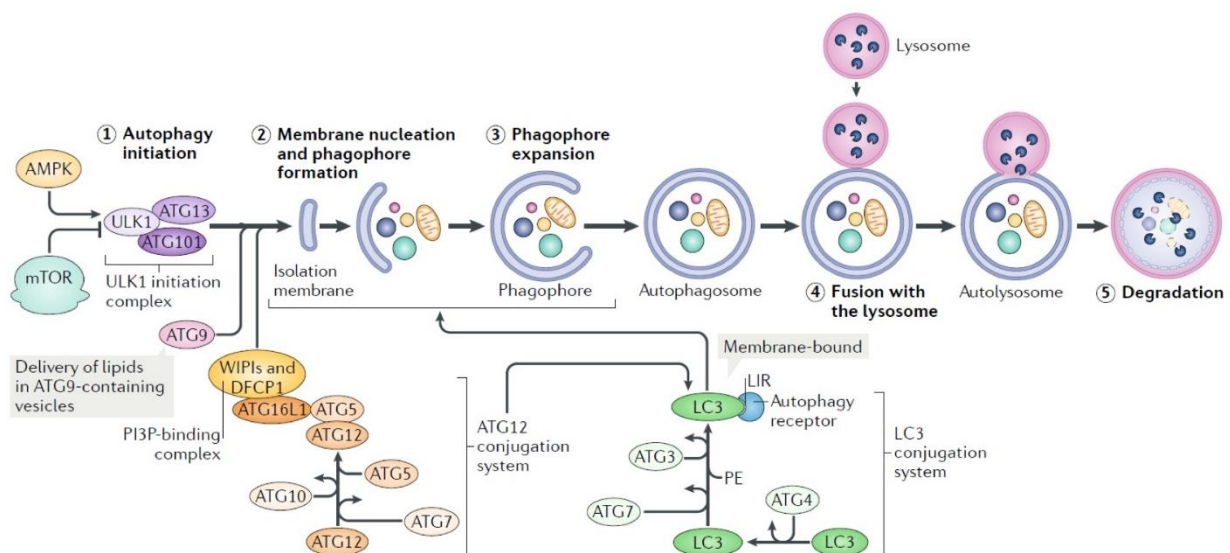


Figure 15. A schematic process and main regulatory machinery of autophagy. The process of autophagy can be divided into five sequential steps: initiation (1), nucleation and phagophore formation (2), expansion (3), fusion with the lysosomes (4) and final degradation (5). where many autophagy-related proteins (ATGs) intervene. (Modified from Hansen et al., 2018).

Two of the key upstream regulators of autophagic response are the AMP activated protein kinase (AMPK) and the mammalian target of rapamycin (mTOR), though with opposite roles. AMPK is activated when nutrients are restricted or energy is scarce and it signals to activate catabolic pathways. AMPK phosphorylates unc-51 like autophagy activating kinase (ULK1) at serines 317 and 777 which promote autophagosome formation (Kim et al., 2011), but also can indirectly activate

autophagy by inhibiting mTOR (Gwinn et al., 2008) or can increase lysosomal production in association with transcription factor EB (TFEB) (Zhao et al., 2020). mTORC1 is a nutrient sensing kinase that is active when nutrients are available, favoring anabolic pathways and growth, and inhibiting autophagy and other catabolic routes. mTORC1 phosphorylates TFEB decreasing its activity, which is considered the master regulator of lysosomal and autophagy-related genes (Roczniak-Ferguson et al., 2012), and also phosphorylates ULK1 at serine 757, which directly inactivates it and thus autophagy (Kim et al., 2011). mTORC1 can also modulate autophagy in indirect ways such as by controlling the production of lysosomes (Roczniak-Ferguson et al., 2012). However, lysosomes as well have a central role in controlling autophagy as they are able to sense nutritional intracellular changes and the activation of mTORC1, TFEB (in collaboration with RAG GTPases) and the initial steps of AMPK glucose and ATP sensing occur at the lysosomes (Ondaro et al., 2022).

Other key proteins in autophagy are the microtubule associated protein light chain 3 (LC3) and the gamma aminobutyric acid receptor associated proteins (GABARAPs) which are proteolytically processed and incorporated into the autophagosome membranes where they interact with many autophagy receptors to select and recruit cargo. In more detail, ATG12 conjugation system, formed by the interaction of ATG5, ATG12, ATG16, WIPI and DFCP1, promotes the conjugation of LC3, which consists of its cleavage by ATG4 to form LC3 I who is then lipidated by binding to phosphatidylethanolamine (PE) to form LC3 II. This form of LC3 is the one that can bind to autophagosome membranes and act in the processing of cargo (Hansen et al., 2018). A last worth-mentioning protein implicated in autophagy is Sequestosome 1 (SQSTM1 or p62) as it binds to ubiquitylated proteins to direct them to autophagosomes for their degradation.

Last, it should be noted that although autophagy and lysosomes are players of the same game, in terms of disease, they can be classified in different groups based on the primary impairment site or the mutated gene, sort of like it occurs with mitochondrial diseases (Jiang & Mizushima, 2014). Thus, some disorders, lysosomal storage disorders, are a group of disorders who primarily have lysosomes affected (Darios & Stevanin, 2020), and others, called autophagy-related diseases, are disorders who mainly have mutations on ATGs and show inability of clearance of unwanted cellular material (Jiang & Mizushima, 2014).

Materials & Methods

Subjects and biopsies. Patients were examined after informed written consent was obtained. All the procedures and examinations, including skin biopsies, were performed approved by the Wellcome Centre for Mitochondrial research (200990), Regional Committee for Medical and Health Research Ethics, Western Norway (IRB.no.000018729), or the Basque Biobank.

Cell culture. Primary human fibroblasts were routinely maintained in Dulbecco's Modified Eagle's Medium (DMEM) (Gibco) containing 25 mM glucose, 1 mM pyruvate supplemented with 10% fetal bovine serum (FBS, Gibco), 5% penicillin and streptomycin (P/S, Gibco), 2 mM GlutaMAX (Gibco), 5% CO₂, at 37°C. All the cell lines were regularly confirmed free of mycoplasma, using the Venor Gem Classic Mycoplasma PCR Detection Kit (Minerva Biolabs).

Immunocytochemistry. For microscopy experiments, approximately 4700 fibroblasts/well were sown on 96-well black microplates (Ibidi). After at least 24 h, cells were treated with the various reagents as follows: 2.5 µM U18666A (U18) 48 h (Abcam), 50 µM chloroquine diphosphate salt (CLQ) 10h (Sigma) and 100 nM rapamycin/sirolimus (Rapa) for 24h (Acofarma) as indicated in the main text and figure legends. For the bromo-deoxyuridine (BrdU, Sigma) incorporation experiments, cells were incubated with BrdU 50 µM for about 12 h before fixation. Cells were fixed with 4% paraformaldehyde (PFA) (Electron Microscopy Sciences) for 20 mins at room temperature (RT). After washing with Phosphate Buffered Saline (DPBS, Gibco), the cells were permeabilized and blocked for 1 h at RT with 10% donkey serum (GeneTex) or goat serum (Sigma Aldrich) in 0.1% Triton X-100, PBS (PBST 0.1%). Cells then were incubated with primary antibodies (see Table M2) in PBST overnight (O/N) at 4°C. After three washes for 5 min with PBST 0.1%, cells were incubated with the appropriate secondary antibodies (see Table M2) 1:450 dilution in 10% goat/donkey serum in PBST 0.1% for 1-2 h at RT. Cells were then washed 3x with PBST 0.1% and 1x with PBS, and Mounting Medium with DAPI (Ibidi) was added.

For free cholesterol and neutral lipid labeling, similar procedure was followed but after PFA fixation and DPBS washing, cells were directly incubated with Filipin III 50 µg/mL (Sigma) for 1 h for cholesterol and with BODIPY™ 493/503 1µg/mL (Invitrogen) for 15 min for neutral lipids, both protected from light. After that, 2x washes of 5 min with PBS 1x were done, and a short incubation of 5 min was done

with SYTOX™ Deep Red 0.5 μ M (Thermo Scientific) to stain the nuclei. A last wash was done with DPBS and Mounting Medium (Ibidi) was added to the wells.

For observing lysosomal activity, and after respective treatments were done, 10 nM LysoTracker™ Red DND-99 (Invitrogen) was added to culturing cells in DMEM for 45 min and after that, cell media was changed to DMEM FluoroBrite™ supplemented with 5% P/S, 10% FBS and 2 mM GlutaMAX to keep the cells in similar conditions but with less background fluorescence signal.

Image capture and analysis. Fluorescent images were acquired through a Nikon Eclipse 80i epifluorescence microscope or a LSM 900 Zeiss confocal microscope, as indicated. Laser power, gain and offset parameters were kept constant for each experiment. The image analysis was performed using the plugins available in Fiji (Image J). Graphpad (Prism) was used to quantify and represent the data shown as charts.

Immunodetection of proteins. For immunoblotting experiments, cells were grown in 25 cm² flasks until high confluency was obtained. Cells were detached with trypsin (0.4% w/v solution, Gibco) and lysed on ice with RIPA buffer (150 mM NaCl, 1.0% TritonX-100, 0.5% sodium deoxycholate, 0.1% SDS, 50 mM Tris, pH 8.0), 1x Halt™ Protease and Phosphatase Inhibitor Cocktail (Thermo Scientific). After incubating on ice for 40 minutes, the samples were centrifuged for 20 minutes at 15,000 g, 4°C to remove cellular debris. Cell fractionation was carried out using the “REAP: A two minute cell fractionation method” (Suzuki et al., 2010). Briefly described, it consists in a first lysis in 0.1% NP40 (Sigma) in PBS, seriated centrifugations including a sonication step, to finally obtain nuclear and cytosolic fractions. Protein concentration was determined by DC protein assay kit (Bio-Rad). Protein samples were prepared in 1x Laemmli loading buffer (BioRad) with DTT and resolved on 7% or 12% Mini-PROTEAN TGX™ Precast Gels (Bio-Rad) using Tris/Glycine/SDS running buffer (Bio-Rad). After electrophoresis, proteins were transferred to Low-Fluorescence PVDF transfer membranes (Thermo Scientific) and blocked with 3% BSA in PBS, 0.1% Tween for 1 h at RT. Membranes were incubated overnight with primary antibodies (see Table S2) in BSA 3% in PBS, 0.1% Tween, at 4°C and, after washes, they were incubated with the appropriate secondary antibody (see Table S2) for 1 h at RT. Proteins were detected using SuperSignal™ West Pico PLUS chemiluminiscent substrate (Thermo Scientific), and immunoblots were acquired in

an iBright FL1500 Imaging System and quantified with iBright Analysis Software. Graphpad (Prism) was used to quantify and represent the data shown as charts.

Transmission electron microscopy. Cells in an 8-well chamber slide were washed with PB 0.1 M ($\text{NaH}_2\text{PO}_4 \cdot \text{H}_2\text{O}$ and Na_2HPO_4) and fixed with 3% glutaraldehyde for 10 min at 37°C and 2 h at RT. After 5 PB washes of 5 min the chamber slide were dried and sent to Centro de Investigación Príncipe Felipe (Valencia). Once the samples were cut and processed, images were taken with a 200 kV and high-resolution TECNAI G2 20 TWIN transmission electron microscope in Sgiker from the University of the Basque Country.

Quantification of mtDNA copy numbers. The mtDNA copy number was quantified as follows: after DNA isolation, real-time quantitative PCR was performed in triplicates on 384-Well Reaction Plates (Applied Biosystems) in final volumes of 13 μL . Each reaction contained 15 ng of DNA template, 1x Power SYBR Green PCR Master Mix (Applied Biosystems) and 0.5 μM of forward and reverse primers. Mitochondrial and nuclear DNA were amplified using primers specific to regions of human t-RNA and B2 microglobulin genes respectively. t-RNA forward sequence (5'-CACCCAAGAACAGGGTTTGT-3') and reverse sequence (5'-TGGCCATGGGTATGTTGTTA-3'). B2 microglobulin forward sequence (5'-TGCTGTCTCCATGTTTGATGTATCT-3') and reverse sequence (5'-TCTCTGCTCCCCACCTCTAAGT-3').

Changes in the mtDNA copy number were determined by using the $2^{-\Delta\Delta\text{Ct}}$ method (Schmittgen, T. D. & Livak, K. J., 2008).

ATP levels analyzed by CellTiter-Glo (Promega). To determine the cellular ATP levels we used the CellTiter-Fluor™ Cell Viability Assay (Promega) that is non-lytic and can be multiplexed with the CellTiter-Glo® 2.0 (Promega). Two thousand cells were seeded per well in a 384 well-plate in 50 μL of DMEM 10% FBS, and after 48 h the medium was replaced with 20 μL of fresh medium according to the specific experimental condition (e.g. 20 mM 2-DG), starting from a common FluoroBrite™ (Gibco) supplemented with penicillin and streptomycin, 10% FBS, with or without 2 mM GlutaMAX™ (Gibco). After 24 h, we added an equal volume (20 μL) of the CellTiter-Fluor™ assay following the manufacturer's instructions, and measured the fluorescent signal to calculate cell viability using Promega's GloMax® Discover Microplate Reader. To measure intracellular ATP, next we added 40 μL 2X

CellTiter-Glo® 2.0 reagent to lyse the cells and after shaking for 15 mins read the luminescence signal using the Promega'sGloMax® Discover Microplate Reader.

Analysis of metabolic flux by Seahorse (Agilent). Mitochondrial respiration was studied using the Seahorse XF96 Extracellular Flux Analyzer (Agilent) and Extracellular Flux Assay Kit (Agilent). This equipment allows to study mitochondrial respiration in living cells and in real time. The analyzer measures the ratio of oxygen consumption (OCR, Oxygen Consumption Rate), as an indicator of mitochondrial respiration. The day before the experiment, 2,000 cells/well were seeded in a 96-well XFe96/XF Pro cell culture microplate (Agilent). The microplate was loaded with Oligomycin 1 μ M (Sigma), Carbonyl cyanide 4-(trifluoromethoxy)phenylhydrazone) (FCCP) 1 μ M (Sigma), and Rotenone plus Antimycin A 0.5 μ M (both Sigma) following the manufacturers instructions. Then, continuous OCR measurements were carried out. Data was normalized to cell number, which was measured by Cresyl violet staining (0.1% solution for 15 min).

Table M1. Compounds, manufacturers and doses

Compound	Manufacturer	Dose
U18666A	Abcam	1.25/2.5 μ M 48 h
Ro488071	TargetMol	2.5 μ M 48 h
Chloroquinediphosphate salt	Sigma Aldrich	50 μ M 10 h
Rapamycin	Santa Cruz Biotechnology/Acofarma	100 nM 24 h
Atglistatin	Santa Cruz Biotechnology	50 μ M 24 h
Isoproterenol	TargetMol	1 μ M 24 h
LDL	Invitrogen	50 μ g/mL 24 h
Cholesterol solution	Promega	10 μ M 24 h
Sandoz-58035	Sigma Aldrich	2 μ g/mL 24 h
MCP-1/CCL2	MedChem Express	50 ng/mL 24 h
Sphingosine-1-phosphate	Sigma Aldrich	4/40 μ M 24/48 h
2-deoxy-D-glucose	Alfa aesar	20 mM 24 h
Rotenone	Glentham life sciences	0.1 μ M 24h

Table M2. Identity, source and dilutions of the primary and secondary antibodies used in the study.

Antibody/Fluorescent compound	Manufacturer	Catalogue #	Dilution for ICC (for WB is 1:1000)
ABCA1 (rabbit)	Novus	NB400	
ABCG1 (rabbit)	Proteintech	13578-1-AP	
Anti-DNA (mouse)	Progen	61014	1:250
Anti-DNA (mouse)	Progen	690014S	1:250
ATAD3 C-ter (mouse)	Santa Cruz Biotechnology	sc-376185	
ATAD3 N-ter (rabbit)	Custom design		1:1000
ATAD3 N-ter P (rabbit)	Proteintech	16610-1-A	1:200
ATAD3B (mouse)	Santa Cruz Biotechnology	sc-514615	1:250
BiP/GRP78 (rabbit)	Abcam	ab21685	1:1000
BrdU (rat)	Abcam	Ab6326	1:250
CES1 (rabbit)	Proteintech	16912-1-AP	
COXIV (rabbit)	Proteintech	11242-1-AP	
CYP11A1 (rabbit)	Novus	NBP1-85368	

EEA1 (mouse)	Santa Cruz Biotechnology	SC-365652	
GAPDH (mouse)	Sigma	G8795	
LAL (rabbit)	Proteintech	12956-1-AP	
LAMP1 (rabbit)	Cell Signalling	D2D11	1:250
LC3A/B (rabbit)	Invitrogen	PA1-16931	
MITOFILIN (rabbit)	Proteintech	10179-1-AP	
MTCO-2 (rabbit)	Proteintech	55070-1-AP	
NDUFB8 (mouse)	Abcam	ab110242	
NDUFB9 (rabbit)	Proteintech	15572-1-AP	
p(S235/236)-S6 (rabbit)	Cell Signalling	4858	
p(S403)-p62 (rabbit)	Cell Signalling	39786	
PERILIPIN 2 (rabbit)	Proteintech	15294-1-AP	1:250
SERAC1 (rabbit)	Proteintech	25729-1-AP	
SR-BI (rabbit)	Proteintech	21277-1-AP	
SRBP2 (mouse)	Santa Cruz Biotechnology	Sc-13552	
TOMM20 (mouse)	Santa Cruz Biotechnology	Sc-17764	1:250

TOMM20 (rabbit)	Proteintech	11802-1-AP	1:250
UCP2 (goat)	Novus	NB100-59742	1:300
Secondary Antibody for ICC/IHC	Manufacturer	Catalogue #	Dilution for ICC/IHC
Goat anti-Rat IgG (H+L) Cross-Adsorbed Secondary Antibody, Alexa Fluor 647	Invitrogen	A-21247	1:500
IgG (H+L) Highly Cross-Adsorbed Donkey anti- Rat, Alexa Fluor™ 488	Invitrogen	A21208	1:500
IgG (H+L) Cross-Adsorbed Goat anti-Rat, Alexa Fluor™ 555	Invitrogen	A23434	1:500
IgG (H+L) Cross-Adsorbed Goat anti-Rat, Alexa Fluor™ 488	Invitrogen	A11006	1:500
Alexa Fluor®-488 goat- anti-mouse IgG	Invitrogen	A11001	1:500
Alexa Fluor®-555goat- anti-mouse IgG	Invitrogen	A21422	1:500
Alexa Fluor®-555goat- anti-rabbit IgG	Invitrogen	A21428	1:500
Alexa Fluor® 488donkey anti-mouse IgG	Invitrogen	A21202	1:500
Alexa Fluor® 555 donkey anti-mouse IgG	Invitrogen	A31570	1:500
Alexa Fluor® 555donkey anti-rabbit IgG	Invitrogen	A31572	1:500
Alexa Fluor® 488donkey anti-rabbit IgG	Invitrogen	A21206	1:500
Alexa Fluor®647donkey anti-mouse IgG	Invitrogen	A31571	1:500
Alexa Fluor® 555donkey anti-sheep IgG	Invitrogen	A21436	1:500
Alexa Fluor®-647 donkey- anti-rabbit IgG	Invitrogen	A32795	1:500
Alexa Fluor®-647 donkey- anti-goat IgG	Invitrogen	A21447	1:500
Secondary Antibody for WB	Manufacturer	Catalogue #	Dilution for WB

Donkey Anti-Goat IgG, HRP	Promega	V8051	1:5000
Goat Anti-Mouse IgG (H+L), HRP	Promega	W4021	1:5000
Goat Anti-Rabbit IgG (H+L), HRP	Promega	W4011	1:5000
Goat Anti-rabbit IgG, AlexaFluor-647 PLUS	Invitrogen	A32733	1:5000
Goat Anti-mouse IgG, AlexaFluor-647 PLUS	Invitrogen	A32728	1:5000

Results

R1.1- ATAD3 disease: genetics and clinical features.

Of the different *ATAD3* mutant cell lines that we have had the opportunity to work with in our laboratory, two novel genotypes have been described and characterized for the first time during this thesis. Our laboratory focuses on characterizing and understanding the cellular and molecular phenotypes associated with human diseases, while the clinical and genetic diagnosis of the patients were determined by our collaborators.

The first case I studied came from a patient assessed in Exeter, United Kingdom. The fibroblasts were from a neonate boy with healthy parents, who was born with bradycardia and had an Apgar score of 3 out of 10, which is strongly indicative of severe illness and poor outcomes. Immediately after birth, the infant had to be resuscitated and was intubated in the neonatal intensive care unit. The principal clinical symptoms were hypotonia, encephalopathy and seizures, hypertrophic cardiomyopathy, fetal akinesia, congenital cataracts and bilateral corneal opacities. Metabolic investigations revealed increased excretion of several Krebs cycle intermediates, such as fumarate, malate and 2-ketoglutarate. This strongly suggested that the tricarboxylic acid cycle (TCA) is blocked, which is a sign of an impaired respiratory chain and so was a clear indication of mitochondrial dysfunction. Death occurred 3 days after birth. Exome sequencing revealed a *de novo* 68 kb monoallelic dominant duplication between sequences with high homology within the *ATAD3* gene-cluster. The duplication was confirmed by PCR and Sanger sequencing, where a 1.2 kb amplicon was detected in the patient but was not present in the DNA sample of either parent, which established that the duplication occurred *de novo*. The same *de novo* heterozygous 68 kb duplication was found in another four unrelated neonates with strikingly similar clinical features and death in infancy. Although one of the four also carried a single intronic nucleotide change this was not predicted to alter RNA splicing and so should not affect the protein sequence (Gunning 2020 Am Journ Hum Genet).

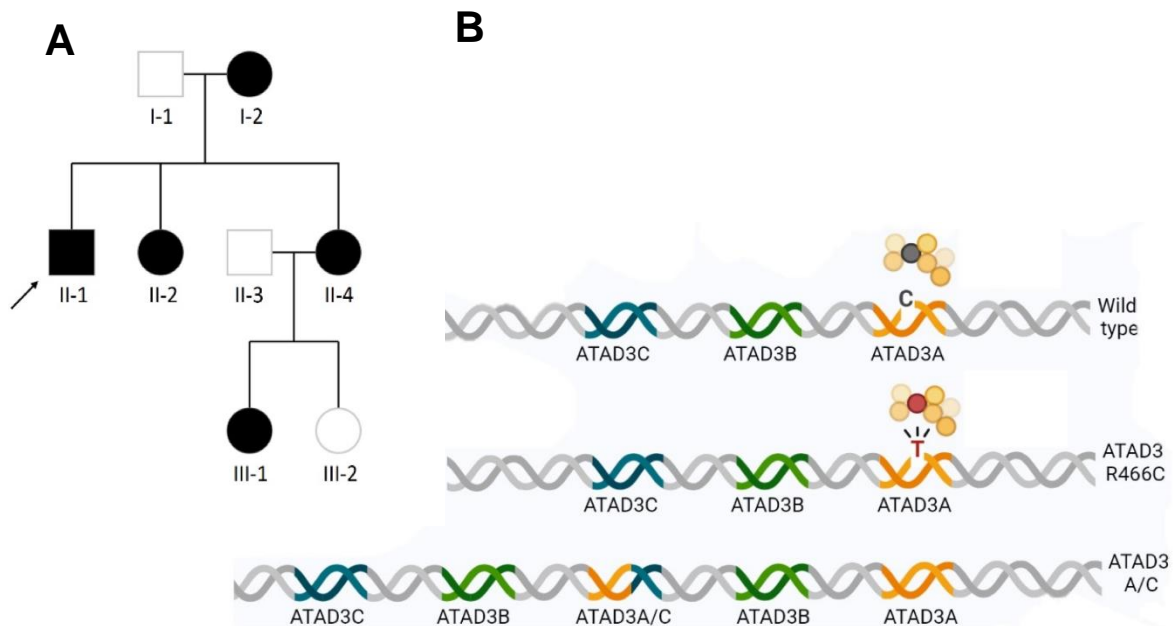
In addition to the *ATAD3A/C* fusion gene, there was also a complete and intact extra copy of *ATAD3B*. To assess whether the extra *ATAD3B* was contributing to the disease, duplications affecting the *ATAD3* gene cluster were evaluated in the Deciphering Developmental Disorders cohort (DDD). Of 32,369 individuals, 61 had a putative monoallelic duplication affecting the region around *ATAD3* gene cluster,

of which 48 were confined to the *ATAD3* genes. All the duplications found in these 48 individuals included *ATAD3B* but not *ATAD3A* and corresponded to apparently unaffected individuals or subjects with mild phenotypes that did not coincide with the severe multisystemic features characteristic of the fatal neonatal syndrome. Therefore, it was concluded that the extra *ATAD3B* contributes little, if at all, to the severe clinical condition, rather the disease arises from the *ATAD3 A/C* fusion variant. This variant predicts an *ATAD3 A/C* fusion protein that differs from the canonical *ATAD3A* protein sequence (isoform II) in 29 residues, seven of which (p.Val450Ile, p.Asn454Cys, p.Gln455His, p.Asp465Ala, p.Arg466Cys, p.Asn468Asp, and p.Glu469Val) reside in the ATPase domain of the protein, owing to the replacement of exons 1-11 in *ATAD3A* and exons 8-12 in *ATAD3C*. Particularly notable are the p.Asn454Cys, which corresponds to the sensor I motif, and p.Arg466Cys, that corresponds to the arginine finger or sensor 2, as both are residues that are known to bind ATP and are essential for ATP hydrolysis in the AAA+ family of ATPases (Ogura et al., 2004; Hanson & Witeheart, 2005). Fibroblasts of this patient were obtained from a skin biopsy and were used to characterize the cellular and molecular changes associated with mutant *ATAD3*, see subsequent sections.

The next case referred to us was a member of a family with five affected individuals spanning three generations. All presented slowly progressive optic atrophy with pale optic discs and retinal nerve fiber layer thinning starting early in life. The adults examined had best corrected visual acuity ranging from 0.25 to 0.5 Snellen, and moderate myopia was common. Most individuals had nyctalopia, various color vision defects and subtle macula changes; however, electroretinograms and visual evoked potentials were normal. Brain MRI was normal among the affected individuals, with the exception of subject II-2, who showed unilateral perineural oedema and central oedema. Subject II-1 (the index case) was assessed neurologically at 21 years old due to unsteady gait, distal lower limb weakness and problems climbing stairs that had been present from early childhood. He also presented learning disability. Examination revealed normal tone, distal muscle atrophy and weakness in the lower limbs and bilateral pes cavus. Deep tendon reflexes were brisk except for absent ankle reflexes. Spinthalamic sensation was reduced in both feet. Ankle reflexes were absent, but patella reflexes were pathologically brisk and there was a positive Babinski reflex on the left. Tone and strength were normal in the arms, but reflexes were all increased and there was a positional tremor. Nerve conduction studies were

consistent with an axonal, predominantly motor, peripheral neuropathy. Analysis of a muscle biopsy from this patient revealed changes related to neuropathy, but mitochondrial DNA deletions were ruled out by long-range PCR and RT-qPCR. Another biopsy, from skin this time, was done to this patient from which fibroblasts were obtained that were used to characterize the cellular and molecular changes associated with mutant *ATAD3*, see subsequent sections.

All five affected individuals presented a heterozygous missense variant in *ATAD3A* c.1396C>T that was not present in the unaffected family members. Thus, the monoallelic point mutation followed a dominant inheritance pattern with full penetrance. It was not found in the gnomad database (Collins et al., 2020) and it is strongly predicted to be a pathogenic substitution (PolyPhen2, Mutationtaster, SIFT and Align) (Ng & Henikoff, 2003). However, because all reached adulthood, the clinical features provoked by this point mutation are considered milder than the multisystemic failure reported for other *ATAD3* mutations, such as deletions and duplications. The missense mutation predicts an arginine to cysteine substitution, at residue 466 of *ATAD3A* isoform II (p.Arg466Cys). This will result in the loss of the arginine finger implicated in ATP hydrolysis in the AAA+ family proteins, and it is the same arginine finger lost as one of the 29 substitutions detected in the *ATAD3* A/C fusion protein (Gunning et al., 2020). Thus, the clinical phenotypes suggest this new *ATAD3A* missense mutation causes a form of autosomal dominant optic atrophy “plus” (DOA+) (ORPHA: 1215).



C

	Walker B
ATAD3A(isf1)	...YAIMTGGDVAPMGREGVTAMHKLFDWANTSRRG <u>LLLFVDEADA</u> FLRKRATEKISEDLRAT 480
ATAD3A(isf2)	...YAIMTGGDVAPMGREGVTAMHKLFDWANTSRRG <u>LLLFVDEADA</u> FLRKRATEKISEDLRAT 432
ATAD3(A/C)	...YAIMTGGDVAPMGREGVTAMHKLFDWANTSRRG <u>LLLFVDEADA</u> FLRKRATEKISEDLRAT 432
ATAD3A(R466C)	...YAIMTGGDVAPMGREGVTAMHKLFDWANTSRRG <u>LLLFVDEADA</u> FLRKRATEKISEDLRAT 432
ATAD3A(isf1)	<u>LNAFLYRTGQHSNKFMLVLASNQPEQFDWAINDRINEMVHFDLPGQEERERLVRMYFDKY</u> 540
ATAD3A(isf2)	<u>LNAFLYRTGQHSNKFMLVLASNQPEQFDWAINDRINEMVHFDLPGQEERERLVRMYFDKY</u> 492
ATAD3(A/C)	<u>LNAFLYRTGQHSNKFML</u> <u>I</u> <u>LASCH</u> <u>PEQFDWAINA</u> <u>C</u> <u>IDVMVHFDLPGQEER</u> <u>A</u> <u>RLVRMY</u> <u>LNEY</u> 492
ATAD3A(R466C)	<u>LNAFLYRTGQHSNKFMLVLASNQPEQFDWAINDR</u> <u>C</u> <u>INEMVHFDLPGQEERERLVRMYFDKY</u> 492
ATAD3A(isf1)	VLKPATEGKQRLKLAQFDYGRKCSEVARL TEGMSGREIAQLAVSWQATAYASEDGVLTEA 600
ATAD3A(isf2)	VLKPATEGKQRLKLAQFDYGRKCSEVARL TEGMSGREIAQLAVSWQATAYASEDGVLTEA 552
ATAD3(A/C)	VLKPATEGK <u>R</u> RLKLAQFDYGRKC <u>L</u> E <u>I</u> ARL TEGMS <u>C</u> RK <u>I</u> AQLAVSWQATAYAS <u>K</u> DGVLTEA 552
ATAD3A(R466C)	VLKPATEGKQRLKLAQFDYGRKCSEVARL TEGMSGREIAQLAVSWQATAYASEDGVLTEA 552
ATAD3A(isf1)	MMDTRVQDAVQQHQQKMCWLKAEGPGRGDESPS 634
ATAD3A(isf2)	MMDTRVQDAVQQHQQKMCWLKAEGPGRGDESPS 586
ATAD3(A/C)	MMD <u>AC</u> <u>VQDF</u> <u>VQ</u> <u>QH</u> <u>Q</u> <u>MM</u> <u>R</u> <u>W</u> <u>L</u> <u>K</u> <u>G</u> <u>E</u> <u>R</u> <u>P</u> <u>G</u> <u>P</u> <u>E</u> <u>D</u> <u>E</u> <u>Q</u> <u>P</u> <u>S</u> S 586
ATAD3A(R466C)	MMDTRVQDAVQQHQQKMCWLKAEGPGRGDESPS 586

Figure 1. Identification of a family with DOA+ associated with a dominant point mutation (R466C) in ATAD3A. (A) pedigree of the family in which affected members carry ATAD3A c.1396C>T, p.R466C (NM_001170535.2) on one allele. **(B)** Schematic representation of the ATAD3 locus in the wild-type, ATAD3 A/C duplication and the ATAD3 R466C point mutants. In ATAD3 A/C only the genetic rearrangement is represented (the specific point mutations are noted in Fig.1B) while the ATAD3A c.1396C>T is represented in the wild type vs. the ATAD3 R466C. The resulting peptide chain is also represented with the Arg466 to Cys change. The different ATAD3 genes (A, B and C) are painted blue, green and orange, respectively. **(C)** Amino acid sequence alignment between parts of ATAD3A isoforms 1 and 2 affected by the ATAD3A/C gene fusion and the arginine finger point mutation. The A/C fusion protein differs at 29 amino acid positions (highlighted in yellow), as described in (Gunning et al., 2020). The individuals with the R466C point mutation have an ATAD3 sequence identical in length to ATAD3A isoform 2 and it only differs in the ATP-binding residue at position 466, which it shares with the ATAD3 A/C fusion protein (red font). Underlined are the residues of the conserved protein kinase domain that form the ATPase region [p.Ile348–p.Asp474; Pfam PF00004]. Marked in a green box is the Walker B ATP binding motif. Residue numbering from [Q9NVI7-2/ NM_001170535.2].

Table 1. Comparison of the most relevant genetic and clinical outcomes in the two ATAD3 patients (ATAD3 A/C and ATAD3 R466C) and compared to patients with biallelic deletions (ATAD3Δ)

	Phenotype	ATAD3 Δ	ATAD3 A/C	ATAD3 R466C
Genetic outcomes	Variant/mutation	38 kb deletion	68 kb duplication	Missense 1396 C>T, R466C
	Zygoty	Biallelic	Monoallelic	Monoallelic
	Dominance	Recessive	Dominant	Dominant
	Inheritance	Parent consanguinity	Unaffected parents	5 affected from 3 generations
Biological outcomes	Sex	Female	Male	Male
Clinical outcomes	Fetal/newborn	Fetal akinesia No-postnatal movements. Absent newborn reflexes.	Fetal akinesia	
	Apgar score		3/10	
	Respiratory	Reduced respiration Cyanosis	Reduced respiration	
	Cardiac		Bradycardia Resuscitation Hypertrophic cardiomyopathy.	
	Muscular	Fiber size variation. Type II predominance.	Hypotonia	Lower limb weakness Distal muscle atrophy
	Cerebral	Encephalopathy Pontocerebellar hypoplasia. Simplified gyration. Thin <i>corpus callosum</i> . Diffuse white matter.	Encephalopathy	Normal MRI
	Cognitive			Learning disability
	General	Micrognathia Clasped thumb. Single palmar crease.	Seizures	Unsteady gait. Inability to climb stairs. Bilateral pes cavus. Absent ankle reflexes. Left babinski reflex. Positional tremor.
	Ocular	Bilateral corneal opacities. Pale optic discs. Corneal edema. Loss of ganglion cells and macula.	Congenital cataracts. Bilateral corneal opacities.	Progressive optic atrophy. Pale optic discs. Retinal nerve fiber layer thinning. Moderate myopia. Nyctalopia. Color vision defects. Subtle macula changes.
	Metabolic	Elevated plasma/urine lactate. Low OXPHOS factors in muscle.	Increased fumarate, malate and α-ketoglutarate	
Survival	Death	Day 4	Day 3	Alive (21 y.o. last when diagnosed)

R1.2- ATAD3 protein-variant expression, identification and organization

Separation of denatured proteins by sodium dodecyl sulfate polyacrylamide gel electrophoresis (SDS-PAGE) and posterior immunoblotting is a relatively fast and easy method to distinguish between copy number variation (CNV) wherever it produces differences in protein abundance.

Using pan specific anti-ATAD3 antibodies, raised in rabbit and mouse able to detect ATAD3A and ATAD3B or ATAD3A alone, respectively, we confirmed differences in abundance. Samples from a patient with the homozygous biallelic deletion (ATAD3 Δ) that predicts an ATAD3A/B fusion product (Desai 2017 Brain) showed a markedly lower signal compared to control lines and other ATAD3 mutants, such that it was barely detectable on occasion (Fig. 2A), matching the results reported by Desai et al. (2017). Although the decrease in the intensity of the band might indicate instability of the mutant protein, as noted by the authors, it could be explained by the fusion gene being expressed under the *ATAD3B* promotor that is considerably weaker than that of *ATAD3A*.

I was also able to confirm that the monoallelic duplication (ATAD3 A/C) increases the signal of both ATAD3B and ATAD3A proteins (Fig. 2A). This is consistent with the theoretical and *in silico* gene rearrangements of the 68 kbp duplication, as it is predicted to have an extra copy of ATAD3B and a fusion protein-product combining ATAD3A and ATAD3C (ATAD3A/C), which differs in 29 amino acids from the canonical ATAD3A sequence (isoform II) but retains the same length (Gunning et al., 2020). Therefore, the increase in the upper band is attributable to the extra copy of *ATAD3B*, while the increase in the lower band is explained by the ATAD3A/C fusion protein. As a corollary, the increase in the two bands indicates the extra copies arising from the duplication event are expressed and are stable, in contrast to many mutant variants that destabilize the proteins resulting in a marked reduced expression both in other ATAD3 variants (Dorison et al., 2020) or other diseases (e.g. MPV17) (Jacinto et al., 2021).

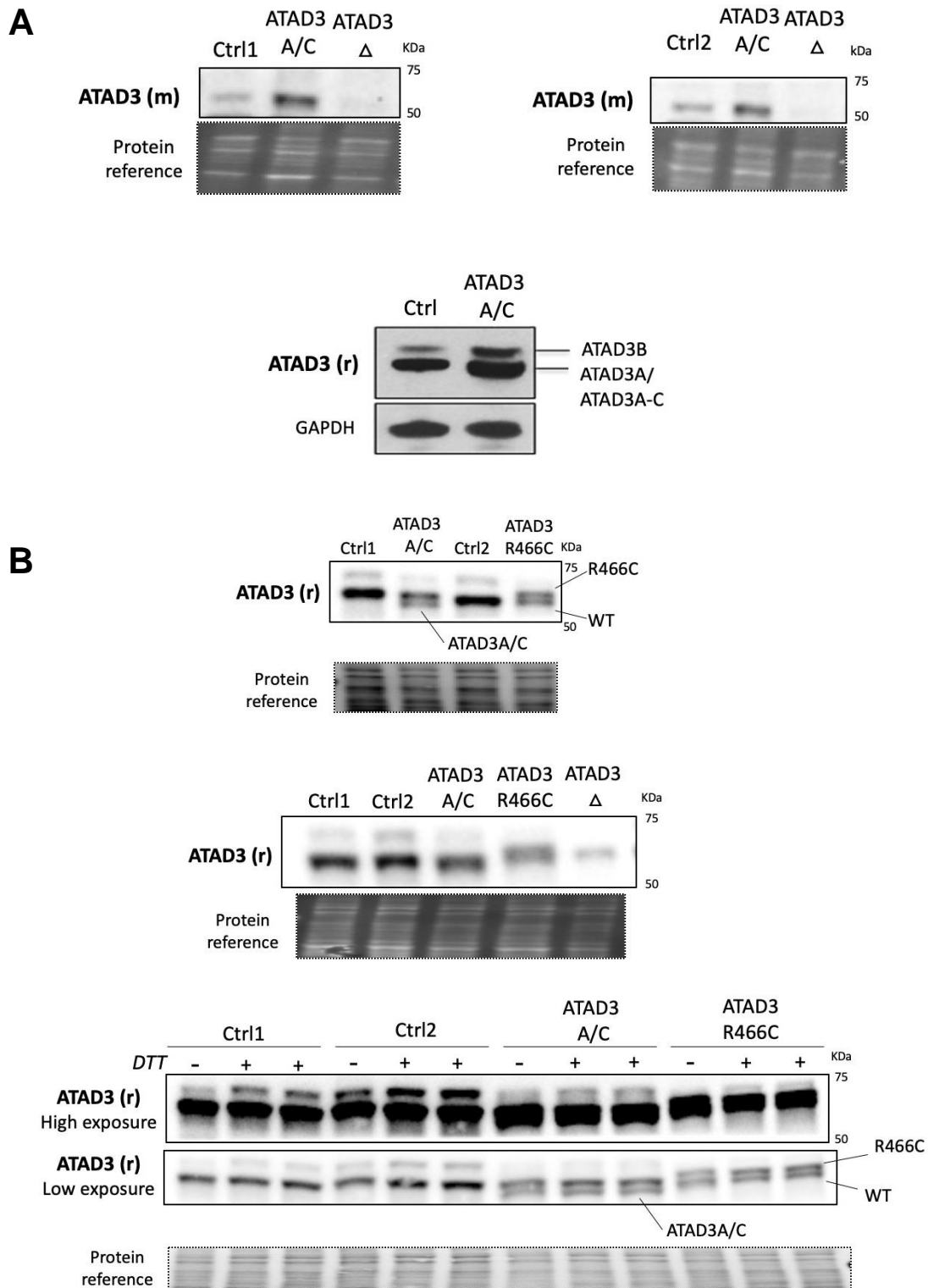


Figure 2. Abundance and mobility changes in ATAD3 protein on SDS-PAGE distinguish ATAD3 mutants from the wild-type protein. (A) Whole cell protein from controls (ctrl), ATAD3 R466C, ATAD3A/C and ATAD3 Δ mutant cell lines, by 11-12% SDS-PAGE and immunolabeled with ATAD3 specific antibodies. **(B)** 8% SDS-PAGE of whole cell protein combined with long running times and lower exposures, irrespective of the denaturant dithiothreitol (DTT, that disrupts disulfide bridges) and subsequent immunolabeling of ATAD3 specific antibodies. Images were acquired by iBright.

Further analyses showed that when denatured protein samples were separated on a gel with a lower pore size (6-8% polyacrylamide, instead of 11-12%), were allowed further separation of the bands of interest (more time in running) and saturation avoided when acquiring the images, more details emerged. Specifically, there were detectable differences in mobility. In the case of the samples from the patients with the duplication, instead of a single broad band there were two distinct bands corresponding to ATAD3A and ATAD3A/C, with the latter running slightly ahead of the wild-type protein (Fig. 2B). Because ATAD3A and ATAD3A/C are of identical size, the difference in mobility is attributable to the 29 amino acid substitutions in ATAD3A/C fusion protein. More surprisingly, samples from the patient with the monoallelic point mutation ATAD3 R466C, also resolved as two distinct ATAD3A species. In this case, the mutant ATAD3 R466C ran marginally slower than the wild type ATAD3A and, so, corresponds to the upper band (Fig. 2B).

As one or more of the amino acid substitutions in ATAD3 A/C and ATAD3 R466C, create new cysteine residues, we speculated the two bands detected under low pore size conditions could be due to an intramolecular conformational change arising from disulfide bonds formed between cysteines (Wiedemann et al., 2020). Therefore, strong reducing conditions were imposed by the denaturant agent dithiothreitol (DTT) that disrupts the disulfide bonds, but this did not produce any change in any of the bands, neither in size, mobility or amount (Fig. 2B). Nevertheless, we cannot exclude the possibility that the new cysteine residues create inappropriate interactions in cells and *in vivo*, in some conditions.

Thus, apart from the changes in abundance produced by differential expression, we have been able to identify several ATAD3 protein species arising from rearrangements in *ATAD3* genes that migrate differently due to presumed structural and conformational changes.

One recognized disease mechanism is mutations that result in protein mistargeting, which will effectively act as loss-of-functions mutations and could additionally have gain of function effects in their new location. Therefore, we evaluated the distribution of ATAD3 in control and patient-derived fibroblasts (ATAD3 A/C and R466C) using a pan-specific antibody to label ATAD3, and imaged by confocal microscopy. The ATAD3 signal was detected in all the mutants studied, mainly in mitochondria, evidenced by colocalization with OMM protein TOMM20 (Fig. 3A and B, and next section). Co-staining of ATAD3 and an antiDNA antibody (that labels both nuclear

and mitochondrial DNA), shows that some of the ATAD3 and mtDNA also coinciding (Fig. 3C), as previous studies have shown (He et al., 2007; Arguello et al., 2021). Hence, the mutant ATAD3 variants are correctly targeted to the mitochondria.

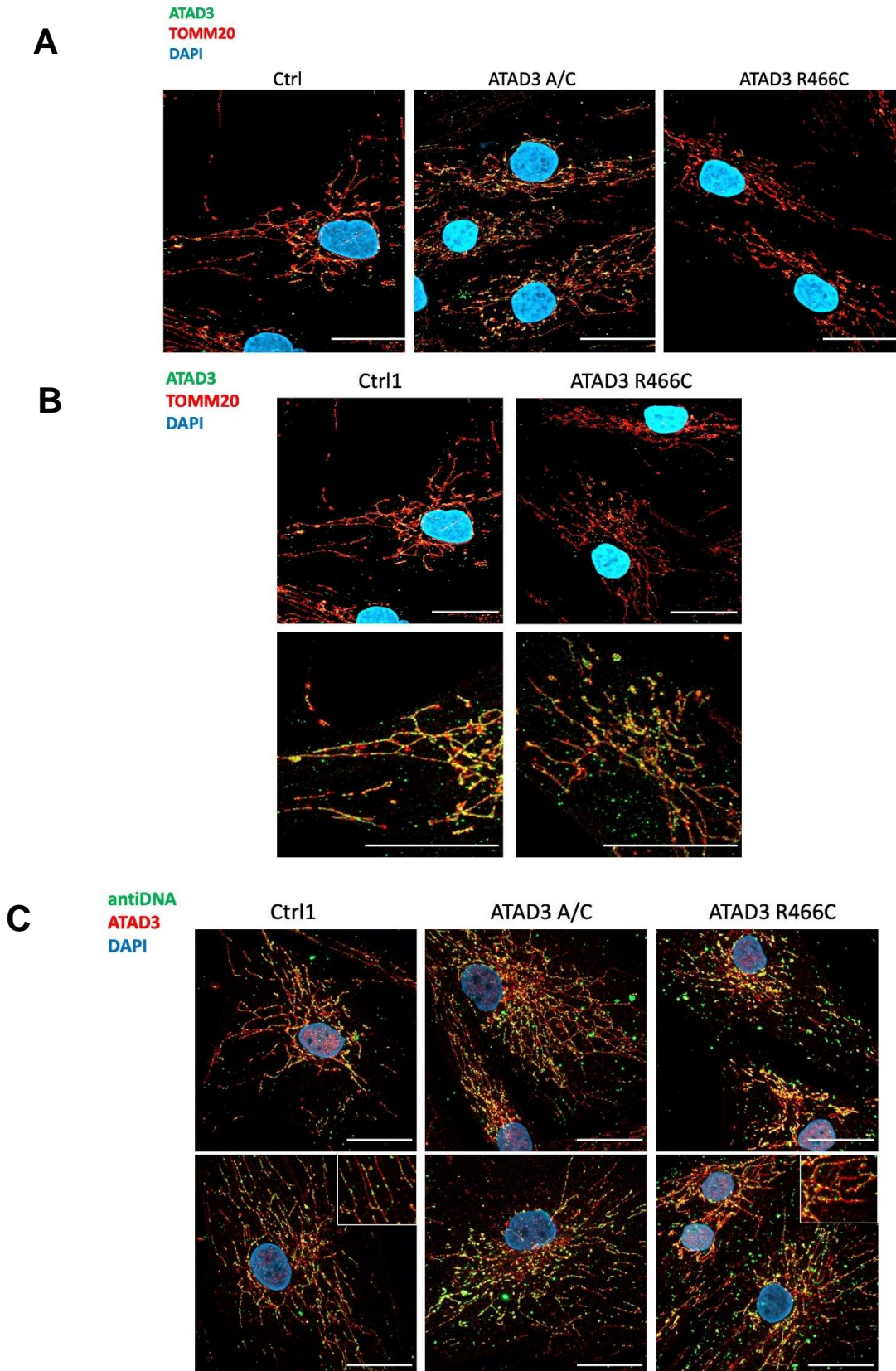


Figure 3. ATAD3 A/C and R466C mutants express ATAD3 and it is targeted to mitochondria and shows colocalization with most of the mitochondrial DNA. (A) Immunostaining of control and ATAD3 mutant cells with the combined anti-ATAD3 (green) and the outer mitochondrial membrane protein specific anti-TOMM20 (red) by confocal microscope at 40x shows specific subcellular localization of ATAD3 to mitochondria. In blue are the nuclei stained with DAPI. **(B)** 63x objective shows the colocalization in higher magnifications. **(C)** Immunostaining of control and ATAD3 mutant cells with a co-staining of ATAD3 (red) with an antibody that labels cellular DNA, antiDNA (green) by confocal microscopy at 40x. Digital zooms are in the upper right side of ctrl and ATAD3 R466C. In blue are the nuclei stained with DAPI.

R1.3- ATAD3 antibodies

During the course of determining the subcellular localization of the ATAD3 mutant proteins, we observed some extra-mitochondrial foci in the vicinity of the nucleus in both control and mutant cells, with an antibody that detected the N-terminal of ATAD3, called anti-ATAD3 N-ter W (Fig. 4). This raised the possibility that ATAD3 was not exclusively a mitochondrial protein. The phenotype reminded us of the labeling and distribution of the endosomes, and, indeed co-staining anti-ATAD3 N-ter W and the early endosomal marker anti-EEA1 (Santa Cruz Biotechnology, SCBT) showed that the extra-mitochondrial punctate signal of anti-ATAD3 N-ter W colocalized with the endosomes (Fig. 5). There were more endosomes than the punctate ATAD3 signal, but the majority of the ATAD3 foci colocalized with the endosomes.



Figure 4. anti-ATAD3 N-ter W antibody shows extra-mitochondrial signal. (A) ATAD3 mutants and controls were co-stained with an antibody specific for N-terminal ATAD3 (a gift of J. Walker), anti-ATAD3 N-ter W (green) and the outer mitochondrial membrane protein with anti-TOMM20 (red) and the images captured by epifluorescent microscopy. In blue are nuclei stained with DAPI.

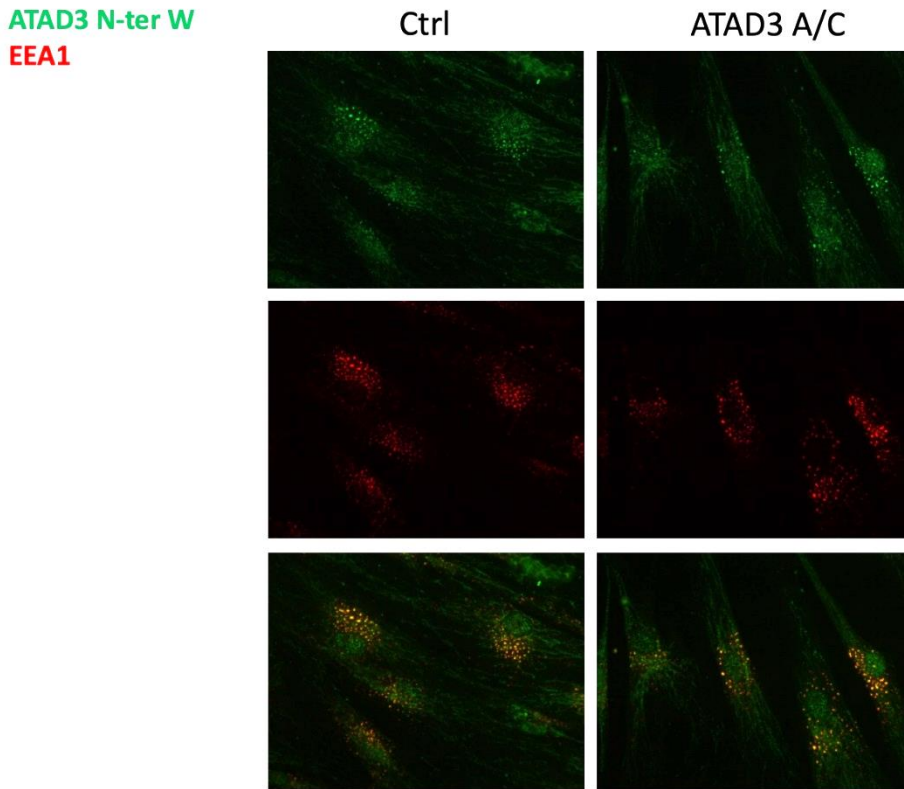


Figure 5. The extra-mitochondrial anti-ATAD3 N-ter W antibody colocalizes with the early endosome antigen 1 (EEA1). ATAD3 A/C mutants and controls (ctrl) were co-stained with the Walker antibody specific for ATAD3 N-terminal, anti-ATAD3 N-ter W (green) and the early endosome antigen 1, EEA1 (red) by epifluorescent microscope.

To determine whether the extra-mitochondrial signal of ATAD3 N-ter W was attributable to ATAD3 protein, we tested additional ATAD3 antibodies. Two antibodies that detected the N-terminal of ATAD3 were used. Both were raised in rabbits using different fragments of the same human ATAD3B protein sequence (GenBank: AAH02542.1). The original antibody, anti-ATAD3 N-ter W, was custom designed against amino acids 44 to 247 of ATAD3B by Dr. J. He working in Dr. J Walker's laboratory (He et al., 2007) and the other, anti-ATAD3 N-ter P, was purchased from Proteintech (catalog number 16610-1-A), raised against amino acids 1 to 270 (Proteintech). Therefore, both include the N-terminal region which is

considered to span from amino acids 1 to 245, but the anti-ATAD3 N-ter P might also recognize the subsequent transmembrane segment, TMS (246-264) (Gilquin et al., 2010). Because ATAD3B only differs in 62 extra amino acids in the C-terminus from isoform II of ATAD3A (Merle et al., 2012) both antibodies recognize ATAD3A protein based on Western Blotting. However, because isoform I contains an extra exon that inserts 48 amino acids at position 92, they may not detect isoform I, or less avidly. Although there is a third paralog in hominids, ATAD3C, these antibodies *in silico* are predicted to detect only a short sequence as ATAD3C is the most different of the ATAD3 proteins.

Two other antibodies were used, one for detecting the C-terminus: anti-ATAD3 C-ter, purchased from SCBT (catalog number sc-376185) and another general one: anti-ATAD3 FL, obtained from Novus (catalog number H00055210-B01P). The first one is raised in mice against the fragment comprising amino acids 407 to 634 of human ATAD3A isoform I (SCBT), which lies within the C-ter. As this fragment is all shared with isoform II, the antibody can also detect this isoform. Furthermore, according to Blastp (NCBI) *in silico*, this antibody can detect ATAD3B (and ATAD3C) with more than 90% alignment. The anti-ATAD3 FL is also raised in mice against full length (FL) human ATAD3A (isoform II) (Novus). Because the antigen is so long and unspecific, this antibody is predicted to target many splice-variants and paralogs.

One last antibody to anti-ATAD3B, was tested (SCBT catalog number sc-514615), which was raised in mice against a fragment comprising amino acids 598 to 615 located in the C-terminus of human ATAD3B. The fact that the antigen is specific to the far end of the C-terminus in ATAD3B, enables this antibody to only detect ATAD3B (isoform I), verified *in silico* with Blastp (NCBI).

Co-staining of human fibroblasts with anti-ATAD3 N-ter W, with either anti-ATAD3 C-ter or anti-ATAD3 FL, showed that only the former labeled extra-mitochondrial foci (Fig. 6A and B). Even the anti-ATAD3 N-ter P, which is the most similar of the antibodies to anti-ATAD3 N-ter W, could not detect the extra-mitochondrial phenotype (Fig. 7B). Further analysis of ATAD3 antibody staining by ICC revealed that both anti-ATAD3 N-ter W and P antibodies labeled signal in the nucleus, especially the anti-ATAD3 N-ter W in contrast to the rest of the ATAD3 antibodies used (Fig. 7A and B). To investigate the signal detected in the nucleus, we performed a cell fractionation to separate both control and ATAD3 mutant cells in fractions, cytoplasmic (C) and nuclear (N), and compared them to whole-cell lysates (W) by

immunoblotting. Two markers appeared to validate the fractionation, tubulin was concentrated in C while lamin A+C was detected only in N, and anti-ATAD3 N-ter W detected signals both in W and C but not in N (Fig. 8); thus, we could not detect the signal observed in the nucleus by ICC with the cell fractionation and subsequent immunoblotting. No other band from a different molecular size was detected in either of the fractions.

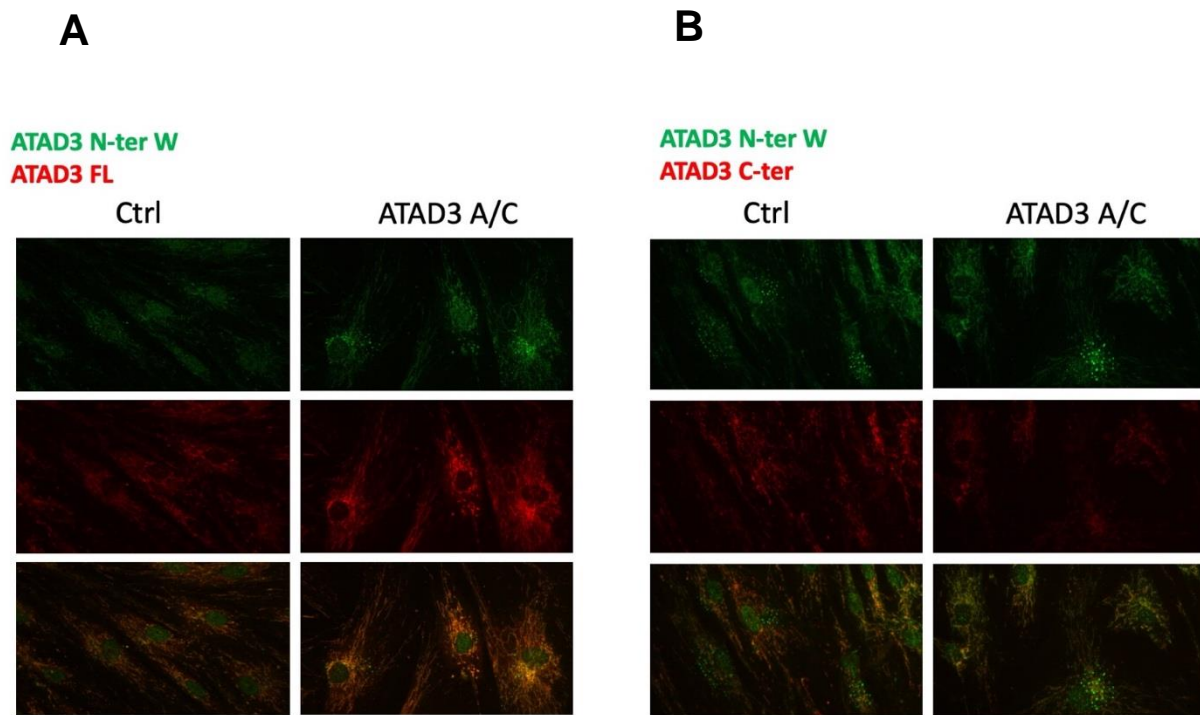


Figure 6. Two commercial antibodies for ATAD3, anti-ATAD3 FL (full length) and anti-ATAD3 C-ter, specific for the C-terminal, do not show the extra-mitochondrial foci. (A) ATAD3 A/C mutants and controls (ctrl) were co-stained with the Walker antibody, anti-ATAD3 N-ter W (green) and the antibody that labels full length ATAD3, ATAD3 FL (red). **(B)** ATAD3 A/C mutants and controls (ctrl) were co-stained with anti-ATAD3 N-ter W (green) and the antibody specific for the C-terminal of ATAD3, ATAD3 C-ter (red) by epifluorescent microscope.

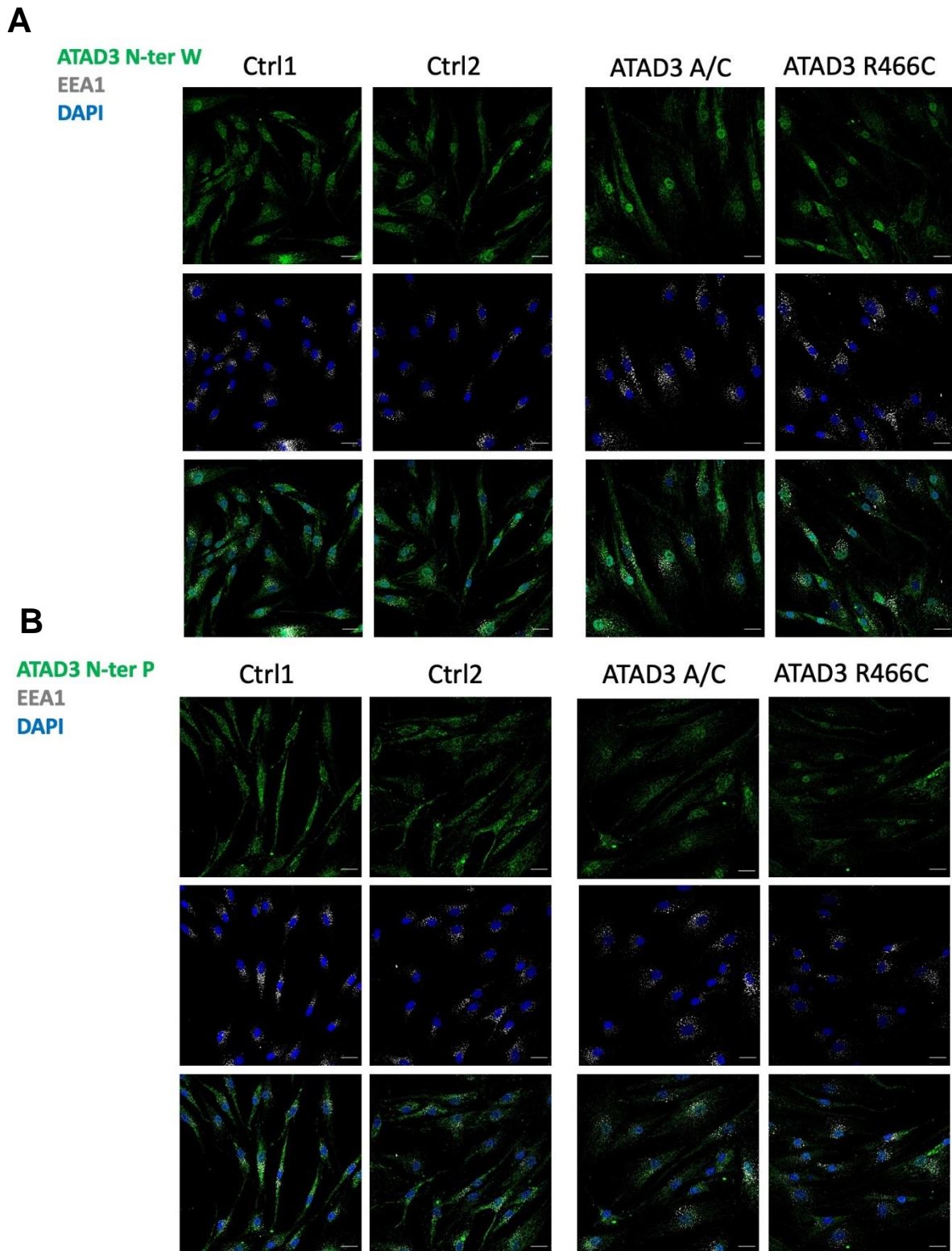


Figure 7. Both ATAD3 antibodies that target the N-terminal produce a nuclear signal. (A) ATAD3 A/C and R466C mutants and controls (ctrl) were co-stained with the Walker antibody, anti-ATAD3 N-ter W (green) and early endosome antigen 1, EEA1 antibody (gray). **(B)** ATAD3 A/C and R466C mutants and controls (ctrl) were co-stained with an antibody specific for ATAD3 N-terminal by Proteintech, anti-ATAD3 N-ter P (green) and early endosome antigen 1, EEA1 antibody (gray). Additionally, the nuclei were stained with DAPI; all stains were detected by confocal microscopy.

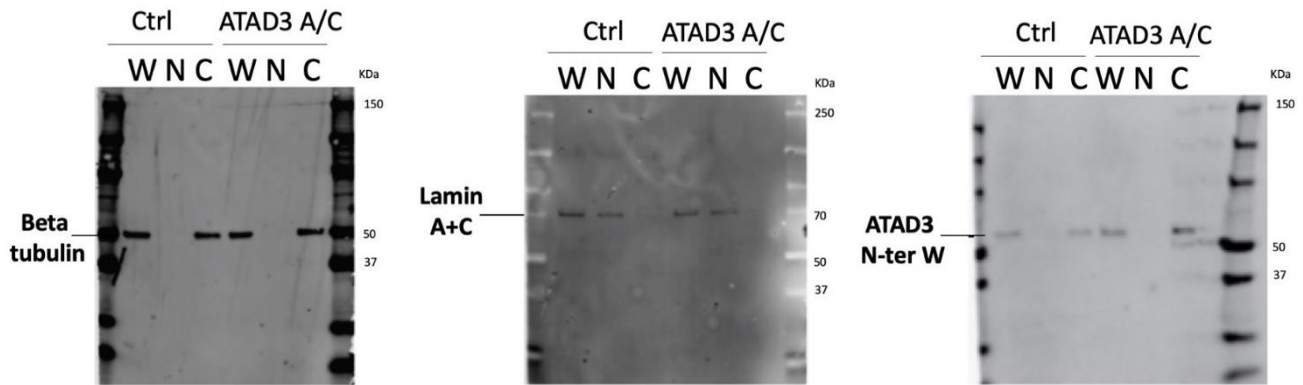


Figure 8. Western blot analysis of cell fractions with the Walker N-ter ATAD3 antibody detects the protein exclusively in the cytoplasm. ATAD3 A/C mutants and control (ctrl) cells were fractionated following the REAP method (Suzuki et al., 2010) and the proteins from the obtained fractions (whole-cell, W, nuclear, N and cytoplasmic, C) were immunostained in separate blots with beta tubulin and lamin A+C, as controls for the fractionation protocol, and the anti-ATAD3 N-ter W antibody. Images were acquired using Typhoon.

We also checked the detection of the anti-ATAD3 N-ter W and P antibodies in several *ATAD3* mutants versus controls by Western Blotting. Immunoblots revealed that the expected 66 and 72 kDa bands corresponding to ATAD3A and ATAD3B / hyperphosphorylated-ATAD3A, respectively (Fang et al., 2010; Li et al., 2014), as well as the specific bands that characterize the different mutants (see section 1.2), could be detected with both antibodies, but no other band revealing the presence of other variants/proteins was detected in either of the blots (Fig. 9).

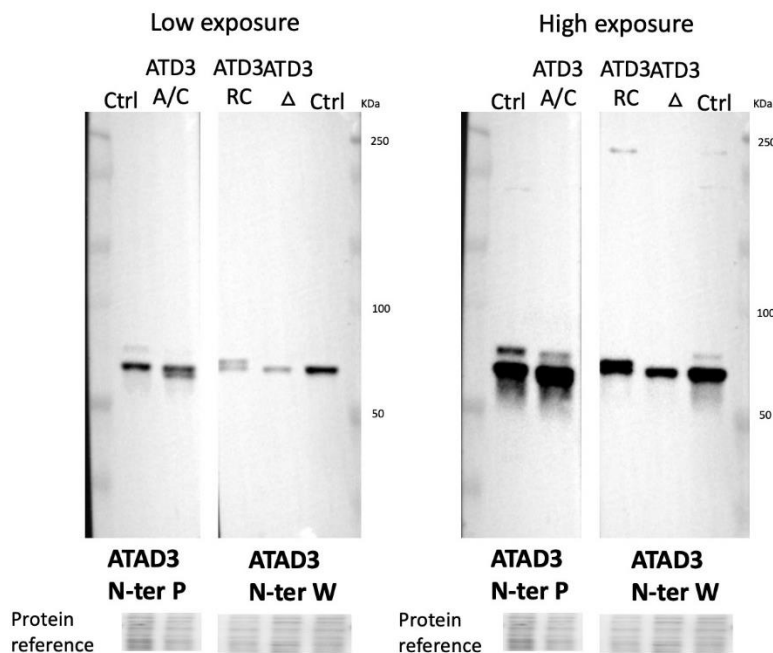
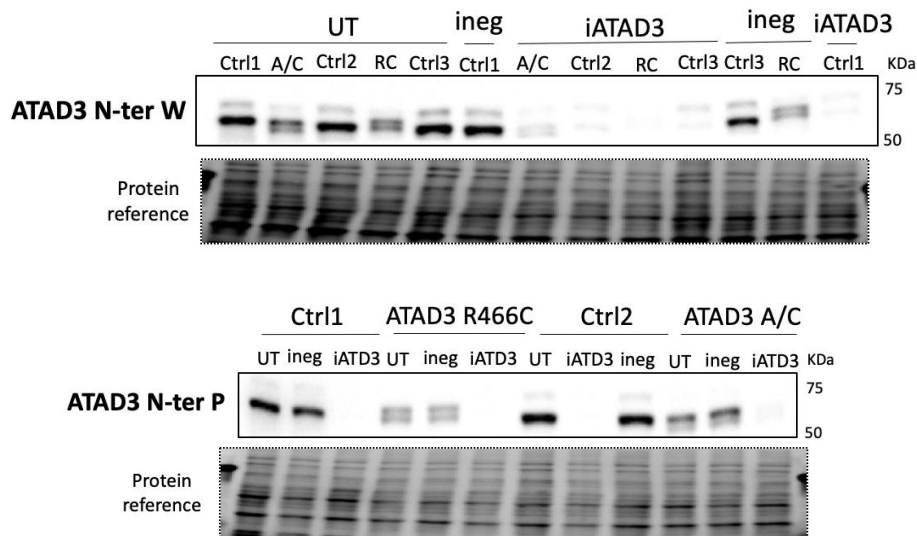


Figure 9. Walker (W) and Proteintech (P) N-ter ATAD3 antibodies exclusively label ATAD3 by western blotting. 8% SDS-PAGE of whole cell protein from controls (ctrl), ATAD3 R466C (ATD3 RC), ATAD3A/C (ATD3 A/C) and ATAD3 Δ (ATD3 Δ) mutant cell lines, combined with long running times and lower exposures, were immunolabeled with anti-ATAD3 N-ter W anti-ATAD3 N-ter P antibodies in separate blots. Images were acquired by iBright.

At this point the likelihood that the custom-made antibody could detect a protein other than ATAD3 was high. To check that, we silenced *ATAD3A* by RNA interference (RNAi) (Fig. 10A) and observed by ICC that the anti-ATAD3 N-ter W signal that localized to mitochondria was greatly diminished, whereas the nuclear and perinuclear punctate stain persisted, and the latter colocalized with EEA1 (Fig. 10B).

A



B

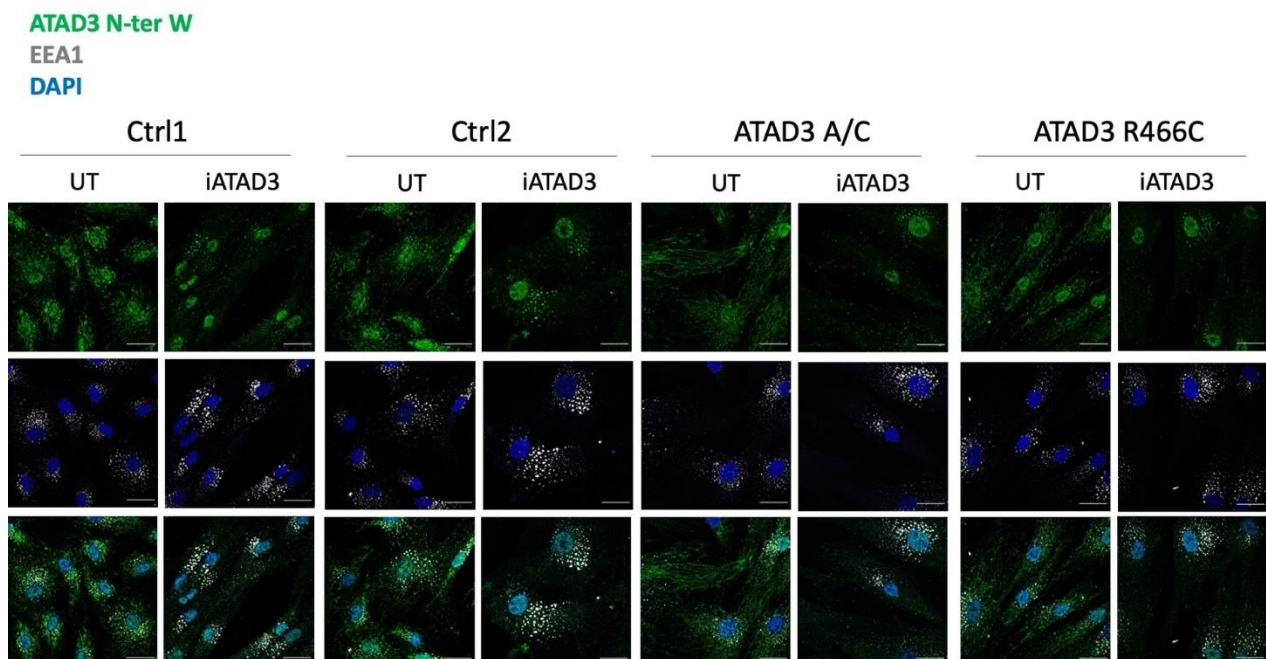


Figure 10. Gene silencing of *ATAD3A* markedly decreased *ATAD3* signal by Western blotting but the nuclear and extra-mitochondrial foci detected by immunofluorescence persisted. (A) 8% SDS-PAGE of whole cell protein from controls (ctrl), *ATAD3* R466C (RC) and *ATAD3A/C* (A/C) mutant cell lines, were immunolabeled with anti-*ATAD3* N-ter P (left blot) and anti-*ATAD3* N-ter W (right blot) antibodies. Each of the cell lines was analyzed when *ATAD3A* was silenced by one of two specific silencers for two rounds of 96 h (i*ATAD3*), versus a silencing control (ineg) and untreated cells (UT). Images were acquired by iBright. **(B)** *ATAD3* A/C and R466C mutants and controls (ctrl) were co-stained with the Walker N-ter *ATAD3* antibody (green), and early endosome antigen 1, EEA1 antibody (gray) by confocal microscopy after *ATAD3A* RNAi (i*ATAD3*) vs. untreated (UT). In blue are the nuclei stained with DAPI.

This indicates that this antibody labels *ATAD3A* and its signal is highly decreased when the protein is silenced, but it also shows that the remaining extra-mitochondrial signal corresponds to something other than *ATAD3A*, which could be *ATAD3B*. However, the *ATAD3B* specific antibody did not stain the perinuclear foci, but it did produce staining reminiscent of the ER, as well as the mitochondria (Fig. 11).

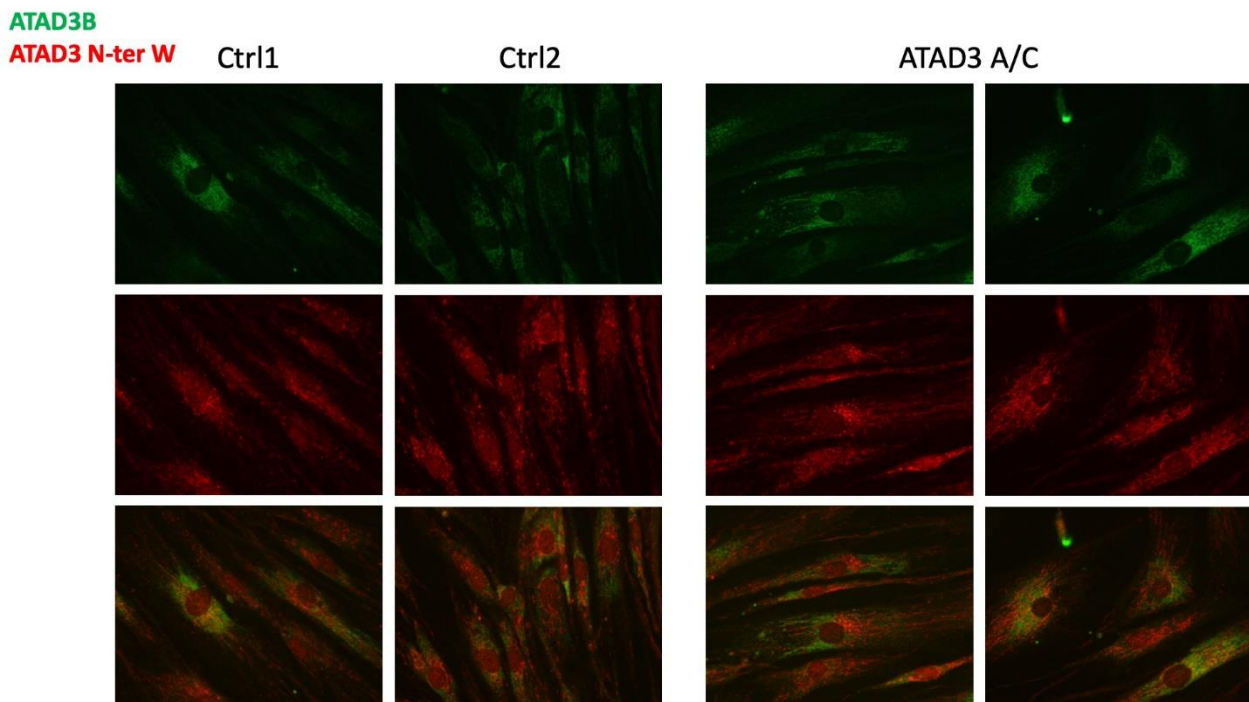


Figure 11. An antibody to *ATAD3B* partly colocalized with anti-*ATAD3* N-ter W, and displayed a distribution reminiscent of the endoplasmic reticulum. *ATAD3* A/C mutants and controls (ctrl) were co-stained with an antibody specific for *ATAD3* N-terminal (red) and an antibody specific for *ATAD3B* (green) by epifluorescence microscopy.

Thus, we next did a co-staining of the *ATAD3B* specific antibody and an antibody that labels the ER chaperone BIP/GRP78, to confirm the colocalization with the ER.

But we also included primary cells from ATAD3 Δ patients and immortalized mouse embryonic fibroblasts (MEF), because these cells do not express ATAD3B. In this experiment, we also treated the cells with the UPR inducer, 2-deoxyglucose (2DG) to enhance the GRP78 signal (Pantic et al., 2021). We observed that the ATAD3B specific antibody colocalized with GRP78 (and thus ER) but there also was signal that did not colocalize with GRP78, confirming its localization to both ER and mitochondria (Fig. 12). However, we also detected signal both in ATAD3 Δ cells and MEFs (Fig.12), indicating the antibody labels ATAD3A or another protein and it is not specific to ATAD3B. Therefore, we could not confirm the punctate phenotype being ATAD3B protein.

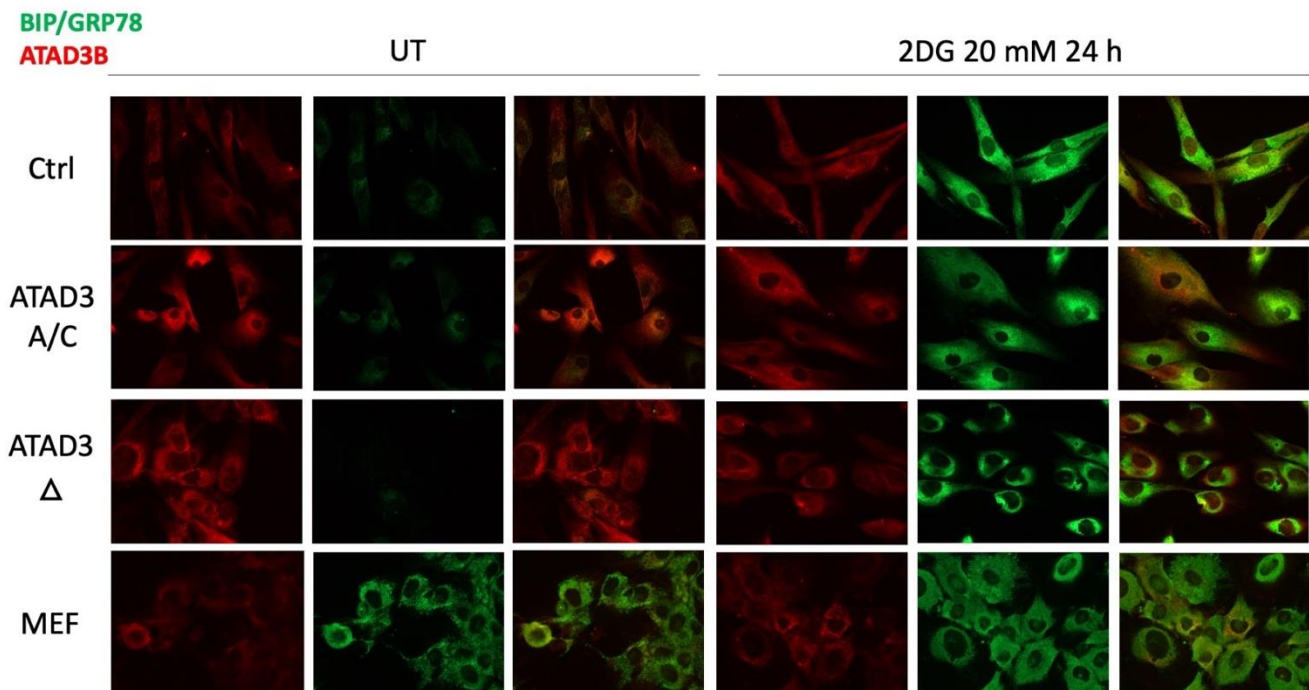


Figure 12. The anti-ATAD3B staining of the endoplasmic reticulum is unrelated to ATAD3 protein as the signal is equally strong in ATAD3 Δ cells and mouse embryonic fibroblasts. ATAD3 A/C and ATAD3 Δ mutants, controls (ctrl) and mouse embryonic fibroblasts (MEFs) were treated without (UT) and with 2-deoxyglucose (2DG), the latter to induce GRP78 signal, and co-stained with an antibody specific for ATAD3B (red) and another for the endoplasmic reticulum protein BIP/GRP78 (green) by epifluorescence microscopy.

R1.4- Mitochondria and mitochondrial DNA phenotypes in ATAD3 mutant human primary fibroblast

Mitochondrial network morphology was observed by labeling the OMM protein TOMM20 via ICC. Control fibroblasts typically displayed a mitochondrial network extending throughout the cytoplasm (Fig. 13). In contrast, many ATAD3 mutant cells had altered mitochondrial morphology, either because the mitochondria network was fragmented or clumped (Fig. 13).

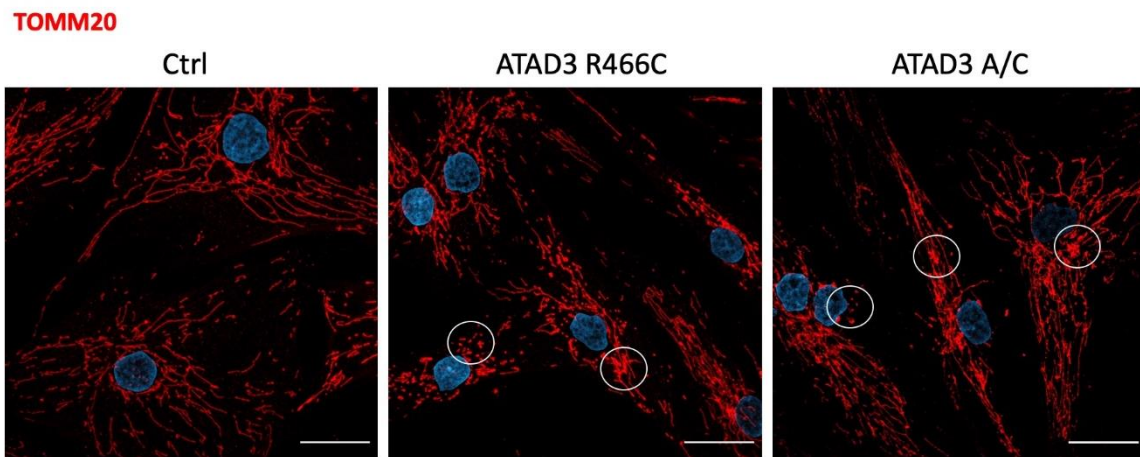
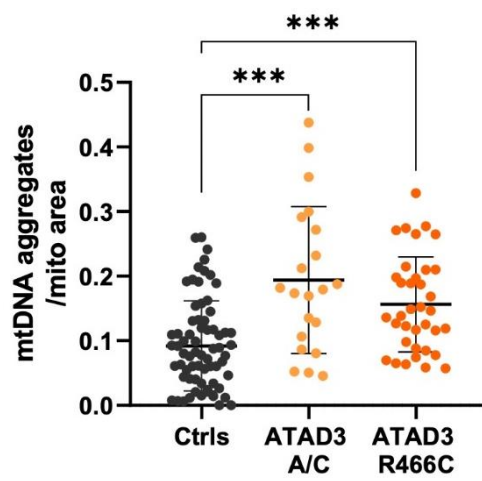
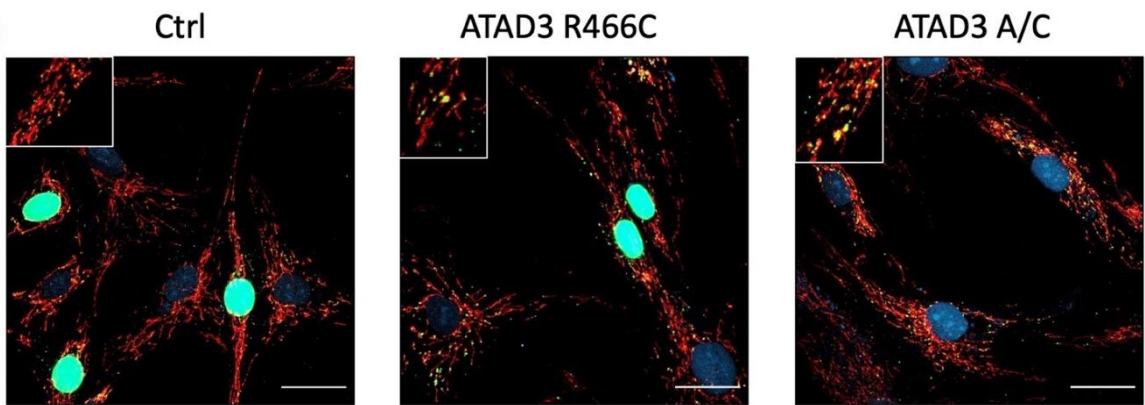


Figure 13. ATAD3 mutant fibroblasts display mitochondrial clumping. Confocal images of control cell lines (Ctrl) and fibroblasts from ATAD3 mutants (R466C and A/C) labeled with an antibody to the outer mitochondrial membrane protein TOMM20 (red) to stain the mitochondrial network. Circles show aberrant mitochondrial morphology - clumping and fragmentation.

Clumping of mitochondria can be related to mtDNA aggregation (e.g. Desai et al., 2017), and altered mtDNA distribution and organization were evident when mtDNA was labeled either with an anti-DNA antibody or an anti-bromodeoxyuridine antibody that binds to the thymidine nucleoside analogs of bromodeoxyuridine (BrdU) that are incorporated in replicating mtDNA when it is provided as a supplement to the culture medium. Compared to control cells, which have mtDNA molecules spread throughout the mitochondrial network that extends across the cell, many *ATAD3* mutant cells contained mtDNA aggregates (Fig.14A and B), suggesting that mtDNA segregation and distribution was impaired as a result of the mutant *ATAD3*. This phenotype is variable and depends on the status of the cells in culture (see Discussion).

A

BrdU
TOMM20
DAPI



B

antiDNA
TOMM20
DAPI

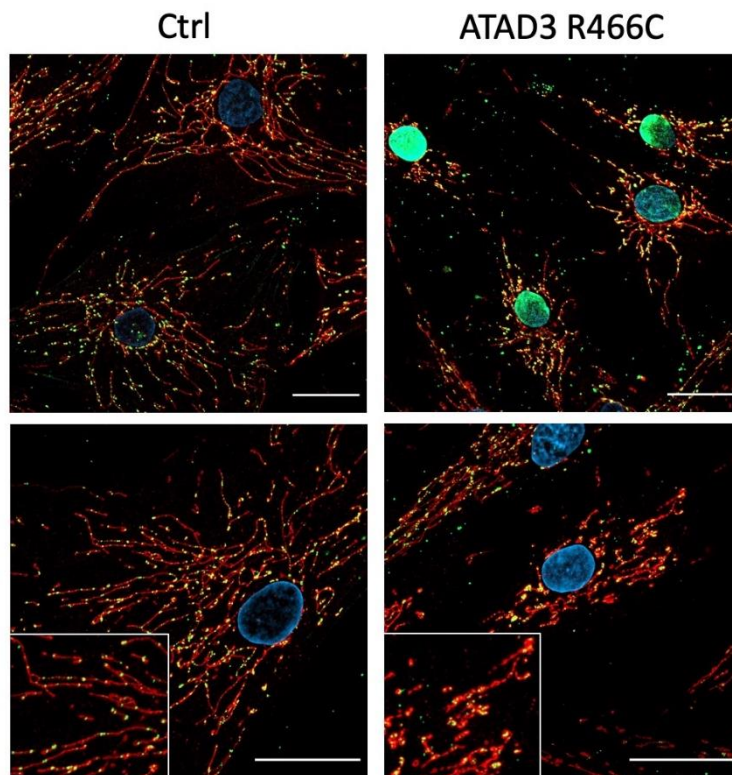


Figure 14. ATAD3 mutant fibroblasts display mitochondrial DNA aggregation. (A) Control (Ctrl) and ATAD3 A/C and R466C mutant fibroblasts immunostained with anti-TOMM20 (red) and anti-BrdU (green), after 50 μ M BrdU supplementation for 12 h and acquired with a confocal microscope at 40x magnification. Boxes are digital zooms showing mtDNA aggregates (in ATAD3 mutant lines). The chart indicates the extent of mtDNA foci aggregated per unit area of TOMM20 in control (ctrl) cells and cells carrying mutant ATAD3 (>30 cells per line; *** $p < 0.001$). **(B)** As panel A, except that the DNA was labeled with anti-DNA antibody, in control (Ctrl) and ATAD3 R466C mutant cells. Lower part images are microscope magnifications with the 63x objective. In blue are the nuclei stained with DAPI.

Although the BrdU-labeling confirmed the mtDNA aggregation phenotype (Fig. 14A), this was not its primary purpose. A pulse labeling of mtDNA with BrdU is an established method of assessing mtDNA synthesis rate (e.g. Pantic et al., 2021). As there was no difference between the BrdU signal of the ATAD3 mutants and controls after a 12 hour pulse, the replication of mtDNA is unimpaired in the ATAD3 mutant fibroblasts, at least under standard culture conditions. Despite the mtDNA aggregation, *ATAD3* mutants had similar levels of mtDNA as control cells, and if something they showed a greater signal, especially ATAD3 A/C cells, (Fig. 14A) rather than a decrease that would be related with a depletion in mtDNA. However, ICC is an imprecise way to measure the level of mtDNA and so, the number of mtDNA copies per cells was quantified by RT-qPCR methodology, the same way as done with *SPG7* mutants in a previous publication by us (De la Casa-Fages et al., 2019) and other groups (Dalla Rosa et al., 2016). The qPCR estimated mtDNA copy number of fibroblasts harboring *ATAD3* mutations was undistinguishable from controls (Fig. 15A and B), as was the abundance of the mtDNA packaging protein, mitochondrial transcription factor A (TFAM) measured by Western Blotting (Fig. 15C). Hence, neither mtDNA synthesis nor copy number seem to be deeply affected by mutant *ATAD3* in proliferating human fibroblasts.

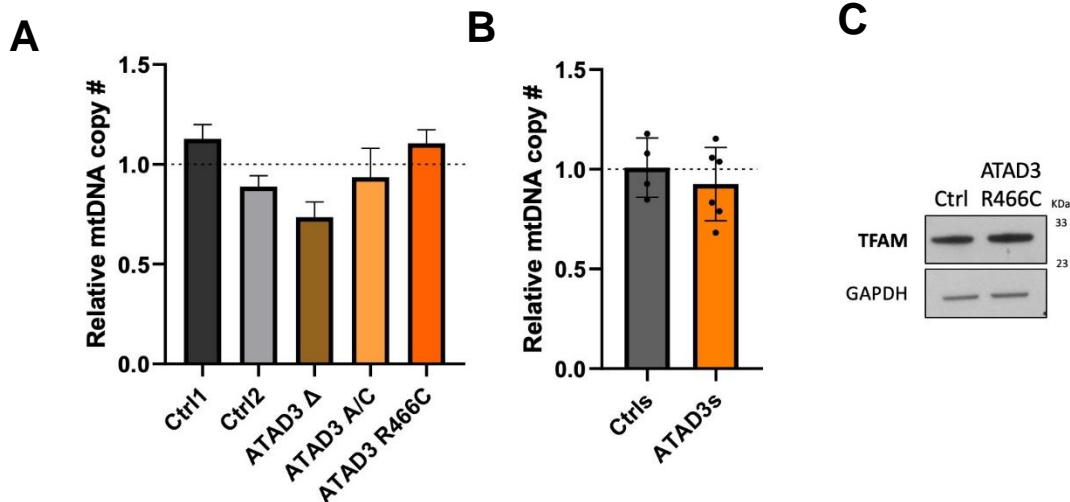


Figure 15. ATAD3 mutants have near normal mitochondrial DNA copy number. (A) Relative mitochondrial DNA (mtDNA) copy level expressed relative to the mean of two controls (ctrl1 and ctrl2) in ATAD3 R466C (dark orange), ATAD3 A/C (pale orange) and ATAD3 Δ (brown) mutant fibroblasts. **(B)** Relative mitochondrial DNA (mtDNA) copy level expressed relative to the mean of controls (gray) versus all three ATAD3 mutants (orange). **(C)** Protein extracted from controls (ctrl) and ATAD3 R466C mutants was separated by 11-12% SDS-PAGE and subsequently immunostained with anti-TFAM (transcription factor A, mitochondrial). GAPDH was used as a loading control.

At the boundary between the matrix and the intermembrane space, in the IMM, cristae greatly expand the surface area where respiratory chain proteins are embedded, augmenting the energy production capacity of the organelle. Mice lacking *Atad3* display disrupted cristae in the mitochondria of their muscle and consequently they suffer an OXPHOS impairment (Moraes 2018 J Cell Sci). On the other hand, cells with the *ATAD3* duplication do not manifest OXPHOS deficiency (Frazier et al., 2021), whereas they do display other abnormalities that are described in detail later in this chapter. Hence, *ATAD3* dysfunction does not seem to be primarily related to cristae maintenance. Nevertheless, we did a rough approximation and checked the status of cristae in *ATAD3* mutant cells by looking at the ultrastructure of the mitochondria via transmission electron microscopy. The images revealed most of the cristae were indistinguishable from controls in most of the mitochondria from the *ATAD3* mutant cells; however, a small fraction of mitochondria, estimated at 10%, was dysmorphic with swollen mitochondria containing few or truncated cristae (Fig.16).

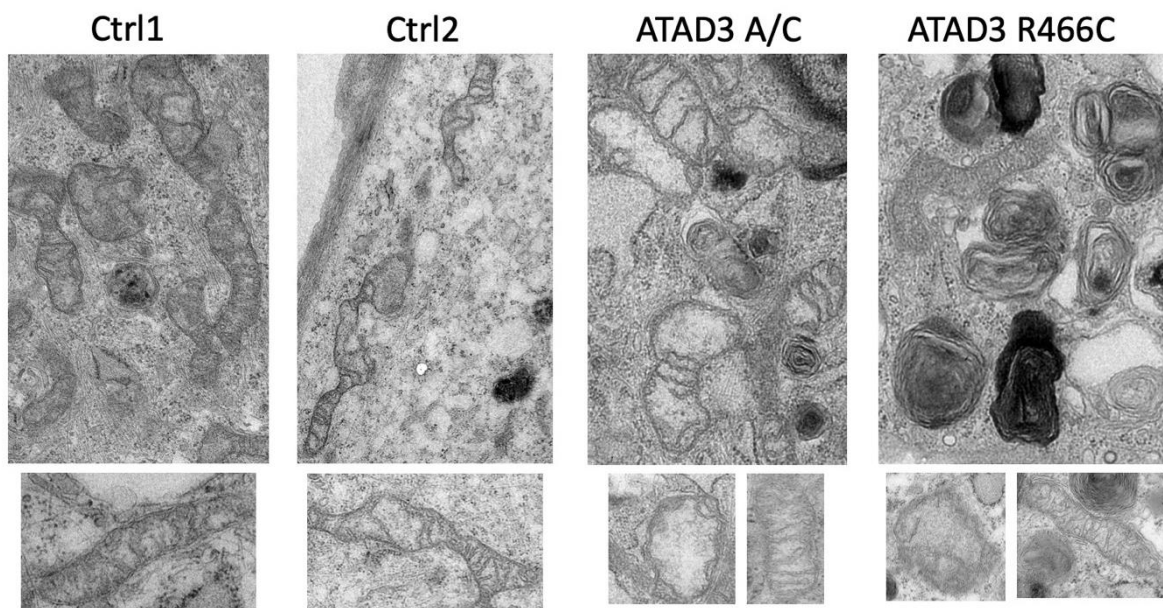


Figure 16. Mitochondrial ultrastructure is similar in controls and ATAD3 mutants, although more aberrant or sparse cristae were detected in the mutants. Transmission electron micrographs of ATAD3 A/C and ATAD3 R466C mutants and control fibroblasts showing mitochondria at different magnifications. In ATAD3 mutants the lower left image shows aberrant mitochondria and the lower right normal-cristae mitochondria.

Mitochondrial crista protein MIC60 or MITOFILIN was also checked by ICC and showed a similar distribution in ATAD3 mutants compared to control cells, thus another indication that cristae structure was not heavily impaired in these ATAD3 mutants (Fig. 17).

A

MIC60/MITOFILIN

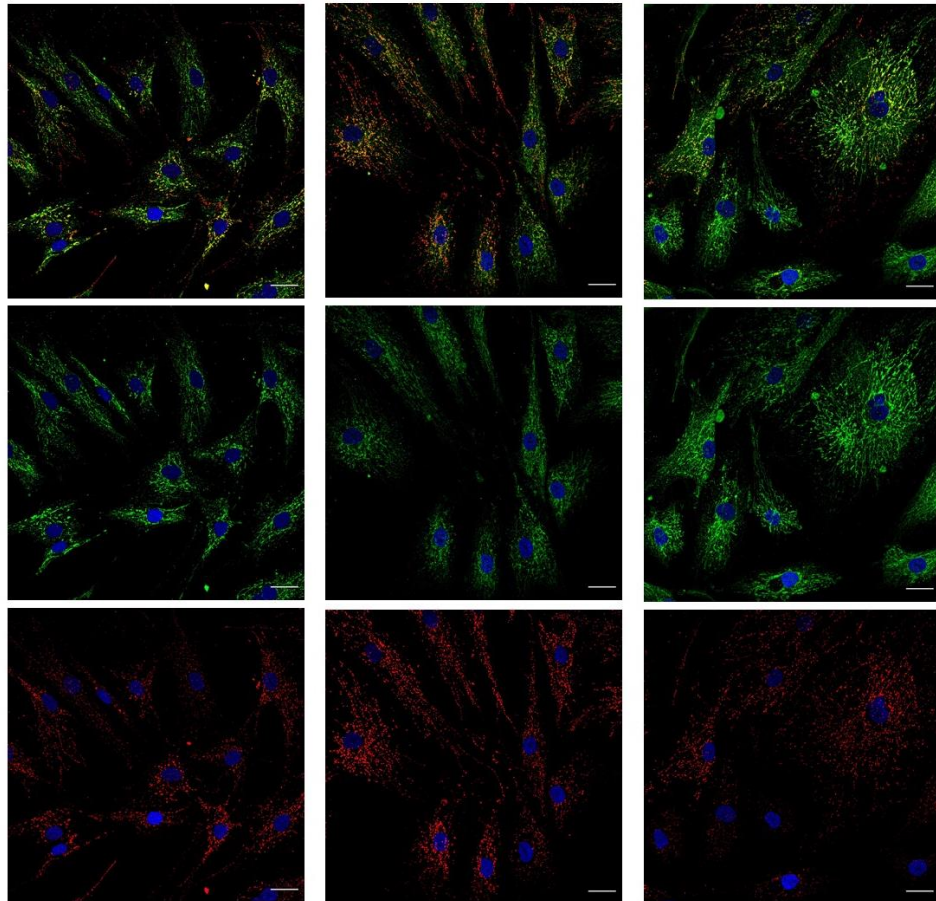
UCP2

DAPI

Ctrls

ATAD3 A/C

ATAD3 R466C



B

MIC60/MITOFILIN

DAPI

Ctrl

ATAD3 A/C

ATAD3 R466C

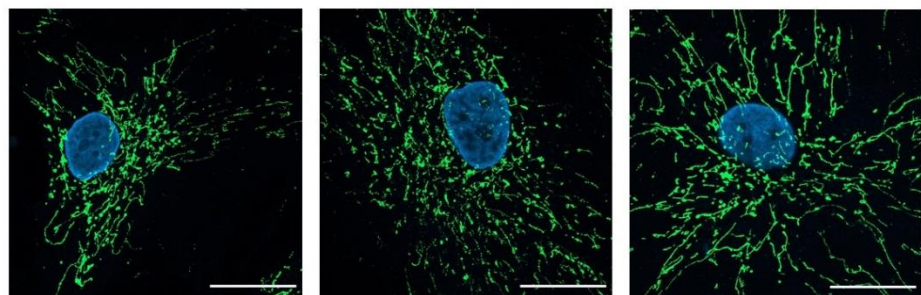
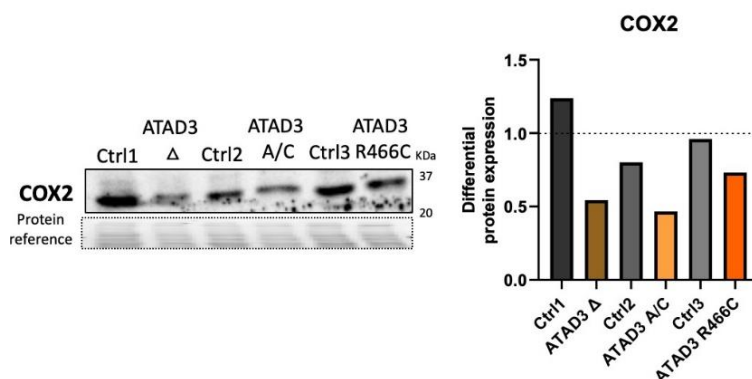


Figure 17. Mitochondrial cristae protein MIC60 shows normal signal and distribution in ATAD3 mutant cells. (A) Mitochondrial crista protein MIC60/MITOFILIN (green) was co-stained together with mitochondrial uncoupling protein 2 (UCP2) in control (ctrl) and ATAD3 A/C and ATAD3 R466C mutant fibroblasts and images were acquired by confocal microscopy. In blue are the nuclei stained with DAPI. **(B)** Microscopy magnifications with 40x objective show MIC60/MITIFOLIN distribution in the control (ctrl) and ATAD3 A/C and ATAD3 R466C mutant fibroblasts. In blue are the nuclei stained with DAPI.

OXPPOS deficiency is a central component of the majority of mitochondrial disorders, and while severe deficiencies are often associated with aberrant or scarce cristae, respiratory chain deficiency is not always directly proportional to cristae. Therefore, we evaluated OXPPOS and energy production in ATAD3 mutants. First, some of the key components of the respiratory chain complexes were analyzed, two proteins of complex IV (COX II and COX IV) and two proteins of complex I (NDUFB8 and NDUFB9), which are the most affected complexes in mitochondrial diseases (see introduction). The steady-state level of the two complexes was lower for ATAD3 A/C mutants as the abundance of all the proteins studied was lower than in controls (Fig. 18), and in some experiments, the decrease in expression in some subunits was equal to that of cells harboring high levels of pathological m.3243A>G, which display severe OXPPOS dysfunction (Pantic et al., 2021).

In contrast, ATAD3 R466C mutants did not show any difference in the abundance of these proteins (Fig. 18) suggesting that complex I and IV were normal in the case of this ATAD3 mutant. For ATAD3 Δ mutants, it has already been reported they have a lower expression of several OXPPOS proteins as the GSEA analyses revealed after RNA-seq and also because the abundance of COXII and NDUFB9 subunits is lower than in control cells (Fig. 18), as reported by (Desai 2017 Brain). Lastly, our collaborators in London, Dr. Taanman (University College London), have carried out a preliminary OXPPOS analysis of the ATAD3 R466C cells and found that respiratory chain enzymes activities are within the normal range (data not shown).



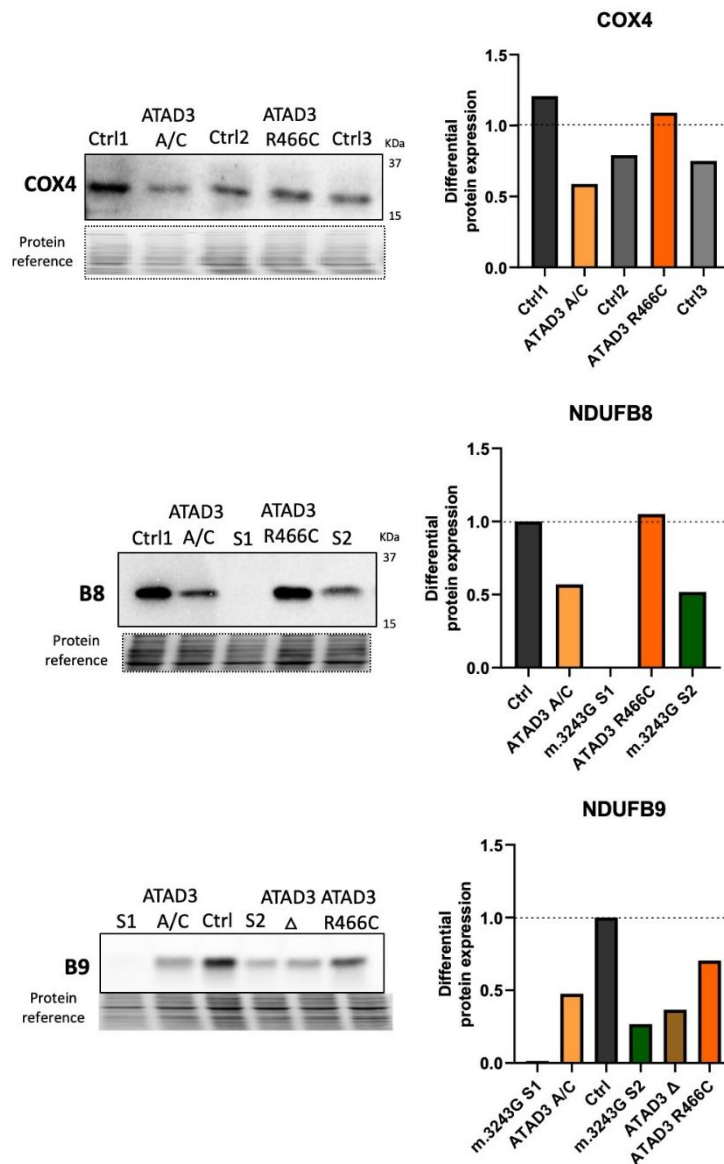


Figure 18. ATAD3 A/C and ATAD3 Δ have lower levels of OXPHOS complex I and IV proteins, while those of ATAD3 R466C are similar to controls. Controls (ctrl), ATAD3 A/C, ATAD3 Δ and ATAD3 R466C mutants and fibroblasts with m.3243G of subjects 1 and 2 (S1 and S2) that have OXPHOS severely affected, especially subject S1, were separated by SDS-PAGE and immunoblotted for components of respiratory complexes I (NDUFB8 and B9) and IV (COX2 and COX4). Images of the blots were acquired by iBright. Quantification of the blots was done normalizing the band intensity to the protein-reference signal and expressed relative to the mean of the control(s).

Additionally, energy production was measured either by a luminescence assay that reports the ATP levels in cells or by the oxygen consumption and media acidification levels via the Seahorse assay. We observed there were differences among the ATAD3 mutant cell lines. ATAD3 Δ mutants showed higher ATP levels (Fig. 19A), but they were not included in the Seahorse experiments, whereas ATAD3A/C cells showed similar ATP levels to controls (Fig. 19A) but they showed lower oxygen consumption rate (OCR) in Seahorse, close to the m.3243G S2 patients (Fig. 19B). It should be noted that m.3243G S1 patients, showed an even lower ATP and OCR

levels (Fig. 19A and B) and they have OXPHOS severely affected, as reported by (Pantic et al., 2021). On the contrary, ATAD3 cells with the R466C mutation did not show any noticeable alteration in the ATP production, and their ATP and OCR levels were similar to control cell lines (Fig. 19A and B). Therefore, we observe a correlation of the severity of the disease produced by the type of mutation or genetic rearrangement in the ATAD3 genes, and the level of impairment in the OXPHOS system that produces energy, being the ATAD3 Δ and ATAD3A/C mutants the most affected ones and the ones that show less ATP amounts.

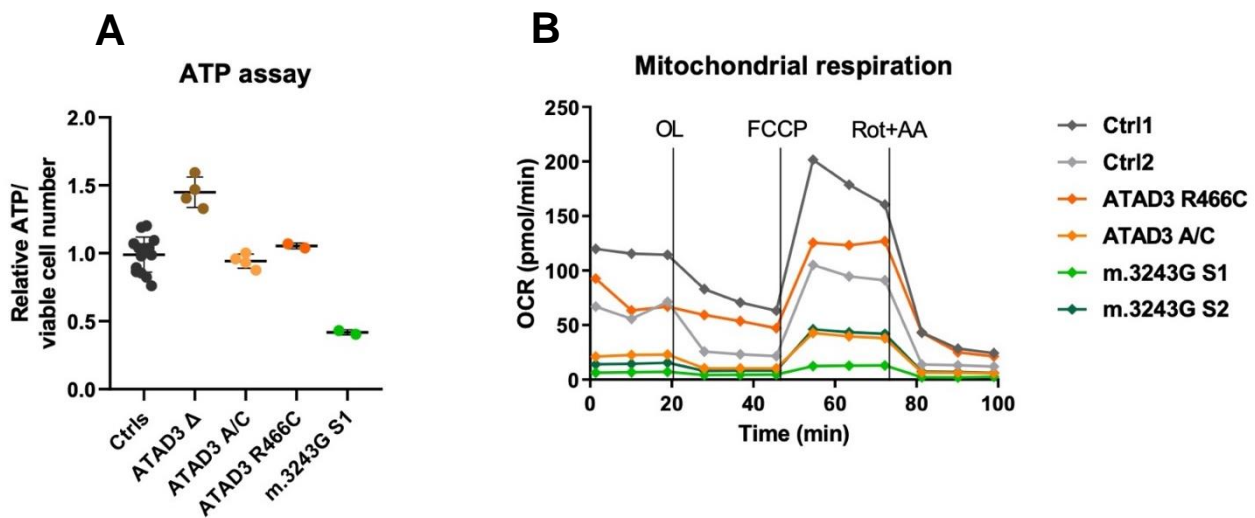


Figure 19. ATAD3 A/C but not R466C has a reduced oxygen consumption rate. ATP (A) and mitochondrial respiration (B) were measured in controls (ctrl), ATAD3 A/C, ATAD3 Δ and ATAD3 R466C mutants and fibroblasts with the MELAS mutation m.3243G subject 1 and 2 (S1 and S2). (A) a luminescent assay (Promega) that measures ATP by Glomax normalized to the viable cells. Values were expressed relative to the mean of controls. (B) Oxygen consumption rate (OCR) of the cells measured using a XF-flux analyzer, Seahorse Instrument. Drugs used in the assay: oligomycin (OL), a respiration uncoupler (FCCP) and rotenone plus antimycin A (Rot+AA).

R1.5- Extra-mitochondria effects of ATAD3 mutants

R1.5.1-Free cholesterol accumulation and the expression of proteins implicated in cholesterol metabolism.

ATAD3 was first linked to cholesterol metabolism by its implication in steroid biosynthesis (Gilquin et al., 2010). Flies lacking *Atad3* have a severe developmental problem and ATAD3 was linked with the transport of cholesterol to mitochondria for

the conversion to pregnenolone, as the first step in steroid hormone biosynthesis (Gilquin et al., 2010 & Rone et al., 2012). Later, it was shown that ATAD3 was involved in the formation of specific cholesterol-rich membrane domains that facilitated Twinkle-nucleoid attachment (Gerhold et al., 2015). Transcriptome analysis of patients with the biallelic deletion in ATAD3 (ATAD3 Δ) also revealed that cholesterol metabolism was one of the most altered pathways and this patient's cells showed elevated intracellular unesterified cholesterol, similar to that found in patients with Niemann-Pick type C disease or control cells treated with the cholesterol trafficking inhibitor compound U18666A (U18) (Desai et al., 2017). Therefore, we checked the intracellular free cholesterol levels using Filipin III in the fibroblasts from the three available *ATAD3* mutants, and discovered all had elevated free cholesterol levels (Fig. 20), as seen previously for the deletion mutant. Although there was variability between experiments and depending on the well-being of the cells in culture (affected by parameters like confluency, passage number, nutrients in the media and so on), the filipin signal was invariably higher in the *ATAD3* mutants than the controls and the mean difference was two-fold (Fig. 20). This increase was similar to the induction in controls produced by inhibiting intracellular cholesterol trafficking with U18 (Fig. 20). The levels were similar for all three mutants, and so do not correlate with disease severity or OXPHOS deficiency.

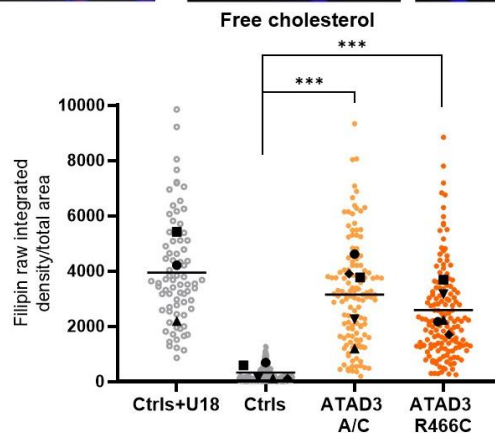
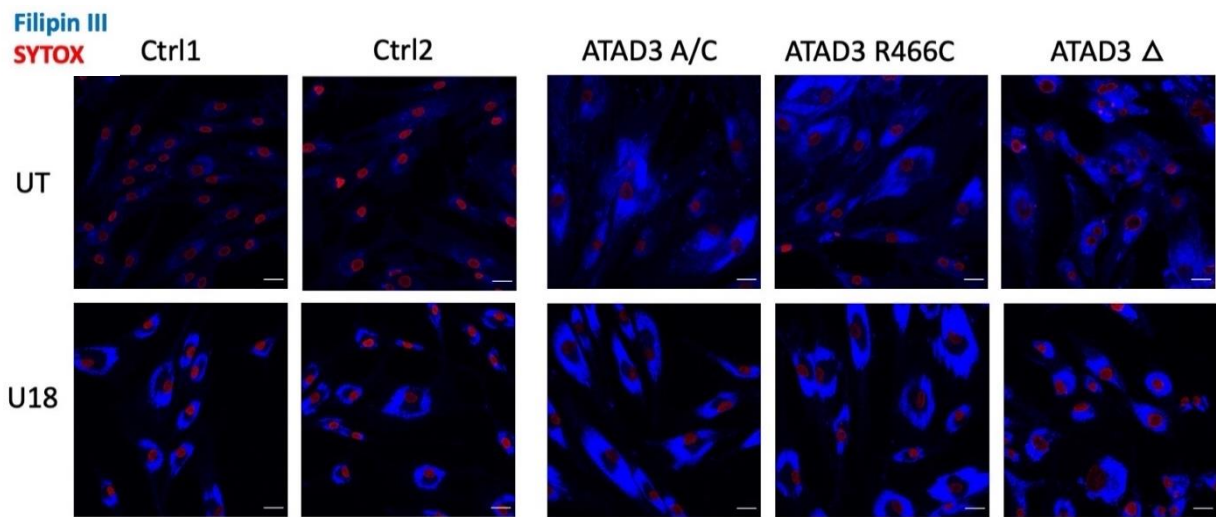


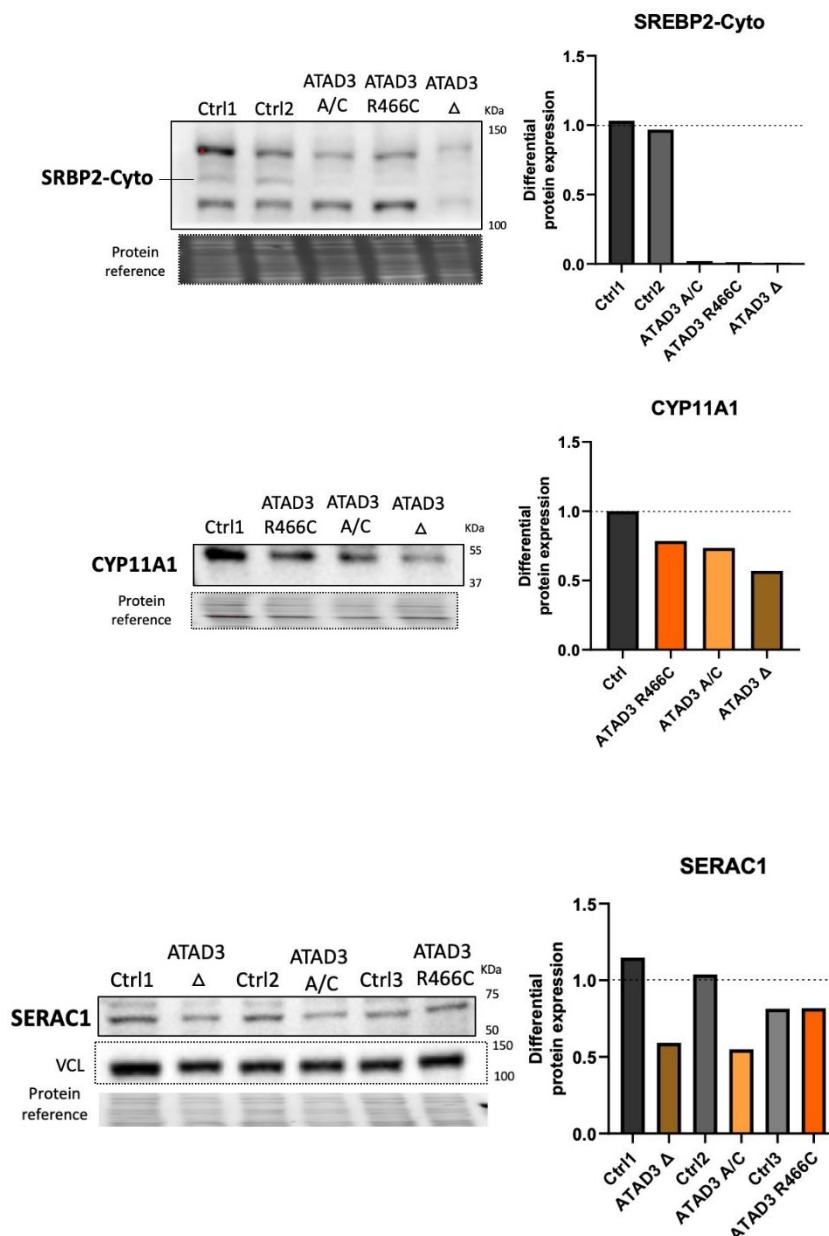
Figure 20. *ATAD3* mutant fibroblasts display elevated unesterified cholesterol. Representative images of Filipin III stained *ATAD3* mutants (*ATAD3* R466C, *ATAD3* A/C and *ATAD3* Δ) and control (Ctrl) fibroblasts, treated with and without the cholesterol trafficking inhibitor U18666A (U18). Quantification of filipin signal (measured as raw integrated density) per total area of the cell, where each point represents a cell and each color a different cell line/condition (>100 cells per line, n=5 independent experiments (represented with different polygons and their mean as a horizontal line), except for Ctrl+U18 where n=3 independent experiments; *** p < 0.001).

In earlier studies in the cells of two patients with mutations in the *ATAD3* gene cluster (one of them *ATAD3* Δ), transcriptomic analysis revealed lipid metabolism as the most altered pathway in endogenous metabolic network analysis, besides the cholesterol pathway, and free-cholesterol was elevated in both to a similar extent (Desai et al., 2017). Therefore, we hypothesized that *ATAD3* mutants universally alter cholesterol homeostasis but they might employ different methods to achieve the same ends.

One way would involve the proteins implicated in the cholesterol biosynthetic pathways. The expression of key enzymes from the pathway of cholesterol biosynthesis was markedly upregulated in *ATAD3* mutants with deletions (Desai et al., 2017). At the protein level, a decrease was detected in the abundance of a cytoplasmic isoform of SREBP2 (Desai et al., 2017), the master regulator of cellular cholesterol synthesis, which is cut at the cytoplasm and translocated to the nucleus to activate cholesterol biosynthesis (Horton et al., 2002). In our hands, *ATAD3* Δ cells also showed a decrease in that cytosolic isoform of SREBP2, as well as *ATAD3* A/C and *ATAD3* R466C cells, but not control lines (Fig. 21A), implying an activation of the cholesterol biosynthetic pathway in *ATAD3* mutant cells. CYP11A1 is a protein involved in the conversion of cholesterol, presumed to be imported by *ATAD3*, to pregnenolone in the mitochondria (Rone et al., 2012). It was one of the most differentially expressed genes in the cells of an *ATAD3* patient (S5) involving severe biallelic genetic rearrangements that led to the deficiency of the *ATAD3B* proteins from the two alleles, but was not that differentially expressed in the cells of *ATAD3* Δ patient (Desai 2017 Brain). Here, when we measured protein abundance in three different *ATAD3* mutants, *ATAD3* Δ , *ATAD3*A/C and *ATAD3* R466C, none showed a substantial difference in CYP11A1 abundance (Fig. 21A). Last, we checked the expression of SERAC1, a protein that has been linked to phospholipid exchange between the endoplasmic reticulum and the mitochondria and is thought to be involved in intracellular cholesterol trafficking (Wortmann et al., 2012). There was some variation in the abundance of SERAC1, but the range in the *ATAD3* A/C and

ATAD3 R466C mutants was similar to controls (Fig. 21A), which suggests SERAC1 expression is not affected in the ATAD3 mutant lines. A decrease, again lower than for S5, was also reported for ATAD3 Δ cells in carboxylestersase 1 (CES1) (Desai et al., 2017), involved in the catabolism of cholesteryl esters (Quiroga et al., 2012). We corroborated those results and observed a subtle decrease in CES1 for ATAD3 Δ cells, but not for ATAD3 A/C cells (Fig. 21B). In the same line, we also checked the expression of lysosomal acid lipase or cholesteryl ester hydrolase (LAL), a protein that converts cholesteryl esters to unesterified cholesterol in the lysosomes and endosomes (Burke & Schubert, 1972). LAL steady-state protein level was reduced in ATAD3 R466C and ATAD3 A/C lines, especially in the latter, (Fig. 21B). This suggests that there might be a shortage of esterified cholesterol in ATAD3 mutant cells, and it strongly argues against the idea that the free cholesterol pool might be a consequence of increased conversion of cholesteryl-esters to free cholesterol.

A



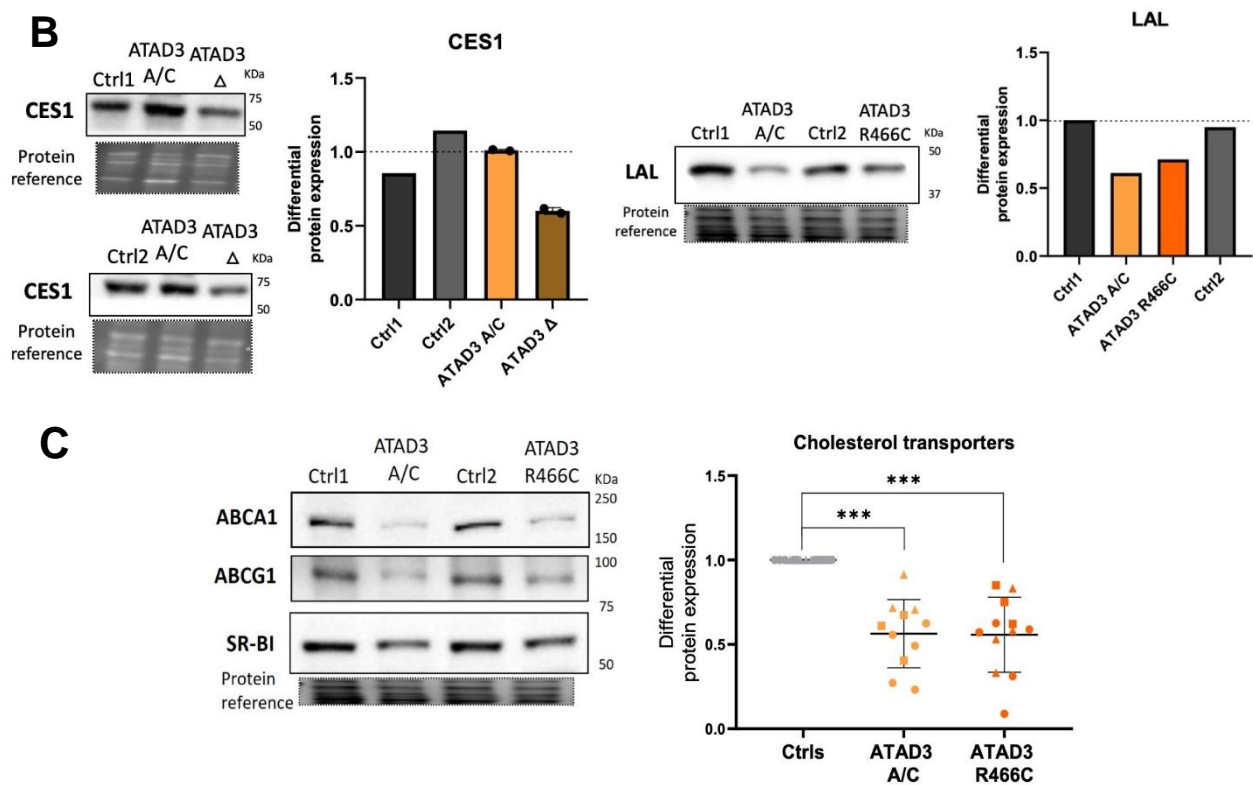


Figure 21. Differential expression of selected proteins involved in cholesterol metabolism in ATAD3 mutant vs. control fibroblast. (A) Controls (ctrl), ATAD3 A/C, ATAD3 Δ and ATAD3 R466C mutants were separated by SDS-PAGE and immunoblotted for key proteins involved in cholesterol metabolism: the cytosolic fragment of the master regulator SREBP2, CYP11A1 involved in steroidogenesis from cholesterol in mitochondria, and SERAC1 related to cholesterol trafficking. Images of the blots were acquired by iBright. Quantification of each blot was done normalizing the band intensity to the protein-reference signal and expressed relative to the mean of control(s). **(B)** Immunoblots of two enzymes involved in cholesteryl ester to free cholesterol conversion like carboxylesterase1 (CES1) and cholesteryl ester hydrolase (LAL), as per panel A. **(C)** Immunoblots of cholesterol efflux proteins (ABCA1, ABCG1 and SR-BI) in ATAD3 R466C and A/C duplication mutants vs. controls. quantification of the three enzymes (circles= ABCA1, squares= ABCG1 and triangles= SR-BI) was done relative to controls where each dot represents an independent experiment and different colors denote each of the cell lines (n=3-5 independent experiments, *** p < 0.001).

Another way of increasing the free cholesterol would be to decrease the efflux of unesterified cholesterol from the cell, which from the four main ways of occurring three are mediated by transmembrane plasma membrane proteins: scavenger receptor class B, type I (SR-BI), and the ATP-binding cassette (ABC) transporters ABCA1 and ABCG1 (Phillips et al., 2014). To determine whether there was a difference in the abundance of these proteins, whole cell protein lysates were separated by SDS-PAGE and after transferring to solid support, immunoblotting revealed that the expression of proteins, ABCA1, ABCG1 and SR-BI, was reduced in the two ATAD3 mutants studied, ATAD3 A/C and ATAD3 R466C, compared to controls (Fig. 21C).

R1.5.2-Neutral lipid accumulation.

Cholesterol metabolism is closely intertwined with other branches of lipid metabolism, such as the previously mentioned steroidogenesis (Gilquin et al., 2010) or neutral lipid metabolism that includes lipid droplets, which have been reported to be accumulated in the neurons of an *Atad3* conditional knockout mouse (Arguello et al., 2021). With that in mind, we wanted to check whether the increase in free cholesterol observed in the ATAD3 mutants was an isolated phenotype or it was rather a general phenomenon affecting other pathways in the lipid metabolism, as well. We used Bodipy™ 493/503 that labels neutral and non-polar lipids with greater accuracy and sensitivity than alternative compounds available in the market, such as Nile Red or Oil Red O (Gozce & Freeman 1994). However, the Bodipy 493/503 signal is barely detectable in most control cell lines, including fibroblasts, exceptions are adipocytes and hepatocytes that contain high levels of non-polar lipids under standard growth conditions. That said, fibroblasts and other cells accumulate neutral lipids and lipid droplets when grown in media supplemented with fatty acids, like oleic or palmitic acid (Rohwedder et al., 2014).

In striking contrast to control fibroblast lines, ATAD3 *mutant* fibroblasts accumulated Bodipy-stained lipids in their cytoplasm in standard culture conditions; i.e., without oleic acid supplementation (Fig. 22). It was important to understand whether the accumulation of free cholesterol was sufficient to trigger an increase in non-polar lipids. Thus, we performed an experiment that affected both the cholesterol biosynthetic pathway, by inhibiting one of its enzymes -oxidosqualene cyclase- with Ro 48-8071 (Ro) and cholesterol intracellular trafficking, by inhibiting NPC1 with U18. Pharmacologically modulating cholesterol metabolism induced a marked increase in free cholesterol in controls (Fig. 23A) similar to that of untreated ATAD3 mutants, while these compounds only had a modest increase in Bodipy signal (Fig. 23B). That said, a colleague has subsequently seen that U18 treatment is accompanied by a substantial increase in Bodipy signal in another cell type (astrocytes), which suggests increased cholesterol levels can provoke altered neutral lipid metabolism, in other conditions or contexts.

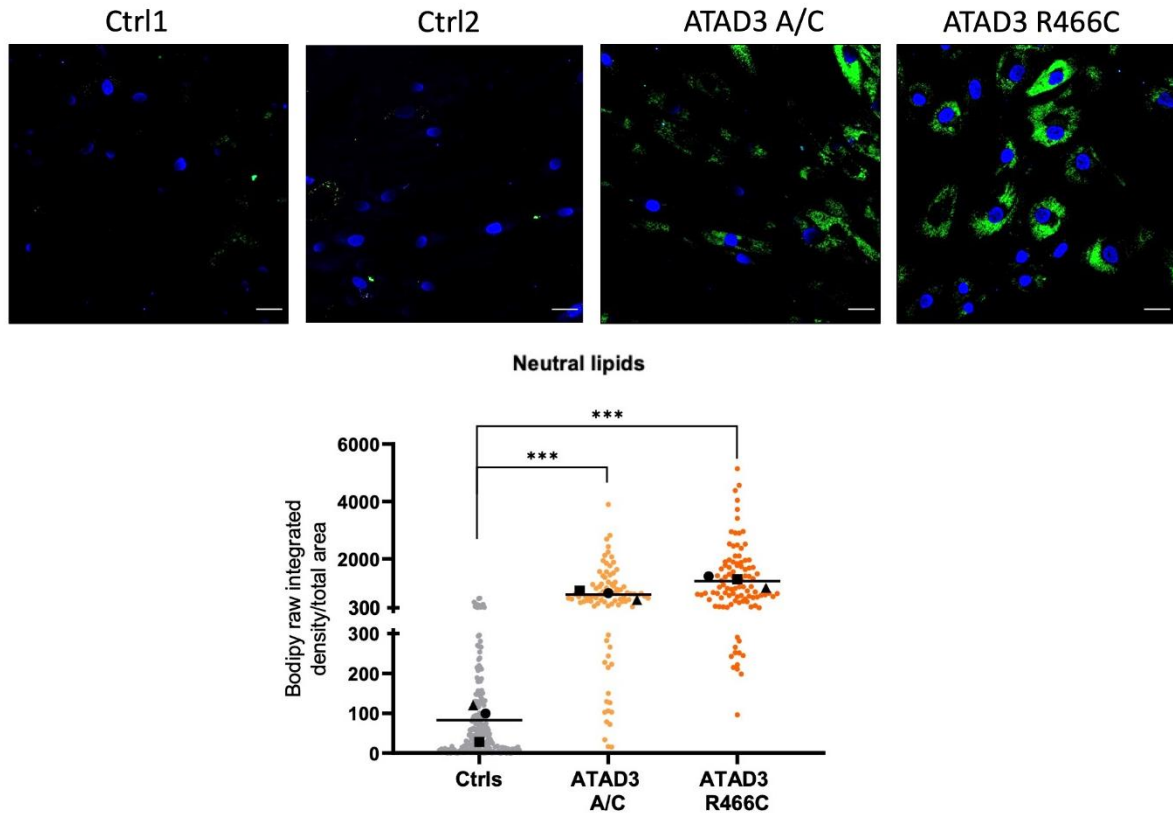
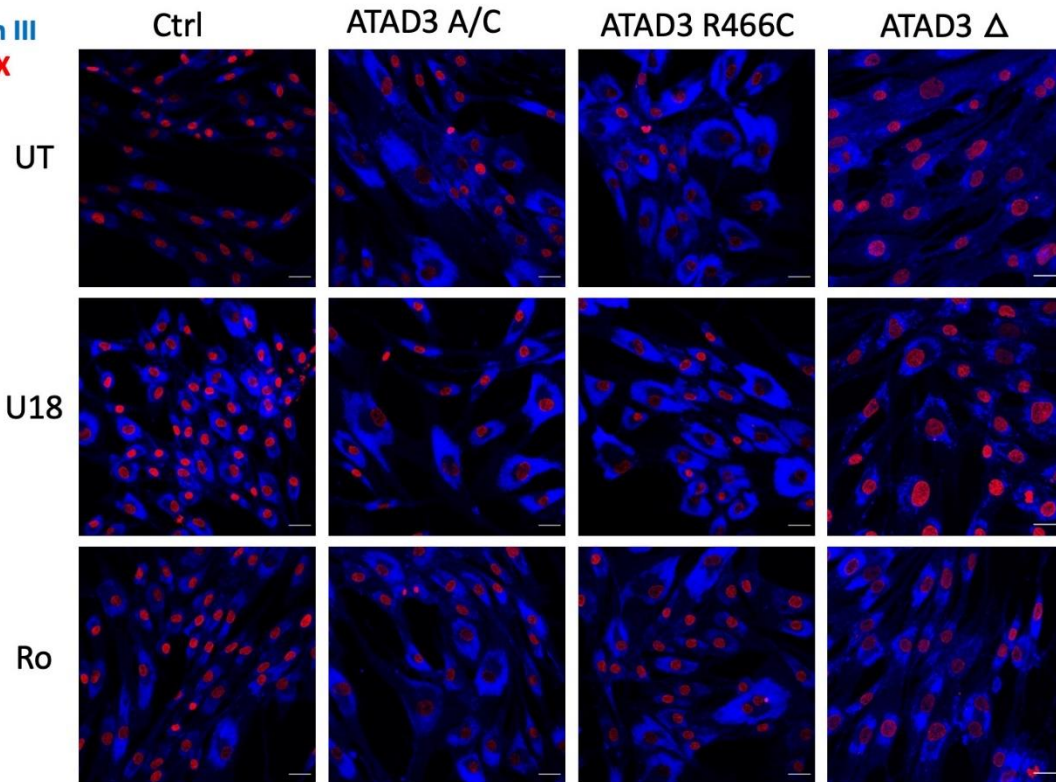
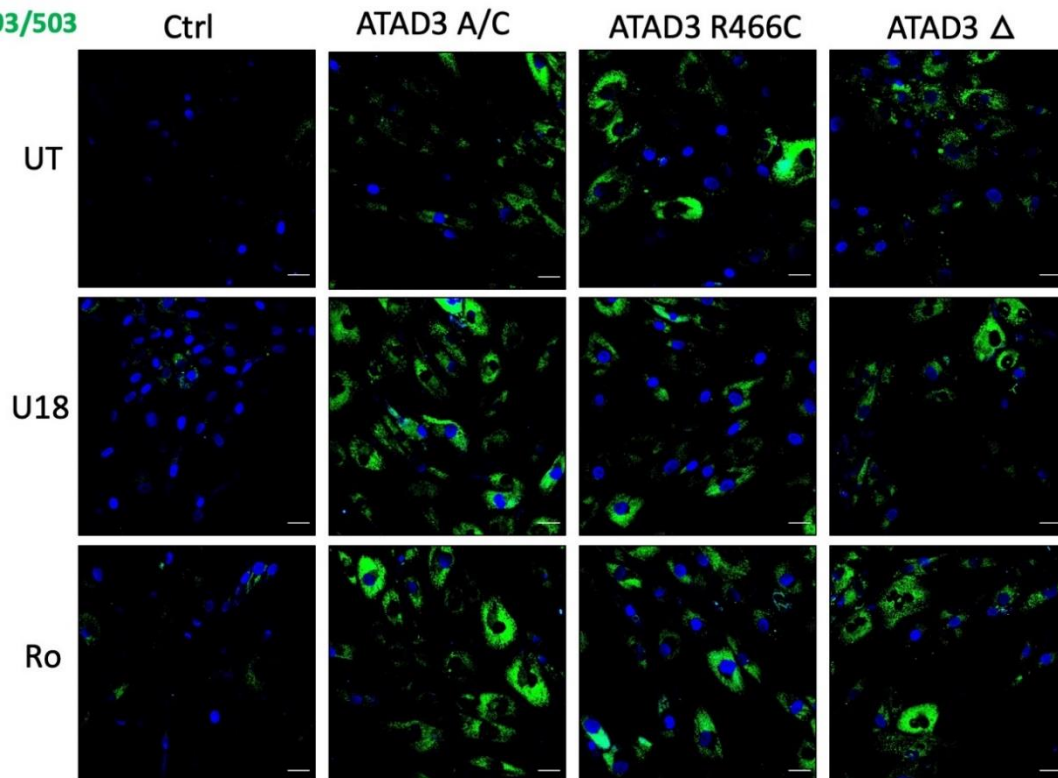


Figure 22. *ATAD3* mutant fibroblasts display elevated neutral lipids. Representative images of control and *ATAD3* mutant fibroblasts grown in standard medium (without oleate) and incubated with BODIPY™ 493/503 to stain accumulated neutral lipids (green) and SYTOX™ Deep Red to mark the nuclei (converted to blue). Chart of Bodipy 493/503 signal (measured as raw integrated density per total area of the cell) from controls and *ATAD3* mutant fibroblasts (> 100 cells per line, n=3 independent experiments; *** p < 0.001 where each of the polygons represent the mean of an experiment).

We also checked the effect of nutrient restriction, respiratory chain impairment and autophagy inhibition on neutral lipid metabolism. We used the glucose analog 2-deoxy glucose (2DG) that reduces glucose and glutamine utilization (Wang et al., 2018), respiratory chain complex I inhibitor rotenone (Rot) and the combination of both (2DG+Rot) which severely inhibits autophagy (Pantic et al., 2021). None of these alterations had an appreciable effect on neutral lipid foci size or abundance (Fig. 24), suggesting neither altered glucose and glutamine utilization, nor respiratory chain insufficiency nor blocked autophagy automatically induces neutral lipid accumulation, at least in the short term.

AFilipin III
SYTOX**B**Bodipy 493/503
SYTOX

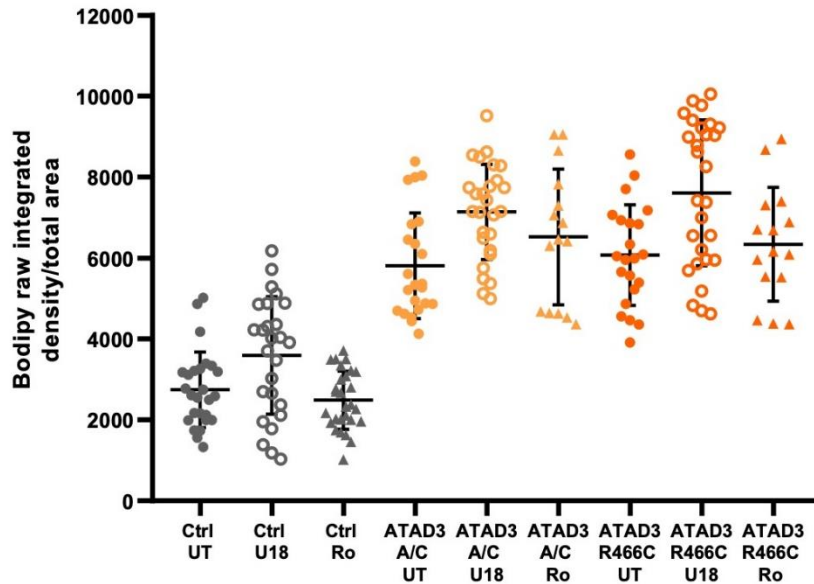


Figure 23. Pharmacological inhibition of cholesterol synthesis and trafficking produces a marked increase in free cholesterol signal in control cells similar to that seen in untreated cells with *ATAD3* mutations, while neutral lipids remain almost unaltered. Control (ctrl) and *ATAD3* mutant cells were treated with or without Ro 48-8071 (Ro) an inhibitor of the cholesterol biosynthetic enzyme, oxidosqualene cyclase, or with U18666A (U18) an inhibitor of intracellular cholesterol trafficking. After 48 h cells were incubated with (A) Filipin III to stain free cholesterol (blue) and SYTOX (red) to label the nuclei or (B) with BODIPY™ 493/503 to stain accumulated neutral lipids (green) and SYTOX™ Deep Red to mark the nucleus (converted to blue). Below a chart of the quantification of Bodipy 493/503 signal (measured as raw integrated density per total area of the cell) from controls and *ATAD3* mutant fibroblasts where each point represents a cell.

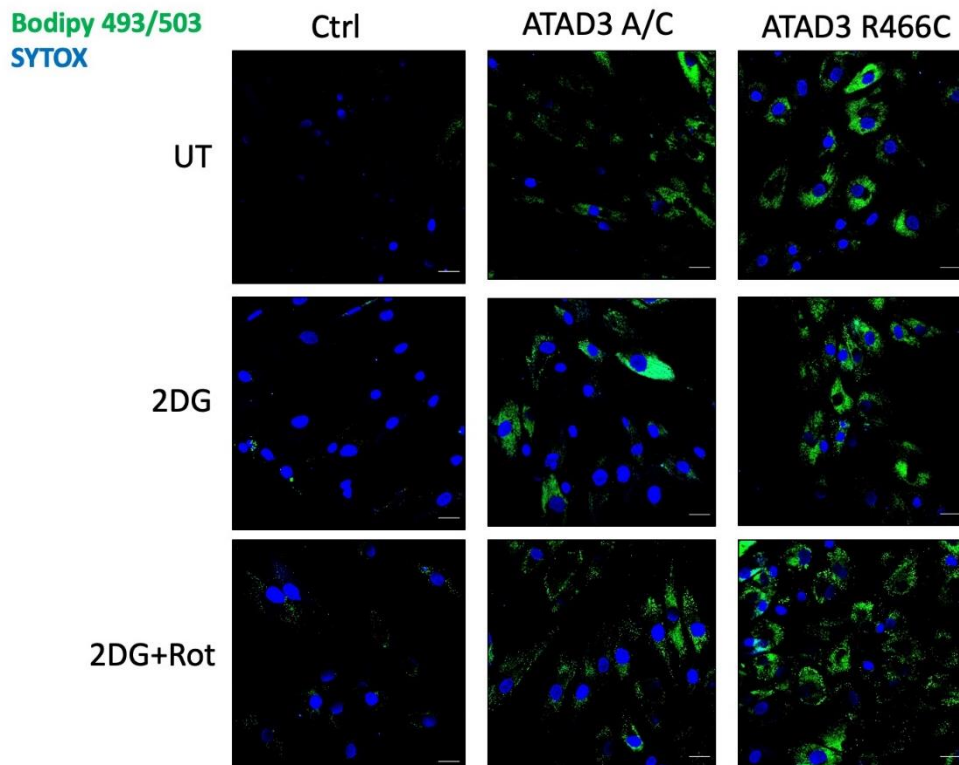


Figure 24. Neutral lipid accumulation is not attributable to inhibition of the respiratory chain or impaired autophagy. 2-deoxy-D-glucose (2DG) alone, to restrict glucose and glutamine utilization, and in combination with inhibition of the respiratory chain (with rotenone, Rot) which blocks autophagy (Pantic et al., 2021), but these treatments have little or no effect on neutral lipid droplet accumulation based on BODIPY™ 493/503 staining (green). Nuclei are labeled with SYTOX™ Deep Red (converted to blue after image capture without any other adjustment of the settings).

R1.5.3-Autophagy: autophagic flux, lysosomal abundance and activity & autophagy intermediates by TEM

The inhibition of autophagy was studied in part because, several ATAD3 mutants have been reported to have altered cellular degradation pathways, like mitophagy in the case of *dAtad3*^{R534W} (Harel et al., 2016) or autophagy in the case of ATAD3 p.G533D (Cooper et al., 2017). Autophagy is a complex process involving endosomes, lysosomes and a group of proteins that follow a series of defined events, to recycle cellular materials. Some of these events are amenable to monitoring and analysis. For instance, detecting and characterizing lysosomes can indicate the status of autophagy, and measuring the accumulation of proteins involved in autophagy when the process is blocked enables autophagic flux to be determined (Klionsky et al., 2012).

The abundance of lysosomes in the ATAD3 mutant fibroblasts was evaluated by immunolabeling the lysosomal membrane protein LAMP1. Based on this marker, ATAD3 mutant cells had many more lysosomes in their cytoplasm compared to control cells (Fig. 25A), and quantification of LAMP1 signal per unit area indicated that the lysosomal number was at least twice normal (Fig. 25A). Another widely used lysosomal marker is LysoTracker™ Red DND-99, which fluoresces at 577/590 nm, as its signal depends on its interaction with lysosomal acidic enzymes, and so indirectly indicates their functional capacity. ATAD3 mutants stained strongly with this dye, also about twice than control cells (Fig. 25B) revealing ATAD3 mutants not only have more lysosomes but that these are active, evidenced by their acidic pH. In agreement with the LAMP1 results, transmission electron microscopy images revealed that the cytoplasm of ATAD3 mutants was packed with autophagic bodies: lysosomes, autophagosomes and autophagolysosomes, whereas control cells had a less crowded cytoplasm, with the usual complement of organelles (Fig. 26). Among all the cellular clutter present in the cytoplasm of ATAD3 mutant cells, there was a

type of structure which was abundant but absent from control cell lines: membrane-whorls (Fig. 26). These are multi-membranous lysosomes that resemble the layered structure of onions or marbles (also called zebra bodies) which are attributed to unprocessed cellular membranes, and are characteristic of lysosomal storage disorders (Parkinson-Lawrence et al., 2010) (Martinet et al., 2014).

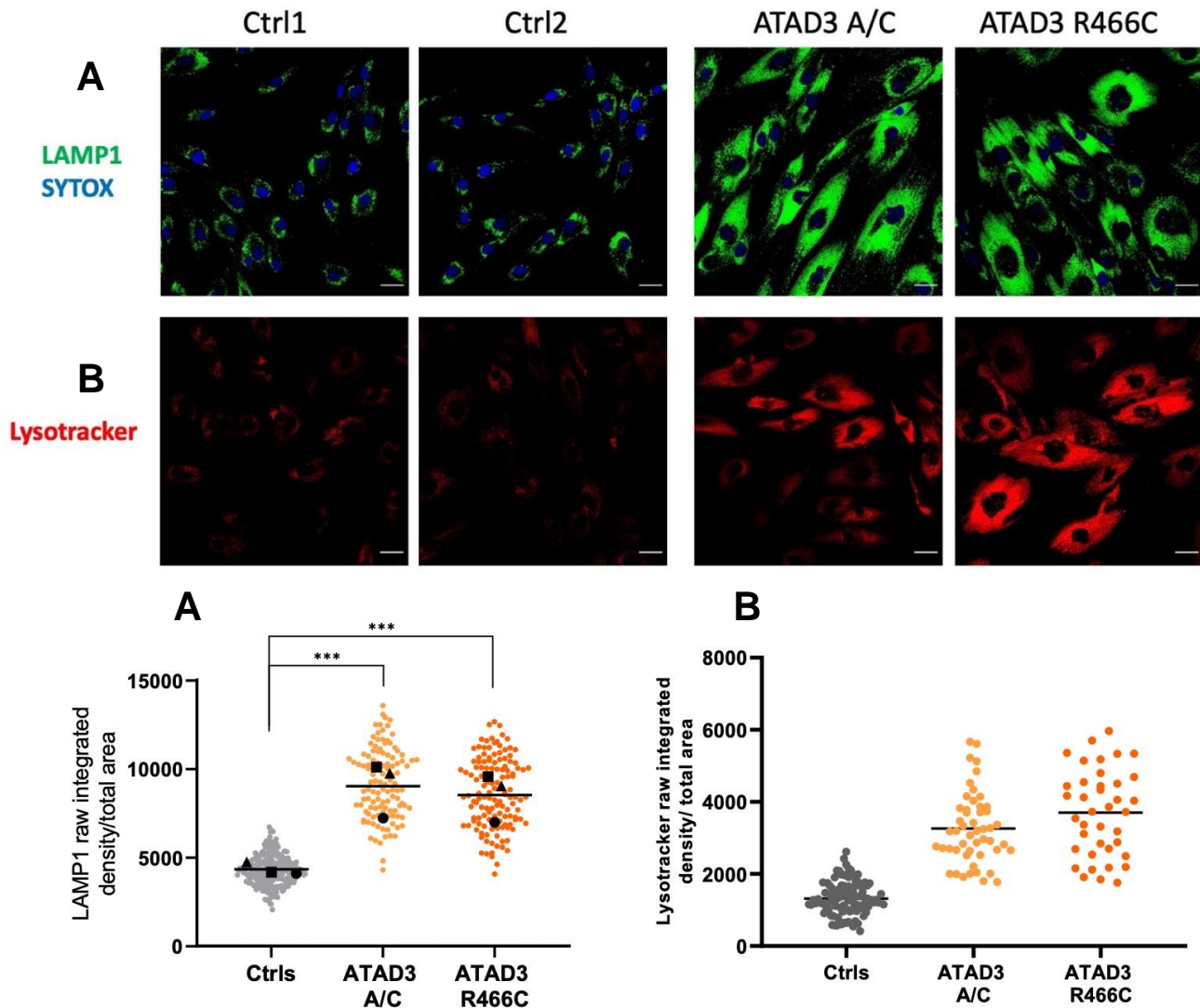
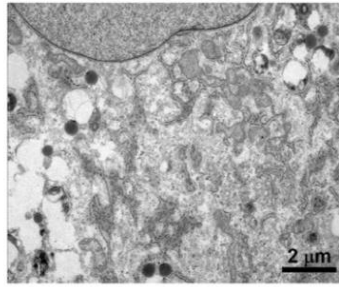
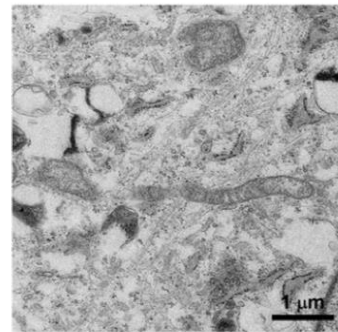
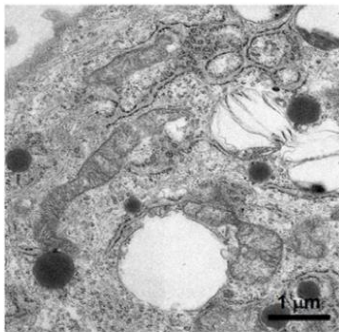
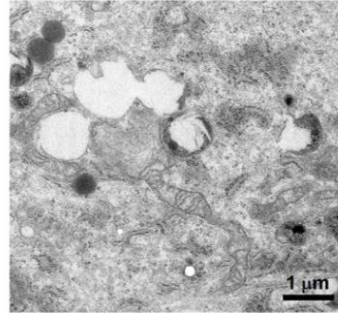
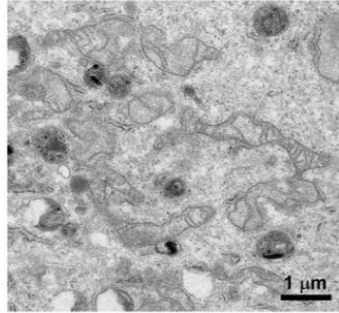
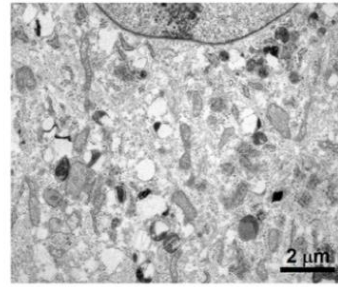


Figure 25. ATAD3 mutants have an increased and active lysosomal pool. ATAD3 A/C and R466C mutant and control (ctrl) fibroblasts stained with an antibody against lysosome-associated membrane protein 1 (LAMP1, green) with SYTOX (blue) stained nuclei (**A**), while the same cell lines were labeled live with an indicator of acidified lysosomes, Lysotracker Red DND-99 (red) (**B**). Both LAMP1 and Lysotracker signals were measured as raw integrated density per total area of the cell from controls and ATAD3 mutant fibroblasts, but > 100 cells per line, n=3 independent experiments; *** p < 0.001 where each of the polygons represent the mean of an experiment for LAMP1, while n=1 for Lysotracker.

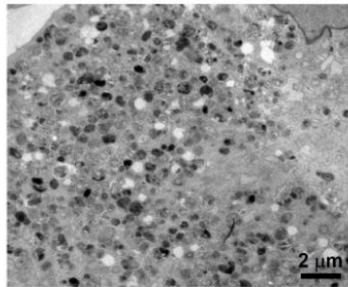
Ctrl1



Ctrl2



ATAD3 A/C



ATAD3 R466C

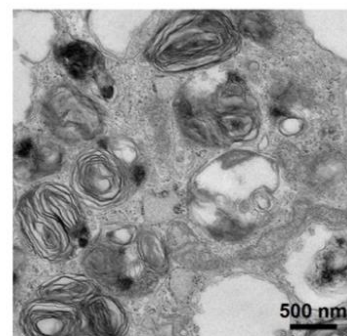
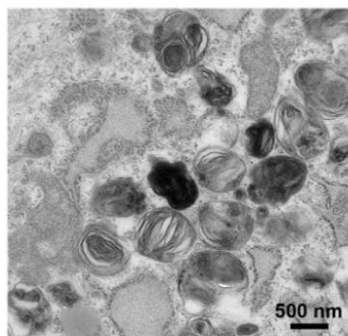
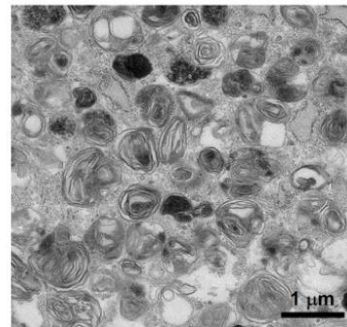
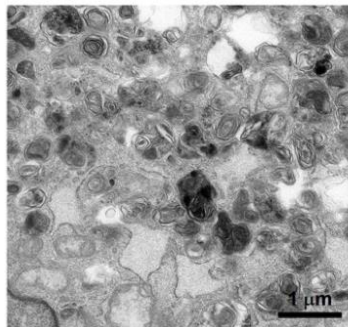
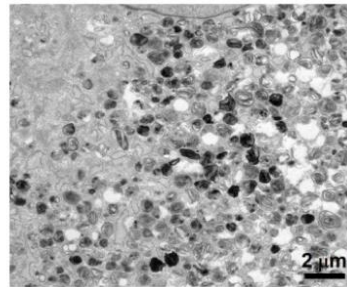


Figure 26. The cytoplasm of *ATAD3* mutant cells contain abnormal structures with membrane-whorls. Transmission electron micrographs of *ATAD3* A/C and R466C mutants and control (ctrl) fibroblasts showing cytoplasmic content at different magnifications.

To check the status of the autophagic flux, we used chloroquine (CLQ) that prevents acidification rendering the lysosomes non-functional (Fig. 28), and unable to fuse with autophagosomes (Klionsky et al., 2012). The abundance of key autophagic proteins, lipidated LC3A/B and phosphorylated SQSTM/p62, were determined by Western Blotting in *ATAD3* mutant versus control fibroblasts. The two proteins increased by an order of magnitude or more after CLQ exposure in control cells, indicating that autophagy was active in the absence of the inhibitor, as expected. The increases in the *ATAD3* mutant cells were occasionally lower, but often similar to the controls, including under the most demanding conditions when key nutrients were restricted (glucose and glutamine) or in the severest *ATAD3* mutant case, such as the *ATAD3* Δ (Fig. 27). Therefore, *ATAD3* mutants have similar autophagic flux to control cell lines, and so the increase in lysosomal numbers is not secondary to impaired autophagy. On the other hand, more lysosomal capacity to achieve the usual autophagic flux indicates that the process must be less efficient than normal, i.e. slower than normal (see Discussion).

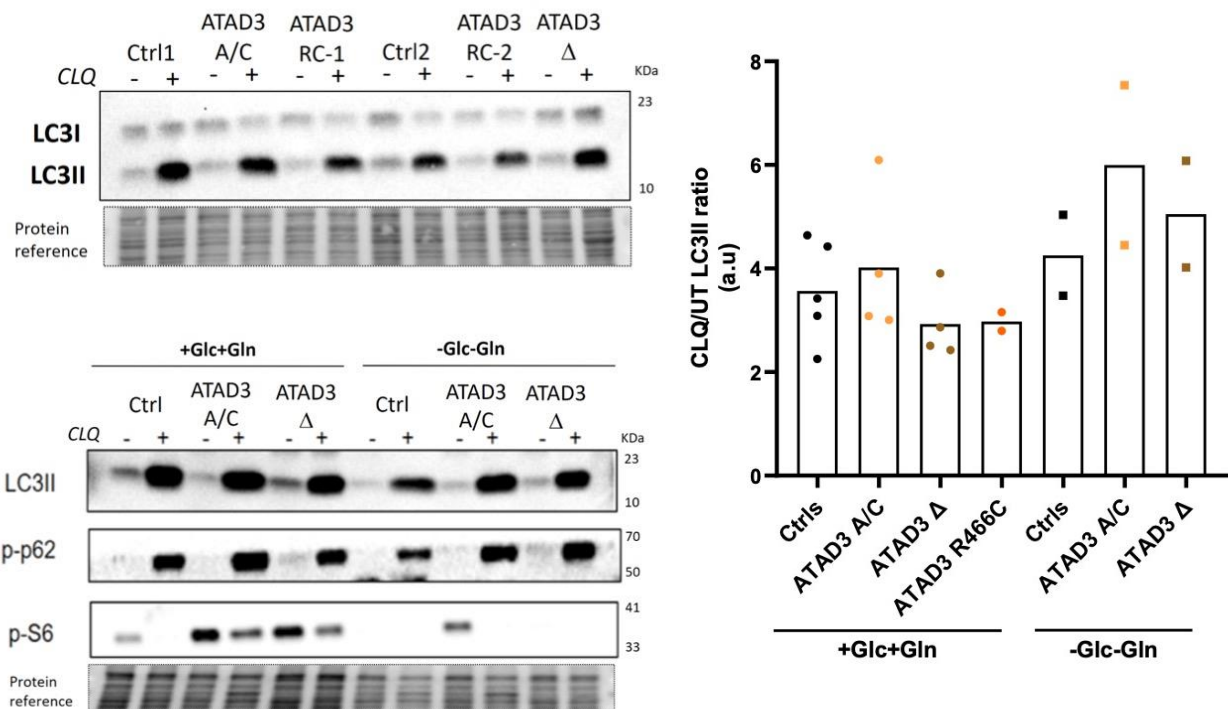
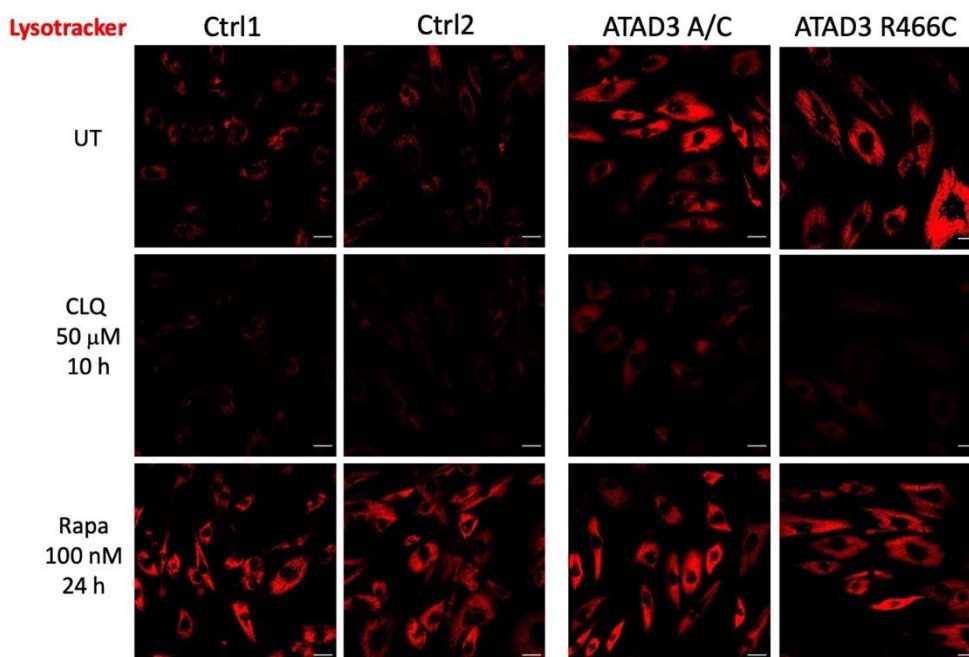


Figure 27. Autophagic flux and mTOR status are little altered in ATAD3 mutants.

ATAD3 A/C, deletion (Δ) and R466C cells (vial 1 (passage 24) and 2 (passage 13)) were treated with and without chloroquine (CLQ), as a way to block autophagy, in parallel with control cells (ctrl) and were grown in medium containing or lacking glucose and glutamine (+Glc+Gln) and (-Glc-Gln), respectively. When not stated it means they were grown in standard medium (with glucose and glutamine). Autophagic flux was analyzed through the observation of lipidation of LC3A/B via immunoblotting (II being the lipidated form). phospho(S403)-p62 proteins was as well analyzed as an autophagy marker, as it accumulates in autophagosomes, whereas p(S235/236)-S6 ribosomal protein is indicative of active mTOR. Quantification of LC3II normalized to protein reference and represented as the ratio of CLQ against the basal (untreated, UT), thus representing the accumulation of lipidated LC3II when autophagic flux is blocked. Each data point represents an independent experiment (n=2-4).

A well-recognized pathway of stimulation of lysosomal production and activity is through their implication on autophagy via the repression of the master regulator protein mTOR, which can occur naturally under nutrient restriction and starvation, or chemically by using its inhibitor Rapamycin (Rapa) (Klionsky et al., 2012). Control and mutant cell lines were treated with CLQ and Rapa to inhibit or increase the lysosomal pool, respectively. After the addition of LysoTracker lysosomes were imaged in live cells, which confirmed they were almost absent in the first case but were highly increased in the second (Fig. 28). However, the lysosomal changes occurring in the ATAD3 mutants were independent of mTOR repression, as the ribosomal protein S6 was phosphorylated at serine 235/236 in the ATAD3 mutant cells (Fig. 27), which is an indicator of active mTOR (Kimball et al., 1999). Note that when cells are subjected to nutrient deprivation, the abundance of the serine 235/236 of the S6 is reduced drastically, indicating mTOR then is inhibited as expected in these conditions (Fig. 27).



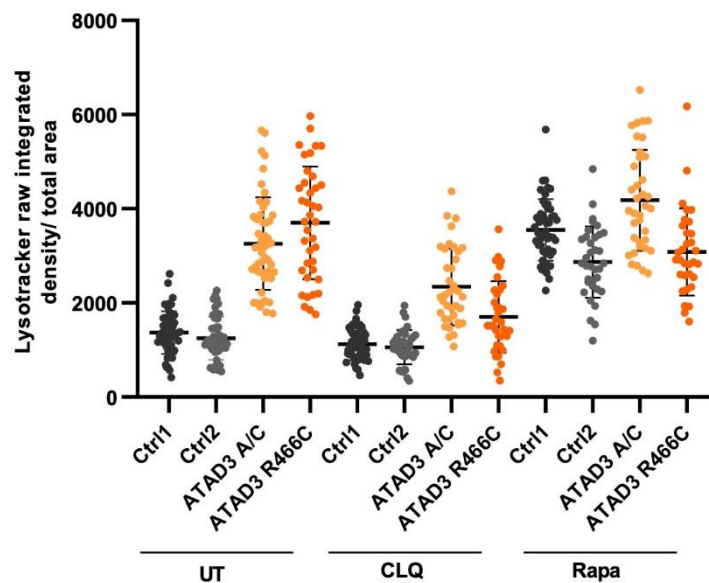


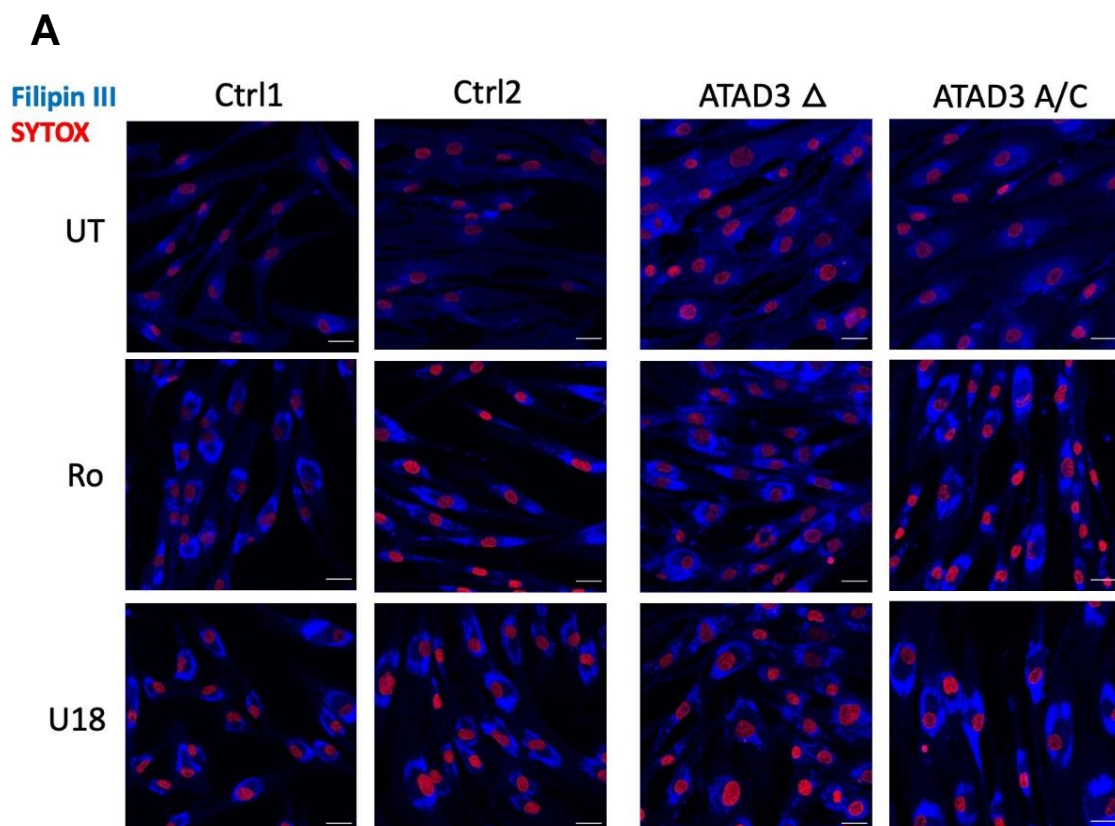
Figure 28. Chloroquine represses while rapamycin stimulates lysosome activity. ATAD3 A/C and R466C cells were grown in standard medium (UT), medium with 50 μ M chloroquine (CLQ) for 10 h to block lysosome activity, or medium with 100 nM rapamycin (Rapa) to stimulate lysosomes (via mTOR inhibition) for 24 h prior to adding LysoTracker™ for 45 mins to detect acidified lysosomes. Quantification of LysoTracker signal was measured as raw integrated density per total area of the cell from controls and ATAD3 mutant fibroblasts with each of the drugs, where each of the dots represent a cell, n=1 experiment.

R1.6- Cholesterol and lipid metabolism modulation as a potential way of identifying, alleviating or treating ATAD3 mutants.

Because cholesterol and lipid metabolism are altered in ATAD3 dysfunction (sections R.1.5.1 and 1.5.2), we focused on modulating them, as this might identify conditions that are beneficial or toxic for *ATAD3* mutant cells. This information could guide dietary management of patients, and help unravel the underlying effects of mutant ATAD3 on cellular pathophysiology, and thereby help in the identification of potential therapeutic targets.

Hence, several nutrient and pharmacological treatments targeting sterol and lipid metabolism were applied to the *ATAD3* mutant fibroblasts. The two principle readouts used were Filipin III staining of the free cholesterol pool and mtDNA distribution and synthesis, via BrdU labeling. The first one because the elevated free-cholesterol is a consistent central cellular phenotype for *ATAD3* mutants. The second one because as well as mtDNA being linked to ATAD3, its replication is an important reporter of the functional status of mitochondria and it directly responds to alterations in the cellular homeostasis.

Similar to the previous modulation with statins (Desai et al., 2017), we decided to start by inhibiting the cholesterol biosynthetic pathway. However, an important reason to use Ro 48-8071 (Ro) instead of statins in our studies was that Ro blocks 2,3-oxidosqualene: lanosterol cyclase (OSC), which is downstream of the statin target, HMG-CoA reductase, and downstream of the branch point of farnesyl pyrophosphate necessary for coenzyme Q synthesis, which might therefore produce a more specific inhibition of cholesterol biosynthesis (Morand et al., 1997). Treatment of control cells with Ro 2.5 μ M for 48 h led to an increase in free-cholesterol (Fig. 29A), similar to that reported for statins (Desai et al., 2017). In the *ATAD3* mutants (duplication and deletion), Ro increased the free cholesterol as well, to that of the Ro-treated controls and similar to the increase observed with U18 (Fig. 29A). Thus, inhibiting cholesterol downstream of the branch-point in its biosynthesis does not alter the impact on cholesterol homeostasis. However, Ro strongly inhibited mtDNA synthesis in both control and *ATAD3* mutant cell lines (Fig. 29B and C). In contrast U18 had no appreciable effect on mtDNA synthesis. The reason for this starkly different effect is not known but it would be worthwhile to check CoQ levels in response to the two treatments.



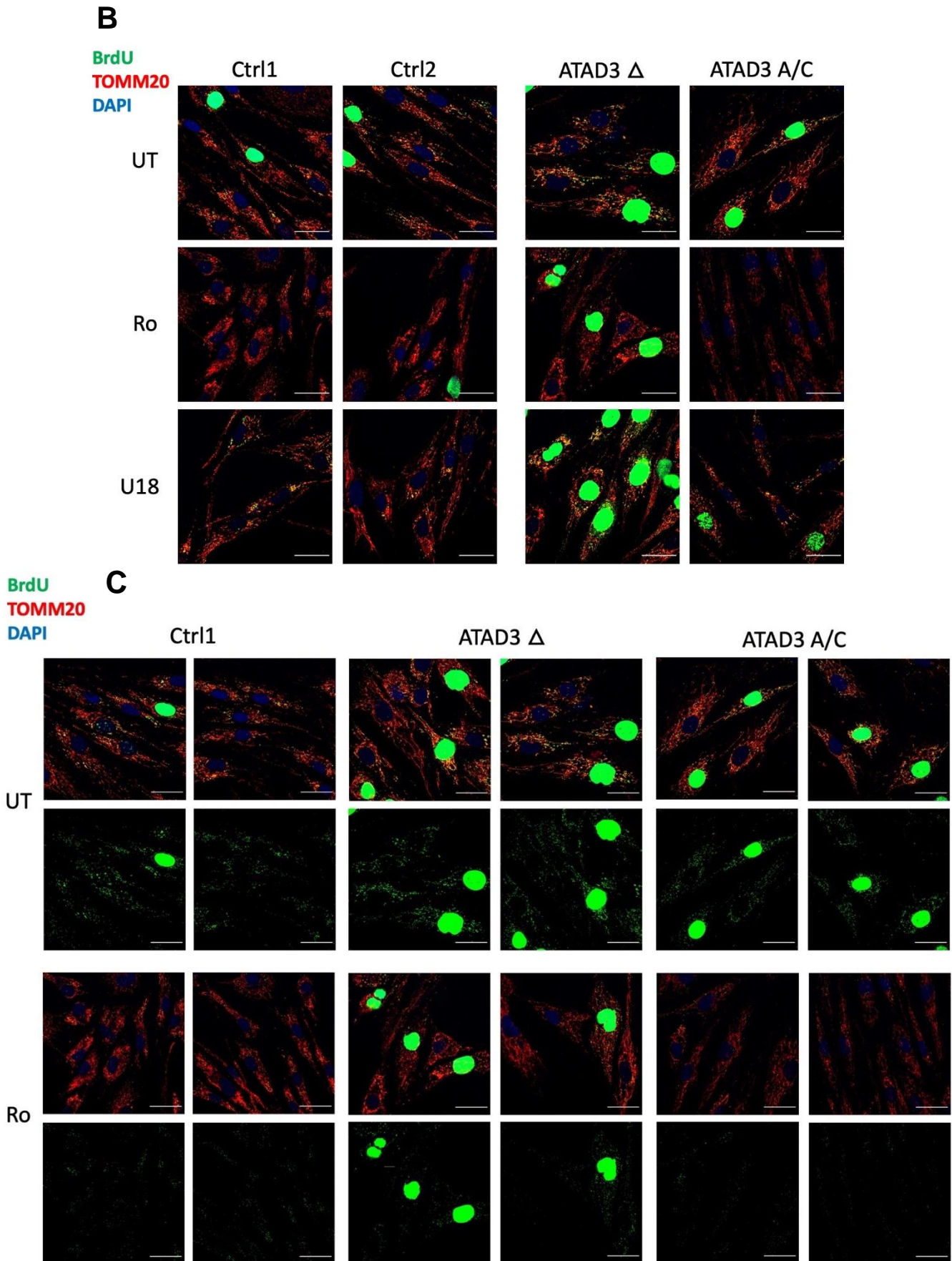


Figure 29. Treatment of cells with Ro 48-8071 produces a marked increase in free cholesterol, similar to U18666A, but only the former inhibits mitochondrial DNA synthesis. Control (ctrl) and *ATAD3* mutant cells were treated with or without Ro 48-8071 (Ro), an inhibitor of the cholesterol biosynthetic enzyme, oxidosqualene cyclase,

or with U18666A (U18) an inhibitor of intracellular cholesterol trafficking. After 48 h cells were incubated with **(A)** Filipin III to stain free cholesterol (blue) and SYTOX (red) to label the nuclei or **(B)** Confocal merged images using a 40 x objective of cells stained with anti-TOMM20 (red) and anti-BrdU (green), after 50 μ M BrdU supplementation for 12 h. In blue, DAPI stained nuclei. **(C)** Merged BrdU and TOMM20 signals, as panel B, only for Ro and UT conditions, and accompanied by BrdU (green) alone to better appreciate the decrease in the mitochondrial DNA synthesis.

The hypothesis that mtDNA is attached to the inner membrane facilitated by cholesterol microdomains predicts that ATAD3 dysfunction could disrupt any element of the microdomains. As well as cholesterol, sphingolipid is an essential component of cholesterol microdomains, and ATAD3 co-purified with a key enzyme of sphingolipid metabolism, SPTLC (He et al., 2012). This enzyme was also found to be upregulated in the transcriptomic analysis performed in two ATAD3 mutants with biallelic deletions (Desai et al., 2017). Therefore, with the objective of assessing the effect of modulating sphingolipids in ATAD3 dysfunction, we used an established bioactive sphingolipid, sphingosine-1-phosphate (S1P), which has been shown to be implicated in many diseases (Maceyka et al., 2012). Treatments of 4 μ M and 40 μ M S1P for 24 and 48 h produced an increase in free-cholesterol, both in control and ATAD3 mutant lines (Fig. 30A and B). However, at the higher dose of 40 μ M 48h free-cholesterol seemed to be differently distributed and aggregates were detected in the cytoplasm, often towards the cell periphery, in more than 60% of the control cells, but in few or none of the ATAD3 A/C cells (Fig. 30A and B). Although it is not known why these cholesterol aggregates form in controls and not in the ATAD3 mutants, S1P was the only treatment that distinguished the mutants from the controls and so provides a hint that altered sphingolipid metabolism is a unique feature of ATAD3 dysfunction

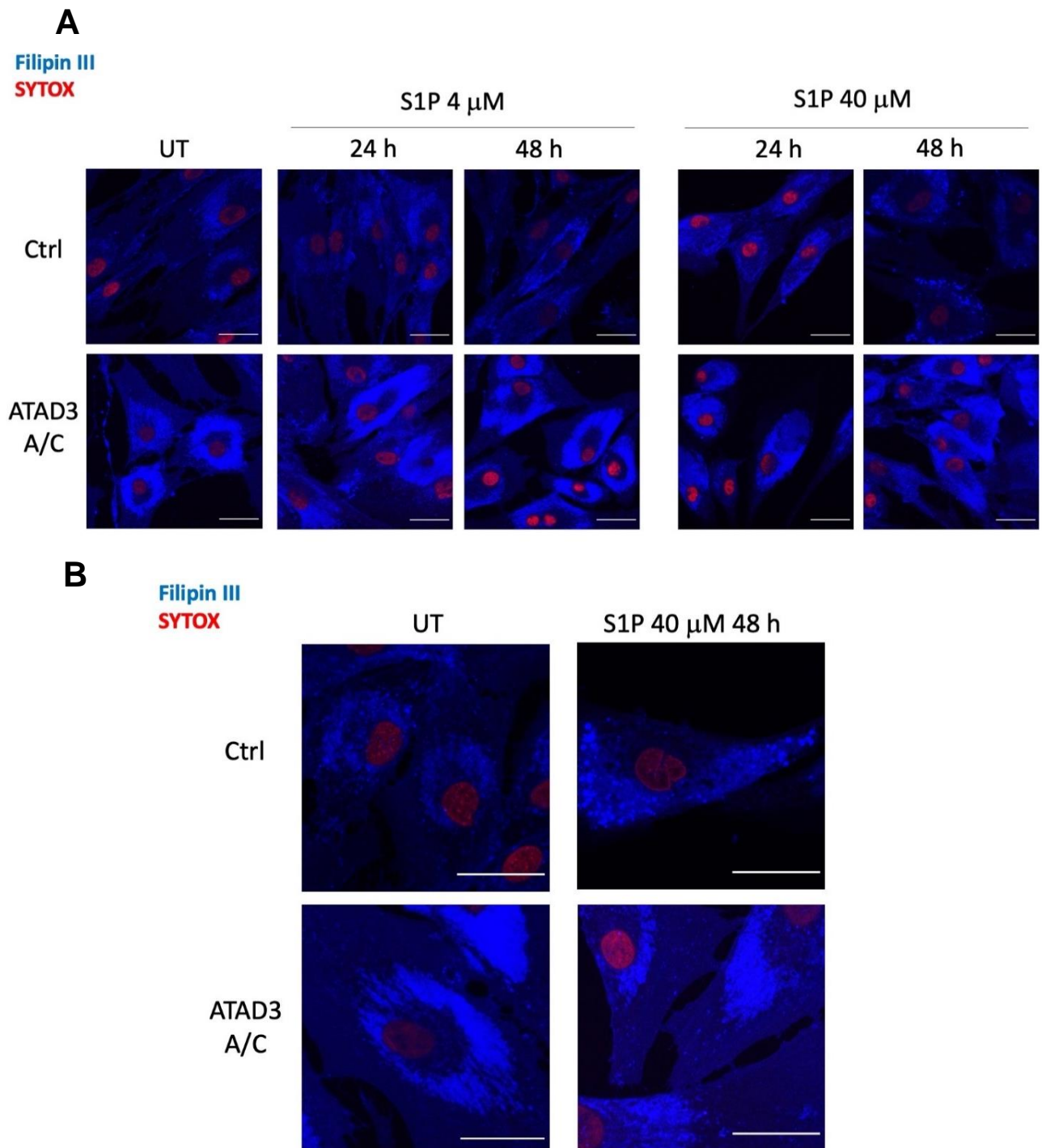


Figure 30. Spingosine-1-phosphate supplementation 40 μ M for 48 h produces free cholesterol foci close to the cell periphery in controls but not in ATAD3 mutants. (A) ATAD3 A/C mutant and control (ctrl) fibroblasts were treated without (UT) and with 4 or 40 μ M sphingosine-1-phosphate (S1P) for 24h and 48h, and subsequently stained with Filipin III to label free cholesterol (blue) and SYTOX (red) to label nuclei. Images were acquired on a confocal microscope at 40x objective. **(B)** Same as panel A but microscope magnifications with a 63x objective for S1P 40 μ M for 48 h versus UT.

When control and mutant cell lines were treated with the high dose of S1P and perilipin 2 was checked, the most ubiquitously expressed lipid droplet protein (Calise et al., 2012; Kawashima et al., 2012) there was an increase for all the cell lines compared to their basal state (Fig. 31), suggesting this treatment enhances neutral lipid production; i.e. that S1P treatment reproduces two features of the ATAD3 mutants in control cells: elevated free cholesterol and the accumulation of neutral lipids. Nonetheless, verification of this with Bodipy needs to be done.

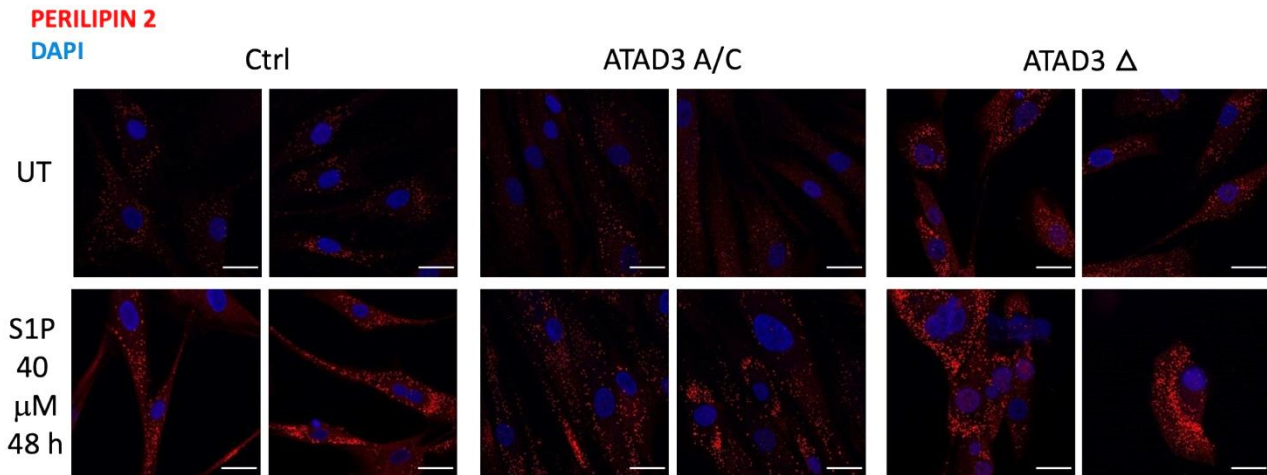


Figure 31. Cells treated with 40 μ M sphingosine-1-phosphate for 48 h have abundant lipid droplet protein, perilipin 2, in their cytoplasm. ATAD3 A/C and ATAD3 Δ mutant and control (ctrl) cells were treated without (UT) and with 40 μ M sphingosine-1-phosphate (S1P) for 48 h and stained with lipid droplet protein marker perilipin 2 (red). In blue are the nuclei stained with DAPI.

Other reported ways of increasing the level of free-cholesterol in cells are the combined treatment of low-density lipoprotein (LDL) and the SOAT1 inhibitor Sandoz-58035 (Sdz), supplementation of cholesterol in the culture media and the use of monocyte chemoattractant protein 1 (MCP1). According to the literature, LDL and Sdz together inhibit cholesterol re-esterification and thus prevent the conversion of ingested cholesterol to cholesteryl esters (Feng et al, 2003). However, we found that it was not necessary to combine the two as individually LDL and Sdz (and combined as well) induced a marked increase in free-cholesterol in controls, similar to U18, and the free-cholesterol in the ATAD3 mutants remained high, with no noticeable variation (Fig.32).

Because of its inherent insolubility, preparing homogenous emulsions of cholesterol is difficult in non-organic solvents, and the cholesterol solution provided by Promega in their Cholesterol/ Cholesterol Ester-Glo™ kit, proved more consistent than our own preparations. When added as a supplement to the growth medium, at 10 μ M for 24 h, it produced a similar effect to LDL and Sdz, as cholesterol was highly increased in controls but no change was detected in the ATAD3 mutants. Nonetheless, small aggregates, close to the periphery of the cell, were observed both in controls and the ATAD3 mutants (Fig.32). However, they seemed different to the aggregates observed with S1P, as in this case they were not exclusive to controls and they appeared in addition to the usual increase in free-cholesterol, forming small clumps, whereas in the case of S1P it seemed the free cholesterol was redistributed into those aggregates.

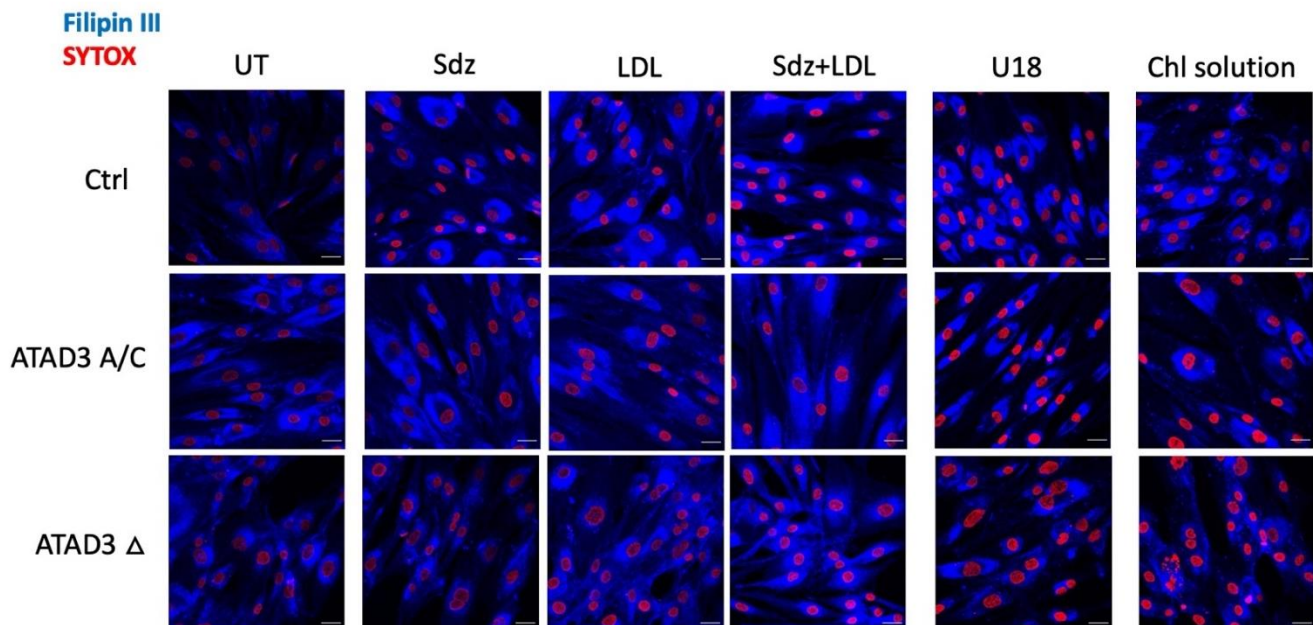


Figure 32. Chemical treatments targeting cholesterol and lipid metabolism and direct cholesterol supplementation increase the free cellular cholesterol pool. ATAD3 A/C and ATAD3 Δ mutant cells were treated with Sandoz-58035 (Sdz) 2 μ g/mL, LDL 50 μ g/mL and the combination of both (Sdz+LDL) for 24h, U18666A (U18) 1.25 μ M for 48h and the cholesterol solution (by Promega) at 10 μ M for 24h, all in a medium with 2% delipidated FBS and fatty acid-free BSA 2 mg/mL, as per Marcil et al., 1999. Free cholesterol was label with Filipin III (blue) and nuclei were stained with SYTOX (red).

Last, MCP1/CCL2 has been reported to decrease the expression of plasma membrane cholesterol transporters ABCA1, ABCG1 and SR-BI via post-translational modification of PI3K/Akt (Huang et al., 2013). In a preliminary experiment, a treatment of 50 ng/mL MCP1 for 24 hours led to a moderate increase in free-

cholesterol both in the mutant and control cell lines, although not to the level of the (untreated) ATAD3 mutants (Fig. 33). Thus, the compound has the expected effect but further work is needed on dosing and duration to assess how well it mimics the ATAD3 mutants.

To gain a fuller picture of how changes in lipid homeostasis impact cholesterol levels and so potentially understand the role of mutant *ATAD3*, Atglistatin (Atglis) and Isoproterenol (ISO) were also tested. Atglis is an inhibitor of adipose triglyceride lipase (ATGL), the rate-limiting enzyme of lipolysis, and it has been reported to inhibit lipolysis in cell lines and mice (Sathyanarayan et al., 2017; Lumaquin et al., 2021). Instead, ISO is a well-known lipolysis inducer that activates the hormone-sensitive lipase (Lumaquin et al., 2021). Both the inhibitor (Atglis, 50 μ M 24 h) and the activator (ISO, 1 μ M 24h) of lipolysis increased the free cholesterol pool, in mutant and control cell lines, albeit not to the level of the ATAD3 mutants (Fig. 33).

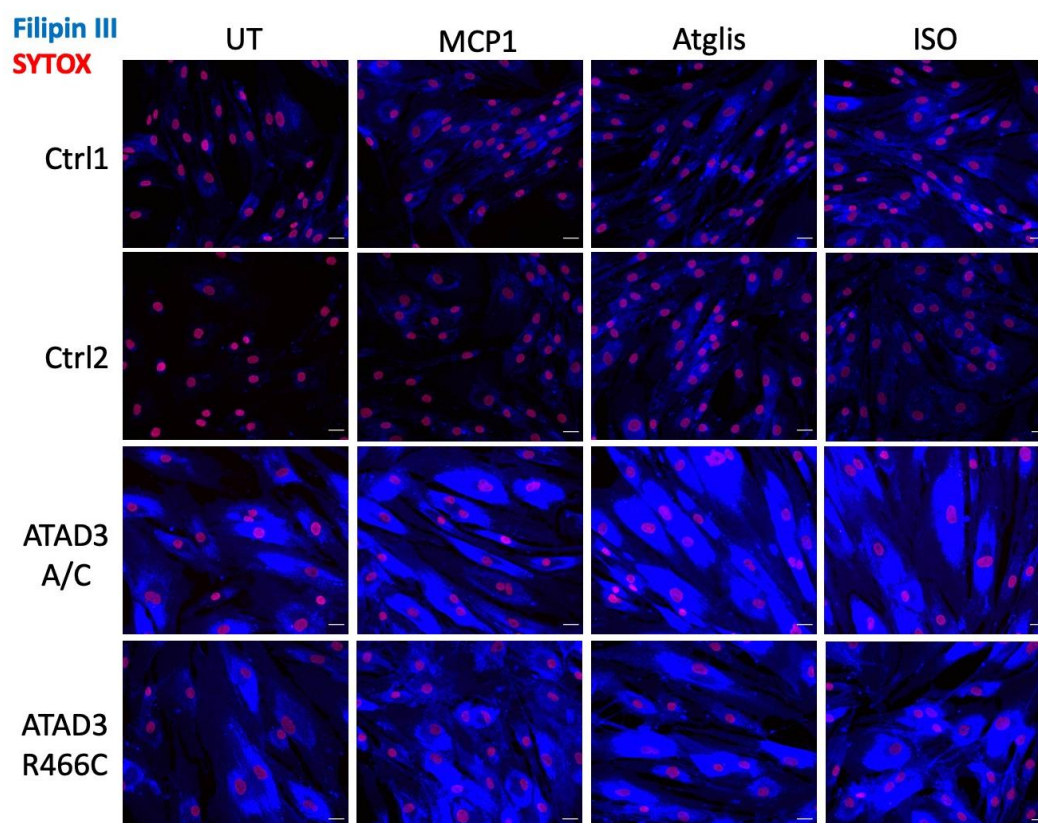


Figure 33. MCP1, Atglistatin and Isoproterenol produce a modest increase in free-cholesterol in all cell lines. ATAD3 A/C and R466C mutant and control (ctrl) cells were treated without (UT) and with 50 ng/mL MCP1/CCL2 for 24h, or the lipolysis inhibitor Atglistatin (Atglis) 50 μ M 24 h or inducer Isoproterenol (Iso) 1 μ M 24h, and stained with Filipin III to label free cholesterol (blue) or SYTOX (red) to label nuclei.

R1.7- Other potential ATAD3 patients

The first patient was a 3 years old boy (at the time of assessment and biopsy obtaining) whose family contacted our group due to the results of a genetic study where a possible *ATAD3* genetic rearrangement was detected. The genetic study had been previously conducted analyzing the exome by next generation sequencing (NGS) and two variants of uncertain significance were detected: a possible rearrangement in *ATAD3A* and a missense heterozygous mutation (c.149C>A, p.Pro50His) in *CPT2*. Specific primers were designed to Sanger sequence the region encoding for *ATAD3A* in the parents and the affected child, but only the parental samples could be amplified, despite the sequencing was repeated three times, suggesting a *de novo* rearrangement in this area had occurred. Reanalysis of the sequencing data by our collaborators Drs. Frazier and Thorburn, of Melbourne Children's Hospital in Australia, failed to detect any clear rearrangement in the *ATAD3* locus. Some *ATAD3B* exons (such as exon 2 and 16) had very low coverage which could indicate the presence of heterozygous deletions in those areas. However, there were no other samples from the same batch and so unequivocal identification of structural variants was not possible. Dr. Frazier also identified a possible AA>TT substitution (p.Lys60Leu) in exon 1 of *ATAD3A*, though because of low coverage in that area it could also be mismapping rather than a genuine change. As several other *ATAD3* disease-causing missense variants have been mapped to nearby residues (p.Phe50Leu, p.Thr53Ile, p.Leu77Arg, p.Leu77Val) p.Lys60Leu could be a credible pathological missense mutation.

The subject was born from non-consanguineous healthy parents (with a previous healthy daughter) in a eutocic delivery that did not require medical assistance. He was first assessed by a neurologist due to a postural motor delay, as he did not walk until two years of age, though he showed good development in other neurological aspects, including cognition. He presented with neurosensorial hearing loss. Although standard metabolic screening was negative, the subject had a carnitine transport deficit. Magnetic resonance showed a deep bilateral white matter alteration, whereas electromyography and electroneurography were normal. The child came for a clinical examination with Dr. Martí in the Donostia University Hospital where I had the opportunity to meet the patient and his mother and attend the examination. He made good contact, talked and responded normally. His eyes were free of nystagmus or ophthalmoplegia with correct motility. He presented no hypotonia or weakness,

but rather a modest hypertonia in the lower limbs without retractions. He had the ability to get up from the floor with Gowers negative, but had unsteady gait with modest spastic paraplegia pattern without tremor. We performed a skin biopsy from which we obtained fibroblasts (named PPA1) for further characterizing ATAD3 associated molecular phenotypes.

Immunoblotting of ATAD3 extracted from PPA1 cells showed a single broad band similar to controls (Fig. 34A). However, PPA1 fibroblasts presented elevated free cholesterol and neutral lipids similar to the established ATAD3 mutant lines (Fig. 34B). There was a markedly lower rate of mtDNA synthesis in the PPA1 fibroblasts compared to controls and the *ATAD3* duplication and deletion mutants. This low rate of DNA synthesis was restricted to the mitochondria as nuclear BrdU staining was at least equal to the controls (Fig. 34C).

Treatments with U18, Ro, LDL (+/- Sdz) and the cholesterol solution all produced increases in free cholesterol in PPA1 (Fig. 35A and B). Because the level was relatively high without treatment the relative increase tended to be less than in the control cells, as seen in the ATAD3 mutants (Fig. 35). The high dose of S1P did not produce the cholesterol aggregates seen in control cells (Fig. 36), providing another similarity with the established *ATAD3* mutants.

Thus, the cholesterol and lipid phenotypes of the PPA1 fibroblasts are compatible with the cells carrying a dysfunctional form of ATAD3. On the other hand, the mtDNA synthesis deficiency is not shared with the established ATAD3 mutants and given that cholesterol homeostasis can be perturbed in many ways it is most likely that a mutation in a gene other than ATAD3 is the cause of the disease. Therefore, further studies are needed on PPA1, and at the moment a second genetic study is being made to sequence the exomes of the patient and the parents to try to determine the genetic defect of this patient.

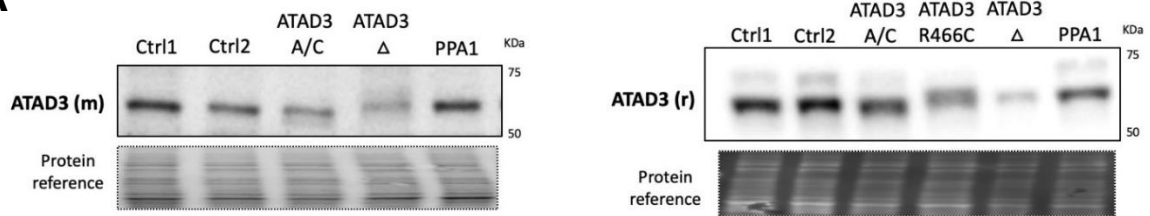
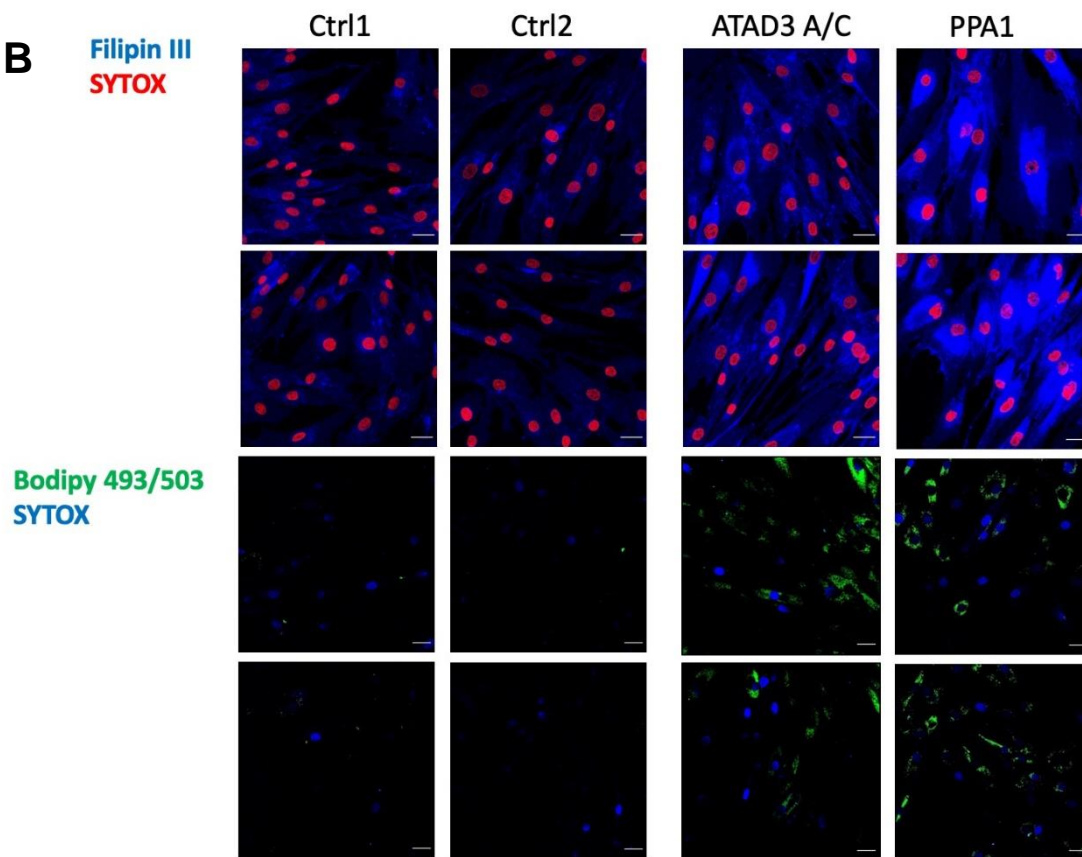
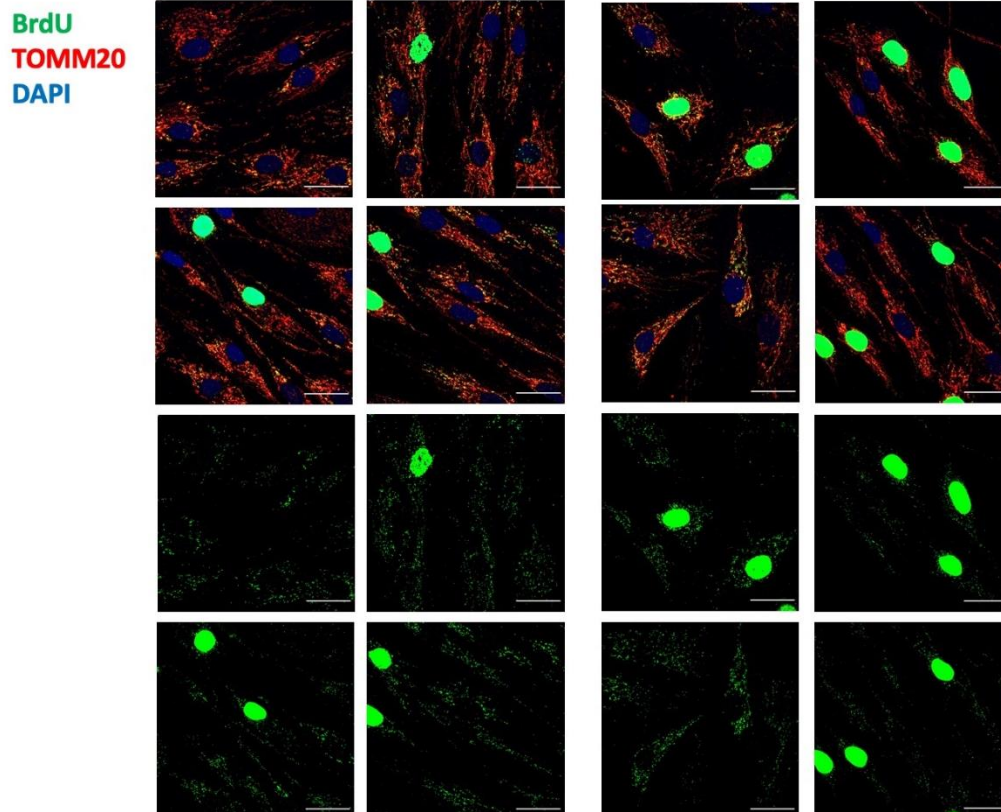
A**B****C**

Figure 34. PPA1 cells display increased free-cholesterol and neutral lipids. (A) Whole cell protein from controls (ctrl), ATAD3 R466C, ATAD3A/C and ATAD3 Δ mutant cell lines, by 8% SDS-PAGE and immunolabeled with ATAD3 specific antibodies, mouse (m) and rabbit (r). Images were acquired by iBright. Controls (Ctrl), ATAD3 A/C mutants and PPA1 cells were stained with **(B)** Filipin III (blue) to label free cholesterol and SYTOX™ Deep Red (red) for nuclei, or **(C)** with BODIPY™ 493/503 (green) to stain neutral lipids and SYTOX™ Deep Red to mark the nuclei (converted to blue), or **(D)** with anti-TOMM20 (red) and anti-BrdU (green), after 50 μ M BrdU supplementation for 12 h. Images were acquired with a confocal microscope at 20x for Filipin and Bodipy, and 40x for BrdU.

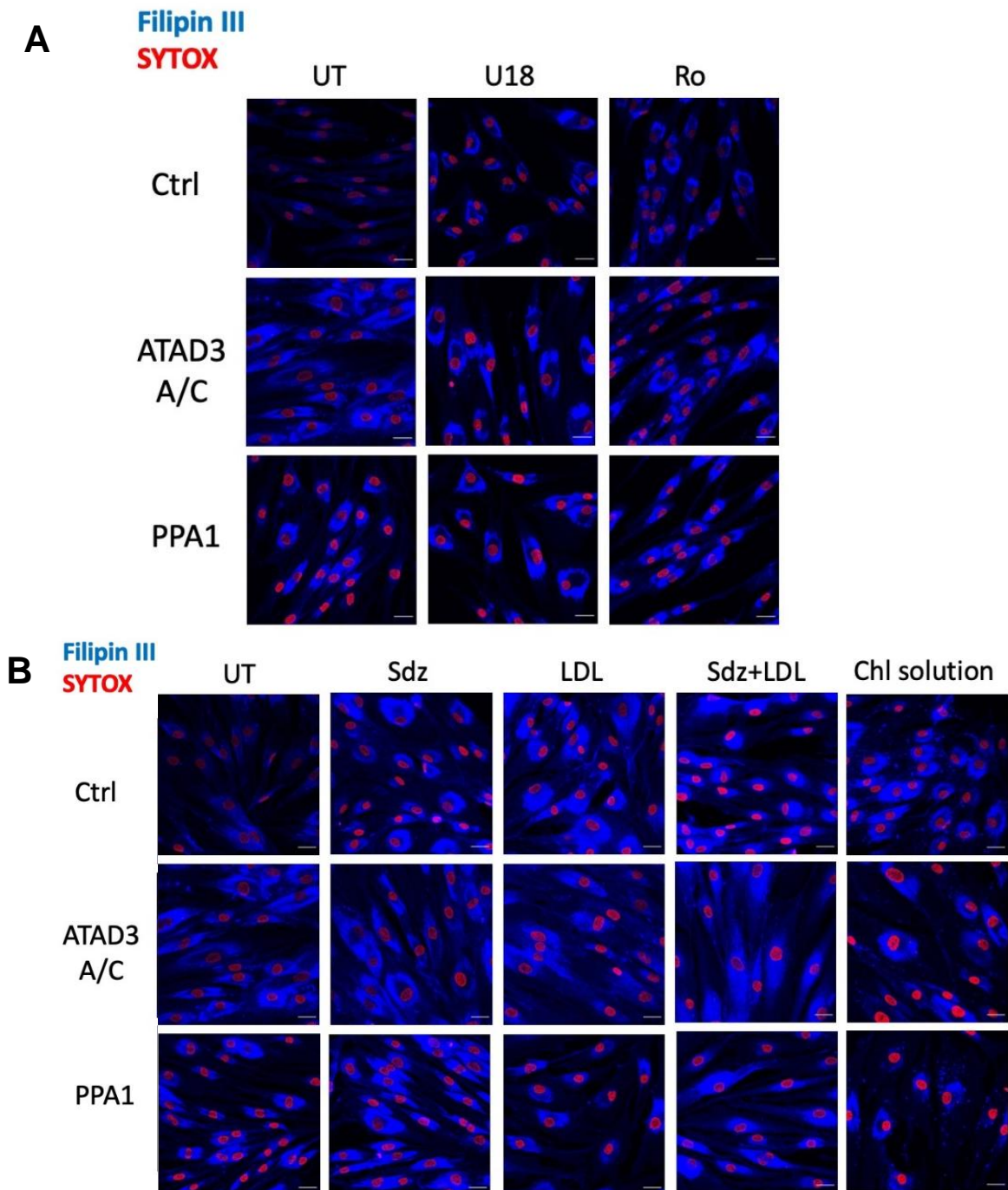


Figure 35. Treatment with U18, Ro, LDL (+/- Sdz) and the cholesterol solution produced increases in free cholesterol in PPA1. Controls (Ctrl), ATAD3 A/C mutants and PPA1 cells were treated with **(A)** U18666A (U18) 1.25 μ M for 48h and the inhibitor of the cholesterol biosynthetic enzyme oxidosqualene cyclase, Ro 48-8071 (Ro) and **(B)** Sandoz-58035 (Sdz) 2 μ g/mL, LDL 50 μ g/mL, both Sdz+LDL, or 10 μ M cholesterol (Promega) for 24h, in a medium with 2% delipidated FBS and 2 mg/mL fatty acid-free BSA, as per Marcil et al., 1999. Free-cholesterol was label with Filipin III (blue) and nuclei were stained with SYTOX (red).

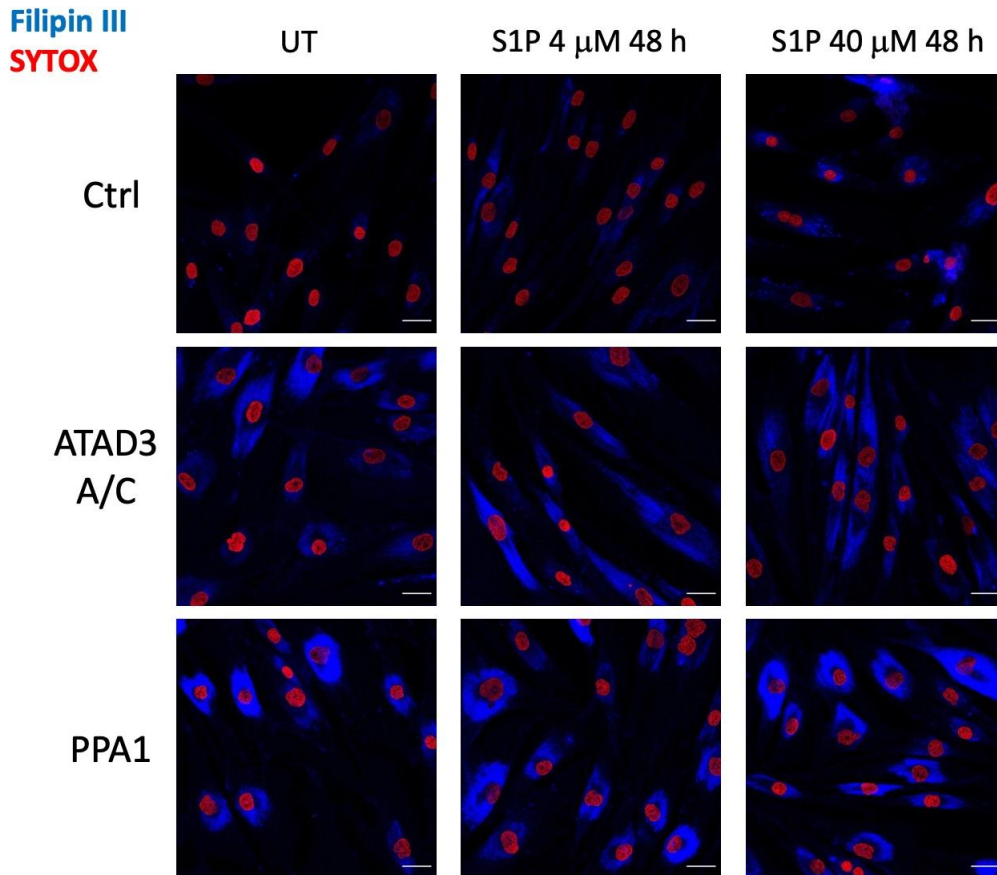


Figure 36. Spingosine-1-phosphate (S1P) supplementation does not produce cholesterol aggregates in PPA1. Controls (Ctrl), ATAD3 A/C mutants and PPA1 cells were treated without (UT) and with sphingosine-1-phosphate (S1P) 4 and 40 μ M for 48h and were later stained with Filipin III to label free cholesterol (blue) or SYTOX (red) to label nuclei.

I additionally screened fibroblasts from a two-year old Turkish boy with a suspected ATAD3 mutation that we called PPA2. The boy carries a homozygous mutation in ATAD3A (c.955G>A, p. Ala319Thr) based on WES analysis. As a first assessment, free cholesterol was tested, revealing staining was as low as the controls (Fig. 37). Although he is a credible case, the lack of the cholesterol phenotype led us to focus on the characterization and experimentation with fibroblasts of the other patients.

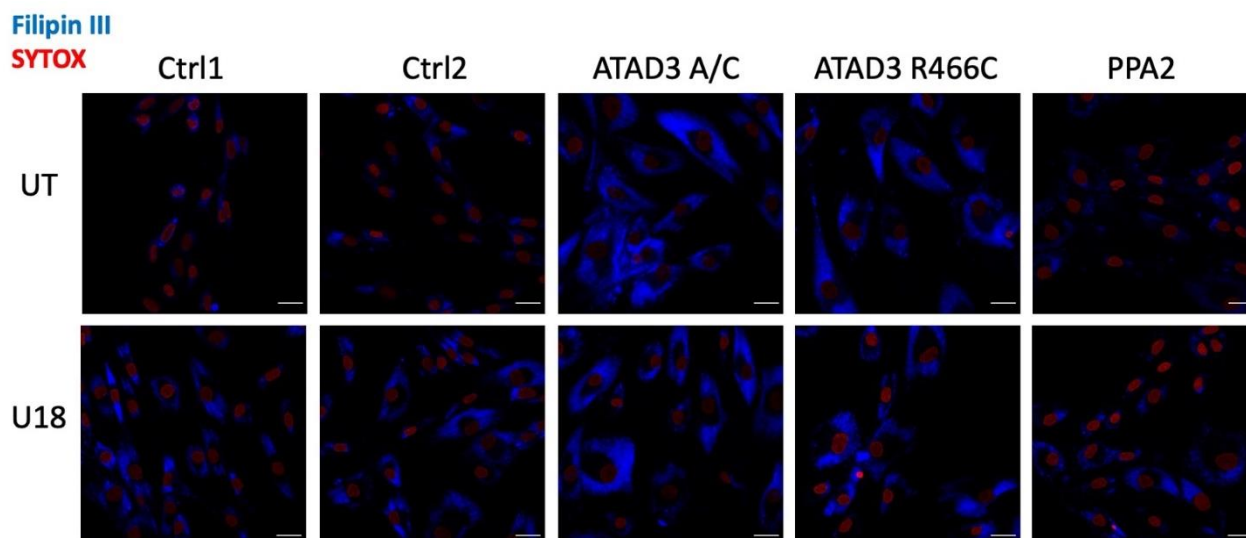


Figure 37. Basal free cholesterol levels in a potential ATAD3 patient, PPA2, are similar to controls. Controls (Ctrl), ATAD3 A/C and R466C mutants and PPA2 cells were stained with Filipin III (blue) to label free cholesterol and SYTOX™ Deep Red (red) for nuclei, both in untreated (UT) and treated with cholesterol trafficking inhibitor U18666A (U18) 1.25 μ M for 24 h, as a control.

Most recently cells for analysis have arrived from a patient from Galicia (Spain), ATAD3 421. He is a newborn, with healthy unrelated parents, that presented fetal akinesia, no postnatal movements, absent newborn reflexes, respiratory insufficiency and macrocephaly. He spent several days after birth in the neonatal intensive care unit. He was also reported to have talipes equinovarus (or clubfoot) and hypertrophic legs. The initial diagnosis was a myotonic dystrophy but later a dystonia episode was reported which suggested neurotransmitter dysregulation. Further examination identified bilateral cataracts, hypertrophic cardiomyopathy, alteration in the carnitine transport and some defects in mitochondrial metabolism (unspecified). Exome sequencing via NGS revealed a monoallelic missense variant (c.388G>T; p.Glu130X) in *ACAD9*, a protein involved in β -oxidation and mutations in that gene are associated with complex I deficiency. As this variant leads to a stop codon, the predicted protein product is expected to be non-functional, though there is no evidence of previous description of this variant in the general population or in specialized data sets, thus further characterization and experimental results would be needed. The sequencing results also revealed a large chromosomal monoallelic deletion comprising approximately a fragment of 62 kb (positions 1386065-1447853) in the short arm of chromosome 1 (1p36.33). This deletion eliminates *ATAD3C*,

ATAD3B and the beginning of *ATAD3A*. The deletion is reminiscent of the previous deletions in *ATAD3*, such as the one studied here, given the association to the severe multisystemic syndrome PHRINL (OMIM: 618810), although the other deletions are recessive. More clinical evaluation is being made and we will analyze the fibroblasts shortly to characterize this patient further.

**Chapter II: Generation of a new
in vivo membrane-bound
cholesterol reporter and its
utilization in the Atad3 R472C
Drosophila model**

Introduction

***Drosophila melanogaster* in the lab**

Drosophila melanogaster, or the common fruit fly, so named as they are naturally found feeding on rotting fruit and vegetables, is an insect from the Diptera order and Drosophilidae family. They were originally made famous at the beginning of the 20th century because with them Dr. Morgan developed the chromosome theory of inheritance (Morgan, 1910). Among other notable milestones, *Drosophila* were central to the discovery of the homeobox genes that determine our body plan, as exemplified by possibly the most famous mutant in all biology, *antennapedia*. To this day, *Drosophila* are a widely used animal model in many labs worldwide, because of their small size, the ease of handling, culturing, and high fecundity. But probably the most important reason is that a range of powerful genetic tools was developed for *Drosophila* to manipulate their small compact genome, and so they can be used to study a wide range of human genetic disorders that affect conserved genes, much more efficiently than say mouse models (Hales et al., 2015).

Flies in the laboratory are usually kept in cylindrical plastic tubes with sterile food at the base, which mainly consists of a mixture of agar, yeast, corn meal, molasses and water. The fly life-cycle at 25°C is approximately 10 days from fertilized egg or embryo to newborn fly, also called an adult, but lowering the temperature slows all stages of the life-cycle (Fig. 16). This effect of low temperature is a feature that researchers exploit for stock maintenance. After fertilization, embryogenesis lasts approximately 24 hours, and is followed by three larval stages called first, second and third instar larval stages. During the first two, where each lasts a day, larvae are still in the food because that is usually where adult flies go to eat and mate. The third instar larval stage typically takes two days and is characterized by the climbing of the larvae up in the vial; therefore, it is common to refer to them as wandering larvae. After these five days, larvae start metamorphosis inside a hard case called the puparium and they are referred to as pupae. This is a period that takes another four to five days where the animal drastically changes at all levels. It will need to degrade larval tissues to form new adult ones from structures called imaginal discs, which are progenitor-deriving distinct cells each developing into different adult structures, such as eyes, wings, legs and so on. Once the metamorphosis is over, adult flies will hatch from the puparium, also referred to as eclosion, and adult flies will continue their lifespan for about 70 days in healthy conditions at 25°C (Ziehm et al., 2013).

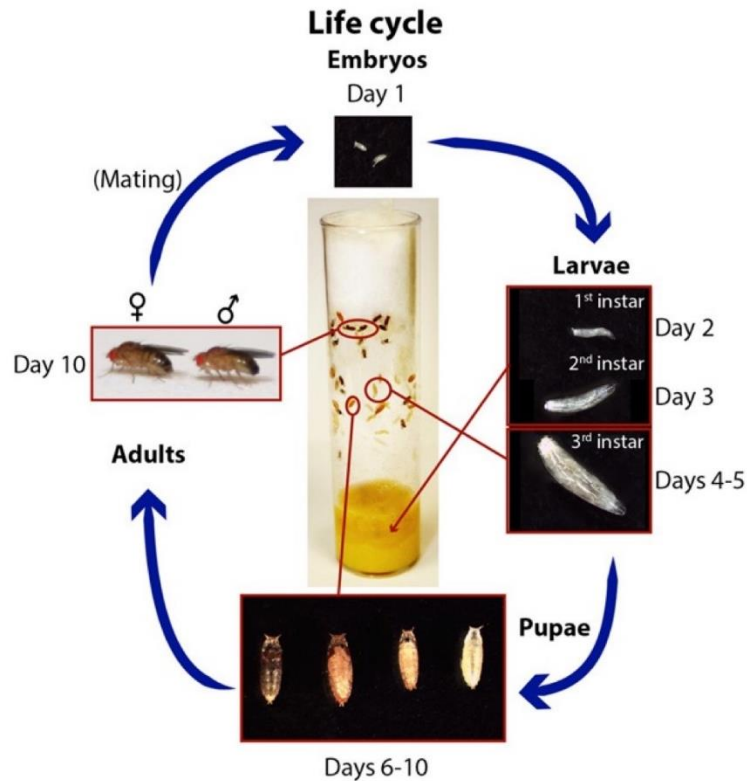


Figure I6. Life cycle of *D. melanogaster*. Each major stage of the life cycle, which is completed in 9–10 days when flies are maintained at 25°C. Embryos hatch from the egg after 1 day and spend about 4 days as larvae in the food. Around day 4-5, third instar larvae crawl out of the food to pupate on the side of the vial. During days 5–9, metamorphosis occurs until adult flies eclose from pupal cases around days 9–10. Cycle restarts when adult flies begin mating about 8 hours after they are born. (Modified from Hales et al., 2015).

From the moment they hatch until they become sexually mature, there is a period of about 8 hours that is a necessary window for the researcher to collect those females, called virgins, for future crosses, facilitated by a characteristic paler and bigger morphology and the presence of the meconium in the abdomen (Fig. I7A). Besides, both newborn male and female virgins, usually show wet and sticky body and wings (Fig. I7C). This is done because once they start breeding females can store sperm from their mate relatives and thus it could produce unwanted progeny in subsequent experimental crosses. Males, on the contrary, can be collected at any time.

Male and female adults can easily be distinguished because males have a characteristic pigmentation in their abdomen, being that the reason why they are called *melanogaster* which in Latin means dark gut, and also show more prominent genitals (Fig. I7B).

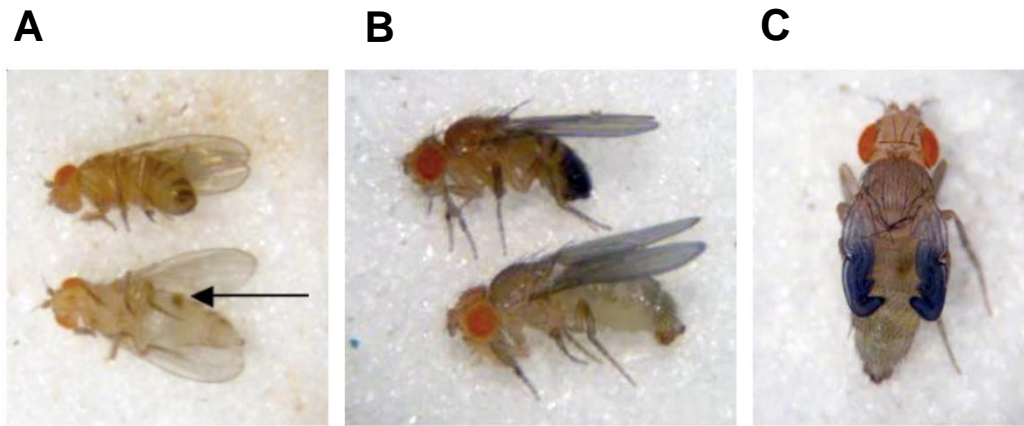


Figure 17. Male and female virgins have several distinguishing characteristics. (A) Two female flies, where the bottom female is more recently born (virgin) and shows the characteristic meconium in the abdomen (arrow). **(B)** Two male flies, where the bottom male shows the typically big genitalia at the end of the abdomen that distinguish them from females. Also note the identifying black abdomen in adult males (melanogaster). **(C)** A newborn virgin fly with typical wet wings after eclosion. (From the Berg lab, University of Washington).

UAS-Gal4 system for targeted gene expression

In yeast, galactose metabolism is transcriptionally regulated by GAL4 only when the upstream activation system (UAS) binds to it. The observation that the yeast UAS-GAL4 system was active in other organisms, such as plants, zebrafish, *Drosophila* and even in human cells, led to the idea of a yeast geneticist and a *Drosophila* geneticist at the Harvard Medical School to generate a targeted gene expression system in the fly (Brand & Perrimon, 1993).

Before the UAS-GAL4 system transgene expression in *Drosophila* in selected tissues or in a transient way could be achieved by using defined promoters or heat shock promoters, respectively; but different transgenic lines had to be created for almost each experiment. The UAS-Gal4 system allowed to create a physically separated system where some transgenic flies would contain the UAS sequence followed by the transgene or the target gene, and other independent ones would have its transcriptional activator (the Gal4 driver), thus as long as these flies were kept separated nothing would occur. However, when the two groups of flies were crossed, the transgene would be expressed depending on the pattern dictated by the expression of the Gal4 (Fig. 18). The system offers multiple combinations as infinite target genes or sequences can be used to cross with the thousands of Gal4 drivers available and many more that can be generated that limit expression to specific cells, tissues and organs (Dahmann, 2016).

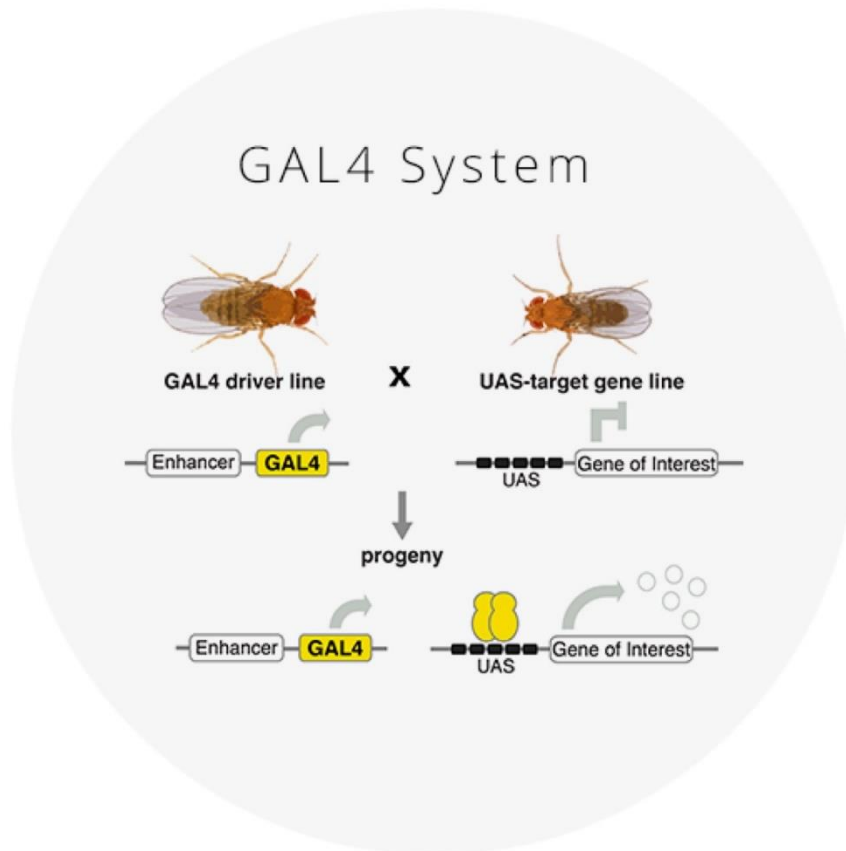


Figure 18. GAL4 driver and UAS-target gene fly lines are generated and maintained as separate stocks. In the absence of GAL4 there is no expression of the target gene. Crossing a fly expressing GAL4 to a fly carrying a UAS-target genes results in targeted gene expression in the progeny of the cross. (Modified from Dahmann, 2016).

Currently, many modified UAS-Gal4 systems exist that include more complex genetic elements that confer additional features to the system. To mention some of the most important modifications: taking advantage of the CRISPR-Cas9 system, UAS transgenes have been modified to reduce or remove expression in a tissue-specific way; GAL80 system has been created that allows the control of the expression of the GAL4 by a temperature-dependent GAL80; or the FLP-out GAL4 system that enables to generate mosaic tissues with cells that express the transgene and cells that do not by expressing the FLP recombinase under a heat shock promoter that will randomly remove a transcription termination signal between the promoter and the Gal4, when a certain temperature shock is induced. All these modified versions of the original system allow further specialization and let the researchers acquire more detailed results that help answering otherwise very complex questions (Dahmann, 2016).

Materials & Methods

Cloning and transgenesis. The original pAAV-GFAP-mKate-FL-D4 plasmid was used as a template to amplify by PCR the sequence encoding the mKate and D4 region of interest with the following primers that contain extra sequences encoding for Bgl II and Not I restriction sites: 5'-atTTGAGATCTcaaa ATG GAGCTGATTAAGGAGAACATG-3' (forward) and 5'-aactaaGCGGCCGC TTAGTTGTAGGTGATGCTGCT-3' (reverse). The PCR product was purified and inserted into the Bgl II and Not I sites of an empty pUASTattB vector using T4 DNA ligase (Bischof et al., 2007). The resulting plasmid was amplified by doing subsequent transformation by heatshock into competent *Escherichia Coli*, colony selection in Ampicillin culture media and purification of the plasmid using the Zippy™ Plasmid Miniprep Kit (Zymmo Research) first and the PureLink® HiPure Plasmid Midiprep Kit (Invitrogen) second. The products obtained after purification were verified by Sanger sequencing (Genewiz) and injected into the following embryos (done by a company): pUASTattB-mKate-ThetaTox-D4 – *y1 w11118; PBac{y+-attP-3B}VK00033* (Venken et al., 2006). Transgenic flies were selected with a *W⁺* marker and were balanced.

For the generation of the UAS-*dAtad3*^{R472C} flies, pUASTattB-dAtad3R472C-V5 construct was generated by performing site-directed mutagenesis PCR using the original pUASTattB-dAtad3aWT-V5 vector as a template (Yap et al., 2021) and the following primers: 5'-tttgattatgccatcaacgatTGC ctggatgaaatggaggagttc-3' (forward) and 5'-gaactccaccatttcatccagGCAatcgttgatggcataatcaaa-3' (reverse), to introduce the arginine to a cysteine substitution. The PCR product was purified and inserted into the EcoR I and Not I sites of an empty pUASTattB vector using T4 DNA ligase (Bischof et al., 2007). The resulting plasmid was treated the same as the pUASTattB-dAtad3R472C-V5 plasmid and the same procedure was followed for transformation and amplification. The products obtained after purification were verified by Sanger sequencing (Genewiz) and injected into the following embryos (done by a company): pUASTattB-dAtad3R472C-V5–*y1 w11118; PBac{y+-attP-3B}VK00037* (Venken et al., 2006). Transgenic flies were selected with a *W⁺* marker and were balanced.

Fly strains and maintenance. The following stocks were obtained from the Bloomington *Drosophila* Stock Center at Indiana University (BDSC): *elav*^{C155}-*Gal4*, *insc-Gal4*, *UAS-GFP-LAMP* (on 2nd chromosome). *dAtad3* RNAi line (v22445) was obtained from VDRC stock center.

To generate flies carrying both *insc-Gal4* and *UAS-GFP-LAMP*, we performed recombination of these two genetic components. The flies carrying *insc-Gal4*, *UAS-GFP-LAMP* were verified by genomic PCR using the following primers. pUAST-F: 5'-AGTGCAAGTTAAAGTGAATC-3' EGFP-R: 5'- CGCCTTCTTGACGAGTTCTTC-3'.

All flies were maintained at room temperature (21°C). All crosses were kept at 25°C.

DNA extraction, PCR, electrophoresis and sequencing. Genomic DNA was extracted from 10 *UAS-dAtad3^{R472C}-V5 Drosophila* from 1-3 lines using the PureLink™ Genomic DNA Mini Kit (Invitrogen). The sequences of 1 kb corresponding to mKate-D4 (with the pUAST primers) or about 1.8 kb corresponding to dAtad3 (with all the primers) were amplified following OneTaq® Hot Start PCR protocol (New England BioLabs) using the following primers: 5'-AGTGCAAGTTAAAGTGAATC-3' (pUAST forward), 5'-GTAGTTTAAACACATTATACAC-3' (pUAST reverse), 5'-GCCAAGGCACGAGTGGATCGC-3' (dAtad3-seq1) and 5'-GTGTTGACTGGTCGCACACC3'- (dAtad3-seq2). An electrophoresis was done to visualize the PCR products and PCR products were purified with the QIAquick PCR purification kit (Qiagen). Last, purified products were sent to GeneWiz for Sanger sequencing.

Drosophila protein extraction and immunoblotting. For the Western Blots from *Drosophila*, we kept a mixture of head, thorax and legs (after removing abdomen and wings) out of 6 flies (3 males and 3 females) from each genotype, or only heads out of 20 flies (10 males and 10 females) from each genotype. These samples were grinded mechanically against the walls of an eppendorf with plastic arrows and chemically with 100 µL of 1x Sample Buffer containing 4x Bolt™ LDS (Invitrogen), 10x Reducing Bolt™ (Invitrogen), RIPA with 1% SDS and 100x protease inhibitor (Invitrogen). They were boiled for 10 minutes at 70-100°C and centrifuged 3 minutes at 15000 rpm to only keep the supernatant. The same amount of total protein (10 µL/well) was loaded in 4-12% Mini-PROTEAN® TGX Stain-Free™ Protein Gels (Bio-Rad) and was run with Bolt™ MES SDS Running Buffer (Invitrogen) for 1h at 100 V

and 10 minutes at 180 V both at RT. Transfer to nitrocellulose membranes (BioRad) was done in Towbin buffer 1x with 10% methanol for 1 h at 10 V. Total protein was stained by red ponceau with the Ponceau S Staining solution (Thermo Fisher) and washed by milliQ water and a picture with the phone was taken. Blocking of the proteins was done with 5% non-fat milk in TBS, 0.05% Tween, for 1 h at RT. Membranes were incubated overnight at 4°C with the following primary antibodies in blocking solution: mouse anti-V5 1:2000 (Invitrogen), mouse anti-ATP5A 1:2000 (Abcam) and mouse anti-actin 1:20000 (MP Biomedicals). The next day rinses and washes were done with TBS, 0.05% Tween, and incubation with the HRP conjugated goat anti-rabbit (Invitrogen) or goat anti-mouse (Invitrogen) secondary antibodies, both at 1:7000 for 1 h at RT. Proteins were detected using Clarity™ Western ECL substrate (BioRad) and images were acquired in a ChemiDoc XRS+ System (BioRad).

Drosophila larval brain dissection and immunohistochemistry. For *Drosophila* brain staining, dissection of third instar larvae was performed as described in Hafer and Schedl (Hafer & Schedl 2006 J Vis Exp). Briefly, brains attached to the cuticle from the third instar larvae were fixed in 500 µl of 4% formaldehyde for 30 minutes at room temperature. The fixation solution was discarded, and the samples were washed in PBS containing 0.3% Triton X-100. The primary antibodies were used for the following dilutions: rabbit anti-GFP 1:1000 (Molecular Probes), rat anti-Miranda 1:500 (Abcam), and mouse anti-Prospero 1:1000 (DSHB). Anti-mouse IgG highly cross-absorbed secondary antibody, Alexa Fluor 488 (Invitrogen), anti-rat IgG cross-absorbed secondary antibody, Cyanine5 (Invitrogen), and anti-rabbit IgG highly cross-absorbed secondary antibody, Alexa 488 (Invitrogen) were used at 1:500. Samples were mounted in Vectashield (Vector Laboratories). Imaging was performed by LSM710 confocal microscope (Zeiss). Images were processed with the Zeiss LSM Image Browser and Adobe Photoshop.

Results

R2.1- Construction of a new membrane-cholesterol reporter for *Drosophila*: mKate-D4

Our attempts to label unesterified cholesterol in fly histological samples with filipin were unsuccessful due to high background and autofluorescence in the larval fat body and brain. In any case, based on our premise that ATAD3 is involved not only in cholesterol transport to the mitochondria, but also its recruitment to mitochondrial membranes, we wanted to be able to detect membrane-embedded cholesterol, instead of unesterified cholesterol. We learned from the literature that there is a naturally occurring protein that has this property: perfringolysin O, a pore-forming toxin from the bacterium *Clostridium perfringens*. D4 is a cholesterol-binding domain of PFO devoid of the pore forming-activity. D4 conjugated to a fluorescent reporter has been used to stain membrane-bound cholesterol in cultured cells (Waheed et al., 2001; Wilhelm et al., 2019). Therefore, we obtained a plasmid that encodes D4 attached to a fluorescent reporter, mKate, from Dr. Mazahir T. Hasan (Achucarro Basque Center for Neuroscience). The plasmid was suitable for expression in human astrocytes. We amplified the D4-mKate portion of the plasmid, and sub-cloned it in plasmids suitable for expressing it in *Drosophila*, taking advantage of the UAS-Gal4 system. We then, transformed the new plasmid and produced sufficient amount and ensured by PCR and sequencing that the new plasmid had been created correctly. After verification, the plasmid was sent to a company that injected it into flies creating a novel *Drosophila* line with the UAS-*mKate-D4* construct. To check the influence in viability exerted by the plasmid and to make sure it would be expressed and would properly label cholesterol in membranes when crossed to flies containing a Gal4 driver, we next performed a series of consecutive crosses to verify that. We detected no phenotypical abnormalities neither in the development, movement or the capacity of procreation of these flies (data not shown) and we successfully detected differences in membrane cholesterol using flies with a *dAtad3* point mutant (R.2.2.2 and R.2.2.3), confirming the new plasmid created for the visualization of membrane-bound cholesterol in *Drosophila* was a success.

R2.2- Generation and characterization of *dAtad3*^{R472C} flies

R2.2.1-Generation of UAS-*dAtad3*(R472C)-V5 flies.

Dr. Wan Hee Yoon was one of the leading authors of the first report of ATAD3 disease (Harel et al., 2016) and is a specialist in *Drosophila* disease models. My original plan for our collaboration with Dr. Yoon's lab was to create a fly model of human ATAD3 R466C, by introducing into flies an additional copy of the equivalent orthologous mutation *dAtad3*^{R472C}; however, in the initial discussion we learned that Dr. Yoon had already created this model because it was one of the most prominent of the 29 amino acid substitutions associated with the ATAD3 monoallelic duplication (described above and in Gunning et al., 2020). On arrival in the Yoon laboratory, I studied three independent *dAtad3*^{R472C} lines. Two were indistinguishable from controls, whereas the third was lethal or had severe phenotypes when expression was restricted (see below). To determine whether the affected line was attributable to *dAtad3*^{R472C}, I screened for the presence of the transgene. For this, genomic DNA was extracted from the three *Drosophila* lines and the sequence encoding the transgene amplified by PCR. All three lines yielded a product that corresponded in size with the sequence of interest (Fig. 38), indicating the transgene from the plasmid injected into the flies had been inserted correctly. Moreover, Sanger sequencing of all three samples confirmed all three had the TGC nucleotide substitution (encodes cysteine) instead of CGT (encodes arginine) in the 1414-16 base positions (Fig. 38), demonstrating the correct insertion of the mutation, identical for the three lines.

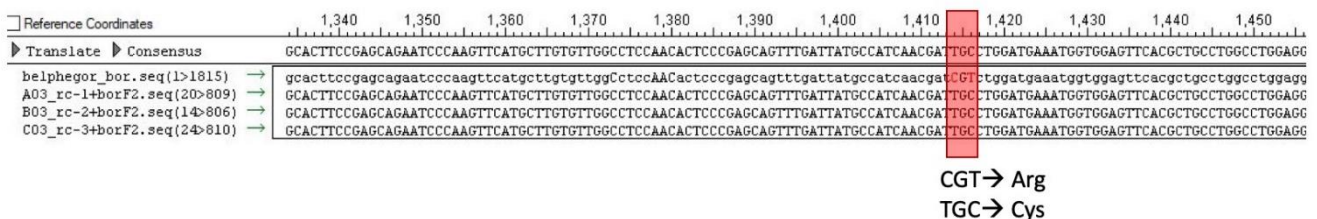
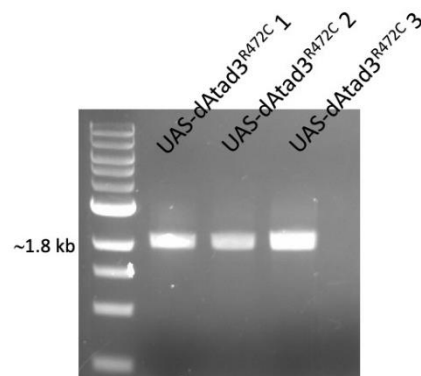


Figure 38. All three of the original UAS-dAtad3^{R472C} lines had a transgene of about 1.8 kb with the correct substitution. The length of the transgene was evaluated after genomic DNA was PCR amplified and run on a gel (upper part). Sanger DNA showed the c.1414-16CGT>TGC; p.Arg>Cys substitution in the three lines (A03, B03 and C03) compared to the wild type dAtad3 sequence (belphegor_bor). Reference coordinates indicates the position in the DNA sequence and each of the letters corresponds to the established nucleotide code (adenine (A), thymine (T), guanine (G) and cytosine (C)).

Having excluded a technical failure in the introduction of the transgene in the sequence, the next logical step was to check its expression in the three different lines, as failure to express the transgene could potentially explain the differences in viability between the three lines. Because the third *Drosophila* line did not produce any viable progeny with most of the Gal4 drivers, protein for analysis was only available from the progeny of the first and second lines. These two lines were crossed with two ubiquitous Gal4 drivers (*Act-Gal4* and *Tub-Gal4*) and a Gal4 driver that restricts expression to the muscle and nervous system (*dAtad3-Gal4*). As the latter Gal4-driver has restricted expression, protein was extracted from a mixture of heads, thoraxes and legs, to obtain protein from expressing tissues. As a control we used transgenic flies with a short sequence encoding the V5 peptide under the control of the UAS promoter but no 'gene-of-interest' (UAS-empty). Both lines were expressing the UAS-dAtad3^{R472C} (labeled by an anti-V5 antibody), though some differences in the abundance of the bands were detected between the two lines under the expression of the three different Gal4 drivers, especially for *Tub-Gal4* and *dAtad3-Gal4* (Fig. 39). Although the first and second lines expressed the mutant dAtad3^{R472} transgene, later it became clear that the level of expression was on the low side and possibly especially so in the head.

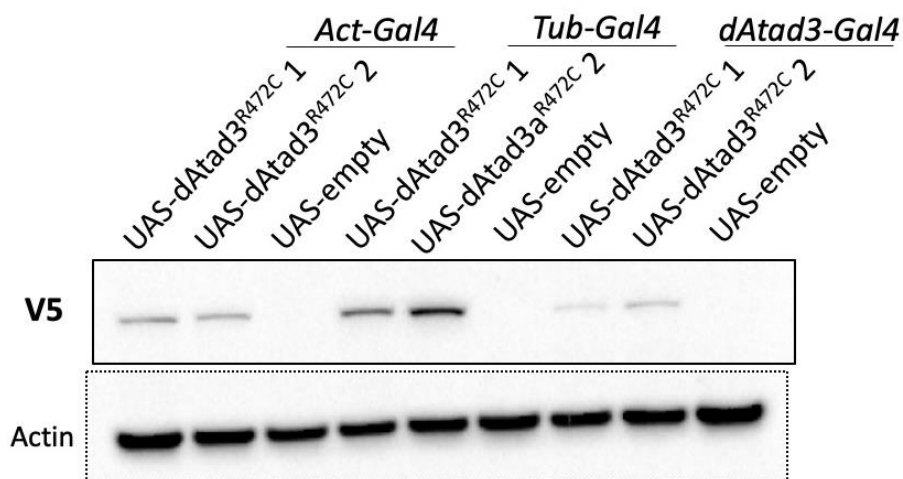


Figure 39. UAS-dAtad3^{R472C} lines 1 and 2 express the transgene under *Act-Gal4*, *Tub-Gal4* and *dAtad3-Gal4* drivers. Protein was extracted from a mixture of head, thorax and legs of UAS-dAtad3^{R472C} lines 1 and 2 and the UAS-empty flies as a control, each of which crossed to ubiquitous (*Act-Gal4* and *Tub-Gal4*) or muscle and nervous system expressing (*dAtad3-Gal4*) Gal4 drivers. Each of the transgenes has a V5-tag to enable posterior antibody detection (anti-V5) and actin was used as a loading control. Images were acquired on ChemiDoc XRS+ System.

The last step that could help explain the differences in viability between the three lines, was to analyze the expression of the transgene under the *ey-Gal4* driver, which at the time was the only Gal4 driver tested that produced some viable flies, in the case of the third line. Since the expression of the *ey-Gal4* driver is restricted to the eye, the optic nerve and part of the brain, only heads were used to extract protein from the progeny of these crosses. Despite all the viable progeny had the same genotype, the third line was further divided in two groups, based on very characteristic phenotypes: flies that were born with normal eyes and flies that had abnormal eyes (indicated with an asterisk). The first and second lines did not express the transgene, like the UAS-empty flies, but the third line did express the transgene, even the asterisk labeled group of the progeny with aberrant eyes (Fig. 40), likewise the flies with an extra copy of wild type *dAtad3*.

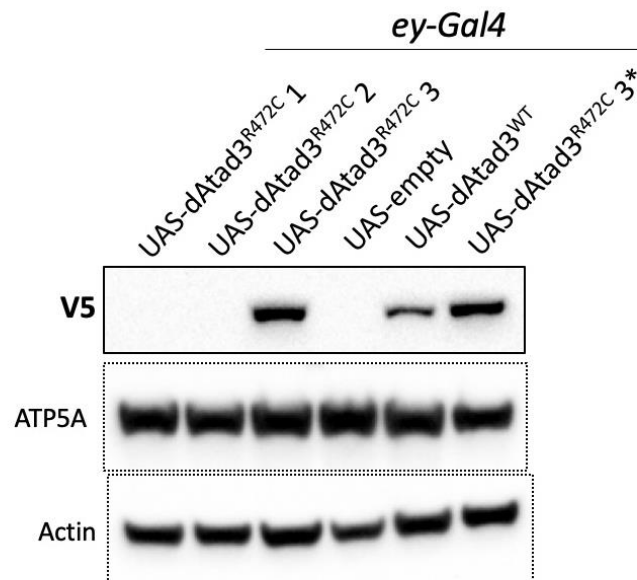


Figure 40. Uniquely UAS-dAtad3^{R472C} line 3 expresses the transgene under *ey-Gal4* driver. Protein was extracted from heads of UAS-dAtad3^{R472C} lines 1, 2, 3 and 3* (only heads with eye-defect phenotypes) and the UAS-empty (empty transgene) and UAS-dAtad3^{WT} (wild type *dAtad3* transgene) flies as controls, each of which crossed to the *ey-*

Gal4 driver, that restricts expression to the eye-optic nerve and part of the brain. The transgenes include a V5-tag to enable antibody detection (anti-V5). Actin and mitochondrial protein ATP5A were used as loading controls. Images were acquired on ChemiDoc XRS+ System.

























In light of the unresolved differences between the three lines, we constructed a new UAS-*dAtad3*^{R472C}-V5 vector. The two nucleotide change to create the R472C substitution was introduced by site-directed mutagenesis PCR of the wild type (WT) version of *Atad3*, using custom designed primers to replace the arginine at residue 472 with cysteine. The PCR product was ligated into an empty plasmid for expression in flies and was transformed, the same way as with the mKate-D4 plasmid. PCR and sequencing were used to confirm that the new plasmid had been generated correctly. After verification, the plasmid was sent to a company that inserted it into flies creating several new *Drosophila* lines with the R472C point mutation in ATAD3. Crossing five of the new lines with the different Gal4 drivers revealed that all gave ostensibly the same results as the third line, indicating the third line was representative of *dAtad3*^{R472C}.

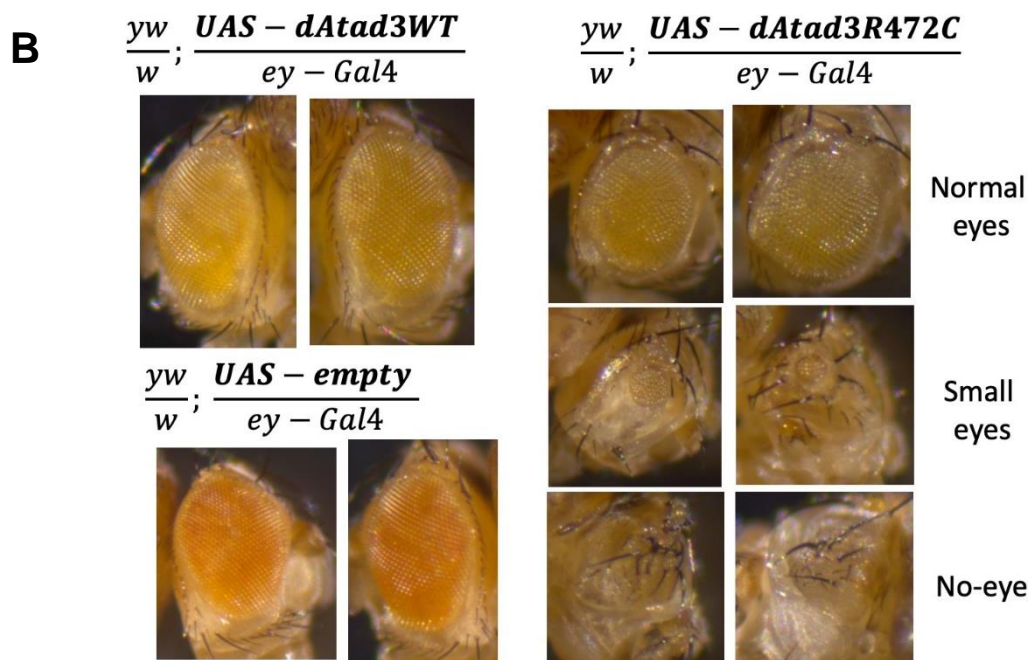
R2.2.2-Mutation severity assessment

To provide functional interpretation of the *dAtad3*^{R472C} point mutation and assess the consequences of the ablation of the arginine finger implicated in the ATP hydrolysis in ATAD3, we started by producing a series of crosses with a range of Gal4 drivers that would express the transgene in a tissue-specific manner. Three Gal4 drivers were used that express the transgene ubiquitously: daughterless-Gal4 (*da-Gal4*), tubulin-Gal4 (*tub-Gal4*) and actin-Gal4 (*act-Gal4*). No adult flies were obtained when the transgene was ubiquitously expressed owing to arrest in pupal eclosion, in two independent UAS-*dAtad3*^{R472C} lines (Fig. 41A). Expression was restricted, to study severity of the mutation in specific tissues, first to the muscle and nervous systems (as these are the most affected tissues in by mutations in *Atad3*) with the *dAtad3*-*Gal4* driver, and then to the neurons alone with the use of a Gal4-driver called Embryonic Lethal Abnormal Vision C155-Gal4 (*elav*^{C155}-*Gal4*). Both Gal4-drivers, when crossed to the UAS-*dAtad3*^{R472C} lines, led to impaired pupal eclosion (Fig. 41A). Only when the expression was much more restricted either by cell type, to the

neuroblast, with inscrutable-Gal4 (*insc-Gal4*), or restricted in time, with the late onset eye and neuronal driver Glass Multimer Reporter-Gal4 (*GMR-Gal4*), viable progeny were obtained (Fig. 41A), with no apparent developmental problems. When we used an eyeless-Gal4 driver (*ey-Gal4*) which limits expression to the eye, optic nerve and part of the brain, the transgene was viable in about 65% (Fig. 41A) of the viable flies about a third of them showed an aberrant eye-phenotype (Fig. 41B). This eye-phenotype included flies that completely lacked one or both eyes or whose shape and size was abnormal, with very small eyes (Fig. 41B). The high lethality when ubiquitously expressing *dAtad3*^{R472C} in flies is similar to that produced by the silencing of *dAtad3* with a RNAi (UAS-*dAtad3* RNAi V22445) (Fig. 41A). These findings indicate that loss of the arginine finger mediating ATP hydrolysis in ATAD3 is highly deleterious in flies. Even when expression is limited to the eye and part of the brain, reduced viability and a severe eye-phenotype is observed. On the other hand, expression restricted to neuroblasts was well tolerated with no loss of viability and no overt phenotypes. Therefore, the more restricted the expression of the mutant *Atad3* variant, the less it affects viability (Fig. 42). Therefore, a spectrum of transgene expression arises that starts from absolute inviability, goes through partial viability with severe phenotypic alterations, and ends in total viability without apparent changes. These last two are windows that allow us to observe the events that occur in the cells during the pathological process caused by the mutation, which would otherwise be very difficult to study due to the severity of the phenotypes that are generated.

A

Transgenes	Gal4 drivers							
	<i>da-Gal4</i>	<i>tub-Gal4</i>	<i>act-Gal4</i>	<i>dAtad3-Gal4</i>	<i>elav¹⁵⁵-Gal4</i>	<i>ey-Gal4</i>	<i>GMR-Gal4</i>	<i>insc-Gal4</i>
UAS- <i>dAtad3</i> ^{R472C} -V5	 Lethal	 Lethal	 Lethal	 Lethal	 Lethal	 Viable 65%	 Viable	 Viable
UAS-empty (UK37)-V5	 Viable	 Viable	 Viable	 Viable	 Viable	 Viable	 Viable	 Viable
UAS- <i>dATAD3</i> RNAi (V22445)	 Lethal	 Lethal	 Lethal	 Lethal	 Lethal	 Lethal	 Viable	 Viable



Progeny's genotype	Cross 1		Cross 2		Viability %		Eye defect %	
	Pupae	F1	Pupae	F1	Cross1	Cross2	Cross1	Cross2
$\frac{yw}{w}; \frac{UAS - dAtad3(R472C)}{ey - Gal4}$	84	55	68	40	65	60	25	42
$\frac{yw}{w}; \frac{UAS - dAtad3WT}{ey - Gal4}$	127	133	132	140	100	100	0	0
$\frac{yw}{w}; \frac{UAS - empty}{ey - Gal4}$	136	143	131	150	100	100	0	0
$\frac{yw}{w}; \frac{UAS - dAtad3 RNAi (V22445)}{ey - Gal4}$	118	0	92	0	0	0	0	0

Figure 41. The orthologous mutation in *Drosophila*, *dAtad3*^{R472C}, is highly deleterious and escapers exhibit abnormal eye-defects. (A) Chart that shows the viability/lethality/partial viability (black, red and orange respectively) of UAS-*dAtad3*^{R472C} expressed under different Gal4 drivers: ubiquitous (*Act-Gal4* and *Tub-Gal4*), muscle and nervous system driver (*dAtad3-Gal4*), neuron driver (*elav*^{C155}-*Gal4*), eye, optic nerve and part of the brain driver (*ey-Gal4*), late onset eye and neuronal driver (*GMR-Gal4*) and neuroblast driver (*insc-Gal4*). UAS-empty (empty transgene) and UAS-*dAtad3* RNAi (RNA interference silent *dAtad3* transgenic fly) were used as controls. **(B)** Light microscope images of the abnormal eye phenotypes of flies expressing UAS-*dAtad3*^{R472C} under the *ey-Gal4* driver seen in ~33% of the viable progeny, compared to the normal eyes of flies expressing no transgene (UAS-empty), or wild-type transgenic *Atad3* (UAS-*dAtad3*^{WT}). Chart with the number of pupae and progeny (F1) from each cross for each of the different genotypes gives the viability % (n F1/n pupae) and in the case of UAS-

dAtad3^{R472C} flies under *ey-Gal4* the percentage of the viable flies that have eye defects (no-eyes or one little eye). Full genotypes are shown.

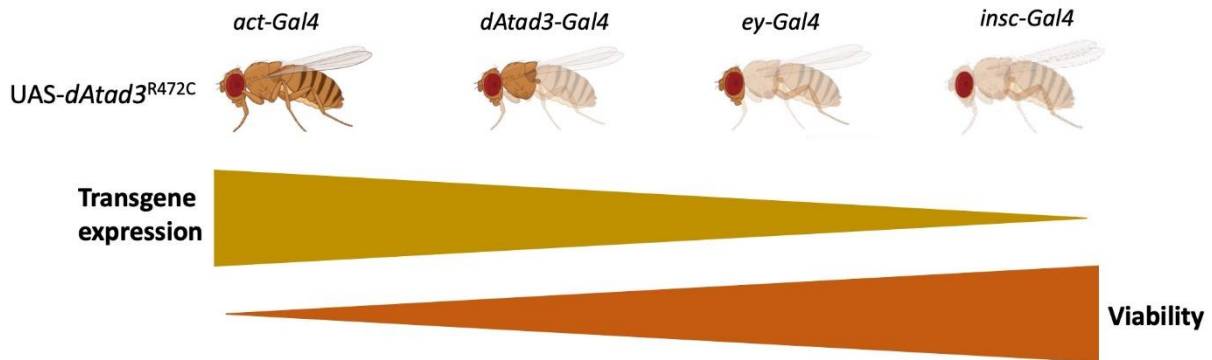


Figure 42. Restricted expression of the UAS-*dAtad3*^{R472C} transgene increases viability. Schematic representation of the increase in viability (orange) when transgene UAS-*dAtad3*^{R472C} is restricted or directed to specific body-parts and tissues (yellow) with the use of different Gal4-drivers, as indicated in the drawings of the flies.

R2.2.3- Membrane-bound cholesterol and lysosomes

A key reason for generating the *Drosophila* model was to determine whether mutant Atad3 produced cholesterol abnormalities. If this were to prove the case, it would a) show that ATAD3's impact on cholesterol metabolism is highly conserved and so would speak to the fundamental function of the protein; b) allow us to determine the effects of mutant Atad3 *in vivo* and c) allow us to study the developmental aspects of the disorder. Because our attempts to label free cholesterol in larval brains and the fat body with Bodipy failed, we decided to develop a new tool to label cholesterol in cellular (and mitochondrial) membranes (see R.2.1.1). The results that follow were carried out in collaboration, as I had to return from Dr. Yoon's lab; thus, we did the conceptualization of the experiments and Dr. Yoon and his staff performed the experiments. We first evaluated the effect of the membrane-bound cholesterol in the UAS-dATAD3^{R472C} larval neuroblasts. Expression of UAS-*mKate-D4* with UAS-*empty* by the neuroblast driver *insc-Gal4* produced a low diffuse mKate (red) signal in neuroblast of control larvae (Fig.43i), spread all over the neuroblast. In contrast, the expression of UAS-*mKate-D4* with UAS-*dAtad3*^{R472C} by *insc-Gal4* showed numerous mKate foci (Fig. 43ii), indicating membrane-bound cholesterol in

dAtad3^{R472C} flies is aggregated in discrete foci, and suggesting cholesterol is also elevated in flies, as in human *Atad3* mutant fibroblast, and accumulated in membranes.

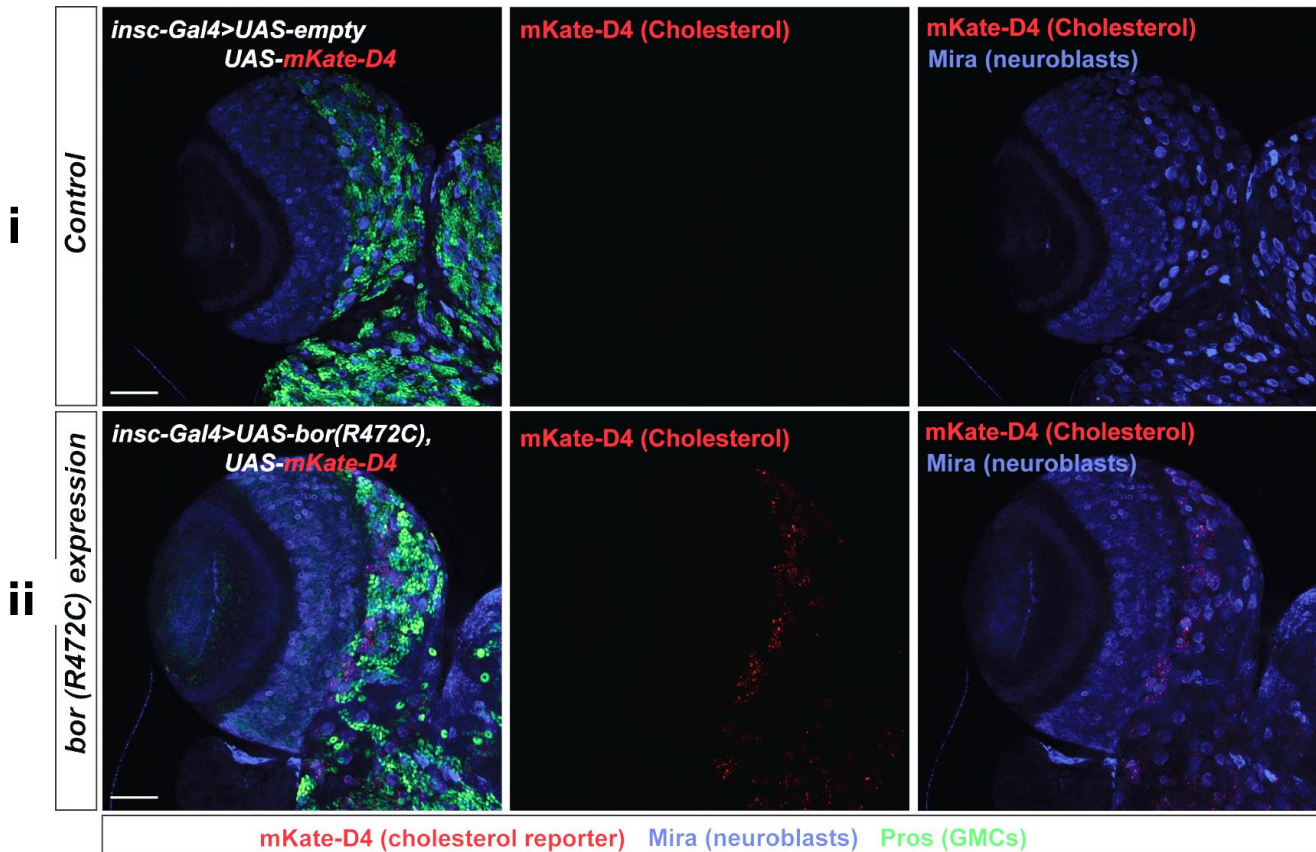


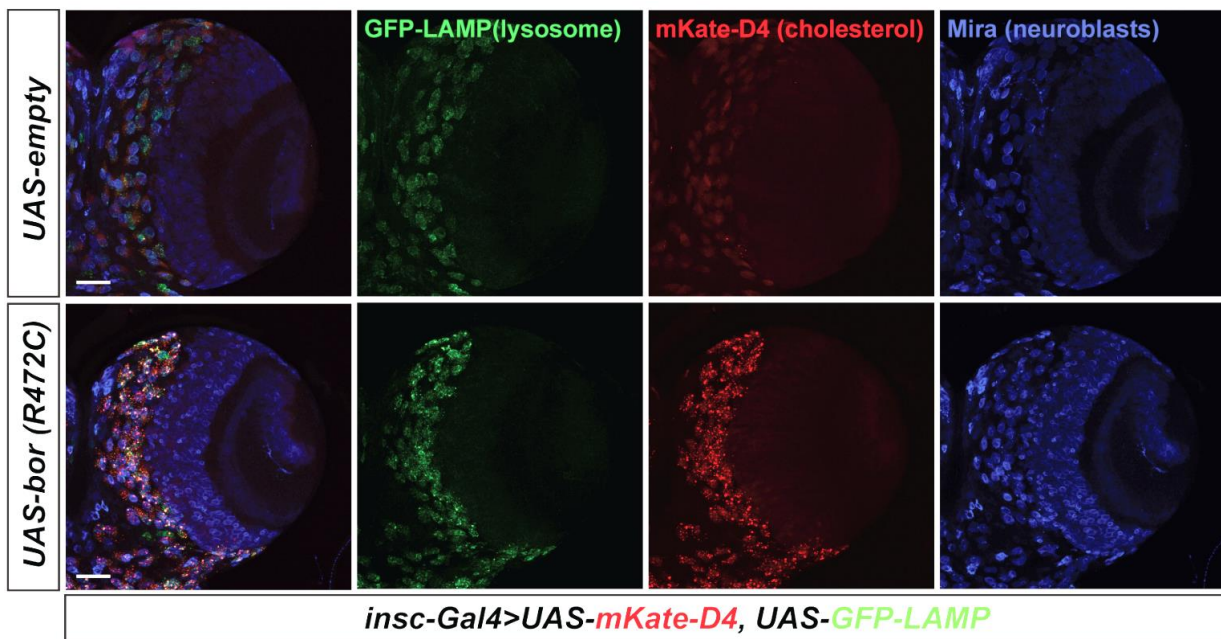
Figure 43. The orthologous mutation in *Drosophila*, *dAtad3*^{R472C} increases membrane-bound cholesterol. Confocal micrographs of *Drosophila* larval brain lobes carrying *insc-Gal4* and UAS-mKate-D4 together with UAS-empty (control), **i**), or UAS-*dAtad3*^{R472C}, **ii**). Neuroblasts are labeled miranda (blue) and ganglion mother cells (GMCs) by Prospero (green). mKate-D4 (red) is the membrane-bound cholesterol reporter. Scale bar= 50 μ M

Having shown that there was a marked increase in lysosomes in the human cell lines with mutant ATAD3 (see R.1.5.3), we suggested to Dr. Yoon that he apply a lysosomal marker in conjunction with the cholesterol marker. He then crossed the double mutant UAS-*mKate-D4* and UAS-*empty/dAtad3*^{R472C} flies with a *Drosophila* line expressing a fluorescently tagged LAMP protein that labels lysosomes *in vivo* (UAS-*GFP-LAMP*) (Pulipparacharuvi., 2005). The resulting *dAtad3*^{R472C} flies when expressed under the *insc-Gal4* driver, showed an increase in the GFP-LAMP signal compared to that observed in UAS-*empty* flies (Fig. 44A) indicating *Drosophila* with mutant *Atad3* also had an elevated pool of lysosomes, similar to human fibroblasts

with mutant *Atad3*. At higher magnification, it could be observed that the neuroblasts with higher amounts of lysosomes were the ones that also had elevated membrane cholesterol signal (Fig. 44B). In fact, in more than a quarter of puncta both mKate-D4 and GFP-LAMP signals were overlapping or juxtaposed (Fig. 44B and C). This strongly suggests that the lysosomes are targeting and ingesting the membranes with a high concentration of cholesterol.

This result is concordant with the TEM images from the human ATAD3 mutant cell lines (see R.1.5.3), i.e., the onion and marble-like lysosomes (membrane-whorls) are inferred to contain cholesterol-engorged membranes, as further elaborated in the Discussion.

A



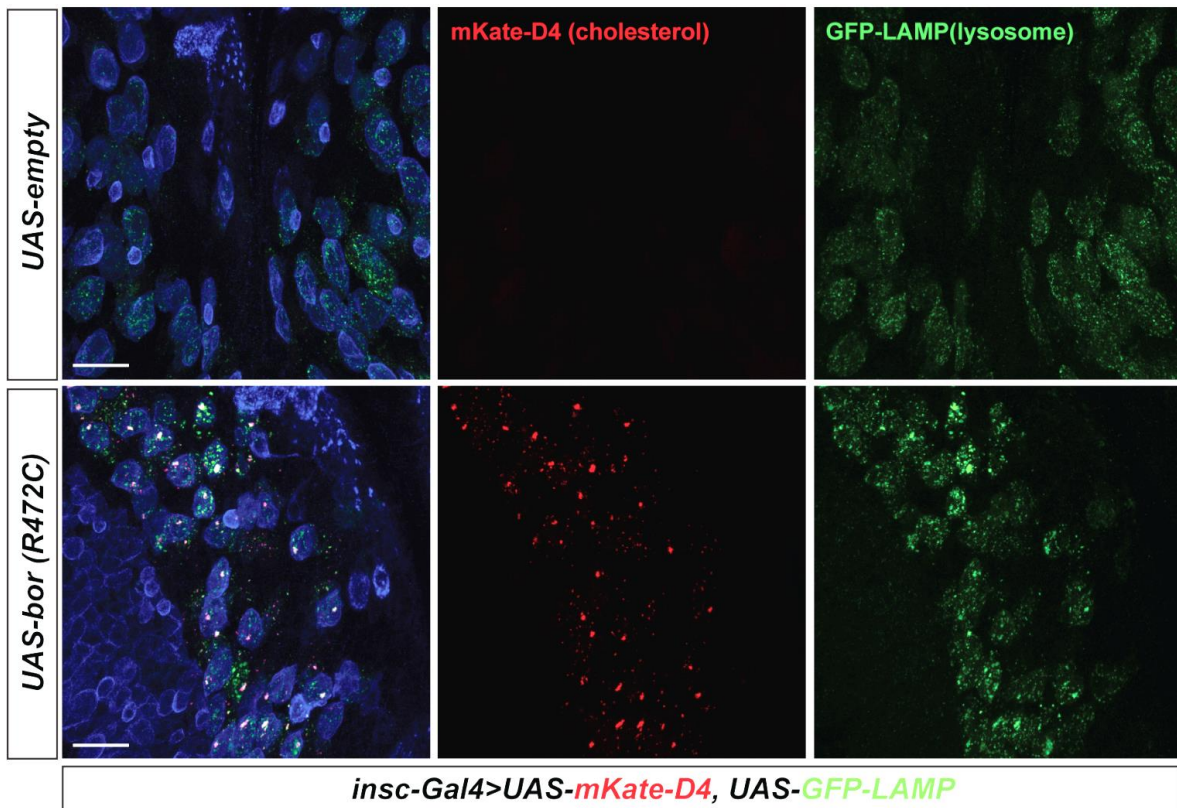
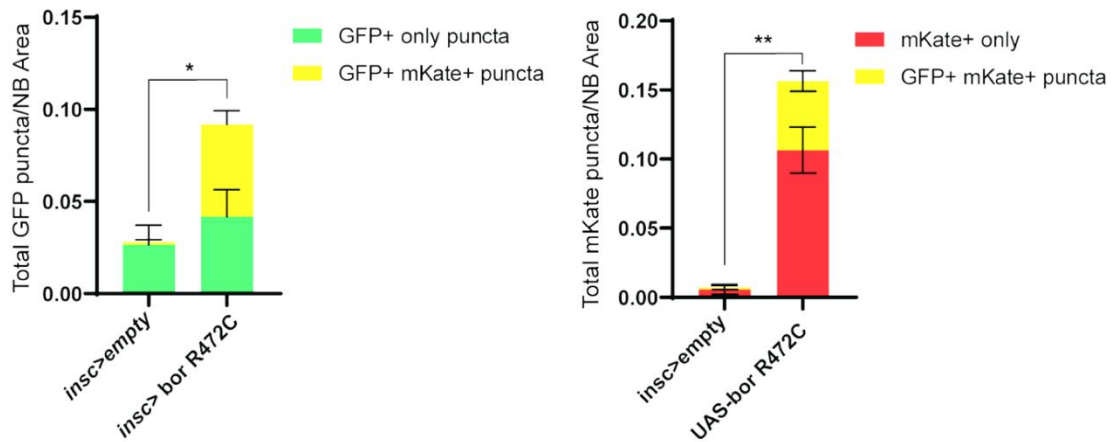
B**C**

Figure 44. *dAtad3*^{R472C} mutant neuroblasts show increased membrane-associated cholesterol together with increased lysosome content. Confocal micrographs of *Drosophila* brain lobes carrying *insc-Gal4*, UAS-GFP-LAMP, and UAS-mKate-D4 together with UAS-empty (control), or UAS-*dAtad3*^{R472C} at a magnification of 20 x. Scale bar 50 μ m, (A) and 63 x; scalebar 20 μ m (B). (C) Quantification of puncta area of GFP-LAMP, mKate-D4, and both signals. Error bars indicate the statistical errors of the mean (SEM). p values were calculated using Student's t test. *p < 0.05, **p < 0.01. Neuroblasts are labeled miranda (blue). GFP-LAMP (green) marks lysosomes. mKate-D4 (red) is the membrane-bound cholesterol reporter.

Discussion

Mitochondrial diseases were originally classified based on clinical presentations since canonical syndromes like Person, Alpers, Leigh, Kearns-Sayre, LHON, Barth, MERRF or MELAS with particular constellations of symptoms had been recognized for decades before their genetic basis was understood. Despite these classifications help, not every patient presents all the symptoms characteristic of a syndrome and some can display just a single symptom. This occurs even in siblings who have a very similar genetic background (even with the exact same variant) but have different clinical presentations, evidencing the power of other epigenetic or environmental factors. As we previously addressed, some of the disorders can begin right after birth but many do not present until adulthood. Some can be acute, sporadic presentations characterized by stroke-like episodes, and many are chronic which worsen over the years. Thus, all these factors complicate the diagnosis of mitochondrial diseases and in many patients, mitochondrial disease is just one of several diagnostic possibilities. Therefore, the identification of pathogenic variants is required to confirm the diagnosis of a mitochondrial disorder. The recognition of a certain cluster of symptoms, close examination of the familial clinical history or knowledge of a geographical prevalent disease may lead to the testing of specific variants, but usually, specific panel-testing, exome or genome Sanger sequencing or next generation sequencing methods are applied, depending on the needs and the budget (Rahman, 2020; Shiau Ng et al., 2021).

In the 1980s and 90s identifying the specific sequence change responsible for a disease among 3 billion nucleotides was an awesome task. The hunt for the cause of high-profile diseases, such as Duchene Muscular Dystrophy and Cystic Fibrosis, involved years of work by huge teams and was followed by scientists around the world with great expectation. The cost is difficult to estimate but would likely come to hundreds of millions of dollars at current rates. Today any curious individual can have their own genome (or at least exome, the part that includes the vast majority of known disease-causing variants) sequenced for about 500 € in an afternoon (Schwarze et al., 2018). Whole exome sequencing was first used to identify an unknown pathological variant in 2009, and the technique exploded shortly thereafter. In the UK, over 100 000 genomes had been sequenced by 2018 in a single coordinated national project targeting rare diseases and cancer (Smedley et al., 2021). Between 2018 and 1995, which was when the first nuclear gene defect responsible for mitochondrial disease was identified – a mutation in succinate dehydrogenase

subunit A (*SDHA*) that produced Leigh syndrome (Bourgeron et al., 1995)- the mitochondrial disease field had identified numerous nuclear gene mutations as the cause of a wide variety of these disorders. For instance, mitochondrial polymerase gamma, encoded by *POLG*, is considered the most common nuclear cause of mitochondrial disease, as more than 200 different mutations in *POLG* have been identified to date (Frazier et al., 2019). Even to this day new gene defects causing mitochondrial disease are coming to light, including for proteins with a well-defined role in mitochondrial biology such as variants in genes that encode for proteins involved in the mitochondrial transcription machinery like the mitochondrial RNA polymerase (*POLRMT*) or the mitochondrial transcription elongation factor (*TEFM*) (Olahova et al., 2021; Van Haute et al., 2023). Often, a major difficulty is that genome sequencing invariably reveals a host of unique variants and so the challenge is to understand which is the cause of the disease. Once the genetic lesion is clear, the next critical step is to identify tissue, cellular and molecular phenotypes that can not only confirm causality, but also provide insights into disease mechanism, with the ultimate goal of developing rational therapies. A few considerations need to be done here as there are some factors that can alter the outcome of the phenotypes in mitochondrial diseases. The variable number of mitochondria among tissues is one of them, with up to 30 times different, and the differential expression of about 25% of mitochondrial proteins between organs is another, but there are many other factors such as the ATP/ADP/AMP ratio or changes in membrane potential (Frazier et al., 2019).

However, functional validation of the identified genetic variants is highly important to verify the causality of the variant for the disease. Nowadays, many available biochemical, molecular and cellular techniques can be used and the importance of laboratory work should be reminded. Recently, all the measurable physical and biochemical traits have begun to study at once, namely phenomics, in combination with sequencing methods to create a computational diagnostic resource (Rahman, 2020).

ATAD3 pathological spectrum: genotype-phenotype correlates and diagnosis

Genotype-phenotype correlations can be useful for diagnostic purposes for which there was a clear need as by 2010, many groups researching mitochondrial diseases had identified patients with ATAD3 variants but were at a loss to know whether these

were pathological, and it was not until 2016 that the first report of pathological mutations in the *ATAD3* gene cluster was published (Harel et al., 2016). Another difficulty here is that mitochondrial diseases often show genetic heterogeneity and pleiotropy. The first occurs when many genes are reported to cause a disorder, such as in the case of Leigh syndrome where more than 75 genes are known to cause it (Lake et al., 2015), though this can also be associated with another underlying problem in not finding characteristic symptoms/phenotypes that distinguish among the different real diseases classified as one big group. Pleiotropy, on the other hand, consists of a gene that is associated to many unrelated phenotypes or shows many distinct clinical manifestations, like in the case of *POLG* that is known to cause a broad range of diseases and syndromes (Cohen et al. 2014), probably because its critical function and the wide variety of disease-causing mutations described, as stated before.

Although *ATAD3* had been reported to be involved in many different cellular tasks and its precise function has not been elucidated yet, it was logical to see *ATAD3* as a pleiotropic protein; however, the *ATAD3* deletions showed that the disease was tightly defined (fatal neonatal cerebellar hypoplasia) and the genetic lesion was unequivocal: a substantial part of the DNA was missing and the amount of the protein expressed was a fraction of normal (Harel et al., 2016; Desai et al., 2017). Thus, *ATAD3* deletions were the obvious mutants for us to further study and to begin the task of characterizing molecular and cellular defects that accompany mutations in *ATAD3*.

The duplication events in *ATAD3A* found during this thesis, which were published in 2020 (Gunning et al., 2020), were reported to cause disease for the first time, broadening the genotype spectrum of *ATAD3*-related disorders. The 68 kb duplication was found in five independent families whose parents lacked the mutation. The clinical phenotypes displayed by the case whose fibroblast we studied and the other neonates with *ATAD3* duplications overlap in some of the symptoms with previously reported cases, such as corneal clouding, cardiomyopathy, hypotonia, white matter changes, seizures, fetal akinesia, and contractures. Furthermore, all subjects from this cohort died within six weeks of life, indicating a severe developmental effect similar to that found in patients with biallelic deletions, that are also very severe (Desai et al., 2017). Further strengthening our findings, Frazier and colleagues reported another 17 cases with the same 68 kb monoallelic

duplication occurring in slightly different breakpoints but between highly homologous regions of *ATAD3A* and *ATAD3C* by non-allelic homologous recombination (Frazier et al., 2021). Their cohort also matched ours in the presentation of the clinical symptoms, with hypertrophic cardiomyopathy, lactic acidosis and perinatal death being nearly almost constant features among all deletion patients, and also shared with biallelic deletion patients (Desai et al., 2017).

The *ATAD3A/C* fusion protein arising from the duplication is uniquely associated with the severe neonatal phenotype and is therefore likely causal, unlike the extra load of *ATAD3B*. The fusion protein differs from *ATAD3A* in 29 amino acid residues within the C-terminal region, including a conserved residue within the ATPase domain, p.Arg466Cys that is conserved in all multimeric AAA+ ATPases. Despite it being located outside the Walker A and B motifs, this residue is necessary for ATP hydrolysis, as it binds to the gamma-phosphate of ATP in the neighboring monomer (Hanson & Whiteheart, 2005). In *SPASTIN*, multiple recurrent missense variants have been reported at the equivalent arginine finger residue (p.499Arg), which have been shown to result in the complete loss of the protein's ATPase activity, causing autosomal-dominant hereditary spastic paraplegia (*SPG4*), through a dominant-negative mechanism (Hazan et al., 1999; Evans et al., 2005).

The same missense variant (p.Arg466Cys) is the only amino acid mutation detected in the other patient that we characterized, *ATAD3 R466C*, (and in its 4 affected relatives), in a monoallelic fashion. Thus, it offers a simplified genetic picture of *ATAD3* dysfunction, which is valuable for the characterization of the molecular effects and consequences at the subcellular level. The evidence for this single amino acid substitution being deleterious is compelling: the mutant allele follows a dominant pattern of inheritance with full penetrance, as all five affected family members display symptoms, and this variant has not been reported in any healthy subject. Some of the clinical features resemble those observed in other milder cases of *ATAD3* dysfunction, such as the muscular and neurological deficiencies, but with additional defects affecting the eye, with optic atrophy and peripheral neuropathy as core features. To a lesser extent, some of the eye-phenotypes are shared with *ATAD3 A/C* patients, as they also present cataracts and corneal opacities. Therefore, we identified a novel variant in a patient that exclusively ablates the arginine finger involved in ATP hydrolysis and expands the clinical manifestations arising from mutations in *ATAD3A*, with a suggested dominant optic atrophy plus (*DOA+*).

The dominance of the p.Arg466Cys variant is supported by the data from *Drosophila*. Ubiquitous, pan-neuronal and neuro-muscular system expression of the orthologous *Drosophila* mutant *Atad3*^{R472C}, caused lethality, strongly suggesting that *dAtad3*^{R472C} is a dominant-negative or a gain-of-function mutation. Restriction of *dAtad3*^{R472C} expression to the eye and part of the nervous system, resulted in partial lethality and escapers frequently exhibited a marked developmental defect in the eye. Neuroblast-specific expression of *dAtad3*^{R472C} also indicated that the loss of the arginine finger produces molecular changes in cholesterol and lysosomes in *Drosophila* that parallel those of human fibroblasts with ATAD3 R466C and ATAD3 A/C.

As both mutants contain the same arginine ablation, an evident genotype-cellular phenotype correlation can be seen, which is also confirmed in the generated *dATAD3*^{R472C} mutant. This also shows the conserved function of ATAD3A, and especially of the ATPase domain, which is clearly affected by the arginine ablation both in human and fly. Furthermore, it suggests the function of the ATPase domain, which remains elusive, is highly probable to be related to cholesterol. Therefore, I hypothesize that depending on the mutation the mutants could have only specific parts or functional domains affected, which would explain why different mutants show different cellular responses and clinical manifestations, while the most severely affected mutants (like the large biallelic deletions or the in vitro knockouts) would have profound protein alterations that would correspond to the severe clinical presentations reported (Desai et al., 2017; Chen et al., 2022). Thus, in cases like ATAD3 R466C the ATPase function of the protein is affected while the protein seems to remain structurally stable, but other mutations could cause alterations that affect the structure or oligomerization capacity of ATAD3 that would produce more structural damages like loss of cristae, diminishing ER-contacts or perturbation of the connections with the nucleoid proteins, that explain the variety of cellular phenotypes and functions attributed to ATAD3A.

When the 68 kb duplication was reported great emphasis was given to the p.R466C substitution because of its established contribution to the ATPase of other AAA+ family members (Gunning et al, 2020). However, the less severe disease in the individuals that uniquely have this change, ATAD3A R466C, indicates that the other mutations make a substantial contribution to ATAD3A loss-of-function in the neonates. All the more, when it is considered that more hexamers will contain at least one affected subunit in the ATAD3 arginine finger cases than those of the individuals

with the ATAD3 A/C duplication. The reason for this is that the latter patients have two good copies of ATAD3A for every mutant, whereas mutant and wild-type ATAD3A protein are predicted to be in equimolar amounts in the ATAD3A R466C patients. There is also no suggestion that one of the mutant proteins is unstable at the level of the protein monomers, although the oligomers have, not yet been analyzed in the case of ATAD3A R466C. Experiments with recombinant proteins would help resolve the issue of the precise impact on ATPase activity and thereby clarify whether hexamers with 1-5 wild-type copies of ATAD3A support limited ATP hydrolysis.

Another useful approach for diagnosis and identification of the mutants is the conventional western blotting where the denaturing conditions produced in the protein extraction process (RIPA, heat and DTT) result in the detection of only simple ATAD3 monomers (also conditioned by the antibody used) of about 66.5 kDa. Our results show that, the different bands detected by Western blotting for the three ATAD3 mutants studied fit with the theoretical and *in silico* predictions made for each of the mutants, and so, we have been able to confirm they are translated into the expected protein product and shown that they can be identified by protein separation and antibody detection, i.e. used for diagnostic purposes in future studies. Finally, all the ATAD3 mutants were evidently stable, which is not the case for many mutant variants, such as the recessive *MPV17* mutants that can also be diagnosed via immunoblotting for being highly unstable and they lack the band corresponding to *MPV17* compared to controls (Dalla Rosa et al., 2016). Characterization of the expressing protein variants offers further possibilities, as ATAD3 forms oligomers; therefore, strategies like blue native electrophoresis (BNE) could be added to the workflow, as this could identify or corroborate many more pathological *ATAD3* mutants. If some oligomers are affected but not others this could aid understanding the functions of the different forms of ATAD3 as well as their respective contributions to the disease.

In agreement to the differences in mobility we observed, Frazier and colleagues also reported in ATAD3 complexes (formed by oligomerization) derived from patients with the same duplication as ours that the main 900 kDa complex migrated a bit faster than the same complex in controls (Frazier et al., 2021). Moreover, ATAD3 complexes were almost imperceptible in patients with biallelic deletions, similar to the low ATAD3 signal detected in our samples and as it has been reported previously

(Harel et al., 2016; Desai et al., 2017). This suggests that despite the interaction with other ATAD3 species or other partner proteins, the structural differences provided by the genetic variants are maintained even in more complex molecular forms.

Exact confirmation that the predicted protein products are translated and expressed stably in the mutant cells, especially when fusion-proteins are generated, is complicated by the limitations of the techniques used and unavailability of specific antibodies to detect each of the variants. For instance, the predicted molecular weight of ATAD3A and the ATAD3 A/C protein arising from the fusion-gene, is almost identical: 66.2 kDa. Some research groups have studied the expression of the different variants in depth, thanks to alternative more complex techniques such as quantitative proteomics, that can be used to detect specific ATAD3 peptides (which will target both unaffected and mutated or rearranged sequences) and compare the abundance, and thus, expression levels in ATAD3 mutants versus controls. Using this technique, Frazier and colleagues showed that patients harboring the deletion expressed ATAD3A about 75% less than controls, similar to ATAD3B levels, and they confirmed that peptides against the deleted regions could not be detected in the patients (Frazier et al., 2021). Similarly, they detected specific peptides against the ATAD3C part present in the fusion-protein in patients with the duplication, that were absent in controls, and an increase in the peptides against ATAD3B and the duplicated ATAD3 A/C sequence was observed, consistent with the effects of the duplication event.

Nevertheless, all the aforementioned techniques despite being more accurate and precise than conventional western blotting, are also more time-consuming, involving long and complicated protocols that are more expensive. Thus, and if directly applying the technicalities reported in our work (like small pore size gel usage and low exposure) combined with appropriate antibodies, a relatively simple western blotting can help detecting ATAD3 variants. Hence, subtle genetic changes that are difficult to decipher by traditional sequencing technologies can be partially solved by analyzing protein samples from patient cells, and can potentially help clinicians in the arduous process of diagnosis.

Going back to the diagnostic process, it should be noted that neither of the ATAD3 subjects displayed obvious evidence of mitochondrial distress in any of the clinical tests performed, despite all of them have a mitochondrial disease, indicating the importance of analyzing nucleus-encoded genes in these cases for proper diagnosis.

ATAD3 locus is now considered by many expert geneticists and clinicians as one of the five most common mitochondrial disease-causing nuclear genes, along with *POLG*, *SURF1*, *PDHA1* and *TAZ* (Frazier et al., 2019). Copy number variants (CNVs) are especially challenging in genomic analyses, both in their detection and interpretation, as the high frequency of benign duplications observed in the *ATAD3* region, coupled with high sequence homology of the three genes, translates into pathogenic duplications potentially being missed when sequencing. Furthermore, the *ATAD3* locus is the only known genomic region underlying mitochondrial disease where segmental duplications lead to recurrent non-allelic homologous recombination events (Frazier et al., 2021). This suggests that systematic CNV analysis, particularly of genomic intervals prone to instability, should be done routinely. Therefore, for all severe neonatal disorders of unknown origin, negative for known mitochondrial variants and mitochondrial nuclear genome panels, the *ATAD3* locus should be considered a potential candidate, and we highlight the importance of carefully evaluating for single nucleotide, copy-number, or structural variants.

OXPHOS *in vivo* and in cell models of *ATAD3* disease

In all mitochondrial diseases, the first place to start is usually oxidative phosphorylation (OXPHOS), as being the principal role of mitochondria, most of the mutations in genes that encode for mitochondrial proteins, tend to produce OXPHOS deficiencies somehow.

Despite the genetic uniformity in the *ATAD3* deletions, and almost no variability in the disease progression, as it was very lethal, OXPHOS deficiency was markedly different between patients, varying in the activity of complexes and in the expression of subunits in fibroblast, muscle or liver (Desai et al., 2017). In the cells of two patients with *ATAD3* deletions where a reduction in the steady-state levels of selected OXPHOS proteins was observed, RNA-Seq and posterior GSEA analysis in cultured fibroblasts indicated a clear reduction in expression of the OXPHOS gene set, as well, (GSEA, Gene Set Enrichment Analysis, The Broad Institute, Harvard University, USA). GSEA analysis also differentiated the two cell lines, with those from the adult case having the milder decrease in the OXPHOS gene-set than the neonate's cells, suggesting that this analysis can be used to stratify patients with mitochondrial diseases, not only those with *ATAD3* disease. Overall, the *ATAD3* deletions were

unusual in that the OXPHOS deficiency was clearer cut in the cells than in solid tissues, whereas in other mitochondrial disorders it is often the reverse.

In my hands, immunoblotting for key OXPHOS subunits from complex I and IV in samples from the two new ATAD3 mutant cell lines (ATAD3 A/C and ATAD3 R466C) typically gave signals similar to controls for ATAD3 R466C, whereas the ATAD3 A/C cell line usually had decreased expression of key OXPHOS components, similar to a m.3243A>G mutant, that invariably showed marked reductions in NDUFB8 and B9. These results suggested that there was no marked OXPHOS deficiency in ATAD3 R466C, at least in cultured cells, and showed that our ATAD3 A/C patient could have defects in some OXPHOS proteins, but these seemed to little alter mitochondrial respiration and ATP levels. More extensive analyses by Dr. Thorburn's group in Australia for other ATAD3 A/C fibroblasts included evaluation of the holoenzymes of the respiratory chain and OXPHOS complexes via BNE (Frazier et al., 2021). In this case, though, contrary to the ATAD3 deletions, OXPHOS deficiency was more prominent in tissue mitochondria than in fibroblast, as the amount of OXPHOS super-complexes as well as complex I and IV activity greatly diminished in the liver and heart mitochondria of the patients with the deletions that explains the cardiomyopathy. OXPHOS deficiency, especially complex I and V and super-complex reduction, was also evident when ATAD3 was ablated both in muscle and brain conditional mice by Dr. Moraes's group in Miami, though in a progressive way, as a worsening in OXPHOS deficiency was reported in older mice (Peralta et al., 2018; Arguello et al., 2021). The different subunits and complexes require interdependence to form stable and functional super-complexes, that is why defects in a single subunit often produce combined complex deficiencies, thus progressively, damage in some complexes can affect other complexes (Protasoni et al., 2020).

Despite all the heterogeneity and variability in OXPHOS between ATAD3 mutations and the affected tissues, complex I deficiency is a common feature. In fact, it is the most common biochemical feature in pediatric mitochondrial diseases, accounting for about one third of all cases (Fassone & Rahman, 2012). Complex I deficiency is usually related to problems in mitochondrial DNA, in several ways. It can be because of structural defects in the mtDNA molecules itself (mutations, deletions) or in the number of these molecules (that can result in mtDNA depletion), or because there are problems somewhere in the process of obtaining the products encoded in mtDNA. Since ATAD3 mutants do not have other mutations in the mtDNA, the first

option is excluded. Modulation of the expression of ATAD3 in aneuploid cells did not change the mtDNA copy number (He et al., 2007; He et al., 2012) and in patients with HAYOS, mtDNA depletion has only occasionally been reported in tissues (Peralta et al., 2018; Arguello et al., 2021) and never to date in cell culture ATAD3 cells. I also corroborated that in the three different ATAD3 mutants available in the lab, excluding mtDNA depletion as the cause of OXPHOS deficiencies in the ATAD3 mutants. Thus, the involvement of ATAD3 in controlling directly or indirectly the mtDNA replication, transcription or translation is the most plausible explanation for the OXPHOS deficiencies.

F₁F₀ ATPase synthase (or complex V) has been reported to form dimers that are necessary in the formation of cristae in the IMM (Kühlbrandt, 2019), thus giving an important structural role to complex V. The levels and activity of complex V were notably decreased in the muscle and brain conditional ATAD3 knockout mice, and in the latter, complex V deficiency preceded any other alteration detected in OXPHOS complexes (Peralta et al., 2018; Arguello et al., 2021). This suggests an early dysfunction of the ATPase synthase unrelated to OXPHOS deficiency which could be controlled by ATAD3 and would affect cristae formation and organization. A last consideration should be made with membrane potential, as it is essential for the generation of an adequate electrochemical gradient for the ultimate purpose of energy production (Frazier et al., 2019). Although, I did not directly assess membrane potential, I indirectly measured ATP synthesis and observed not clear changes in the ATP production in the studied ATAD3 mutant fibroblast. Our observations of the cristae structure by electron microscopy showed some abnormal mitochondria in the ATAD3 mutant cells, but most importantly, the majority of them displayed perfectly normal morphology and cristae. Thus, again, this indicates differences between tissue and cell samples and suggests cristae and OXPHOS impairment is not a central alteration to ATAD3 diseases, unlike for many mitochondrial diseases. Recently, it has been demonstrated that each crista functions as an independent bioenergetic subunit with their own membrane potential, which prevents the failure of specific cristae spreading to the rest (Wolf et al., 2019). That same publication provides a useful method for characterizing these distinct potentials by the combined use of several dyes, microscopy and image analysis software that could be applied to the ATAD3 mutant cells to decipher the exact contribution of membrane potential to the disease pathogenesis.

ATAD3 mitochondrial DNA and nucleoids

Just as OXPHOS perturbations do not follow a simple pattern in ATAD3 mutants, mitochondrial DNA phenotypes are also mixed. We observed an altered mitochondrial morphology that disrupted the mitochondrial network and formed condensed and clustered areas in both fibroblasts with the ATAD3 A/C monoallelic duplication and the ATAD3 R466C substitution. Moreover, with a DNA staining, and even with certain nucleoid proteins like GRSF1, both lines showed mitochondrial DNA aggregates within the condensed areas, in line with previous observations in the rest of the ATAD3 variants reported by us and other groups (Desai et al., 2017; Gunning et al., 2020; Dorison et al., 2020; Arguello et al., 2021). On the other hand, mtDNA synthesis can be higher or lower in the *ATAD3* mutants. Desai and colleagues reported that one deletion mutant line had slow mtDNA synthesis, whereas my experience of the three mutant ATAD3 lines was that mtDNA synthesis rates tended to be equal to controls, or if anything, increased, although the latter could also be a secondary effect of increased mitophagy (see the discussion of autophagy below).

As the ATAD3 mutants that show the mtDNA aggregation phenotype are very different from a genetic point of view, we think these are secondary changes, consequences of altered structural and functional properties in ATAD3 mutant proteins, but above all, useful as another assay in the cellular test battery that distinguishes and helps identifying potential ATAD3 patients. However, these phenotypes appear in only a fraction of the cells, in the ATAD3 A/C mutant it was estimated to be less than 40% of the cells, and we observed yet unknown culturing conditions can vary their appearance. To clarify, since our culturing conditions are kept under strict controls, we deduced that the most prominent candidate to be causing the variation in the mitochondrial phenotypes in our cultures is something in the fetal bovine serum (FBS) supplemented in the media, which contains many different and sometimes unspecified compounds that could have potentially altered the phenotypes with the several batch changes performed during the years.

Anyhow, the distribution of mtDNA (and nucleoid) along the mitochondrial network seems to be modified in ATAD3 mutant cells. Hence, this suggests an abnormal distribution of the nucleoids and relates ATAD3 to playing a role in nucleoid

organization, that could possibly affect the functionality of those nucleoids, which would explain the aforementioned OXPHOS deficiencies.

The relationship of ATAD3 with mtDNA and the nucleoid is unquestionable: it co-purifies with mtDNA under the most stringent conditions, including ones that strip TFAM from the mtDNA (He et al., 2007), it resolves on iodixanol gradients with mtDNA and mitochondrial ribosomes, and in cultured cells ATAD3 silencing radically alters mtDNA topology and disrupts mtDNA multimers held together by detergent-resistant protein, which are putative segregation intermediates and downregulates mitochondrial protein synthesis in human embryonic kidney cells (He et al., 2007; He et al., 2012). Therefore, the aggregation phenotype is compatible with ATAD3 having a direct role in mtDNA segregation as earlier proposed (He et al., 2007). However, it is not conclusive, as ATAD3 malfunction could indirectly disrupt mtDNA organization by first altering the mitochondrial membrane organization.

The evidence for this hypothesis is robust. First of all, ATAD3 is a transmembrane protein that is known to be regularly distributed along the mitochondrial network (Arguello et al., 2021). This structural role of ATAD3 has dual functions, as it has been proposed to serve as a scaffold crucial in membrane architecture (He et al., 2013; Arguello et al., 2021), but also because with that distribution it promotes the interaction with many partner proteins in both the OMM/cytoplasmic end, where it can interact with ER proteins, and the IMM end, where it mainly relates to nucleoid proteins. Because ATAD3 co-purifies with cholesterol rich domains where most of mtDNA is also present and ATAD3 is enriched in mitochondria-ER contact sites, this further evidences the structural role of ATAD3 in mitochondrial membrane architecture, where it is the common factor involved in the regulation of all those different interactors.

ATAD3 and cholesterol

Mitochondria have very low basal cholesterol levels, however, it is known to be crucial to tightly regulate mitochondrial cholesterol levels as well as its organization, as these can impact the biophysical and functional properties of mitochondrial membranes (Elustondo et al., 2016). Despite the existence of classical lipid rafts associated to sphingolipids is still unknown in the mitochondria, probably due to

these low amounts, it has been reported that cholesterol forms functionally distinct microdomains, that are essentially cholesterol-rich platforms (Rukmini et al., 2001; Zhang et al., 2009; Gerhold et al., 2015). ATAD3 has been shown to be linked with these cholesterol-rich platforms in the IMM allowing the binding of mtDNA molecules/nucleoid proteins to the membrane, promoting the processing and expression of mtDNA (He et al., 2007; Gerhold et al., 2015). Furthermore, ATAD3 has been reported to be implicated in mitochondrial cholesterol import, which has exhaustively been studied in steroidogenesis (Rone et al., 2012; Issop et al., 2015). These studies also pointed out the involvement of ER contact sites, being the ER the place where endogenous cholesterol is synthesized and a key cholesterol supplier for mitochondria (Elustondo et al., 2016), evidencing once more the link between cholesterol and ATAD3.

The aforementioned RNA-Seq analysis of the two ATAD3 deletion lines revealed altered cholesterol and lipid metabolism as the most affected pathways by MetaCore analysisTM (Desai et al., 2017). While this was an important finding it did not prime the study, rather it opened up a research line which provided powerful and unbiased confirmatory evidence for the hypothesis that cholesterol homeostasis was disrupted in ATAD3 disease.

Besides by transcriptomics, Desai and colleagues also showed elevated free cholesterol in fibroblast with ATAD3 deletions and this phenotype was similar to that found in patients with pathological mutations in *NPC1*, which have Niemann-Pick type C (Desai et al., 2017). This is a classic lysosomal storage disorder that accumulates abnormal amounts of lipids, mainly free cholesterol and sphingolipids, in the cytoplasmic lysosomes and endosomes which results in neurodegeneration (Karten et al., 2009). Moreover, both the ATAD3 deletion and the *NPC1* mutant cells exhibited mtDNA aggregation, which could also be achieved by pharmacologically perturbing cholesterol metabolism (with statins or U18666A, which alter cholesterol biosynthesis and trafficking, respectively) (Desai et al., 2017). This raised the question of whether cholesterol perturbation could directly impact mtDNA, which I tackle it further below.

My analysis of new ATAD3 variants showing that the monoallelic ATAD3 duplication and the ATAD3 R466C point mutant produce the same increase in the cellular free-cholesterol pool as the ATAD3 deletions is hugely important in establishing perturbed

cholesterol homeostasis as a core cellular disease phenotype. While the high cholesterol level is not exclusively restricted to *ATAD3* mutant lines, *NPC1* mutants being an obvious exception, my findings suggest it is a valuable laboratory diagnostic tool for differential diagnosis that can be performed by any laboratory that has skin fibroblast lines and a basic epifluorescent microscope. In our laboratory it is already established as the lead assay for assessing the credentials of putative new causes of *ATAD3* disease.

Apart from the elevated levels of free cholesterol, I report here a modest upregulation in cholesterol biosynthesis (increased expression of *SREBP2*), a decreased expression of cholesterol efflux transporters (downregulation of *ABCA1*, *ABCG1* and *SR-BI*) and a decrease in cholesterol de-esterification (reduced expression of *LAL*) in the *ATAD3* mutant cells studied, which suggests an overall unbalanced cellular homeostasis. Specifically, the first two are two ways that explain the elevated free cholesterol phenotype, especially the decrease in the plasma membrane transporters, as all of the transporters were significantly diminished in the *ATAD3* mutants. The reduced *LAL* expression means that the conversion of esterified cholesterol to free cholesterol is decreased, probably because the *ATAD3* mutant cells want to prevent more accumulation of free cholesterol that is already high due to the marked decrease in the plasma membrane cholesterol transporters.

An unusual neutral lipid accumulation was also observed in these cells, as it is not typical to have a neutral lipid accumulation in basal conditions in a cell-type like fibroblasts, which suggests the dysregulation is more extended than cholesterol metabolism and also affects other branches of lipid metabolism. With the use of two cholesterol modulating agents, unesterified cholesterol was highly increased in all the cell lines whereas neutral lipids were almost unaltered, also when glucose and glutamine were restricted, respiratory chain was impaired and autophagy was inhibited. These results indicate that the increase of free cholesterol does not necessarily imply an increase in neutral lipids and that these pathways do not seem to be regulating neutral lipid metabolism, which suggests neutral lipid accumulation in *ATAD3* mutant cells is not secondary to altered cholesterol metabolism, but is rather a downstream, or an independent phenomenon.

A similar cascade of events with the accumulation of free cholesterol, neutral lipids, and the rest of the cholesterol-related phenotypes has been reported in the pathogenesis of non-alcoholic fatty liver disease (NAFLD) (Arguello et al., 2015) and recently an overexpression in ATAD3A has been reported in human and rat with NAFLD pathology (Chen et al., 2022), which proposes that there are other factors that can upregulate ATAD3 and produce similar cellular alterations as described in ATAD3 disorders, without ATAD3 being mutated. The publication by Chen and colleagues, who belong to an old ATAD3 research group led by Dr. Papadopoulos (in California), also generated a deletion and a point mutation in ATAD3A exon 7 by CRISPR-Cas9 in human hepatocellular carcinoma cells, where they observed similar cellular phenotypes as those described in our ATAD3 mutants. Altered mitochondrial morphology, cristae loss and decreased ATP production, elevated free cholesterol without any evident sign of changes in key genes and enzymes involved in cholesterol metabolism, to what the authors suggest ATAD3A might regulate cholesterol export from the cell. Most of these phenotypes are shared with our *ATAD3* mutants, and the rest, like cristae loss or notable ATP decrease, as previously discussed, seem to be more downstream effects of ATAD3 dysfunction and could be mutation specific.

Although, our attempts to label free cholesterol in the flies were unsuccessful, we were able to generate a new tool to label membrane associated cholesterol in the *Drosophila* model: mKate-D4. To our knowledge, this is the first application of the D4-cholesterol reporter *in vivo*, not only in *Drosophila* but other animal models as well, and its evident ability to reveal changes in cholesterol in biological membranes clearly has considerable potential to answer many questions related to perturbed cholesterol homeostasis in a wide variety of animal models of human diseases.

The D4 cholesterol reporter demonstrates that *Atad3* dysfunction leads to elevated cholesterol incorporation in membranes *in vivo*, implying cholesterol metabolism is as well affected in these mutants and suggesting high free cholesterol levels in flies, as observed in the human cells with mutant ATAD3. Flies lack the cholesterol biosynthetic enzyme system of vertebrates and obtain all their cholesterol from the diet (Niwa & Niwa, 2011), and yet the observed cholesterol dysregulation is common to the flies and human and seems to be evolutionarily conserved, as is the *ATAD3* gene. This further evidences the implication of ATAD3 in cholesterol metabolism and excludes alterations in cholesterol biosynthesis as the primary way of producing the

increase in cholesterol. Thanks to some of the results presented in this thesis (like the decreased expression of the plasma membrane cholesterol transporters) we are beginning to explain the way the cells do that, but to date the causes behind the elevated cholesterol in ATAD3 mutants still remain unknown.

However, we can infer that, when ATAD3 is mutated there is an increase in the cellular demand for cholesterol, free and membrane-bound, as it is elevated irrespective of the type of mutation both in human and flies. This, together with already established data, enlightens the hypothesis that ATAD3 is a protein closely involved in mitochondrial cholesterol metabolism. Therefore, we propose a model where genetic alterations in ATAD3 produce a loss of its native function primarily implicated in the uptake of cholesterol to mitochondrial membranes. As cholesterol in cellular membranes needs to be tightly regulated (Jaureguiberry et al., 2010), ATAD3's loss of function is compensated by what we think is an adaptive response that accumulates free cholesterol in the cytoplasm and where, inevitably, part of it will go to cellular membranes, by the law of mass action. That accumulation will occur mainly by reducing the expression of cholesterol transporters in the plasma membrane, but we know certain proteins involved in the metabolism of cholesterol are also the differentially regulated, opening up the need to further study the way and the causes of elevated cholesterol (Fig. D1).

Autophagy and lysosomes in relationship to cholesterol in the ATAD3 mutants

The principal effect of excess cholesterol will be to increase membrane rigidity, which is known to disrupt a swathe of cell and organ functions (Luo et al., 2020). One way to mitigate the problem of an over-abundance of membrane-embedded cholesterol would be to remove the affected regions via autophagy. ATAD3 mutants showed little variation in autophagic flux compared to control cells (observed as LC3II and phospho-p62 levels with and without CLQ treatment), not even under nutrient restriction conditions (without glucose and glutamine availability in the media) that are known to promote autophagy by suppressing mTOR (Sengupta et al., 2010). Indeed, when subjected to those starving conditions, both ATAD3 mutants and controls displayed low levels of phospho-S6, implying that mTOR was suppressed (as mTOR activates phospho-S6) to let activate autophagy (Sengupta et al., 2010), indicating that nutrient restriction was working. However, the increase in phospho-S6 observed in basal ATAD3 mutants, theoretically would imply an inhibited

autophagic flux, which did not correspond to my results, that show there is no such decrease as evidenced either in LC3II and phospho-p62 levels. Thus, the possibility of autophagy in ATAD3 mutants (or at least under yet unidentified reasons) being regulated by an mTOR independent pathway should be considered, as suggested to occur under certain conditions like Ca^{2+} unavailability from ER to mitochondria (Ahumada-Castro et al., 2019; Sarkar et al., 2009). This would further emphasize the role of ATAD3 as a mitochondria-associated membrane (MAM) interactor and would relate ATAD3 with mitochondrial Ca^{2+} regulation and autophagy.

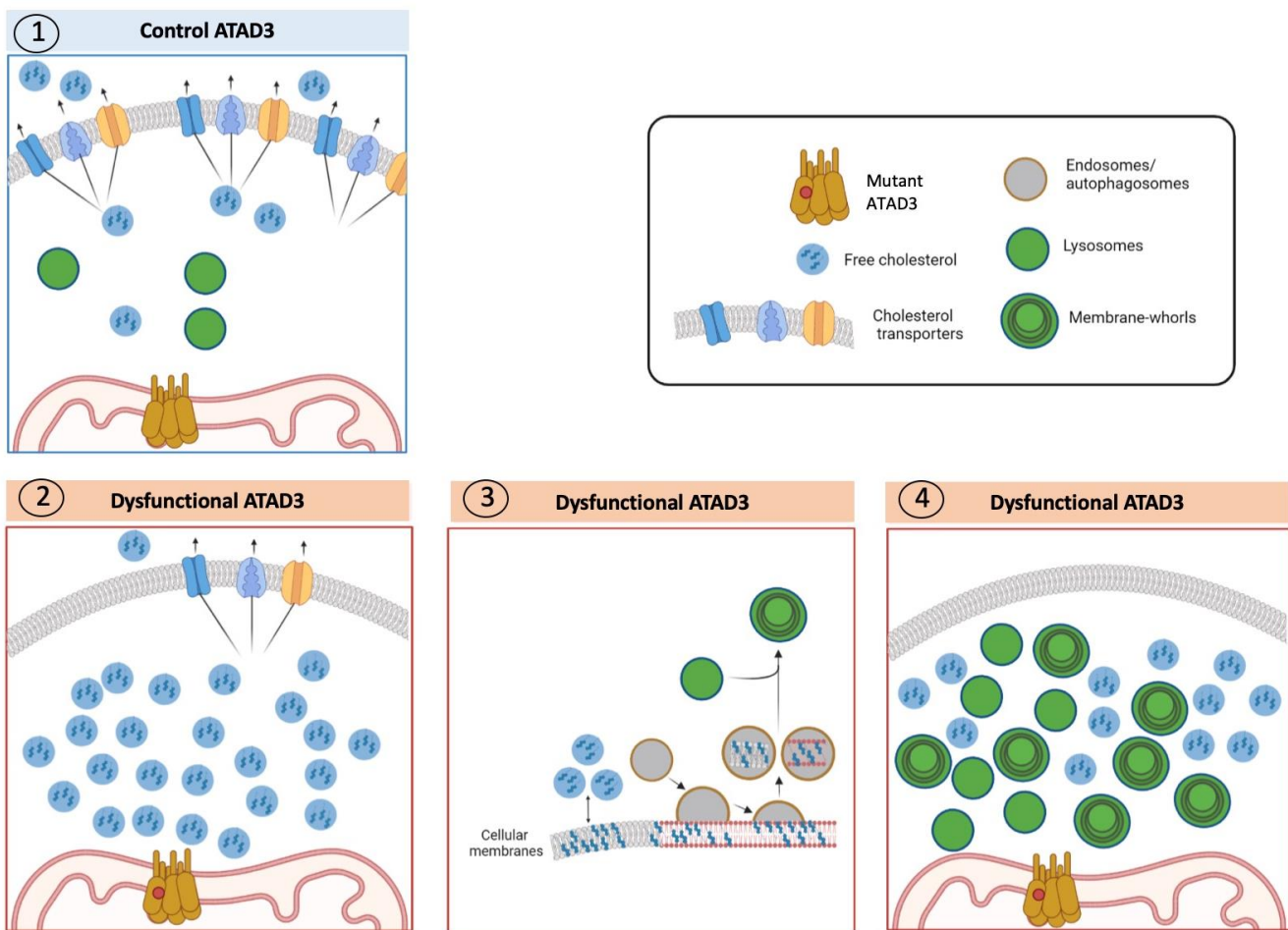


Figure D1. Model of the ATAD3 Molecular Disease Mechanism. Healthy controls (blue panel) have normal cholesterol efflux, which maintains intracellular cholesterol at an appropriate level to achieve the desired amount of cholesterol incorporation in membranes (1). ATAD3 mutant cells (red panels) are unable to incorporate cholesterol in mitochondrial membranes as normal and so they reduce cholesterol transporter abundance and accumulate intracellular free cholesterol (2). Consequently, more cholesterol will be incorporated in cellular membranes in an unregulated manner, following the law of mass action. Although this haphazard approach enables mitochondrial membranes to acquire sufficient cholesterol for basic functions, many membrane areas receive an excess of cholesterol, which triggers the activation of the

endolysosomal pathway (i.e. increase lysosomal mass and activity) to remove these aberrant membranes (3). However, cholesterol-rich membranes are difficult to digest leading to many lysosomes with membrane-whorls (4).

Accordingly, the increase in the lysosomes, observed both in human and fly, that would otherwise suggest that autophagy is increased, in an mTOR independent scenario could be explained by the necessity of augmenting the lysosomal pool due to the high demand of them digesting excess cholesterol in membranes, as we have been able to detect in the fly with the D4 cholesterol reporter. In the *Drosophila* neuroblasts, the lysosomes contain a substantial amount of the membrane-bound cholesterol, based on the mKate-D4 signal coinciding with the lysosomal marker LAMP-GFP, and this is concordant with the accumulation of membrane-whorls observed in electron micrographs of ATAD3 mutant fibroblasts.

Often, the presence of these cytoplasmic inclusions has been observed in patients with lysosomal storage disorders that present mutations in lysosomal acid hydrolases (Stromme et al., 1996). Though an exhaustive characterization of lysosomal enzyme activity has not been performed, ATAD3 patients show an acidic lysosomal environment stained by LysoTracker, which indicates that potentially lysosomes have ideal conditions to perform their digesting function. Therefore, we hypothesize that the increase in the presence of membrane-whorls observed in ATAD3 mutants has to do with the accumulation of free cholesterol that will inevitably produce an indiscriminate insertion of cholesterol in cellular membranes creating regions with a high cholesterol content, and will generate a response to try to degrade those. As part of that response we identified the increase in the endolysosomal pathways, but because such membranes are difficult to digest, the augmented lysosome response is unable to prevent the membrane-bound cholesterol reaching levels much higher than controls and excess cholesterol membranes accumulate as cytoplasmic inclusions in the mutants (membrane-whorls) (Fig. D1). Therefore, excess cholesterol in membranes is predicted to be a key pathogenic component of ATAD3 disease, which could secondarily lead to lysosomal dysfunction or exhaustion, and create a state equivalent to established lysosomal disorders (Parkinson-Lawrence et al., 2010). Similar responses and cellular outcomes have been reported in HSP patients with mutations in *SPG15* that also share clinical symptoms with ATAD3 mutants (such as white matter changes, retinal defects, cognitive impairment and tremor) (Renvoisé et al., 2014), which once again (Cooper et al., 2017) shows the overlapping of these two diseases at the mutational, cellular and clinical levels. Our hypothesis also evidences

the need of further studying lipolysis and lipophagy pathways (Zhang et al., 2022) as they may be altered in the ATAD3 mutants and implicated in the generation of aberrant inclusion bodies. Last, it is important to mention that even if the appearance of membrane-whorls has been reported in many neurological diseases (such as GM2 gangliosidosis, Fabry, Farber or Gaucher diseases) (Stromme et al., 1996) to our knowledge, this is the first time this kind of inclusions have been reported in at least two different ATAD3 mutants (R466C point mutant and duplication), opening the door to explore another yet unknown aspect of cell biology to tackle every aspect implicated in the pathophysiology of the disease.

Altered autophagy and mitophagy (the specific part of the autophagic process that degrades the aberrant mitochondria) have been previously described in some of the ATAD3 mutants, not only in human but also in *Drosophila* (Harel et al., 2016; Cooper et al., 2017; Yap et al., 2021; Chen et al., 2022). Not all of them use the same methods to assess autophagy: some base their result on electron micrographs, some detect the changes in expression of autophagic intermediates by immunoblotting, but overall, few use the classic LC3B I/II detection combined with chloroquine or bafilomycin autophagy blockers. Furthermore, we found that irrespective of the detection method, they all find accumulation of autophagic intermediates in the cells (lysosomes, autophagosomes, p62, LC3) and most of them conclude this means autophagy/mitophagy is increased. I would like to use this opportunity to remind to the scientific community studying autophagy, the importance of measuring the flux, needing to block autophagy to properly report it, and emphasize on carefully interpreting their results, as in many cases an accumulation of autophagic intermediates means autophagy is blocked and thus, those intermediates cannot degrade and accumulate. To mention one example, Cooper and colleagues observe lower bands of p62, which is degraded during autophagy, in an ATAD3 mutant fibroblast comparing to controls, to which they state it is suggestive of an upregulated autophagy. However, they do not seem to consider that when adding bafilomycin, ergo when blocking the autophagic flux, there is no change in the band, which would be increased if autophagy had been upregulated. Therefore, in their case, it would have been more appropriate to say that their ATAD3 mutant shows an impaired autophagy, as p62 is low and even when flux is blocked it does not increase much, suggesting a low flux. But more importantly, under starving conditions (which seem to be fine by the diminish of phospho-S6) autophagy is not increased, contrary to

what occurs in their controls, indicating an impaired autophagy (Cooper et al., 2017). Thus, when studying autophagy definitely blocking autophagic flux helps properly assessing it.

Modulation of cholesterol and lipid metabolism: mechanistic insights and future therapies for ATAD3 disease

The idea that beneficial treatments for mitochondrial diseases might target processes outside the organelle seems counter-intuitive at first; however, two such pathways have been successfully modulated, at least in mouse models. Mice deficient in the OXPHOS complex I subunit NADH dehydrogenase (ubiquinone) Fe-S protein 4 (NDUSF4) have been used by many groups as a mouse model of respiratory chain deficiency and mitochondrial disease. Johnson et al. and colleagues showed that the mTOR inhibitor rapamycin, while failing to have any impact on the underlying complex I deficiency, nevertheless, dramatically extends the life of NDUSF4 deficient mice (Johnson et al., 2013). Likewise, hypoxia improves survival in the same mouse model without restoring respiratory chain capacity (Grange et al., 2021).

When altered cholesterol and lipid metabolism were found to be striking and consistent features of *ATAD3* mutants in the course of this thesis, they appeared ideal targets for modulation, as there are an array of well defined and extensively analysed drugs that act on these branches of cell metabolism. Hence, the simple hypothesis was that lowering the cholesterol pool or inhibiting lipid production might restore homeostasis and attenuate the *ATAD3* mutant related phenotypes. At the same time, the application of modulators of cholesterol and lipid metabolism could clarify the molecular disease mechanism and the changes provoked by *mutant ATAD3*.

A major problem regarding cholesterol modulation is that interventions frequently do not have the expected effect. We can, for instance, restrict glycolysis and the respiratory chain at will, but lowering the free cholesterol pool is much more challenging. HMG-CoA reductase is the rate-limiting step for cholesterol biosynthesis and yet its inhibition with statins in control cells increases rather than decreases the cholesterol pool and causes mtDNA aggregation similar to mutant *ATAD3* (Desai et al., 2017). Ro acts on 2,3-oxidosqualene: lanosterol cyclase (OSC), downstream of statins, but again it increases the free-cholesterol pool in control cells. These

compounds had little effect on the cholesterol levels of *ATAD3* mutant cells and certainly did not lower the free cholesterol pool. Hence, at least in the cell culture models there is currently no evidence that statins or Ro would be effective drugs. That said, it would be helpful to learn if the plasma membrane cholesterol transporters are repressed by these compounds, as this would indicate that this is the standard signalling response to conserve cellular cholesterol levels; i.e. that it is shared with *ATAD3* mutants. Furthermore, statins are highly effective drugs *in vivo*, so it may be that they would be beneficial in *ATAD3* disease after all. Unfortunately, for all its merits, the *Drosophila* model is no help in this matter, as flies do not synthesize cholesterol, and a mouse model is needed. There are available the muscle and brain conditional knockout mice described earlier, although they are extreme, and so if they proved not to benefit from statins, this treatment should still be considered for a knock-in mouse equivalent to the R466C mutation.

Although Ro did not prove any more useful than statins in resolving the problem of the high levels of cholesterol in the *ATAD3* mutant lines, it revealed a new mitochondrial phenotype. In both control and *ATAD3* mutant cells, a Ro treatment of 2.5 μ M for 24 h strongly inhibited mitochondrial DNA synthesis. This provides another demonstration that altered cholesterol metabolism has a profound impact on mitochondria and mtDNA in particular, and so strengthens the proposed cholesterol-mtDNA axis. Further experiments need to be done to determine i) whether other cholesterol biosynthesis inhibitors such as statins also inhibit mtDNA synthesis, ii) the longer-term repercussions of inhibiting mtDNA replication via targeting cholesterol biosynthesis, iii) whether this is coupled to changes in mtDNA turnover, and iv) whether either synthesis or degradation is altered to a different extent in the *ATAD3* mutants versus the controls.

Rather than for therapeutic purposes, MCP1 was expected to exacerbate or mimic aspects of *ATAD3* dysfunction, as it represses the expression of the plasma membrane cholesterol transporters (one of the key new readouts identified in this thesis). In control cells, a short-term MCP1 treatment of 24 hours induced a modest increase in the free cholesterol pool, but well short of the levels seen in the *ATAD3* mutants or in controls treated with U18. Although U18 was not tested in parallel with MCP1, it typically induces an increase in free cholesterol equal to that seen in the untreated *ATAD3* mutants; hence, it is evident that at a dose of 50 ng/mL for 24 hours

MCP1 is considerably less potent than U18 2.5 μ M for 48h. Thus, higher doses, but more especially, longer-term MCP1 treatments are needed to determine whether the pool eventually increases to the level of *ATAD3* mutants, as this would enable us to determine whether this cascades to membrane-embedded cholesterol and lysosomes, which could provide strong corroborating evidence for the model (Fig. D1). Therefore, it could be done as a follow up experiment of the aforementioned Ro and statin treatment and subsequent membrane transporter expression check. The first would tell us about the mechanism of increasing cholesterol, and this one would tell us if the reduced cholesterol efflux via the transporters is sufficient to induce the cholesterol and lysosomal changes found associated to *ATAD3* dysfunction.

MCP1 is ideal in that it targets the transporters that we see repressed in the *ATAD3* mutant, but U18 can answer some of the same questions. Does elevated free cholesterol lead inexorably to increased membrane-embedded cholesterol and lysosomal expansion? The first of these can be addressed by introducing the mKate-D4 construct into human-cell compatible plasmids, which is work in progress, or by electron microscope analysis of U18-treated control cells, to see whether membrane whorls appear, as occurs in the *ATAD3* mutants, as I have shown. The second can be evaluated by LysoTracker and LAMP1 staining, as applied to the *ATAD3* mutants and control (untreated) cells. In preliminary experiments, LAMP1 signal in cells treated with U18 for 48 h was markedly higher than untreated cells in some cases but not others. These experiments need to be confirmed and extended in parallel with further tests of MCP1, but they suggest that high free cholesterol levels are sufficient to induce lysosomal expansion.

As we have seen neutral lipids are present at exceptionally high levels in *ATAD3* mutants without the need to challenge with oleate, targeting lipid degradation was a potential way to restore lipid homeostasis, and perhaps that of cholesterol in parallel. However, the application of Atglis and ISO, which have opposite effects on lipolysis, both increased free cholesterol. Although the effect on neutral lipids has not yet been assessed, these initial findings provide further evidence that increasing cholesterol levels is facile, whereas decreasing them is a much greater challenge.

Because we still lack a treatment that decreases the free cholesterol pool in the *ATAD3* mutants, it leaves open the questions of to what extent it is a compensatory

response, and how much it causes or contributes to the disease. Our working hypothesis is that mitochondrial membranes and particularly the inner membrane lacks cholesterol in the absence of ATAD3, which is so necessary for a correct nucleoid functioning and for maintaining a proper structure of mitochondria. Hence, we attribute the increase in free cholesterol to a programmed response that is designed to ensure that the IMM receives the minimal amount of cholesterol at the correct sites to maintain its basic integrity. Although, the targeted approach was entirely logically, the difficulties encountered suggest the best approach may be to switch to an unbiased and comprehensive chemical library screen. The difficulty with such screens is that testing thousands of different compounds in parallel means that there is little scope to vary the conditions or the duration. Another approach would be to disable the cholesterol biosynthesis pathway on an *ATAD3* mutant background, which would enable cholesterol to be manipulated via the culture medium. This option would enable to know whether there is a minimum cholesterol threshold that the cells need, and it could be a situation that could distinguish the *ATAD3* mutants and the controls. There is no such problem in the fly, as it obtains all its cholesterol from the diet, and so, experiments altering the dietary cholesterol content are currently underway.

The elevated free cholesterol pool was a marked cellular abnormality of *ATAD3* mutants shared with Niemann-Pick type C disease and so was from the outset likely to be of pathological relevance. The finding that cholesterol aggregates form in cellular membranes *in vivo* owing to mutant *ATAD3*, represents compelling evidence that this is a major abnormality, as excess cholesterol in membranes has been a recognized cause of heart disease for decades (Goldstein & Brown, 2015). The changes in lysosomes are logically a direct consequence of the cholesterol aggregates, both because the membrane whorls, in functional lysosomes, of *ATAD3* mutant cells suggest a marked increase in an abnormal substrate, and the fly studies demonstrate that many of the membrane-bound cholesterol aggregates coincide with the enlarged lysosomes. All that said, direct evidence that lysosomes are central to the disease remains to be demonstrated.

While cholesterol proved difficult to manipulate in a controlled manner, lysosomes are more tractable. Their activity can be inhibited and activated with a number of well-characterized chemicals. I focused on chloroquine as the inhibitor of lysosomes,

having used it to monitor autophagic flux and rapamycin as the activator, as it was used as a positive control for testing LysoTracker. In short-term experiments in human cells, CLQ at a dose of 50 μ M for 24-96 hours did not affect the survival or growth of *ATAD3* mutant cells anymore than controls. While longer-term experiments are planned, these compounds are ideal for testing in the fly model as we have two phenotypes that can be scored with ease: lethality and abnormal eyes. Pilot experiments suggest CLQ is more toxic to *dAtad3* mutants than controls, whereas we encountered problems of microbial contamination with rapamycin. Nevertheless, the fly model holds promise for resolving the fundamental question of whether and to what extent lysosomal function is required to mitigate the ATAD3 dysfunction. Should rapamycin improve either of the fly phenotypes it would indicate that it was a potential treatment for ATAD3 disease.

Sphingolipids

As with any result it is important to look beyond the immediate phenotype no matter how striking or compelling. This was why we studied neutral lipids after seeing the elevated free cholesterol pool, as it might be that the primary problem is related more to lipid than cholesterol metabolism. It is particularly important to maintain a reasonably broad perspective and scour the data for other clues in the case of ATAD3, as its precise function is not known. Considering all that we know about ATAD3, sphingolipid is the clear alternative to cholesterol as the essence of the problem. First, sphingolipid is a core component of cholesterol microdomains and so its absence could cause cholesterol aggregation and structural problems (Luo et al., 2020). Second, sphingolipidoses is the cause of multiple forms of lysosomal storage disorders, including NPC disease (Karten et al., 2009). Third, transgenic *ATAD3* co-purified two components of the serine palmitoyltransferase, long chain base subunits (SPTLC), which are the first enzymes of sphingolipid metabolism (He et al., 2012); and fourth, *SPTLC1* and *SPTLC2* were among the genes whose expression was most altered in the *ATAD3* deletion mutants (Desai et al., 2017).

For these reasons we consider it notable that sphingosine supplementation was the only treatment that distinguished the ATAD3 mutants from the controls, even though the distinguishing feature was not dramatic. While S1P increased free cholesterol both in all the cells, it produced cholesterol foci close to the cell periphery exclusively

in the control cells. It is not clear why this is, but it might indicate that this reflects a greater excess of sphingosine in the control cells – that is, the ATAD3 mutant cells have lower levels of sphingosine and so do not shunt cholesterol-sphingolipid complexes to the cell periphery. In any case, on the basis that there was a perceivable difference, we will prioritize S1P treatment in the *dAtad3* mutant flies.

ATAD3 antibodies

A last consideration should be made about the antibodies used to detect ATAD3. Both in ATAD3 mutant and control fibroblast, we detected by ICC a perinuclear signal in some of the cells, that did not colocalize with mitochondria, as it should. Of all 4 different antibodies tried to detect ATAD3 in different ways, the extra-mitochondrial foci phenotype was only detected by a non-commercial ATAD3 antibody (anti-ATAD3 N-ter W), while the rest, that were commercial, could not detect it. The most similar antibody to anti-ATAD3 N-ter W was anti-ATAD3 N-ter P which was raised in the same specie (rabbit) and against almost the same sequence (44-247 vs. 1-245, respectively, that corresponds to the N-terminal) differing in the lack of coverage of the initial region by the first, which does not explain the different detection of the two antibodies. Our results show that this is not unspecific labeling of the antibody, as the punctate signal colocalized specifically with some of the early endosomes, suggesting a possible internalization of ATAD3 by endosomes and implying a biological process had occurred, which ruled out unspecific labeling of an artefact, for example. Assuming this is true, a plausible explanation could be that anti-ATAD3 N-ter W is simply a better antibody that has a more sensitive detection of the protein, while anti-ATAD3 N-ter P would have a higher limit of detection and would not be able to bind to other forms of ATAD3 localizing to the endosomes. The fact that anti-ATAD3 N-ter W needs to be diluted approximately 25x than anti-ATAD3 N-ter P for ICC, also indicates the detection levels and sensitivity of both antibodies are different. In concordance with this hypothesis, the nuclear signal, which was detected by both antibodies, was more prominent with anti-ATAD3 N-ter W.

Cell fractionation and posterior immunoblotting of the separated proteins seemed to have worked correctly as the internal controls used localized where they corresponded (tubulin in the cytoplasmic fraction and lamin A+C in the nuclear fraction). However, the reasons for not having detected the punctate endosomal phenotype in the cytoplasmic fraction can be various. It could that endosomes are

lost from the cytoplasmic fraction during the process of fractioning cells. The use of another internal control such as another antibody to detect endosomes (like the anti-EEA1 used for ICC) would verify this hypothesis. It could, as well, be that the ATAD3 in the cytoplasmic fraction, unlike by ICC, is too little to be detected by this methodology, either because a gradual loss of protein during the steps of this protocol occurs or because some difference in respect to ICC affects the stability or detection capacity of the endosomal ATAD3 signal that should be detected in the cytoplasmic fraction. To sort this issue, the use of another type of fractionation that also separates mitochondrial content could be helpful, as the majority of ATAD3 signal should be detected in the mitochondrial fraction and thus could serve us to establish the main basal signal and continue from there.

Nevertheless, the experiment with interference RNA (RNAi) showed us that anti-ATAD3 N-ter W labeled other peptides whose signal was not decreased by the RNAi and corresponded to the endosomal localizing punctate and nuclear ATAD3 signals. Despite the experiment with ATAD3B antibody did not shed any light to the nature of the punctate phenotype, we demonstrated the anti-ATAD3B (SCBT) is not a valid antibody to label ATAD3B. Thus, as RNAi does not seem to affect the intensity of the punctate and nuclear signals, but it greatly diminishes mitochondrial ATAD3, as expected, the strongest current hypothesis is that the extra-mitochondrial signal corresponds to other proteins that are not ATAD3. These could be any protein unrelated to ATAD3 that shares epitope with the epitope from ATAD3 localizing to mitochondria that anti-ATAD3 N-ter W detects and that for unknown reasons translocates to the endosomes and the nucleus, or it could be an isoform, a cleaved part or another ATAD3 specie that also for unknown reasons shows that translocating property. In that sense, several proteins that have been reported to interact with ATAD3 and co-fractionate in sucrose gradient organelle fractions, such as apoptosis inducing factor and mouse achaete-scute homolog 2 (AIF and MASH2), are known to translocate from the mitochondrial membranes to the nucleus where they exert different functions as transcription factors (Fang et al., 2010; Goller et al., 2013). Further studies to better understand the nature of these interactions and the translocating property should be made, as the possibility that ATAD3 co-translocates with these proteins exists, the same way they interact and appear together in fractions.

Overall, we conclude anti-ATAD3 N-ter W is an antibody that has a higher detection capacity but this implies that it also will detect other still unknown species. Thus, we think this could be an important consideration in the research of many groups (Dr. Thorburn, Dr. Frazier and Dr. Spinazzola to mention some) and publications (Desai et al. 2020; Frazier et al., 2021 for instance) that have used and currently use the anti-ATAD3 N-ter W worldwide either provided by Dr. J. Walker or our group.

Approach to other diseases

In addition to revealing a credible and coherent molecular disease mechanism for ATAD3 mutants, this study has important ramifications for other pathologies, given that ATAD3 disease overlaps with hereditary spastic paraplegia, type I interferonopathies, Huntington's disease, nonalcoholic fatty liver disease and lysosomal storage disorders (Cooper et al., 2017; Lepelley et al., 2021; Zhao et al., 2019; Chen et al., 2022). Moreover, the current knowledge on ATAD3 can help us study other AAA+ ATPases that belong to the same family and could have similar properties, like SPG7-AFG3L2, or more distant connections like presenilins and apolipoproteins E3/E4 (APOE 3/4) that produce Alzheimer's disease, and have to do with cholesterol and lipid metabolism and dysregulation. Some of these issues and topics, especially ER-mitochondria contacts and AAA+ ATPases in association to other diseases, are being studied by other members of my group and will be further addressed in more detail in their respective PhD dissertations.

Conclusions

1. Genetic duplications in the *ATAD3* locus are associated with a dominant disease that manifests as a fatal infantile neuro-cardiac developmental syndrome.
2. Ablation of the arginine finger implicated in ATP hydrolysis in *ATAD3A* produces a dominant optic atrophy with associated neurological symptoms (DOA+).
3. Loss of the equivalent arginine finger in an extra copy of the *Drosophila* homolog of *ATAD3* (*dAtad3^{R472C}*) halves viability and causes developmental defects.
4. Mitochondrial OXPHOS and ATP deficits are secondary effects of *ATAD3* pathogenesis.
5. Mutations and rearrangements in *ATAD3* disrupt the mitochondrial network and produce mitochondrial DNA aggregation.
6. Perturbed cholesterol homeostasis is a core molecular feature of fibroblasts carrying pathological *ATAD3* variants, and so can be used as a diagnostic tool. An increased pool of free cholesterol is associated with decreased expression of the cholesterol efflux transporters ABCA1, ABCG1 and SR-BI.
7. The “arginine finger” *ATAD3* mutant leads to the formation of cholesterol aggregates in cell membranes that will inevitably disrupt membrane integrity and function.
8. Mutations and rearrangements in the *ATAD3* locus cause intracellular neutral lipid accumulation, which involves other branches of lipid metabolism in *ATAD3* disease.
9. Pharmacological modulation of different target-proteins involved in lipolysis, cholesterol and sphingolipid metabolism all produce an increase in free

cholesterol, with sphingolipids emerging as the most promising candidate related to ATAD3 (dys)function.

10. Mutant *ATAD3* fibroblast have an increased lysosomal pool, without marked autophagic alteration, to clear the membrane-embedded cholesterol aggregates in the *ATAD3* mutant cells. However, these are difficult to digest substrates and so they accumulate in lysosomes forming membrane whorls that are characteristic of lysosomal storage disorders.
11. Membrane-cholesterol can be labeled *in vivo* in *Drosophila* via the transgenic expression of cholesterol binding domain, D4, fused to a fluorescent reporter, mKate, as done in the *dAtad3^{R472}* transgenic fly, where cholesterol accumulation and aggregation were detected. Hence, mKate-D4 represents a new tool that can be studied in a wide range of fly disease models where aberrant cholesterol metabolism is known or suspected.
12. As the *ATAD3* arginine finger mutation is dominant, it could reflect a function distinct from the normal activity of ATAD3; however, the increase in the cholesterol pool and subsequent elevated incorporation in membranes is best explained as an adaptive response to the loss of function of ATAD3
13. The non-commercial anti-ATAD3 antibody that targets to the N-terminal of the protein and is widely distributed throughout the world, has to be used carefully as it labels unknown extra-mitochondrial species.
14. Fibroblast-extracted protein separation with subsequent antibody detection distinguishes different ATAD3 variants that combined with free cholesterol labeling can be used as a routine first-approach to identify potential ATAD3 patients.

Bibliography

- Ahumada-Castro, U., Silva-Pavez, E., Lovy, A., Pardo, E., Molgó, J., & Cárdenas, C. (2019). MTOR-independent autophagy induced by interrupted endoplasmic reticulum-mitochondrial Ca²⁺ communication: a dead end in cancer cells. *Autophagy*, *15*(2), 358–361. <https://doi.org/10.1080/15548627.2018.1537769>
- Akman, G., Desai, R., Bailey, L. J., Yasukawa, T., Rosa, I. D., Durigon, R., Holmes, J. B., Moss, C. F., Mennuni, M., Houlden, H., Crouch, R. J., Hanna, M. G., Pitceathly, R. D. S., Spinazzola, A., & Holt, I. J. (2016). Pathological ribonuclease H1 causes R-loop depletion and aberrant DNA segregation in mitochondria. *Proceedings of the National Academy of Sciences of the United States of America*, *113*(30), E4276–E4285. <https://doi.org/10.1073/pnas.1600537113>
- Al Madhoun, A., Alnaser, F., Melhem, M., Nizam, R., Al-Dabbous, T., & Al-Mulla, F. (2019). Ketogenic diet attenuates cerebellar atrophy progression in a subject with a biallelic variant at the ATAD3A locus [response to letter]. *Application of Clinical Genetics*, *12*, 163–165. <https://doi.org/10.2147/TACG.S224520>
- AlAyed, A., Samman, M., Peer-Zada, A., & Almannai, M. (2020). Harel-Yoon syndrome: the first case report from Saudi Arabia. *Journal of Biochemical and Clinical Genetics*, *3*(April), 22–27. <https://doi.org/10.24911/jbcgenetics/183-1585816398>
- Alston, C. L., Rocha, M. C., Lax, N. Z., Turnbull, D. M., & Taylor, R. W. (2017). The genetics and pathology of mitochondrial disease. *Journal of Pathology*, *241*(2), 236–250. <https://doi.org/10.1002/path.4809>
- Anderson, S., Bankier, A. T., Barrell, B. G., de Bruijn, M. H., Coulson, A. R., Drouin, J., Eperon, I. C., Nierlich, D. P., Roe, B. A., Sanger, F., Schreier, P. H., Smith, A. J., Staden, R., & Young, I. G. (1981). Sequence and organization of the human mitochondrial genome. *Nature*, *290*(5806), 457–465. <https://doi.org/10.1038/290457a0>
- Arguello, G., Balboa, E., Arrese, M., & Zanlungo, S. (2015). Recent insights on the role of cholesterol in non-alcoholic fatty liver disease. *Biochimica et Biophysica Acta - Molecular Basis of Disease*, *1852*(9), 1765–1778. <https://doi.org/10.1016/j.bbadis.2015.05.015>
- Arguello, T., Peralta, S., Antonicka, H., Gaidosh, G., Diaz, F., Tu, Y. T., Garcia, S., Shiekhattar, R., Barrientos, A., & Moraes, C. T. (2021). ATAD3A has a scaffolding role regulating mitochondria inner membrane structure and protein assembly. *Cell Reports*, *37*(12), 110139. <https://doi.org/10.1016/j.celrep.2021.110139>
- Baudier, J. (2018). ATAD3 proteins: brokers of a mitochondria–endoplasmic reticulum connection in mammalian cells. *Biological Reviews*, *93*(2), 827–844. <https://doi.org/10.1111/brv.12373>
- Bellusci, M., Paredes-Fuentes, A. J., Ruiz-Pesini, E., Gómez, B., Martín, M. A., Montoya, J., & Artuch, R. (2021). The genetic landscape of mitochondrial diseases in Spain: A nationwide call. *Genes*, *12*(10). <https://doi.org/10.3390/genes12101590>
- Bischof, J., Maeda, R. K., Hediger, M., Karch, F., & Basler, K. (2007). An optimized transgenesis system for Drosophila using germ-line-specific phiC31 integrases. *Proc. Natl. Acad. Sci. U. S. A.* *104*, 3312–3317. <https://doi.org/10.1073/pnas.0611511104>
- Bloise, R., & Reinhart, C. (1981). Epaissement De Pulpes - Modelisation Du Processus Discontinu. *Industrie Minerale, Les Techniques*, *109*(6), 437–441.

<https://doi.org/10.1172/JCI200215593.Lipid>

- Bogehagen, D. F., Rousseau, D., & Burke, S. (2008). The layered structure of human mitochondrial DNA nucleoids. *Journal of Biological Chemistry*, *283*(6), 3665–3675. <https://doi.org/10.1074/jbc.M708444200>
- Bonekamp, N. A., & Larsson, N. G. (2018). SnapShot: Mitochondrial Nucleoid. *Cell*, *172*(1–2), 388–388.e1. <https://doi.org/10.1016/j.cell.2017.12.039>
- Bourgeron, T., Rustin, P., Chretien, D., Birch-Machin, M., Bourgeois, M., Viegas-Péquignot, E., Munnich, A., & Rötig, A. (1995). Mutation of a nuclear succinate dehydrogenase gene results in mitochondrial respiratory chain deficiency. *Nature Genetics*, *11*(2), 144–149. <https://doi.org/10.1038/ng1095-144>
- Brand, a H., & Perrimon, N. (1993). *Ature. Development (Cambridge, England)*, *118*(2), 401–415.
- Burke, J. A., & Schubert, W. K. (1972). Deficient activity of hepatic acid lipase in cholesterol ester storage disease. *Science*, *176*(4032), 309–310. <https://doi.org/10.1126/science.176.4032.309>
- Calise, S., Blescia, S., Cencetti, F., Bernacchioni, C., Donati, C., & Bruni, P. (2012). Sphingosine 1-phosphate stimulates proliferation and migration of satellite cells. Role of S1P receptors. *Biochimica et Biophysica Acta - Molecular Cell Research*, *1823*(2), 439–450. <https://doi.org/10.1016/j.bbamcr.2011.11.016>
- Calvo, S. E., & Mootha, V. K. (2010). The mitochondrial proteome and human disease. *Annual Review of Genomics and Human Genetics*, *11*, 25–44. <https://doi.org/10.1146/annurev-genom-082509-141720>
- Carrodegua, J. A., Theis, K., Bogehagen, D. F., & Kisker, C. (2001). Crystal structure and deletion analysis show that the accessory subunit of mammalian DNA polymerase γ , PolyB, functions as a homodimer. *Molecular Cell*, *7*(1), 43–54. [https://doi.org/10.1016/S1097-2765\(01\)00153-8](https://doi.org/10.1016/S1097-2765(01)00153-8)
- Carvalho, C. M. B., & Lupski, J. R. (2016). Mechanisms underlying structural variant formation in genomic disorders. *Nature Reviews. Genetics*, *17*(4), 224–238. <https://doi.org/10.1038/nrg.2015.25>
- Chen, L., Li, Y., Sottas, C., Lazaris, A., Petrillo, S. K., Metrakos, P., Li, L., Ishida, Y., Saito, T., Garza, S., & Papadopoulos, V. (2022). Loss of mitochondrial ATPase ATAD3A contributes to nonalcoholic fatty liver disease through accumulation of lipids and damaged mitochondria. *The Journal of Biological Chemistry*, *298*(6), 102008. <https://doi.org/10.1016/j.jbc.2022.102008>
- Cheng, J., Ohsaki, Y., Tauchi-Sato, K., Fujita, A., & Fujimoto, T. (2006). Cholesterol depletion induces autophagy. *Biochemical and Biophysical Research Communications*, *351*(1), 246–252. <https://doi.org/10.1016/j.bbrc.2006.10.042>
- Chinnery, P. F. (2022). Primary Mitochondrial Disorders Overview. *GeneReviews*®, 1–16.
- Chinnery, P. F., Elliott, H. R., Hudson, G., Samuels, D. C., & Relton, C. L. (2012). Epigenetics, epidemiology and mitochondrial DNA diseases. *International Journal of Epidemiology*, *41*(1), 177–187. <https://doi.org/10.1093/ije/dyr232>

- Collins, R. L., Brand, H., Karczewski, K. J., Zhao, X., Alföldi, J., Francioli, L. C., Khera, A. V., Lowther, C., Gauthier, L. D., Wang, H., Watts, N. A., Solomonson, M., O'Donnell-Luria, A., Baumann, A., Munshi, R., Walker, M., Whelan, C. W., Huang, Y., Brookings, T., ... Talkowski, M. E. (2020). A structural variation reference for medical and population genetics. *Nature*, *581*(7809), 444–451. <https://doi.org/10.1038/s41586-020-2287-8>
- Cooper, H. M., Yang, Y., Ylikallio, E., Khairullin, R., Woldegebriel, R., Lin, K. L., Euro, L., Palin, E., Wolf, A., Trokovic, R., Isohanni, P., Kaakkola, S., Auranen, M., Lonqvist, T., Wanrooij, S., & Tynismaa, H. (2017). ATPase-deficient mitochondrial inner membrane protein ATAD3a disturbs mitochondrial dynamics in dominant hereditary spastic paraplegia. *Human Molecular Genetics*, *26*(8), 1432–1443. <https://doi.org/10.1093/hmg/ddx042>
- Copeland, W. C. (2008). Inherited mitochondrial diseases of DNA replication. *Annual Review of Medicine*, *59*, 131–146. <https://doi.org/10.1146/annurev.med.59.053006.104646>
- Dahmann, C. (2016). *Drosophila - Methods and Protocols* (C. Dahmann (ed.); Second Ed.). Springer Protocols.
- Dalla Rosa, I., Cámara, Y., Durigon, R., Moss, C. F., Vidoni, S., Akman, G., Hunt, L., Johnson, M. A., Grocott, S., Wang, L., Thorburn, D. R., Hirano, M., Poulton, J., Taylor, R. W., Elgar, G., Martí, R., Voshol, P., Holt, I. J., & Spinazzola, A. (2016). MPV17 Loss Causes Deoxynucleotide Insufficiency and Slow DNA Replication in Mitochondria. *PLoS Genetics*, *12*(1). <https://doi.org/10.1371/journal.pgen.1005779>
- Darios, F., & Stevanin, G. (2020). Impairment of Lysosome Function and Autophagy in Rare Neurodegenerative Diseases. *Journal of Molecular Biology*, *432*(8), 2714–2734. <https://doi.org/10.1016/j.jmb.2020.02.033>
- De la Casa-Fages, B., Fernández-Eulate, G., Gamez, J., Barahona-Hernando, R., Morís, G., García-Barcina, M., Infante, J., Zulaica, M., Fernández-Pelayo, U., Muñoz-Oreja, M., Urtasun, M., Olaskoaga, A., Zelaya, V., Jericó, I., Saez-Villaverde, R., Catalina, I., Sola, E., Martínez-Sáez, E., Pujol, A., ... López de Munaín, A. (2019). Parkinsonism and spastic paraplegia type 7: Expanding the spectrum of mitochondrial Parkinsonism. *Movement Disorders*, *34*(10), 1547–1561. <https://doi.org/10.1002/mds.27812>
- Desai, R., Frazier, A. E., Durigon, R., Patel, H., Jones, A. W., Dalla Rosa, I., Lake, N. J., Compton, A. G., Mountford, H. S., Tucker, E. J., Mitchell, A. L. R., Jackson, D., Sesay, A., Di Re, M., van den Heuvel, L. P., Burke, D., Francis, D., Lunke, S., McGillivray, G., ... Spinazzola, A. (2017). ATAD3 gene cluster deletions cause cerebellar dysfunction associated with altered mitochondrial DNA and cholesterol metabolism. *Brain*, *140*(6), 1595–1610. <https://doi.org/10.1093/brain/awx094>
- DiMauro, S. (2004). Mitochondrial diseases. *Biochimica et Biophysica Acta - Bioenergetics*, *1658*(1–2), 80–88. <https://doi.org/10.1016/j.bbabi.2004.03.014>
- Dorison, N., Gaignard, P., Bayot, A., Gelot, A., Becker, P. H., Fourati, S., Lebigot, E., Charles, P., Wai, T., Therond, P., & Slama, A. (2020). Mitochondrial dysfunction caused by novel ATAD3A mutations. *Molecular Genetics and Metabolism*, *131*(1–2), 107–113. <https://doi.org/10.1016/j.ymgme.2020.09.002>
- Elustondo, P., Martin, L. A., & Karten, B. (2017). Mitochondrial cholesterol import. *Biochimica et Biophysica Acta - Molecular and Cell Biology of Lipids*, *1862*(1), 90–101. <https://doi.org/10.1016/j.bbalip.2016.08.012>

- Evans, K. J., Gomes, E. R., Reisenweber, S. M., Gundersen, G. G., & Lauring, B. P. (2005). Linking axonal degeneration to microtubule remodeling by Spastin-mediated microtubule severing. *Journal of Cell Biology*, *168*(4), 599–606. <https://doi.org/10.1083/jcb.200409058>
- Fang, H. Y., Chang, C. L., Hsu, S. H., Huang, C. Y., Chiang, S. F., Chiou, S. H., Huang, C. H., Hsiao, Y. T., Lin, T. Y., Chiang, I. P., Hsu, W. H., Sugano, S., Chen, C. Y., Lin, C. Y., Ko, W. J., & Chow, K. C. (2010). ATPase family AAA domain-containing 3A is a novel anti-apoptotic factor in lung adenocarcinoma cells. *Journal of Cell Science*, *123*(7), 1171–1180. <https://doi.org/10.1242/jcs.062034>
- Fassone, E., & Rahman, S. (2012). Complex I deficiency: Clinical features, biochemistry and molecular genetics. *Journal of Medical Genetics*, *49*(9), 578–590. <https://doi.org/10.1136/jmedgenet-2012-101159>
- Feng, B., Yaol, P. M., Li, Y., Devlin, C. M., Zhang, D., Harding, H. P., Sweeney, M., Rong, J. X., Kuriakose, G., Fisher, E. A., Marks, A. R., Ron, D., & Tabas, I. (2003). The endoplasmic reticulum is the site of cholesterol-induced cytotoxicity in macrophages. *Nature Cell Biology*, *5*(9), 781–792. <https://doi.org/10.1038/ncb1035>
- Frazier, A. E., Compton, A. G., Kishita, Y., Hock, D. H., Welch, A. E., Amarasekera, S. S. C., Rius, R., Formosa, L. E., Imai-Okazaki, A., Francis, D., Wang, M., Lake, N. J., Tregoning, S., Jabbari, J. S., Lucattini, A., Nitta, K. R., Ohtake, A., Murayama, K., Amor, D. J., ... Thorburn, D. R. (2021). Fatal perinatal mitochondrial cardiac failure caused by recurrent de novo duplications in the ATAD3 locus. *Med (New York, N.Y.)*, *2*(1), 49–73. <https://doi.org/10.1016/j.medj.2020.06.004>
- Frazier, A. E., Holt, I. J., Spinazzola, A., & Thorburn, D. R. (2017). Reply: Genotype-phenotype correlation in ATAD3A deletions: Not just of scientific relevance. *Brain*, *140*(11), e67. <https://doi.org/10.1093/brain/awx240>
- Frazier, A. E., Thorburn, D. R., & Compton, A. G. (2019). Mitochondrial energy generation disorders: Genes, mechanisms, and clues to pathology. *Journal of Biological Chemistry*, *294*(14), 5386–5395. <https://doi.org/10.1074/jbc.R117.809194>
- Gerdes, F., Tatsuta, T., & Langer, T. (2012). Mitochondrial AAA proteases - Towards a molecular understanding of membrane-bound proteolytic machines. *Biochimica et Biophysica Acta - Molecular Cell Research*, *1823*(1), 49–55. <https://doi.org/10.1016/j.bbamcr.2011.09.015>
- Gerhold, J. M., Cansiz-Arda, S., Lohmus, M., Engberg, O., Reyes, A., Van Rennes, H., Sanz, A., Holt, I. J., Cooper, H. M., & Spelbrink, J. N. (2015). Human Mitochondrial DNA-Protein Complexes Attach to a Cholesterol-Rich Membrane Structure. *Scientific Reports*, *5*, 1–15. <https://doi.org/10.1038/srep15292>
- Gilquin, B., Taillebourg, E., Cherradi, N., Hubstenberger, A., Gay, O., Merle, N., Assard, N., Fauvarque, M.-O., Tomohiro, S., Kuge, O., & Baudier, J. (2010). The AAA + ATPase ATAD3A Controls Mitochondrial Dynamics at the Interface of the Inner and Outer Membranes. *Molecular and Cellular Biology*, *30*(8), 1984–1996. <https://doi.org/10.1128/mcb.00007-10>
- Goldstein, J. L., & Brown, M. S. (2015). Genes to Statins. *Cell*, *161*(1), 161–172. <https://doi.org/10.1016/j.cell.2015.01.036.A>

- Goller, T., Seibold, U. K., Kremmer, E., Voos, W., & Kolanus, W. (2013). Atad3 Function Is Essential for Early Post-Implantation Development in the Mouse. *PLoS ONE*, *8*(1). <https://doi.org/10.1371/journal.pone.0054799>
- Goto, Y., Nonaka, I., & Horai, S. (1990). A mutation in the tRNA(Leu)(UUR) gene associated with the MELAS subgroup of mitochondrial encephalomyopathies. *Nature*, *348*(6302), 651–653. <https://doi.org/10.1038/348651a0>
- Grange, R. M. H., Sharma, R., Shah, H., Reinstadler, B., Goldberger, O., Cooper, M. K., Nakagawa, A., Miyazaki, Y., Hindle, A. G., Batten, A. J., Wojtkiewicz, G. R., Schleifer, G., Bagchi, A., Marutani, E., Malhotra, R., Bloch, D. B., Ichinose, F., Mootha, V. K., & Zapol, W. M. (2021). Hypoxia ameliorates brain hyperoxia and NAD⁺ deficiency in a murine model of Leigh syndrome. *Molecular Genetics and Metabolism*, *133*(1), 83–93. <https://doi.org/10.1016/j.ymgme.2021.03.005>
- Greaves, L. C., Nooteboom, M., Elson, J. L., Tuppen, H. A. L., Taylor, G. A., Commane, D. M., Arasaradnam, R. P., Khrapko, K., Taylor, R. W., Kirkwood, T. B. L., Mathers, J. C., & Turnbull, D. M. (2014). Clonal Expansion of Early to Mid-Life Mitochondrial DNA Point Mutations Drives Mitochondrial Dysfunction during Human Ageing. *PLoS Genetics*, *10*(9). <https://doi.org/10.1371/journal.pgen.1004620>
- Gunning, A. C., Strucinska, K., Muñoz Oreja, M., Parrish, A., Caswell, R., Stals, K. L., Durigon, R., Durlacher-Betzer, K., Cunningham, M. H., Grochowski, C. M., Baptista, J., Tysoe, C., Baple, E., Lahiri, N., Homfray, T., Scurr, I., Armstrong, C., Dean, J., Fernandez Pelayo, U., ... Ellard, S. (2020). Recurrent De Novo NAHR Reciprocal Duplications in the ATAD3 Gene Cluster Cause a Neurogenetic Trait with Perturbed Cholesterol and Mitochondrial Metabolism. *American Journal of Human Genetics*, *106*(2), 272–279. <https://doi.org/10.1016/j.ajhg.2020.01.007>
- Hales, K. G., Korey, C. A., Larracuente, A. M., & Roberts, D. M. (2015). Genetics on the fly: A primer on the drosophila model system. *Genetics*, *201*(3), 815–842. <https://doi.org/10.1534/genetics.115.183392>
- Hanes, I., McMillan, H. J., Ito, Y., Kernohan, K. D., Lazier, J., Lines, M. A., & Dymont, D. A. (2020). A splice variant in ATAD3A expands the clinical and genetic spectrum of Harel-Yoon syndrome. *Neurology: Genetics*, *6*(4), 3–7. <https://doi.org/10.1212/NXG.0000000000000452>
- Hansen, M., Rubinsztein, D. C., & Walker, D. W. (2018). Autophagy as a promoter of longevity: insights from model organisms. *Nature Reviews Molecular Cell Biology*, *19*(9), 579–593. <https://doi.org/10.1038/s41580-018-0033-y>
- Hanson, P. I., & Whiteheart, S. W. (2005). AAA+ proteins: Have engine, will work. *Nature Reviews Molecular Cell Biology*, *6*(7), 519–529. <https://doi.org/10.1038/nrm1684>
- Harel, T., Yoon, W. H., Garone, C., Gu, S., Coban-Akdemir, Z., Eldomery, M. K., Posey, J. E., Jhangiani, S. N., Rosenfeld, J. A., Cho, M. T., Fox, S., Withers, M., Brooks, S. M., Chiang, T., Duraine, L., Erdin, S., Yuan, B., Shao, Y., Moussallem, E., ... Lupski, J. R. (2016). Recurrent De Novo and Biallelic Variation of ATAD3A, Encoding a Mitochondrial Membrane Protein, Results in Distinct Neurological Syndromes. *American Journal of Human Genetics*, *99*(4), 831–845. <https://doi.org/10.1016/j.ajhg.2016.08.007>
- Hazan, J., Fonknechten, N., Mavel, D., Paternotte, C., Samson, D., Artiguenave, F., Davoine, C. S., Cruaud, C., Dürr, A., Wincker, P., Brottier, P., Cattolico, L., Barbe, V., Burgunder,

- J. M., Prud'homme, J. F., Brice, A., Fontaine, B., Heilig, R., & Weissenbach, J. (1999). Spastin, a new AAA protein, is altered in the most frequent form of autosomal dominant spastic paraplegia. *Nature Genetics*, 23(3), 296–303. <https://doi.org/10.1038/15472>
- He, J., Cooper, H. M., Reyes, A., Di Re, M., Kazak, L., Wood, S. R., Mao, C. C., Fearnley, I. M., Walker, J. E., & Holt, I. J. (2012). Human C4orf14 interacts with the mitochondrial nucleoid and is involved in the biogenesis of the small mitochondrial ribosomal subunit. *Nucleic Acids Research*, 40(13), 6097–6108. <https://doi.org/10.1093/nar/gks257>
- He, J., Cooper, H. M., Reyes, A., Di Re, M., Sembongi, H., Gao, J., Neuman, K. C., Fearnley, I. M., Spinazzola, A., Walker, J. E., & Holt, I. J. (2012). Mitochondrial nucleoid interacting proteins support mitochondrial protein synthesis. *Nucleic Acids Research*, 40(13), 6109–6121. <https://doi.org/10.1093/nar/gks266>
- He, J., Mao, C. C., Reyes, A., Sembongi, H., Di Re, M., Granycome, C., Clippingdale, A. B., Fearnley, I. M., Harbour, M., Robinson, A. J., Reichelt, S., Spelbrink, J. N., Walker, J. E., & Holt, I. J. (2007). The AAA+ protein ATAD3 has displacement loop binding properties and is involved in mitochondrial nucleoid organization. *Journal of Cell Biology*, 176(2), 141–146. <https://doi.org/10.1083/jcb.200609158>
- Holt, I.J., Harding, A. E., & Morgan-Hughes, J. A. (1988). Deletions of muscle mitochondrial DNA in patients with mitochondrial myopathies. *Nature*, 331(6158), 717–719. <https://doi.org/10.1038/331717a0>
- Holt, I.J. (2019). Survey and summary: The mitochondrial R-loop. *Nucleic Acids Research*, 47(11), 5480–5489. <https://doi.org/10.1093/nar/gkz277>
- Holt, I.J., & Jacobs, H. T. (2014). Unique features of DNA replication in mitochondria: A functional and evolutionary perspective. *BioEssays*, 36(11), 1024–1031. <https://doi.org/10.1002/bies.201400052>
- Holt, I.J., Lorimer, H. E., & Jacobs, H. T. (2000). Coupled Leading-and Lagging-Strand Synthesis of Mammalian Mitochondrial DNA eubacteria. Replication of the H strand on this model is proposed to initiate at a single site (O H), and to proceed unidirectionally until two-thirds of the way around the These. *Cell*, 100, 515–524.
- Huang, C. X., Zhang, Y. L., Wang, J. F., Jiang, J. Y., & Bao, J. L. (2013). MCP-1 impacts RCT by repressing ABCA1, ABCG1, and SR-BI through PI3K/Akt posttranslational regulation in HepG2 cells. *Journal of Lipid Research*, 54(5), 1231–1240. <https://doi.org/10.1194/jlr.M032482>
- Hubstenberger, A., Labourdette, G., Baudier, J., & Rousseau, D. (2008). ATAD 3A and ATAD 3B are distal 1p-located genes differentially expressed in human glioma cell lines and present in vitro anti-oncogenic and chemoresistant properties. *Experimental Cell Research*, 314(15), 2870–2883. <https://doi.org/10.1016/j.yexcr.2008.06.017>
- Hubstenberger, A., Merle, N., Charton, R., Brandolin, G., & Rousseau, D. (2010). Topological analysis of ATAD3A insertion in purified human mitochondria. *Journal of Bioenergetics and Biomembranes*, 42(2), 143–150. <https://doi.org/10.1007/s10863-010-9269-8>
- Hughes, D. T., Brar, K. K., Morris, J. L., Subramanian, K., Krishna, S., Gao, F., Rieder, L.-S., Freeman, J., Smith, H. L., Jukes-Jones, R., Nunnari, J., Prudent, J., Butcher, A. J. &

- Mallucci, G. R. (2022). PERK-ATAD3A interaction protects mitochondrial proteins synthesis during ER stress. *BioRxiv*, 2022.07.24.501280. <https://doi.org/10.1101/2022.07.24.501280>
- Hung, V., Lam, S. S., Udeshi, N. D., Svinkina, T., Guzman, G., Mootha, V. K., Carr, S. A., & Ting, A. Y. (2017). Proteomic mapping of cytosol-facing outer mitochondrial and ER membranes in living human cells by proximity biotinylation. *ELife*, 6, 1–39. <https://doi.org/10.7554/eLife.24463>
- Iborra, F. J., Kimura, H., & Cook, P. R. (2004). The functional organization of mitochondrial genomes in human cells. *BMC biology*, 2, 9. <https://doi.org/10.1186/1741-7007-2-9>
- Ikonen, E. (2008). Cellular cholesterol trafficking and compartmentalization. *Nature Reviews Molecular Cell Biology*, 9(2), 125–138. <https://doi.org/10.1038/nrm2336>
- Issop, L., Fan, J., Lee, S., Rone, M. B., Basu, K., Mui, J., & Papadopoulos, V. (2015). Mitochondria-Associated membrane formation in hormone-stimulated leydig cell steroidogenesis: Role of ATAD3. *Endocrinology*, 156(1), 334–345. <https://doi.org/10.1210/en.2014-1503>
- Jacinto, S., Guerreiro, P., de Oliveira, R. M., Cunha-Oliveira, T., Santos, M. J., Grazina, M., Rego, A. C., & Outeiro, T. F. (2021). MPV17 Mutations Are Associated With a Quiescent Energetic Metabolic Profile. *Frontiers in Cellular Neuroscience*, 15(March), 1–11. <https://doi.org/10.3389/fncel.2021.641264>
- Jaureguiberry, M. S., Tricerri, M. A., Sanchez, S. A., Garda, H. A., Finarelli, G. S., Gonzalez, M. C., & Rimoldi, O. J. (2010). Membrane organization and regulation of cellular cholesterol homeostasis. *Journal of Membrane Biology*, 234(3), 183–194. <https://doi.org/10.1007/s00232-010-9245-6>
- Jiang, P., & Mizushima, N. (2014). Autophagy and human diseases. *Cell Research*, 24(1), 69–79. <https://doi.org/10.1038/cr.2013.161>
- Johns, D. R., Neufeld, M. J., & Park, R. D. (1992). An ND-6 mitochondrial DNA mutation associated with leber hereditary optic neuropathy. *Biochemical and Biophysical Research Communications*, 187(3), 1551–1557. [https://doi.org/10.1016/0006-291X\(92\)90479-5](https://doi.org/10.1016/0006-291X(92)90479-5)
- Johnson, S. C., Yanos, M. E., Kayser, E., Quintana, A., Castanza, A., Uhde, L., Hui, J., Wall, V. Z., Oh, K., Wasko, B. M., Ramos, F. J., Palmiter, R. D., Peter, S., Morgan, P. G., Sedensky, M. M., & Kaeberlein, M. (2013). mTOR Inhibition Alleviates Mitochondrial Disease in a Mouse Model of Leigh Syndrome. *Science*, 342(6165), 1524–1528. <https://doi.org/10.1126/science.1244360.mTOR>
- Karnkowska, A., Vacek, V., Zubáčová, Z., Treitli, S. C., Petrželková, R., Eme, L., Novák, L., Žárský, V., Barlow, L. D., Herman, E. K., Soukal, P., Hroudová, M., Doležal, P., Stairs, C. W., Roger, A. J., Eliáš, M., Dacks, J. B., Vlček, Č., & Hampl, V. (2016). A eukaryote without a mitochondrial organelle. *Current Biology*, 26(10), 1274–1284. <https://doi.org/10.1016/j.cub.2016.03.053>
- Karten, B., Peake, K. B., & Vance, J. E. (2009). Mechanisms and consequences of impaired lipid trafficking in Niemann-Pick type C1-deficient mammalian cells. *Biochimica et Biophysica Acta - Molecular and Cell Biology of Lipids*, 1791(7), 659–670. <https://doi.org/10.1016/j.bbalip.2009.01.025>

- Kasamatsu, H., Robberson, D. L., & Vinograd, J. (1971). A novel closed-circular mitochondrial DNA with properties of a replicating intermediate. *Proceedings of the National Academy of Sciences of the United States of America*, 68(9), 2252–2257. <https://doi.org/10.1073/pnas.68.9.2252>
- Kawashima, T., Yamazaki, R., Matsuzawa, Y., Yamaura, E., Takabatake, M., Otake, S., Ikawa, Y., Nakamura, H., Fujino, H., & Murayama, T. (2012). Contrary effects of sphingosine-1-phosphate on expression of α -smooth muscle actin in transforming growth factor β 1-stimulated lung fibroblasts. *European Journal of Pharmacology*, 696(1–3), 120–129. <https://doi.org/10.1016/j.ejphar.2012.09.038>
- Kim, J., Kundu, M., Viollet, B., & Guan, K. L. (2011). AMPK and mTOR regulate autophagy through direct phosphorylation of Ulk1. *Nature Cell Biology*, 13(2), 132–141. <https://doi.org/10.1038/ncb2152>
- Kim, M., Schulz, V., Brings, L., Schoeller, T., Kühn, K., & Vierling, E. (2021). mTERF18 and ATAD3 are required for mitochondrial nucleoid structure and their disruption confers heat tolerance in *Arabidopsis thaliana*. *New Phytologist*, 232(5), 2026–2042. <https://doi.org/10.1111/nph.17717>
- Kimball, S. R., Shantz, L. M., Horetsky, R. L., & Jefferson, L. S. (1999). Leucine regulates translation of specific mRNAs in L6 myoblasts through mTOR-mediated changes in availability of eIF4E and phosphorylation of ribosomal protein S6. *Journal of Biological Chemistry*, 274(17), 11647–11652. <https://doi.org/10.1074/jbc.274.17.11647>
- Klionsky, D. J., Abdalla, F. C., Abeliovich, H., Abraham, R. T., Acevedo-Arozena, A., Adeli, K., Agholme, L., Agnello, M., Agostinis, P., Aguirre-Ghiso, J. A., Ahn, H. J., Ait-Mohamed, O., Ait-Si-Ali, S., Akematsu, T., Akira, S., Al-Younes, H. M., Al-Zeer, M. A., Albert, M. L., Albin, R. L., Alegre-Abarrategui, J., ... Zuckerbraun, B. (2012). Guidelines for the use and interpretation of assays for monitoring autophagy. *Autophagy*, 8(4), 445–544. <https://doi.org/10.4161/auto.19496>
- Klionsky, D. J., & Emr, S. D. (2000). Autophagy as a regulated pathway of cellular degradation. *Science (New York, N.Y.)*, 290(5497), 1717–1721. <https://doi.org/10.1126/science.290.5497.1717>
- Kolesar, J. E., Wang, C. Y., Taguchi, Y. V., Chou, S. H., & Kaufman, B. A. (2013). Two-dimensional intact mitochondrial DNA agarose electrophoresis reveals the structural complexity of the mammalian mitochondrial genome. *Nucleic Acids Research*, 41(4), 1–14. <https://doi.org/10.1093/nar/gks1324>
- Kühlbrandt, W. (2015). Structure and function of mitochondrial membrane protein complexes. *BMC Biology*, 13(1), 1–11. <https://doi.org/10.1186/s12915-015-0201-x>
- Kühlbrandt W. (2019). Structure and Mechanisms of F-Type ATP Synthases. *Annual review of biochemistry*, 88, 515–549. <https://doi.org/10.1146/annurev-biochem-013118-110903>
- Kukat, C., Wurm, C. A., Spähr, H., Falkenberg, M., Larsson, N. G., & Jakobs, S. (2011). Super-resolution microscopy reveals that mammalian mitochondrial nucleoids have a uniform size and frequently contain a single copy of mtDNA. *Proceedings of the National Academy of Sciences of the United States of America*, 108(33), 13534–13539. <https://doi.org/10.1073/pnas.1109263108>

- Lackner L. L. (2014). Shaping the dynamic mitochondrial network. *BMC biology*, 12, 35. <https://doi.org/10.1186/1741-7007-12-35>
- Lake, N. J., Compton, A. G., Rahman, S., & Thorburn, D. R. (2016). Leigh syndrome: One disorder, more than 75 monogenic causes. *Annals of Neurology*, 79(2), 190–203. <https://doi.org/10.1002/ana.24551>
- Lang, L., Loveless, R., & Teng, Y. (2020). Emerging links between control of mitochondrial protein atad3a and cancer. *International Journal of Molecular Sciences*, 21(21), 1–14. <https://doi.org/10.3390/ijms21217917>
- Laura L. Clay Montier, Janice Deng, and Y. B. (2009). Number matters: control of mammalian mitochondrial DNA copy number. *Journal Genetics and Genomics*, 36(3), 125–131. <https://doi.org/10.1080/00497878.2016.1120114>
- Lepelley, A., Della Mina, E., Van Nieuwenhove, E., Waumans, L., Fraitag, S., Rice, G. I., Dhir, A., Frémond, M. L., Rodero, M. P., Seabra, L., Carter, E., Bodemer, C., Buhas, D., Callewaert, B., de Lonlay, P., De Somer, L., Dymont, D. A., Faes, F., Grove, L., Holden, S., ... Crow, Y. J. (2021). Enhanced cGAS-STING-dependent interferon signaling associated with mutations in ATAD3A. *The Journal of experimental medicine*, 218(10), e20201560. <https://doi.org/10.1084/jem.20201560>
- Li, S., Lamarche, F., Charton, R., Delphin, C., Gires, O., Hubstenberger, A., Schlattner, U., & Rousseau, D. (2014). Expression analysis of ATAD3 isoforms in rodent and human cell lines and tissues. *Gene*, 535(1), 60–69. <https://doi.org/10.1016/j.gene.2013.10.062>
- Li, S., & Rousseau, D. (2012). ATAD3, a vital membrane bound mitochondrial ATPase involved in tumor progression. *Journal of Bioenergetics and Biomembranes*, 44(1), 189–197. <https://doi.org/10.1007/s10863-012-9424-5>
- Lightowers, R. N., Taylor, R. W., & Turnbull, D. M. (2015). Mutations causing mitochondrial disease: What is new and what challenges remain? *Science*, 349(6255), 1494–1499. <https://doi.org/10.1126/science.aac7516>
- Lumaquin, D., Johns, E., Montal, E., Weiss, J. M., Ola, D., Abuhashem, A., & White, R. M. (2021). An in vivo reporter for tracking lipid droplet dynamics in transparent zebrafish. *ELife*, 10, 1–25. <https://doi.org/10.7554/eLife.64744>
- Luo, J., Yang, H., & Song, B. L. (2020). Mechanisms and regulation of cholesterol homeostasis. *Nature Reviews Molecular Cell Biology*, 21(4), 225–245. <https://doi.org/10.1038/s41580-019-0190-7>
- Maceyka, M., Harikumar, K. B., Milstien, S., & Spiegel, S. (2012). Sphingosine-1-phosphate signaling and its role in disease. *Trends in Cell Biology*, 22(1), 50–60. <https://doi.org/10.1016/j.tcb.2011.09.003>
- Martin, B. W. F., & Mentel, M. (2010). The Origin of Mitochondria Mitochondria : A Ubiquitous and Diverse Family of Organelles The Endosymbiotic Origin of Mitochondria. *Nature education*, January 2010, 1–5.
- Martinet, W., Timmermans, J. P., & De Meyer, G. R. Y. (2014). Methods to assess autophagy in situ - Transmission electron microscopy versus immunohistochemistry. In *Methods in Enzymology* (1st ed., Vol. 543). Elsevier Inc. <https://doi.org/10.1016/B978-0-12-801329-8.00005-2>

- Merle, N., Féraud, O., Gilquin, B., Hubstenberger, A., Kieffer-Jacquinet, S., Assard, N., Bennaceur-Griscelli, A., Honnorat, J., & Baudier, J. (2012). ATAD3B is a human embryonic stem cell specific mitochondrial protein, re-expressed in cancer cells, that functions as dominant negative for the ubiquitous ATAD3A. *Mitochondrion*, *12*(4), 441–448. <https://doi.org/10.1016/j.mito.2012.05.005>
- Mhatre V. Ho, Ji-Ann Lee, and K. C. M., & Dien et al., 2013. (2008). AMPK phosphorylation of raptor mediates a metabolic checkpoint. *Molecular Cell*, *23*(1), 1–7. <https://doi.org/10.1016/j.molcel.2008.03.003>.AMPK
- Minczuk, M., He, J., Duch, A. M., Ettema, T. J., Chlebowski, A., Dzionek, K., Nijtmans, L. G. J., Huynen, M. A., & Holt, I. J. (2011). TEFM (c17orf42) is necessary for transcription of human mtDNA. *Nucleic Acids Research*, *39*(10), 4284–4299. <https://doi.org/10.1093/nar/gkq1224>
- Morand, O. H., Aebi, J. D., Dehmlow, H., Ji, Y. H., Gains, N., Lengsfeld, H., & Hember, J. (1997). Ro 48-8071, a new 2,3-oxidosqualene:lanosterol cyclase inhibitor lowering plasma cholesterol in hamsters, squirrel monkeys, and minipigs: Comparison to simvastatin. *Journal of Lipid Research*, *38*(2), 373–390. [https://doi.org/10.1016/s0022-2275\(20\)37449-6](https://doi.org/10.1016/s0022-2275(20)37449-6)
- Morgan, T. H. (1910). Sex limited inheritance in Drosophila. *Science (New York, N.Y.)*, *32*(812), 120–122. <https://doi.org/10.1126/science.32.812.120>
- Na, J. H., Lee, W. K., & Yu, Y. G. (2018). How do we study the dynamic structure of unstructured proteins: A case study on nopp140 as an example of a large, intrinsically disordered protein. *International Journal of Molecular Sciences*, *19*(2). <https://doi.org/10.3390/ijms19020381>
- Ng, P. C., & Henikoff, S. (2003). SIFT: Predicting amino acid changes that affect protein function. *Nucleic Acids Research*, *31*(13), 3812–3814. <https://doi.org/10.1093/nar/gkg509>
- Ng, Y. S., Bindoff, L. A., Gorman, G. S., Klopstock, T., Kornblum, C., Mancuso, M., McFarland, R., Sue, C. M., Suomalainen, A., Taylor, R. W., Thorburn, D. R., & Turnbull, D. M. (2021). Mitochondrial disease in adults: recent advances and future promise. *The Lancet Neurology*, *20*(7), 573–584. [https://doi.org/10.1016/S1474-4422\(21\)00098-3](https://doi.org/10.1016/S1474-4422(21)00098-3)
- Nicholls, T. J., Nadalutti, C. A., Motori, E., Sommerville, E. W., Gorman, G. S., Basu, S., Hoberg, E., Turnbull, D. M., Chinnery, P. F., Larsson, N.-G., Larsson, E., Falkenberg, M., Taylor, R. W., Griffith, J. D., & Gustafsson, C. M. (2018). Topoisomerase 3α Is Required for Decatenation and Segregation of Human mtDNA. *Molecular Cell*, *69*(1), 9-23.e6. <https://doi.org/10.1016/j.molcel.2017.11.033>
- Niwa, R., & Niwa, Y. S. (2011). The fruit fly drosophila melanogaster as a model system to study cholesterol metabolism and homeostasis. *Cholesterol*, *2011*. <https://doi.org/10.1155/2011/176802>
- Ogura, T., Whiteheart, S. W., & Wilkinson, A. J. (2004). Conserved arginine residues implicated in ATP hydrolysis, nucleotide-sensing, and inter-subunit interactions in AAA and AAA+ ATPases. *Journal of Structural Biology*, *146*(1–2), 106–112. <https://doi.org/10.1016/j.jsb.2003.11.008>
- Oláhová, M., Peter, B., Szilagyí, Z., Diaz-Maldonado, H., Singh, M., Sommerville, E. W.,

- Blakely, E. L., Collier, J. J., Hoberg, E., Stránecký, V., Hartmannová, H., Bleyer, A. J., McBride, K. L., Bowden, S. A., Korandová, Z., Pecinová, A., Ropers, H. H., Kahrizi, K., Najmabadi, H., ... Taylor, R. W. (2021). POLRMT mutations impair mitochondrial transcription causing neurological disease. *Nature Communications*, *12*(1), 1–13. <https://doi.org/10.1038/s41467-021-21279-0>
- Ondaro, J., Hernandez-Eguiazu, H., Garciandia-Arcelus, M., Loera-Valencia, R., Rodriguez-Gómez, L., Jiménez-Zúñiga, A., Goikolea, J., Rodriguez-Rodriguez, P., Ruiz-Martinez, J., Moreno, F., Lopez de Munain, A., Holt, I. J., Gil-Bea, F. J., & Gereñu, G. (2022). Defects of Nutrient Signaling and Autophagy in Neurodegeneration. *Frontiers in Cell and Developmental Biology*, *10*(March), 1–27. <https://doi.org/10.3389/fcell.2022.836196>
- Pantic, B., Ives, D., Mennuni, M., Perez-Rodriguez, D., Fernandez-Pelayo, U., Lopez de Arbina, A., Muñoz-Oreja, M., Villar-Fernandez, M., Dang, T. mai J., Vergani, L., Johnston, I. G., Pitceathly, R. D. S., McFarland, R., Hanna, M. G., Taylor, R. W., Holt, I. J., & Spinazzola, A. (2021). 2-Deoxy-D-glucose couples mitochondrial DNA replication with mitochondrial fitness and promotes the selection of wild-type over mutant mitochondrial DNA. *Nature Communications*, *12*(1). <https://doi.org/10.1038/s41467-021-26829-0>
- Parkinson-Lawrence, E. J., Shandala, T., Prodoehl, M., Plew, R., Borlace, G. N., & Brooks, D. A. (2010). Lysosomal storage Disease: Revealing lysosomal function and physiology. *Physiology*, *25*(2), 102–115. <https://doi.org/10.1152/physiol.00041.2009>
- Peeters-Scholte, C. M. P. C. D., Adama Van Scheltema, P. N., Klumper, F. J. C. M., Everwijn, S. M. P., Koopmans, M., Hoffer, M. J. V., Koopmann, T. T., Ruivenkamp, C. A. L., Steggerda, S. J., Van Der Knaap, M. S., & Santen, G. W. E. (2017). Genotype-phenotype correlation in ATAD3A deletions: Not just of scientific relevance. *Brain*, *140*(11), e66. <https://doi.org/10.1093/brain/awx239>
- Peralta, S., Goffart, S., Williams, S. L., Diaz, F., Garcia, S., Nissanka, N., Area-Gomez, E., Pohjoismäki, J., & Moraes, C. T. (2018). ATAD3 controls mitochondrial cristae structure in mouse muscle, influencing mtDNA replication and cholesterol levels. *Journal of Cell Science*, *131*(13). <https://doi.org/10.1242/jcs.217075>
- Peralta, S., González-Quintana, A., Ybarra, M., Delmiro, A., Pérez-Pérez, R., Docampo, J., Arenas, J., Blázquez, A., Ugalde, C., & Martín, M. A. (2019). Novel ATAD3A recessive mutation associated to fatal cerebellar hypoplasia with multiorgan involvement and mitochondrial structural abnormalities. *Molecular Genetics and Metabolism*, *128*(4), 452–462. <https://doi.org/10.1016/j.ymgme.2019.10.012>
- Phillips, M. C. (2014). Molecular mechanisms of cellular cholesterol efflux. *Journal of Biological Chemistry*, *289*(35), 24020–24029. <https://doi.org/10.1074/jbc.R114.583658>
- Protasoni, M., Pérez-Pérez, R., Lobo-Jarne, T., Harbour, M. E., Ding, S., Peñas, A., Diaz, F., Moraes, C. T., Fearnley, I. M., Zeviani, M., Ugalde, C., & Fernández-Vizcarra, E. (2020). Respiratory supercomplexes act as a platform for complex III -mediated maturation of human mitochondrial complexes I and IV . *The EMBO Journal*, *39*(3), 1–19. <https://doi.org/10.15252/embj.2019102817>
- Pulipparacharuvil, S., Ali Akbar, M., Ray, S., A. Sevrioukov, E., S. Haberman, A., Rohrer, J., Krämer, H. (2005). *Drosophila* Vps16A is required for trafficking to lysosomes and

- biogenesis of pigment granules. *J Cell Sci*, 118 (16): 3663–3673. <https://doi.org/10.1242/jcs.02502>
- Quiroga, A. D., Li, L., Trötz Müller, M., Nelson, R., Proctor, S. D., Köfeler, H., & Lehner, R. (2012). Deficiency of carboxylesterase 1/esterase-x results in obesity, hepatic steatosis, and hyperlipidemia. *Hepatology*, 56(6), 2188–2198. <https://doi.org/10.1002/hep.25961>
- Renvoisé, B., Chang, J., Singh, R., Yonekawa, S., FitzGibbon, E. J., Mankodi, A., Vanderver, A., Schindler, A. B., Toro, C., Gahl, W. A., Mahuran, D. J., Blackstone, C., & Pierson, T. M. (2014). Lysosomal abnormalities in hereditary spastic paraplegia types SPG15 and SPG11. *Annals of Clinical and Translational Neurology*, 1(6), 379–389. <https://doi.org/10.1002/acn3.64>
- Reyes, A., Kazak, L., Wood, S. R., Yasukawa, T., Jacobs, H. T., & Holt, I. J. (2013). Mitochondrial DNA replication proceeds via a “bootlace” mechanism involving the incorporation of processed transcripts. *Nucleic Acids Research*, 41(11), 5837–5850. <https://doi.org/10.1093/nar/gkt196>
- Richter-Dennerlein, R., Oeljeklaus, S., Lorenzi, I., Ronsör, C., Bareth, B., Schendzielorz, A. B., Wang, C., Warscheid, B., Rehling, P., & Dennerlein, S. (2016). Mitochondrial Protein Synthesis Adapts to Influx of Nuclear-Encoded Protein. *Cell*, 167(2), 471–483.e10. <https://doi.org/10.1016/j.cell.2016.09.003>
- Roczniak-Ferguson, A., Petit, C. S., Froehlich, F., Qian, S., Ky, J., Angarola, B., Walther, T. C., & Ferguson, S. M. (2012). The transcription factor TFEB links mTORC1 signaling to transcriptional control of lysosome homeostasis. *Science Signaling*, 5(228), ra42. <https://doi.org/10.1126/scisignal.2002790>
- Roger, A. J., Muñoz-Gómez, S. A., & Kamikawa, R. (2017). The Origin and Diversification of Mitochondria. *Current Biology*, 27(21), R1177–R1192. <https://doi.org/10.1016/j.cub.2017.09.015>
- Rohwedder, A., Zhang, Q., Rudge, S. A., & Wakelam, M. J. O. (2014). Lipid droplet formation in response to oleic acid in Huh-7 cells is mediated by the fatty acid receptor FFAR4. *Journal of Cell Science*, 127(14), 3104–3115. <https://doi.org/10.1242/jcs.145854>
- Rone, M. B., Midzak, A. S., Issop, L., Rammouz, G., Jagannathan, S., Fan, J., Ye, X., Blonder, J., Veenstra, T., & Papadopoulos, V. (2012). Identification of a dynamic mitochondrial protein complex driving cholesterol import, trafficking, and metabolism to steroid hormones. *Molecular Endocrinology*, 26(11), 1868–1882. <https://doi.org/10.1210/me.2012-1159>
- Rorbach, J., Gao, F., Powell, C. A., D’Souza, A., Lightowers, R. N., Minczuk, M., & Chrzanowska-Lightowers, Z. M. (2016). Human mitochondrial ribosomes can switch their structural RNA composition. *Proceedings of the National Academy of Sciences of the United States of America*, 113(43), 12198–12201. <https://doi.org/10.1073/pnas.1609338113>
- Rosing, H. S., Hopkins, L. C., Wallace, D. C., Epstein, C. M., & Weidenheim, K. (1985). Maternally inherited mitochondrial myopathy and myoclonic epilepsy. *Annals of neurology*, 17(3), 228–237. <https://doi.org/10.1002/ana.410170303>
- Rossignol, R., Faustin, B., Rocher, C., Malgat, M., Mazat, J. P., & Letellier, T. (2003).

- Mitochondrial threshold effects. *Biochemical Journal*, 370(3), 751–762. <https://doi.org/10.1042/BJ20021594>
- Rukmini, R., Rawat, S. S., Biswas, S. C., & Chattopadhyay, A. (2001). Cholesterol organization in membranes at low concentrations: Effects of curvature stress and membrane thickness. *Biophysical Journal*, 81(4), 2122–2134. [https://doi.org/10.1016/S0006-3495\(01\)75860-2](https://doi.org/10.1016/S0006-3495(01)75860-2)
- Sacconi, S., Salviati, L., Nishigaki, Y., Walker, W. F., Hernandez-Rosa, E., Trevisson, E., Delplace, S., Desnuelle, C., Shanske, S., Hirano, M., Schon, E. A., Bonilla, E., De Vivo, D. C., DiMauro, S., & Davidson, M. M. (2008). A functionally dominant mitochondrial DNA mutation. *Human Molecular Genetics*, 17(12), 1814–1820. <https://doi.org/10.1093/hmg/ddn073>
- Sarkar, S., Ravikumar, B., Floto, R. A., & Rubinsztein, D. C. (2009). Rapamycin and mTOR-independent autophagy inducers ameliorate toxicity of polyglutamine-expanded huntingtin and related proteinopathies. *Cell Death and Differentiation*, 16(1), 46–56. <https://doi.org/10.1038/cdd.2008.110>
- Sathyanarayan, A., Mashek, M. T., & Mashek, D. G. (2017). ATGL Promotes Autophagy/Lipophagy via SIRT1 to Control Hepatic Lipid Droplet Catabolism. *Cell Reports*, 19(1), 1–9. <https://doi.org/10.1016/j.celrep.2017.03.026>
- Schaffrik, M., Mack, B., Matthias, C., Rauch, J., & Gires, O. (2006). Molecular characterization of the tumor-associated antigen AAA-TOB3. *Cellular and Molecular Life Sciences*, 63(18), 2162–2174. <https://doi.org/10.1007/s00018-006-6200-x>
- Schon, E. A., DiMauro, S., & Hirano, M. (2012). Human mitochondrial DNA: roles of inherited and somatic mutations. *Nature Reviews. Genetics*, 13(12), 878–890. <https://doi.org/10.1038/nrg3275>
- Schwarze, K., Buchanan, J., Taylor, J. C., & Wordsworth, S. (2018). Are whole-exome and whole-genome sequencing approaches cost-effective? A systematic review of the literature. *Genetics in Medicine*, 20(10), 1122–1130. <https://doi.org/10.1038/gim.2017.247>
- Sen, A., Kallabis, S., Gaedke, F., Jüngst, C., Boix, J., Nüchel, J., Maliphol, K., Hofmann, J., Schauss, A. C., Krüger, M., Wiesner, R. J., & Pla-Martín, D. (2022). Mitochondrial membrane proteins and VPS35 orchestrate selective removal of mtDNA. *Nature Communications*, 13(1), 1–20. <https://doi.org/10.1038/s41467-022-34205-9>
- Sengupta, S., Peterson, T. R., & Sabatini, D. M. (2010). Regulation of the mTOR complex 1 pathway by nutrients, growth factors, and stress. *Molecular Cell*, 40(2), 310–322. <https://doi.org/10.1016/j.molcel.2010.09.026>
- Skopkova, M., Stufkova, H., Rambani, V., Stranecky, V., Brennerova, K., Kolnikova, M., Pietrzykova, M., Karhanek, M., Noskova, L., Tesarova, M., Hansikova, H., & Gasperikova, D. (2023). ATAD3A-related pontocerebellar hypoplasia: new patients and insights into phenotypic variability. *Orphanet Journal of Rare Diseases*, 18(1), 92. <https://doi.org/10.1186/s13023-023-02689-3>
- Smedley, D., Smith, K. R., Martin, A., Thomas, E. A., McDonagh, E. M., Cipriani, V., Ellingford, J. M., Arno, G., Tucci, A., Vandrovцова, J., Chan, G., Williams, H. J., Ratnaik, T., Wei, W., Stirrups, K., Ibanez, K., Moutsianas, L., Wielscher, M., Need, A., ... Caulfield, M.

- (2021). 100,000 Genomes Pilot on Rare-Disease Diagnosis in Health Care — Preliminary Report. *New England Journal of Medicine*, 385(20), 1868–1880. <https://doi.org/10.1056/nejmoa2035790>
- Strømme, P., Månsson, J. E., Scott, H., Skullerud, K., & Hovig, T. (1997). Encephaloneuropathy with lysosomal zebra bodies and GM2 ganglioside storage. *Pediatric Neurology*, 16(2), 141–144. [https://doi.org/10.1016/S0887-8994\(96\)00298-6](https://doi.org/10.1016/S0887-8994(96)00298-6)
- Subczynski, W. K., Pasenkiewicz-Gierula, M., Widomska, J., Mainali, L., & Raguz, M. (2017). High Cholesterol/Low Cholesterol: Effects in Biological Membranes: A Review. *Cell Biochemistry and Biophysics*, 75(3–4), 369–385. <https://doi.org/10.1007/s12013-017-0792-7>
- Tang, J. X., Thompson, K., Taylor, R. W., & Oláhová, M. (2020). Mitochondrial OXPHOS biogenesis: Co-regulation of protein synthesis, import, and assembly pathways. *International Journal of Molecular Sciences*, 21(11), 1–32. <https://doi.org/10.3390/ijms21113820>
- Turner, C., Killoran, C., Thomas, N. S. T., Rosenberg, M., Chuzhanova, N. A., Johnston, J., Kemel, Y., Cooper, D. N., & Biesecker, L. G. (2003). Human genetic disease caused by de novo mitochondrial-nuclear DNA transfer. *Human Genetics*, 112(3), 303–309. <https://doi.org/10.1007/s00439-002-0892-2>
- van den Ouweland, J. M. W., Lemkes, H. H. P. J., Ruitenbeek, W., Sandkuijl, L. A., de Vijlder, M. F., Struyvenberg, P. A. A., van de Kamp, J. J. P., & Maassen, J. A. (1992). Mutation in mitochondrial tRNA^{Leu}(UUR) gene in a large pedigree with maternally transmitted type II diabetes mellitus and deafness. *Nature Genetics*, 1(5), 368–371. <https://doi.org/10.1038/ng0892-368>
- Van Haute, L., O'Connor, E., Díaz-Maldonado, H., Munro, B., Polavarapu, K., Hock, D. H., Arunachal, G., Athanasiou-Fragkouli, A., Bardhan, M., Barth, M., Bonneau, D., Brunetti-Pierri, N., Cappuccio, G., Caruana, N. J., Dominik, N., Goel, H., Helman, G., Houlden, H., Lenaers, G., ... Horvath, R. (2023). TEFM variants impair mitochondrial transcription causing childhood-onset neurological disease. *Nature Communications*, 14(1), 1–21. <https://doi.org/10.1038/s41467-023-36277-7>
- Venken, K. J., He, Y., Hoskins, R. A., & Bellen, H. J. (2006). P[acman]: a BAC transgenic platform for targeted insertion of large DNA fragments in *D. melanogaster*. *Science (New York, N.Y.)*, 314(5806), 1747–1751. <https://doi.org/10.1126/science.1134426>
- Ventorim, R. Z., de Oliveira Mendes, T. A., Trevizano, L. M., dos Santos Camargos, A. M., & Guimarães, V. M. (2018). Impact of the removal of N-terminal non-structured amino acids on activity and stability of xylanases from *Orpinomyces* sp. PC-2. *International Journal of Biological Macromolecules*, 106, 312–319. <https://doi.org/10.1016/j.ijbiomac.2017.08.015>
- Vincent, A. E., Grady, J. P., Rocha, M. C., Alston, C. L., Rygiel, K. A., Barresi, R., Taylor, R. W., & Turnbull, D. M. (2016). Mitochondrial dysfunction in myofibrillar myopathy. *Neuromuscular Disorders*, 26(10), 691–701. <https://doi.org/10.1016/j.nmd.2016.08.004>
- von Kleist-Retzow, J. C., Cormier-Daire, V., de Lonlay, P., Parfait, B., Chretien, D., Rustin, P., Feingold, J., Rötig, A., & Munnich, A. (1998). A high rate (20%-30%) of parental consanguinity in cytochrome-oxidase deficiency. *American journal of human genetics*,

63(2), 428–435. <https://doi.org/10.1086/301957>

- Waheed, A. A., Shimada, Y., Heijnen, H. F., Nakamura, M., Inomata, M., Hayashi, M., Iwashita, S., Slot, J. W., & Ohno-Iwashita, Y. (2001). Selective binding of perfringolysin O derivative to cholesterol-rich membrane microdomains (rafts). *Proceedings of the National Academy of Sciences of the United States of America*, 98(9), 4926–4931. <https://doi.org/10.1073/pnas.091090798>
- Wallace, D. C., Zheng, X. X., Lott, M. T., Shoffner, J. M., Hodge, J. A., Kelley, R. I., Epstein, C. M., & Hopkins, L. C. (1988). Familial mitochondrial encephalomyopathy (MERRF): genetic, pathophysiological, and biochemical characterization of a mitochondrial DNA disease. *Cell*, 55(4), 601–610. [https://doi.org/10.1016/0092-8674\(88\)90218-8](https://doi.org/10.1016/0092-8674(88)90218-8)
- Wang, F., Zhang, S., Vuckovic, I., Jeon, R., Lerman, A., Folmes, C. D., Dzeja, P. P., Herrmann, J., Clinic, M., Core, C. M., Clinic, M., & Clinic, M. (2018). Glycolytic Stimulation is not a Requirement for M2 Macrophage Differentiation. *Cell Metabolism*, 28(3), 463–475. <https://doi.org/10.1016/j.cmet.2018.08.012>. Glycolytic
- Wei, W., Schon, K. R., Elgar, G., Orioli, A., Tanguy, M., Giess, A., Tischkowitz, M., Caulfield, M. J., & Chinnery, P. F. (2022). Nuclear-embedded mitochondrial DNA sequences in 66,083 human genomes. *Nature*, 611(7934), 105–114. <https://doi.org/10.1038/s41586-022-05288-7>
- Wiedemann, C., Kumar, A., Lang, A., & Ohlenschläger, O. (2020). Cysteines and Disulfide Bonds as Structure-Forming Units: Insights From Different Domains of Life and the Potential for Characterization by NMR. *Frontiers in Chemistry*, 8(April), 1–8. <https://doi.org/10.3389/fchem.2020.00280>
- Wilhelm, L. P., Voilquin, L., Kobayashi, T., Tomasetto, C., & Alpy, F. (2019). Intracellular and Plasma Membrane Cholesterol Labeling and Quantification Using Filipin and GFP-D4. *Methods in molecular biology* (Clifton, N.J.), 1949, 137–152. https://doi.org/10.1007/978-1-4939-9136-5_11
- Wolf, D. M., Segawa, M., Kondadi, A. K., Anand, R., Bailey, S. T., Reichert, A. S., Bliet, A. M., Shackelford, D. B., Liesa, M., & Shirihai, O. S. (2019). Individual cristae within the same mitochondrion display different membrane potentials and are functionally independent. *The EMBO Journal*, 38(22). <https://doi.org/10.15252/embj.2018101056>
- Yap, Z. Y., Park, Y. H., Wortmann, S. B., Gunning, A. C., Ezer, S., Lee, S., Duraine, L., Wilichowski, E., Wilson, K., Mayr, J. A., Wagner, M., Li, H., Kini, U., Black, E. D., Monaghan, K. G., Lupski, J. R., Ellard, S., Westphal, D. S., Harel, T., & Yoon, W. H. (2021). Functional interpretation of ATAD3A variants in neuro-mitochondrial phenotypes. *Genome Medicine*, 13(1), 1–22. <https://doi.org/10.1186/s13073-021-00873-3>
- Zhang, S., Peng, X., Yang, S., Li, X., Huang, M., Wei, S., Liu, J., He, G., Zheng, H., Yang, L., Li, H., & Fan, Q. (2022). The regulation, function, and role of lipophagy, a form of selective autophagy, in metabolic disorders. *Cell Death and Disease*, 13(2), 1–11. <https://doi.org/10.1038/s41419-022-04593-3>
- Zhao, B., Dierichs, L., Gu, J. N., Trajkovic-Arsic, M., Axel Hilger, R., Savvatakis, K., Vega-Rubinde-Celis, S., Liffers, S. T., Peña-Llopis, S., Behrens, D., Hahn, S., Siveke, J. T., & Lueong, S. S. (2020). TFEB-mediated lysosomal biogenesis and lysosomal drug sequestration confer resistance to MEK inhibition in pancreatic cancer. *Cell Death Discovery*, 6(1). <https://doi.org/10.1038/s41420-020-0246-7>

- Zhao, Y., Sun, X., Hu, D., Prosdocimo, D. A., Hoppel, C., Jain, M. K., Ramachandran, R., & Qi, X. (2019). ATAD3A oligomerization causes neurodegeneration by coupling mitochondrial fragmentation and bioenergetics defects. *Nature Communications*, *10*(1). <https://doi.org/10.1038/s41467-019-09291-x>
- Zheng, Y. Z., Berg, K. B., & Foster, L. J. (2009). Mitochondria do not contain lipid rafts, and lipid rafts do not contain mitochondrial proteins. *Journal of Lipid Research*, *50*(5), 988–998. <https://doi.org/10.1194/jlr.M800658-JLR200>
- Ziehm, M., Piper, M. D., & Thornton, J. M. (2013). Analysing variation in *Drosophila* aging across independent experimental studies: A meta-analysis of survival data. *Aging Cell*, *12*(5), 917–922. <https://doi.org/10.1111/accel.12123>

Appendix

Publications during the PhD

-De la Casa-Fages, B., Fernández-Eulate, G., Gamez, J., Barahona-Hernando, R., Morís, G., García-Barcina, M., Infante, J., Zulaica, M., Fernández-Pelayo, U., **Muñoz-Oreja, M.**, Urtasun, M., Olaskoaga, A., Zelaya, V., Jericó, I., Saez-Villaverde, R., Catalina, I., Sola, E., Martínez-Sáez, E., Pujol, A., Ruiz, M., Schlüter A, Spinazzola A, Muñoz-Blanco JL, Grandas F, Holt I, Álvarez V, López de Munain, A. (2019). Parkinsonism and spastic paraplegia type 7: Expanding the spectrum of mitochondrial Parkinsonism. *Movement disorders: official journal of the Movement Disorder Society*, 34(10), 1547–1561. <https://doi.org/10.1002/mds.27812>

-Gunning, A. C., Strucinska, K., **Muñoz-Oreja, M.**, Parrish, A., Caswell, R., Stals, K. L., Durigon, R., Durlacher-Betzer, K., Cunningham, M. H., Grochowski, C. M., Baptista, J., Tysoe, C., Baple, E., Lahiri, N., Homfray, T., Scurr, I., Armstrong, C., Dean, J., Fernandez Pelayo, U., Jones, A. W. E., Taylor RW, Misra VK, Yoon WH, Wright CF, Lupski JR, Spinazzola A, Harel T, Holt IJ Ellard, S. (2020). Recurrent De Novo NAHR Reciprocal Duplications in the ATAD3 Gene Cluster Cause a Neurogenetic Trait with Perturbed Cholesterol and Mitochondrial Metabolism. *American journal of human genetics*, 106(2), 272–279. <https://doi.org/10.1016/j.ajhg.2020.01.007>

-Pantic, B., Ives, D., Mennuni, M., Perez-Rodriguez, D., Fernandez-Pelayo, U., Lopez de Arbina, A., **Muñoz-Oreja, M.**, Villar-Fernandez, M., Dang, T. J., Vergani, L., Johnston, I. G., Pitceathly, R. D. S., McFarland, R., Hanna, M. G., Taylor, R. W., Holt, I. J., & Spinazzola, A. (2021). 2-Deoxy-D-glucose couples mitochondrial DNA replication with mitochondrial fitness and promotes the selection of wild-type over mutant mitochondrial DNA. *Nature communications*, 12(1), 6997. <https://doi.org/10.1038/s41467-021-26829-0>

-Fernandez-Pelayo, U., **Muñoz-Oreja, M.**, Villar-Fernandez, M., Aiestaran-Zelaia, I., Sánchez-Guisado, M.J., Pantic, B., Elicegui, A., Zufiria, M., Lopez de Arbina, A., Gegg, M., Alonso-Martin, S., RuizCabello, J., Gil-Bea, F., Spinazzola, A., Lopez de Munain, A. & Holt, I.J. (2022). Energy scarcity induces stress granule and inclusion body formation. **Under review.**

-**Muñoz-Oreja M**, Sandoval S, Perez-Rodriguez D, Bruland O, Fernandez-Pelayo U, Villar-Fernandez M, Lopez de Arbina A, Park Y, Martí-Carrera I, Hazan M, Gegg M, Bredrup C, Knappskog P, Varhaug V, Bindoff LA, Spinazzola A, Yoon WH, Holt IJ. (2023). ATAD3 dysfunction increases membrane-bound cholesterol levels resulting in membrane accumulation in lysosomes. **Submitted manuscript.**

-Lopez de Arbina A, Mosqueira-Martin L, Gonzalez K, **Muñoz-Oreja M**, Perez-Rodriguez D, Villar-Fernandez M, Fernandez-Pelayo U, Osinalde N, Vallejo-Illarramendi A, Spinazzola A, Holt IJ. Mitochondrial DNA replication is regulated by lipid-raft protein ERLIN2 and calcium. (2023) **Under review.**

-Zufiria, M., Gerenu, G., Pikatza-Menoio, O., Bengoetxea, X., Jiménez, A., Garciandia, M., Arnold-García, O., Ondaro, J., Elicegui, A., Fernández-Pelayo, U.,

Muñoz-Oreja, M., Aiastui, A., García-Verdugo, J.M., Herranz-Pérez, V., Poza, J.J., Ruiz-Onandi, R., Fernández-Torrón, R., Espinal, J.B., Zulaica, M., Iruzubieta, P., Fernández-Eulate, G., Riancho, J., Vallejo-Illarramendi, A., Holt, I.J., Blázquez, L., López de Munain, A., Alonso-Martín, S & Gil-Bea, F. (2023). Dysregulated FOXO1 activity drives skeletal muscle intrinsic dysfunction in amyotrophic lateral sclerosis. **Under review.**

-Scientific dissemination article: **Muñoz-Oreja M**, Fernandez-Pelayo U, Holt IJ. (2018). Mitokondriak eta zahartzea. *Elhuyar*.331:74-74